Monitoring of Unvented Roofs with Fibrous Insulation, Diffusion Vents, and Interior Vapor Control in a Cold Climate

Building America Report - 2001

September 2020

K. Ueno and J.W. Lstiburek

Abstract:

This research involved construction of a conditioned test hut in a cold climate (Climate Zone 5A) with multiple side-by-side instrumented roof rafter bays. This work examined seven experimental unvented roofs and one code-compliant control hybrid ccSPF-cellulose roof over three winters and following summers. Examined variables included insulation material (fiberglass and cellulose), the presence or absence of a ridge diffusion vent (vapor-open material at the roof ridge to promote drying), the effect of various interior vapor control membranes (fixed and variable permeance), the effect of interior relative humidity, and the effect of interstitial airflow (from the interior into the cavity). This experiment was run over three winters, changing variables of interior conditions, roof configurations/materials, and the addition of intentional air leakage.

Monitoring of Unvented Roofs with Fibrous Insulation, Diffusion Vents, and Interior Vapor Control in a Cold Climate

September 2020

Monitoring of Unvented Roofs with Fibrous Insulation, Diffusion Vents, and Interior Vapor Control in a Cold Climate

FOREWORD

The U.S. Department of Energy (DOE) Building America Program has been a source of innovations in residential building energy performance, durability, quality, affordability, and comfort for more than 20 years. This world-class research program partners with industry to bring cutting-edge innovations and resources to market.

In cooperation with the Building America Program, Building Science Corporation is one of many Building America teams working to drive innovations that address the challenges identified in the program's Research-to-Market Plan.

This report, "Monitoring of Unvented Roofs with Fibrous Insulation, Diffusion Vents, and Interior Vapor Control in a Cold Climate," covers research on replacing currently code-compliant polyurethane spray foam in unvented roof assemblies with lower-cost fibrous insulation (cellulose or fiberglass). Specific research questions include determining the best approach to these types of assemblies by varying parameters such as interior vapor retarders and outward drying mechanisms (vapor diffusion vents). Implementing unvented roofs in a moisture-safe manner with air-permeable fibrous fill insulations could potentially reduce the first cost of unvented roof designs, allowing for more widespread use. Building unvented roofs in a cost-effective, airtight, and moisture-safe manner opens up options for high-performance house designers and builders.

As the technical monitor of the Building America research, the National Renewable Energy Laboratory encourages feedback and dialogue on the research findings in this report as well as others. Send any comments and questions to building.america@ee.doe.gov.
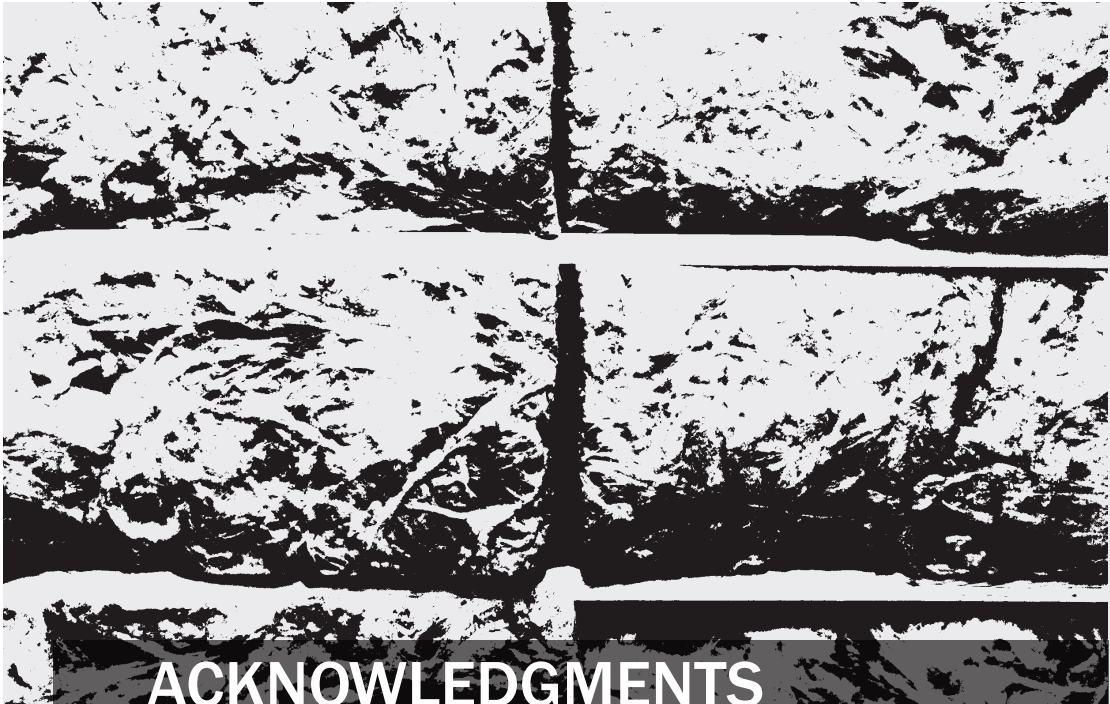
ACKNOWLEDGMENTS

Photo Credits

Cover, from top to bottom: Photos from iStock 182149008, 178447161, 184944590, 467972591;

Page ii and iii: Photo from iStock 182149008;

Page v: Photo by Dennis Schroeder, NREL 28764;

Page vi: Photo from iStock 183245764;

Page vii: Photo from iStock 496703961;

Page viii: Photo from iStock 148484827;

Page ix, x, xi: Photos from Building Science Corporation
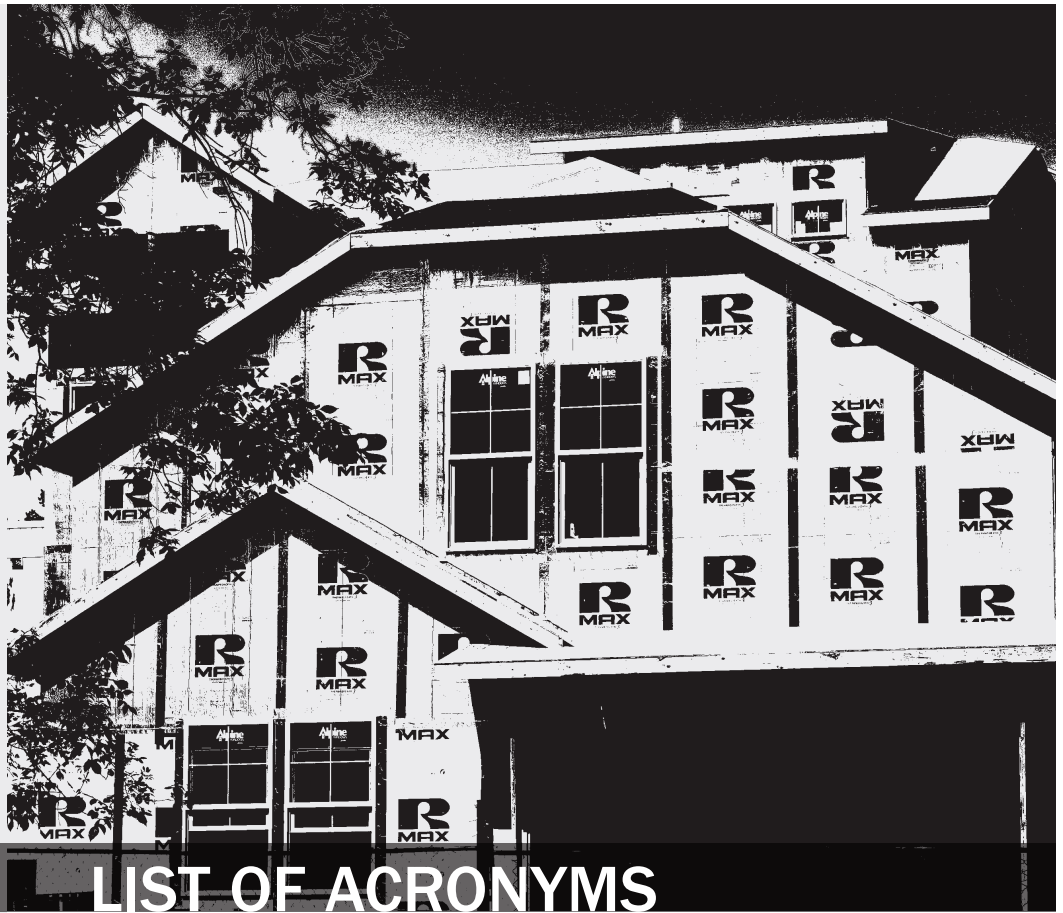
LIST OF ACRONYMS

ccSPF	closed-cell spray polyurethane foam
CFM	cubic feet per minute
DV	diffusion vent
EqLA	equivalent leakage area
FG	fiberglass
HDD	heating degree days
ICC	International Code Council
IRC	International Residential Code for One- and Two-Family Dwellings
MC	moisture content
MDI	methyl diisocyanate
OSB	oriented strand board
PCF	pounds per cubic foot
RH	relative humidity
SVR	smart vapor retarder (variable permeance)
T	temperature
VB	vapor barrier (fixed-perm in this research)

EXECUTIVE SUMMARY

Unvented roof assemblies have been accepted in North American building codes since 2007; code-compliant construction calls for a minimum thickness of "air-impermeable insulation" (based on climate zone) to avoid cold-weather condensation and moisture risks. This is typically implemented with polyurethane spray foam insulation; however, negatives of this material include high first cost and possible adverse environmental impacts. Implementing unvented roofs in a moisture-safe manner with air-permeable fibrous fill insulations (e.g., fiberglass or cellulose) could potentially reduce the first cost of unvented roof designs, allowing for more widespread use. Building unvented roofs in a cost-effective, airtight, and moisture-safe manner opens up options for high-performance house designers and builders.

This research involved construction of a conditioned test hut in a cold climate (climate zone 5A) with multiple side-by-side instrumented roof rafter bays. This work examined seven experimental unvented roofs and one code-compliant control hybrid closed-cell spray polyurethane foam (ccSPF)/cellulose roof over three winters and the following summers. Examined variables include insulation material

(fiberglass and cellulose), the presence or absence of a ridge diffusion vent (vapor-open material at the roof ridge to promote drying), the effect of various interior vapor control membranes (fixed and variable permeance), the effect of interior relative humidity (RH), and the effect of interstitial airflow (from the interior into the cavity). This experiment lasted three winters, with changing variables of interior conditions, roof configurations/materials, and the addition of intentional air leakage.

Winter 1 (2016–2017) was run at "normal" (30%–40%) interior RH conditions. All the non-diffusion-vent roofs (Roofs 3, 4, 5, and 6) remained at high RH levels (95%–100%) for most of the winter, only showing significant drying in spring. Condensation and high sheathing moisture contents (MCs) were also measured. Despite these indications of problems in these roofs, the calculated mold index values remained below 3 (failure threshold of visible mold without magnification). In contrast, the roofs with a variable-perm vapor retarder and a diffusion vent (Roofs 2 and 7) showed the safest performance: Winter 1 data for these roofs indicated the lowest moisture accumulation out of all the roofs, and no measurements exceeding danger thresholds.

Winter 2 (2017–2018) was run at an elevated interior RH (constant 50% RH). Given the poor performance of the non-diffusion-vent roofs in Winter 1, they were eliminated in Winter 2 and replaced with the "small" and "tight" diffusion vent roofs. Higher interior RH levels resulted in worse moisture performance across all roofs; all were at higher risks than Winter 1, with

evidence of condensation at the ridges of all roofs. This included roofs that showed acceptable behavior in Winter 1. The exception was the code-compliant spray foam and cellulose roof (Roof 8), which showed few signs of durability risks. Mold index calculations remained below 3 in Winter 2's data. However, ridge disassembly in summer 2018 revealed mold spotting on sheathing and framing in all fibrous insulation roofs, with some of the worst damage in the tight diffusion vent roofs.

Winter 3 (2018–2019) was run at 50% RH interior conditions, and air leakage was added in late winter (February 2019). Insulation settling was noted between Winter 2 and Winter 3, so all roofs were reinsulated between winters with a complete and dense rafter cavity fill. Interior conditions were first run at 50% RH without air injection, which is identical to Winter 2's conditions. All roofs showed less moisture accumulation than Winter 2, likely demonstrating the effect of suppressing airflow with a complete cavity fill (elimination of air voids due to insulation settling). This finding from early Winter 3 indicates that these unvented fibrous insulation roof assemblies can function with acceptable moisture risks even at high (50%) interior RH levels, if insulation is installed in a void-free manner. However, consistently assuring this level of quality in field installations will be difficult to achieve.

Interior air was injected into north-side roof cavities in late winter; the system induced a small (~0.5 cubic feet per minute [CFM]) leak per roof bay, which is consistent with a small imperfection in relatively airtight construction. This resulted in severe localized wetting (30%–40% MC sheathing maximums), which is a risk range for mold growth and decay. However, disassembly during the following summer showed

no indication of moisture distress at the sheathing, including mold growth, staining, or physical damage.

Other observations that apply over multiple winters include:

- Inward vapor drives were found to be a non-issue with any roofs with variable-perm interior air and vapor control layers. The only issue found with inward vapor drives was liquid water condensation near the ridge at the fixed-perm (1 perm) fiberglass roofs.

- The §R806.5 code-compliant hybrid ccSPF-cellulose roof (Roof 8) consistently showed safe behavior compared to the experimental fiberglass and cellulose roofs.

- All research was conducted using dark-colored roof shingles; lighter-colored roofs have been linked with moisture-related failures due to lower temperatures and less inward solar drying. The north-facing roof still had significant summertime solar gain (peak values ~550 W/m2). Lighter-colored roofing would make these assemblies more vulnerable to wintertime moisture accumulation.

Based on this research, unvented all-fibrous insulation assemblies have greater moisture risks than current code-compliant non-air-permeable insulation or exterior insulation assemblies. These fibrous insulation-only unvented roofs can function in a moisture-safe manner, especially with measures that increase their drying (ridge-top diffusion vent and variable-perm interior vapor retarder), at lower interior RH levels, or with a complete cavity fill. However, widespread adoption of unvented fibrous roof assemblies will likely result in an unacceptable failure rate. In addition, air injection indicated that the assemblies are still highly vulnerable to small air leaks (0.5 CFM), which result in significant localized sheathing moisture uptake.

Finally, the high moisture accumulation and visible mold growth seen in the test roofs after Winter 2 (despite mold index values in the safe range) indicate that these roofs can have significant moisture risks at high interior RH levels.

As a result, it is difficult to recommend these experimental all-fibrous insulation assemblies for any application that might experience high wintertime humidity levels. Although wintertime humidity levels in cold climates are commonly in the 30% RH or lower range, inadvertent operation at 40%–50% RH in winter is becoming more common. This occurs in modern construction with greater airtightness, low outdoor air change rates, and in particular, buildings with high occupant densities (e.g., multifamily construction). Given these risks, acceptance of these assemblies for general use and code acceptance is not recommended.

Unvented fibrous roof assemblies might be useful in retrofit situations, where a failing assembly must be addressed, but interior/exterior demolition followed by code-compliant assemblies (polyurethane spray foam and/or exterior rigid insulation overclad) is not a realistic, affordable, or acceptable option. Unfortunately, there is no code provision allowing "use only to address existing failing assemblies."

Overall, this research has run fibrous insulation unvented roof assemblies through a variety of conditions and exposures; further research on this topic may be of limited value, given the demonstrated risks of these assemblies. A possible exception might be monitoring of "short slope" story-and-a-half (Cape Cod-style) roof assemblies retrofitted with unvented fibrous insulation. This could reduce installation costs and improve R-values in these geometries.

Table of Contents

List of Figures

List of Tables

1 Introduction

Unvented roof assemblies have been accepted in North American building codes for more than a decade (International Code Council [ICC] 2007); code-compliant construction calls for a minimum thickness of "air-impermeable insulation" (based on climate zone) to avoid cold-weather condensation and moisture risks. This is typically implemented with polyurethane spray foam insulation. However, this insulation material—while effective—has a high first cost and possible negative environmental impacts. Implementing unvented roofs in a moisture-safe manner with fibrous fill insulations (e.g., fiberglass, cellulose, mineral fiber) could potentially reduce the first cost of unvented roof designs, allowing for more widespread use. Building unvented roofs in a cost-effective, airtight, and moisture-safe manner opens up options for high-performance house designers and builders.

The experimental work described in this report involved construction of a conditioned test hut in a cold climate (climate zone 5A) with multiple side-by-side instrumented roof rafter bays. These test bays compared code-compliant construction with experimental options. Experimental variables included:

- The presence or absence of a ridge diffusion vent—with vapor-open material at the roof ridge to promote drying, which has been researched in previous work (Ueno and Lstiburek 2015, 2016a, 2016b)

- The effect of various interior vapor control membranes (fixed and variable permeance)

- The choice of cavity insulation material (blown fiberglass or cellulose)

- The effect of interior relative humidity (RH).

Temperature, RH, and wood moisture content (MC) data were collected and analyzed; this work covers three winters of monitoring, with data from the following spring/summers demonstrate drying of assemblies. The objective of this research is to determine what combination of materials/assemblies have the best performance, and whether or not their associated moisture risk is acceptable for code acceptance.

1.1 Unvented Roof Advantages and Disadvantages

Unvented roofs can have higher first costs and more potential moisture/durability risks than conventional vented roof/attic assemblies. However, they are useful in high-performance construction for multiple reasons.

Living space within the sloped roof area is a common design, but vented cathedral assemblies often have poor thermal and moisture performance (due to air leakage and limited insulation depth). Furthermore, more complex roof geometries (e.g., hips, dormers, roof-wall connections) are difficult to vent. Building an attic as conditioned space brings ductwork and air-handling

equipment into the conditioned space, negating duct leakage losses; this measure can also improve building airtightness and address construction issues such as protecting wet pipe sprinklers. Using a "hybrid" approach of spray foam and fibrous fill insulation can lower the cost of high-R roof assemblies, but is more logistically involved (requires two insulator trips/crews).

1.2 Previous Work

High-performance home builders have built compact roof assemblies using fibrous fill insulation with a hygrothermal "flow-through" design (allowing outward drying/moisture flow). These assemblies use a vapor permeable membrane on the exterior of the rafter cavity, a ventilated cavity, and a nail base sheathing. Moisture monitoring of these assemblies shows extremely safe performance (Corson 2015).

However, this flow-through roof design is a complicated assembly that requires excellent quality control and unconventional building materials and techniques. In terms of existing buildings, this assembly is better suited to a "deep energy retrofit," or a major reconstruction of the exterior thermal enclosure, rather than typical energy retrofits in the weatherization category.

European practitioners and high-performance North American home builders have been building unvented roof assemblies using dense-pack cellulose insulation and a variable permeance interior vapor retarder (475 High Performance Building Supply, 2015, 2016a, 2016b). The public information available to date indicates good performance. However, the North American practitioners who build these assemblies are high-performance builders (Passive House or similar) with excellent quality control. It is unclear whether these assemblies are viable when built by typical builders and trades.

Previous Building America-funded research monitored unvented roof assemblies in a cold climate (Chicago, climate zone 5A; Ueno and Lstiburek 2015). That work demonstrated that an unvented cellulose roof assembly has high moisture risks when subjected to high interior RHs (Figure 1). That work also demonstrated that a diffusion vent provides limited drying ability— insufficient to avoid failures. The project also showed that dense-pack cellulose had lower moisture risks than commodity fiberglass batt insulation. However, this work did not study the effect of interior vapor control beyond latex paint (Class III vapor retarder, ~10 perms). Lower interior permeance could control moisture entry into the cavity sufficiently to minimize risks.

7 Unvented Cellulose
6 Diffusion Vent Cellulose
5 Top Vent Fiberglass-GWB
4 Top Vent Fiberglass
3 Top Vent Cellulose
2 Top Vent Cellulose-GWB

GWB = gypsum wall board interior finish

1 Vented

Figure 1. Disassembly of Chicago unvented roof assemblies at conclusion of experiment

Previous Building America-funded research also monitored unvented roof assemblies in hot-humid climates (Houston and Orlando, climate zone 2A; Ueno and Lstiburek 2015, 2016a, 2016b). Two attics were monitored—one in Houston, TX, with asphalt shingles, and the other in Orlando, FL, with concrete barrel tiles; both were monitored for multiple years. The unvented roof assemblies were insulated with loose-fill fiberglass (adhered or netted, respectively), with no intentional interior air barrier between the insulation and the conditioned attic space.
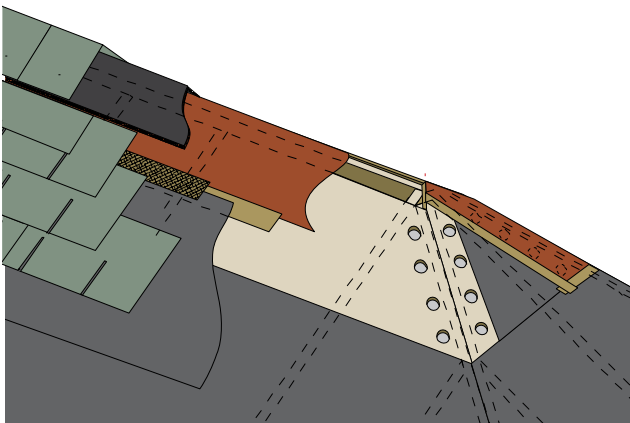
Figure 2. Houston diffusion vent design at the roof ridge and hip

Figure 3. Houston diffusion vent showing ridge condition

The roofs were equipped with a diffusion vent, which is an opening at the ridge and hips covered with a water-resistant but vapor-open membrane (Houston configuration shown in Figure 2 and Figure 3). As a control comparison, portions of the roof were constructed as a typical unvented roof (vapor-impermeable self-adhered membrane at ridge). Collected data indicate that the diffusion vent roof shows greater moisture safety and less wintertime moisture accumulation than the conventional, unvented roof design. The unvented roof had winter periods of 95%–100% RH, with other sensors indicating possible condensation; high moisture levels were concentrated at the roof ridge. In contrast, the diffusion vent roofs had drier conditions. In the

spring, as outdoor temperatures warmed, all roofs dried well into the safe range (10% MC or less).

1.3 Cost-Effectiveness

The primary improvement of unvented roofs with fibrous insulation is not an improvement in energy performance per se, but the reduction in the installed cost of an unvented roof (insulated at the roofline). Code-compliant unvented roofs require premium insulation materials, such as spray foams, rigid foam plastic board, or semi-rigid mineral fiber, which have an associated cost penalty.

The installed cost of closed-cell spray polyurethane foam (ccSPF) varies widely based on contractor availability, the size of the installation, regional pricing, feedstock (crude oil) prices, and access (e.g., requirement for lifts or scaffolding, confined space installation). However, a typical installed price used for estimation purposes is about $1/board foot (1 in. × 12 in. × 12 in.), although pricing may vary in practice from $0.45 to $1.40/board foot.

Figure 4 shows a comparison of insulation material costs based on big box home center pricing gathered from 2007 through 2011. The comparison shows the normalization metric of $/ft^2·R value, which normalizes the area costs based on the R-values. The figure shows values for extruded polystyrene, polyisocyanurate, fiberglass, cellulose, SPF, and mineral fiber. The ccSPF is included in the graph with a caveat: no isolated material cost for ccSPF is shown, because it is effectively manufactured and installed as a single step. An estimate was made using the $1/board foot price and dividing by 2 (50% materials and 50% labor). The graph shows that ccSPF is priced comparably to the rigid board foam plastic products (extruded polystyrene and polyisocyanurate), which are both substantially more expensive than cavity fill fibrous insulation such as fiberglass or cellulose.
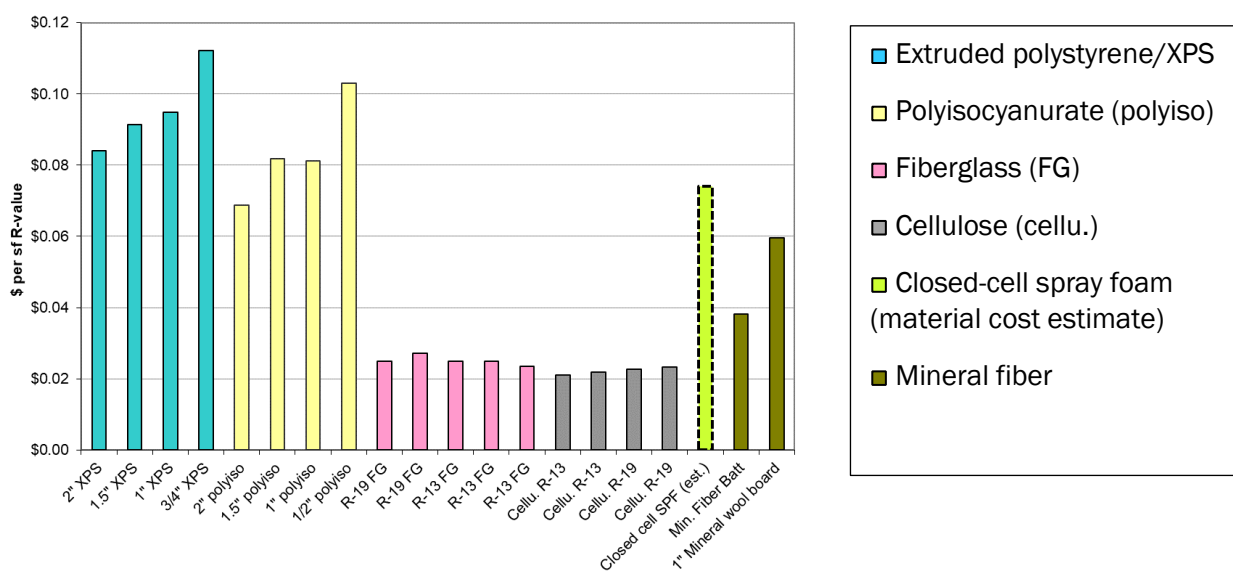
Figure 4. Insulation material costs (no installation), in $/ft²·R-value

Assuming that a typical installation is 50% materials and 50% labor, a 3- to 4-fold reduction in material cost would result in ~30%–40% reduction in installed cost of this measure, assuming equal R-values and equal labor impact. However, this reduction will likely be taken up by increased labor in the fibrous insulation installation, given the requirement for netting and/or interior membranes, instead of a sprayed approach.

The difference in insulation material cost becomes more important as higher R values are adopted in the code. For instance, the 2012 International Energy Conservation Code (ICC 2012b) calls for R-49 ceiling insulation in climate zones 4 through 8 (previously R-38 to R-49) and R-38 in climate zones 1 and 2 (previously R-30). Greater thicknesses of closed-cell spray foam are economically penalized by the fact that a pause is required between ~2 in. "lifts" to allow for heat dissipation/exothermic reaction, resulting in more installer movement and lower efficiency.

1.4 Tradeoffs and Previous Lessons Learned

Benefits of unvented roof assemblies include energy savings due to the elimination of duct conductive and air leakage losses, and improved airtightness by shifting the enclosure geometry to the roof line, especially in complicated geometries such as dormer, kneewalls, and Cape Cod-style houses.

One conclusion from the Houston and Orlando work (Ueno and Lstiburek 2016a, 2016b) is that when switching from spray foam to fibrous (air permeable) insulation, air barrier detailing—especially at roof-wall connections—is critical. Figure 5 shows an infrared image during depressurization air leakage testing with cold exterior conditions; complicated roof-wall interfaces were a common source of air leakage.

Some incremental cost will need to be absorbed by ensuring air barrier performance when implementing unvented roofs with fibrous insulation. However, the design of the proposed cold-climate assemblies includes an interior air/vapor barrier/retarder, which would nominally fulfill this role.
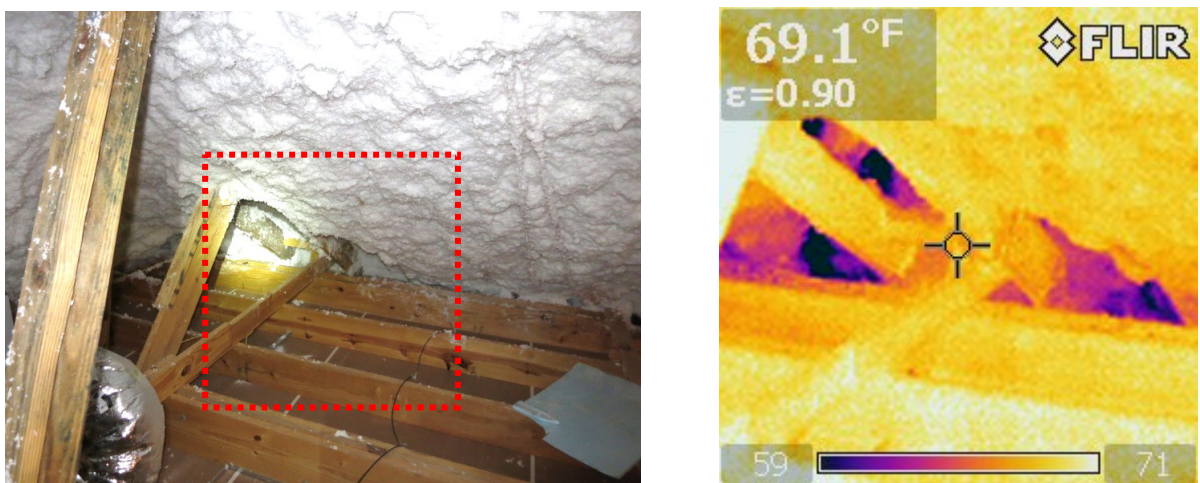
Figure 5. Air leakage at roof-to-wall details at dormer/intersecting roofs

Switching from spray foam to fibrous insulation in unvented roof assemblies can have positive or negative effects on durability. The durability risk of fibrous insulation is that it is more vulnerable to cold-weather interior-sourced air leakage condensation. In fact, this is the greatest reason for caution before implementing this assembly on a wider scale. On the other hand, closed-cell spray foam has low vapor permeance, thus reducing inward drying of wetted sheathing. There are no endemic failures of these assemblies due to this lack of drying, but fibrous insulation could allow for enhanced drying of small, limited roof bulk water leakage. This is discussed by Salonvaara et al. (2013).

2 Test Hut and Roof Construction

2.1 Test Hut Overview

The unvented roof field research and long-term monitoring were conducted at a test hut in Westford, Massachusetts (27 miles northwest of Boston), in climate zone 5A. The test hut has a 32 ft. x 16 ft. footprint, with multiple north-south roof bays, and the long axis faces east-west (Figure 6).
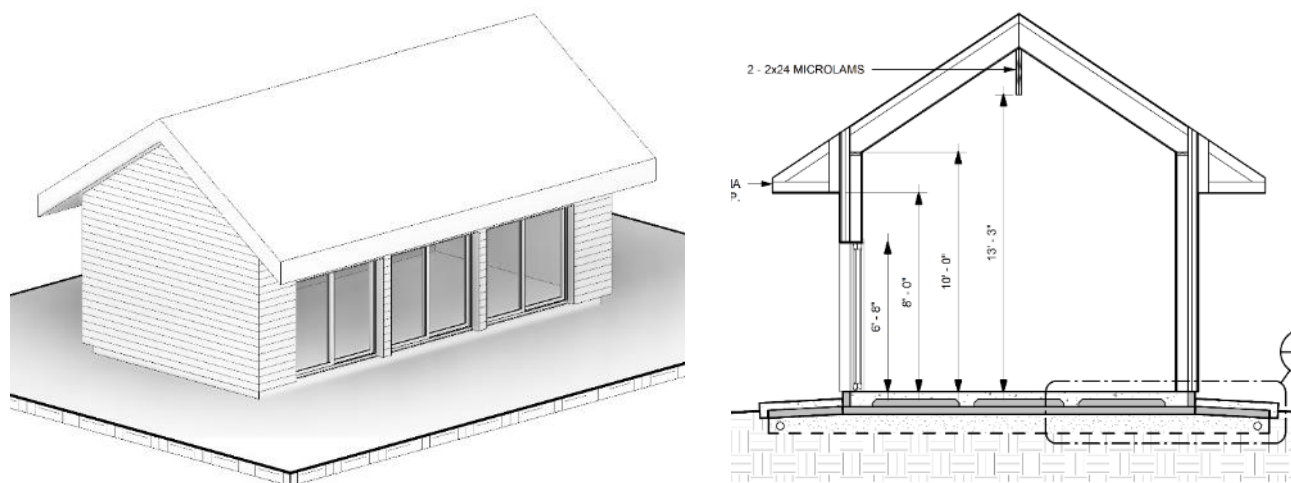
Figure 6. Isometric (left) and building section (right) of test hut

Overview images of the completed test hut are shown in Figure 7, including the south elevation (left), and an overview of the site in winter, putting the test hut exposure in context (right).

Figure 7. Completed test hut south elevation (left), overview image of surroundings (right)

2.2 Construction Detailing

The test hut structure is wood stick frame (Figure 8, left); the wall and roof are sheathed with oriented strand board (OSB) with an integrated air and water barrier surface, detailed with taped seams (Figure 8, right). Walls are 2x6, insulated with closed-cell spray polyurethane foam

(ccSPF) insulation and 4-in semi-rigid mineral fiber continuous exterior insulation, and have horizontal wood shiplap siding.

Figure 8. Test hut during framing (left); roof-to-wall air barrier connection (right)

Roof-to-wall connections are a common air barrier failure point. This was addressed by building the roof-wall junction as a direct connection between the exterior roof and wall sheathing, with a taped seam (Figure 8, right and Figure 9, left). Eave and rake end roof overhangs were then attached, after completion of the air barrier detailing (Figure 9, right).

Figure 9. Roof-to-wall air barrier connection (left), eaves and rakes attached (right)

The rafters have a 14.75-in. deep cavity for a targeted R-49 insulation value, per 2012 International Energy Conservation Code (ICC 2012a) requirements for climate zone 5A. This framing depth was achieved by stacking 2x12 and 2x4 nominal framing lumber rafters (Figure 10, left). The roof has an 8:12 slope.

The rafter bays are framed 24-in. on center (nominal). "Guard" bays are installed between experimental bays and at the roof gable ends/edges (to avoid corner/edge effects on experimental bays). A fluid-applied air and vapor barrier is applied to the sides of the guard bays (Figure 10,

right), providing hygrothermal isolation/separation to each experimental bay. The guard bays are insulated with closed-cell spray foam and cellulose "flash-and-blow" assemblies; one of these guard bays will be instrumented as a code-compliant control comparison. Details of the layout of the experimental and guard bays are shown later in the report in Figure 24 and Figure 25.

Figure 10. 2x12 and 2x4 rafters (left), air and vapor barrier on guard bay rafters (right)

The 32-ft. long test hut provides sixteen 2-ft. wide rafter bays; assuming two end guard bays, this leaves fourteen remaining bays. Assuming half of the bays are guard bay separations, this leaves seven experimental bays.

The exterior of the roof assembly is per typical builder practice, including dark-colored asphalt shingles (α≈0.95/high solar absorptance), vapor-impermeable self-adhered membrane underlayment (0.05 perm), and 5/8-in. OSB sheathing (Figure 11). The roof sheathing is 5/8-in. nominal thickness, with an integrated air and water barrier surface. Self-adhered membrane was used in lieu of more typical #30 felt underlayment to provide worst-case limitations on outward drying, even though asphalt shingles are essentially vapor impermeable. Previous work (Ueno and Lstiburek 2015) demonstrated that asphalt shingles and #30 felt underlayment are not a significant source of inward-driven moisture.

Figure 11. Self-adhered underlayment (left) and asphalt shingles (right)

Guard bays were insulated with 4 in. of ccSPF (Figure 12, left); netting was stapled to the rafters for installation of blown-in cellulose and fiberglass in the experimental bays (Figure 12, right). Cellulose insulation was installed in experimental and guard bays (hybrid flash-and-blow); blown fiberglass insulation was installed in experimental bays only.

Figure 12. ccSPF insulation in guard bays (left); netting installation for blown insulation (right)

Interior vapor control membranes were installed on the test bays, with material varying per assembly (Figure 13, left). The interior vapor control membrane was detailed as an air barrier at each bay, sealing to the rafter faces, ridge beam, and wall top plate.

The first seal iteration used double-sided tape between framing and membrane, followed by single-sided housewrap tape from the membrane to the rafter (Figure 13, right). However, after failures (see Section 12.2 Interior Air Barrier/Vapor Retarder Issues), a multistep process was used to improve the air seal. This included (a) removal of all old tapes and seals, (b) contact spray adhesive (3M 90) on the face of the wood rafter, (c) double-sided tape on the rafter to form a primary seal (Saint-Gobain Norbond foam tape), (d) high-performance housewrap tape on the rafter as a secondary seal (Dow Weathermate Construction Tape), and (e) use of a roller and/or squeegee to improve the adhesive bond.

Figure 13. Interior vapor control membranes (left), double-tape air sealing detail (right)

Space conditioning was provided by a wall-mounted ductless heat pump (commonly called a minisplit), located at the middle of the north-facing wall (Figure 14, left, red oval). In addition, a through-wall exhaust fan (70 cubic feet per minute [CFM] nominal capacity, 28 CFM initial measured flow) was installed in the gable end wall to control interior moisture levels via wintertime air exchange (Figure 14, left, gold circle).

The test hut has multiple south-facing sliding glass doors for its future use as a solar-tempered shed. For the duration of the experiment, the doors were covered with interior solar-control roll-down shades to reduce unwanted temperature excursions from solar gain (Figure 14, right).

Figure 14. Mechanical systems (left) and solar control shades (right)

The various steps of roof construction are shown in the following figures for the north-facing roof, including instrumentation (Figure 15), insulation (Figure 16 and Figure 17), vapor retarder installation, and air sealing (Figure 17 and Figure 18).

Figure 15. North-facing roof bays after instrumentation

Figure 16. North-facing roof bays after spray foam installation

Figure 17. North-facing roof bays after netted fibrous insulation installation

Figure 18. North-facing roof bays after vapor control membrane installation

2.3 Roof Experimental Variables

The test hut contains multiple north/south-oriented rafter test bays. Each experimental assembly is composed of two opposing roof bays to provide two "contributing" roof slopes to each ridge condition.

A typical test hut experimental roof bay (with cellulose insulation) is shown in Figure 19, depicting the exterior wall with 4-in. exterior rigid mineral fiber insulation.
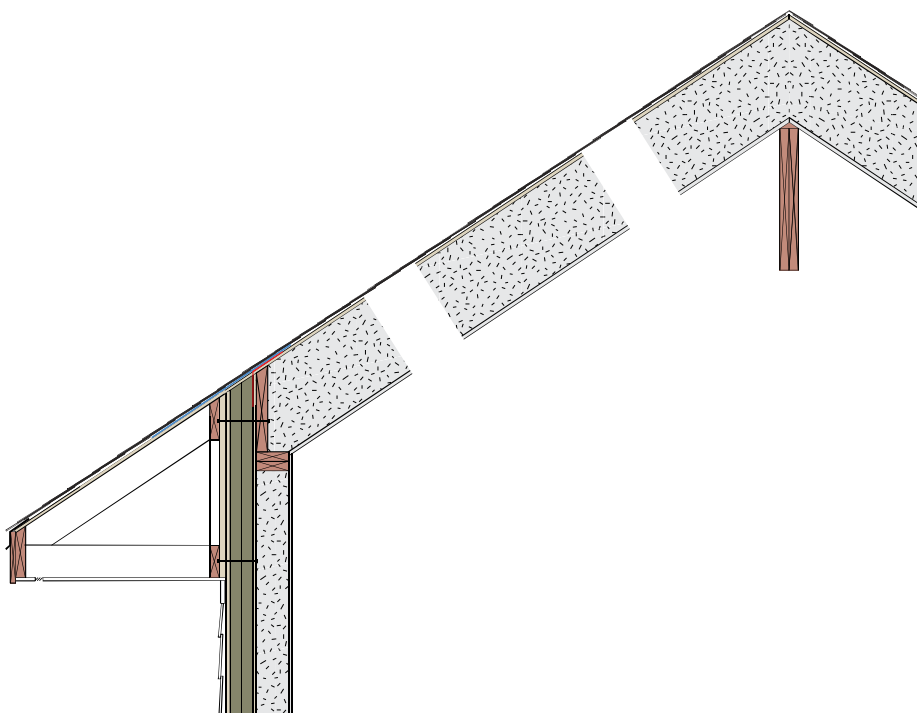
Figure 19. Typical test hut experimental roof bay with cellulose cavity insulation

The experimental variables include:

Insulation material: variables include dense-pack cellulose and blown fiberglass. Fiberglass batt was not considered for this testing, because few practitioners tend toward this option, and to limit the number of test variables.

- Cellulose insulation was installed in test and guard bays (as flash-and-blow) behind netting as a dense-pack installation, at a density of 3.5 pounds per cubic foot (PCF) based on a bag count (material weight). Assuming R-3.5 per in., the cellulose experimental bays are nominal ~R-52. Insulation density measurements during decommissioning of the experiment are covered in Section 18.2: Density Measurements.

- Fiberglass insulation was installed at a density of 1.4 PCF, based on a timed installation technique. Based on rafter thickness and the manufacturer's stated R-value (R-4 per in.), the fiberglass bays are nominal ~R-59. Insulation density measurements during decommissioning of the experiment are covered in Section 18.2: Density Measurements.

- ccSPF was used in the flash-and-blow guard bay assemblies. These assemblies are code-compliant hybrid ccSPF and cellulose roofs, per §R806.5 in the 2012 International Residential Code (IRC) (ICC 2012b), and are shown in Figure 20. Assuming R-6.25/in. for ccSPF, the guard bays are nominal ~R-63. The two insulation materials are installed in thicknesses to achieve a ratio of R-values consistent with the code table (40% air impermeable/60% air permeable) for climate zone 5A.

- One issue raised is that differential R-values in the guard and experimental bays might affect experimental roof sheathing temperatures. Two-dimensional thermal simulations demonstrated that there is insignificant influence on middle-of-bay conditions, where instrumentation is located. These results are detailed further in the appendices in Section 10.3: Roof Assembly Thermal Simulations.
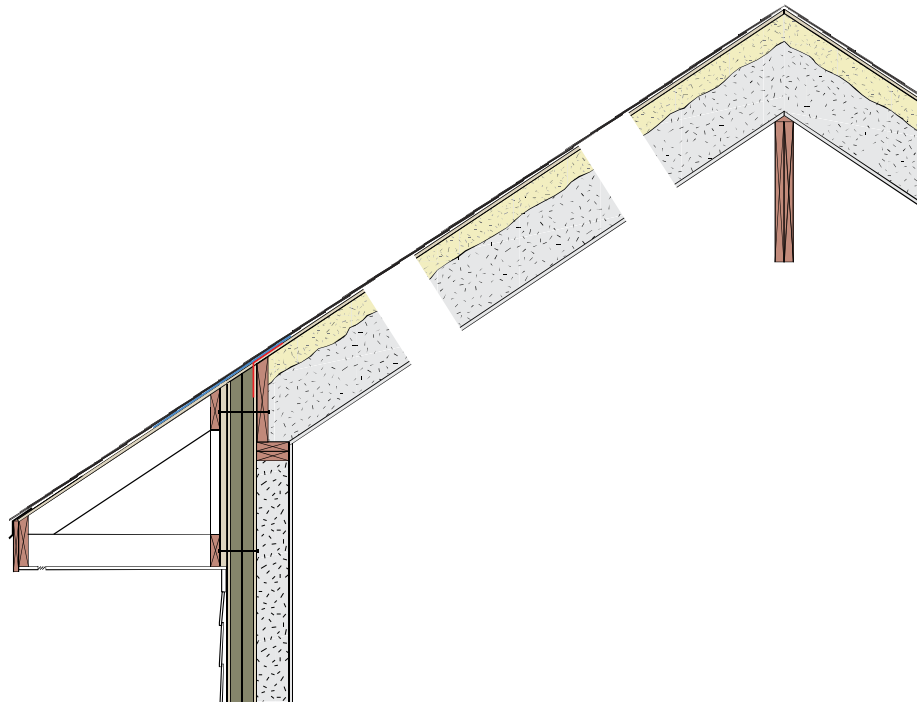
Figure 20. Typical test hut guard roof bay with hybrid spray foam/cellulose insulation

Interior vapor control: variables include several variable-permeance membranes (known as smart vapor retarders [SVRs]) and fixed-permeance membranes. The manufacturers' vapor permeance data for the installed interior vapor control membranes are plotted in Figure 21. Kraft facing (as used in fiberglass batts) is also shown for reference.
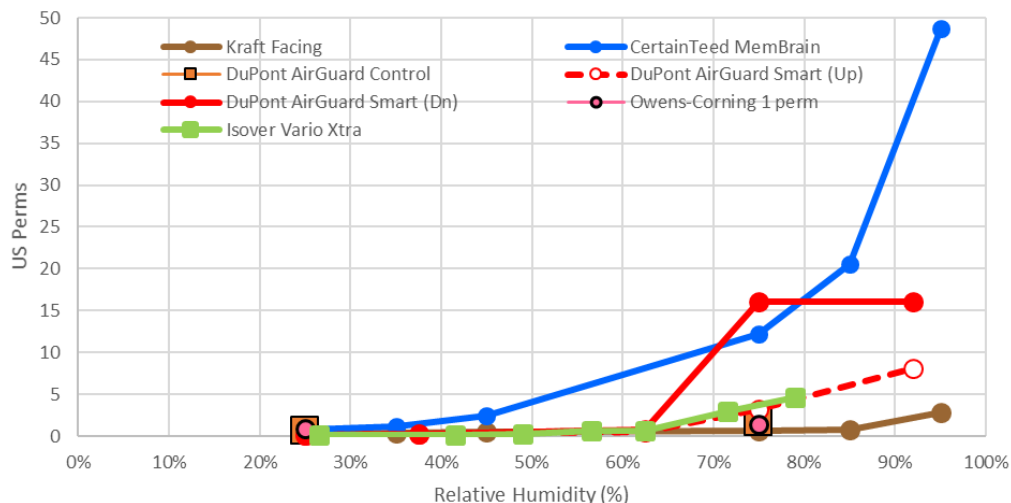
Figure 21. Vapor permeance curves for various interior vapor control materials

The fixed-permeance membranes include Owens Corning High Performance Conditioned Attic netting (0.8 dry cup/1.4 wet cup) for fiberglass experimental attics and DuPont AirGuard Control (0.7 perm nominal) for the cellulose attics.

The initial variable-permeance membranes include CertainTeed MemBrain (0.8 perm dry cup, 12.2 perm wet cup) for fiberglass experimental attics and DuPont AirGuard Smart Gen2 (~1 perm dry cup, 3–16 perm wet cup depending on test direction) for the cellulose attics. In later work, two rafter bays (one fiberglass, one cellulose) were retrofitted with a variable-perm interior vapor retarder with lower mid-range permeances. This material was Isover Vario Xtra (0.1 perm dry cup, ~3 perm wet cup).

The DuPont and Isover products are commercially available in the European market but not in North America.

Diffusion vent: a ridge diffusion vent is installed in some bays to allow outward drying at the ridge, where moisture accumulation typically occurs. These diffusion vents are similar to details used in Houston and Orlando diffusion vent roof research (Ueno and Lstiburek 2016a; 2016b). A ~6-in. opening is cut through the roof sheathing at the ridge (~3 in. each side of the ridge), and covered with a strip of a highly vapor-permeable roof membrane (tear-resistant polyethylene terephthalate fabric with a diffusive waterproof dispersion coating; 214 perms dry cup, 550 perms wet cup), as shown in Figure 22 (left). This material is Dörken Delta-Foxx. The diffusion vent is then covered with an off-the-shelf ridge vent, as used for ventilated roof assemblies (Figure 22, right).

Figure 22. Diffusion vent ridge detail, showing taped membrane (left) and ridge vent cap (right)

In Winter 1, assemblies with and without diffusion vents were compared to determine whether they are required to provide sufficient drying. The non-diffusion-vent roofs had vapor-impermeable self-adhered membrane (0.05 perm) over the ridge area. In Winter 2, several assemblies were modified based on Winter 1's results. The non-diffusion-vent roofs had poor performance and were replaced with assemblies that examine the effect of lower vapor permeance and smaller diffusion vents.

Specifically, the ridge detail is highly vapor-open (300+ perms), and is 6-in. wide, comprising roughly 3% of the roof area flat plane (roughly a 1:30 ventilation ratio). This provides disproportionate drying to the assembly compared to typical code ventilation ratios or surface areas. Therefore, the four non-diffusion-vent roofs were retrofitted with a 2-in. wide diffusion vent slot at the ridge; this is roughly a 1:100 ventilation ratio. Two roofs were covered with the same 300+ perm membrane used at the other diffusion vent roofs (Dörken Delta Foxx), per Figure 23 (right). The other two roofs were covered with a less vapor-open membrane that still allows outward drying (DuPont Tyvek Commercial Wrap, 23 perms dry cup, 28 perms wet cup), per Figure 23 (left).
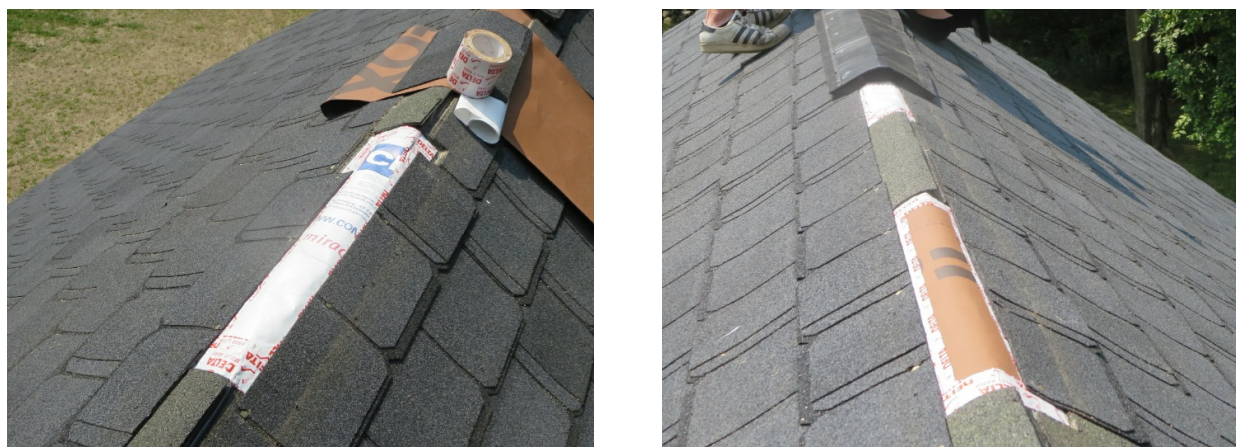
Figure 23. Diffusion vent material installation and ridge cap coverage

Control comparison: The final roof bay is a guard bay, which was instrumented as a code-compliant control comparison (Figure 20). Roof #8 and other guard bays were built as roof assemblies that meet the current code requirements for unvented roofs/conditioned attics (§R806.5 in 2012 IRC; ICC 2012b).

Roof assembly matrix: the resulting roof test assemblies for Winter 1 are shown in Table 1, listing the combinations of insulation, interior vapor control, diffusion vent, and short name. The assemblies for Winter 1, 2, and 3 are shown later in Table 2, Table 3, and Table 4, respectively.

Table 1. Roof Assembly Test Matrix (Winter 1)
Note that FG = fiberglass, VB = vapor barrier; DV = diffusion vent; nDV = no diffusion vent; SVR = smart vapor retarder; cell = cellulose; and ccSPF = closed-cell spray polyurethane foam

Roof #	Insulation	Interior Vapor Barrier	Diffusion Vent	Short Name
1	Fiberglass	Fixed perm (Owens Corning 1 perm)	Yes	FG-VB-DV
2	Fiberglass	Variable perm (MemBrain)	Yes	FG-SVR-DV
3	Fiberglass	Fixed perm (Owens Corning 1 perm)	No	FG-VB-nDV
4	Fiberglass	Variable perm (MemBrain)	No	FG-SVR-nDV
5	Dense pack cellulose	Fixed perm (DuPont 1 perm)	No	Cell-VB-nDV
6	Dense pack cellulose	Variable perm (DuPont Variable)	No	Cell-SVR-nDV
7	Dense pack cellulose	Variable perm (DuPont Variable)	Yes	Cell-SVR-DV
8	ccSPF + cellulose flash-and-blow §R806.5	None	No	ccSPF-Cell

A lateral cross section of the test hut roof is shown in Figure 24 and Figure 25, with the experimental and guard bays called out. The figures also show air/vapor barrier (green) used to hygrothermally isolate experimental bays, the instrumentation wiring penetration at the guard bay (to limit interior air leakage into the test bays), and the relevant interior vapor control layers.
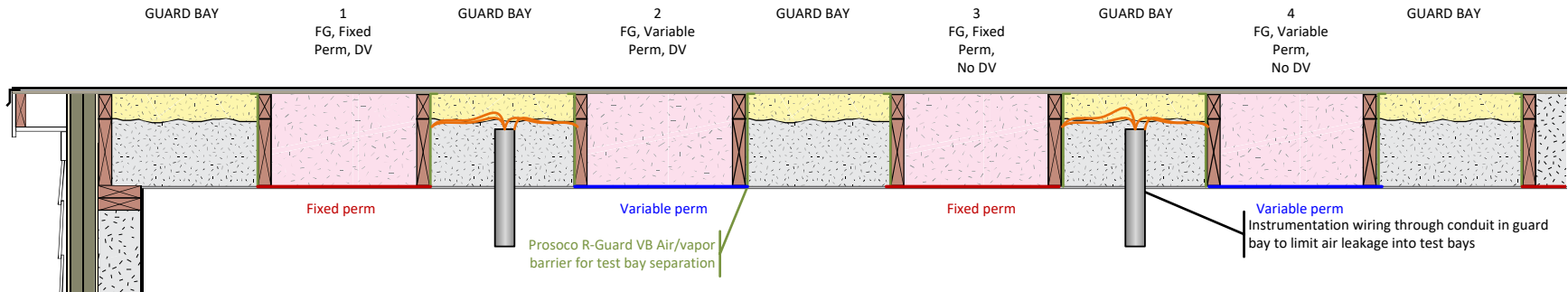
Figure 24. Test hut lateral roof cross section, showing Roofs 1 through 4 (FG = fiberglass; DV = diffusion vent)
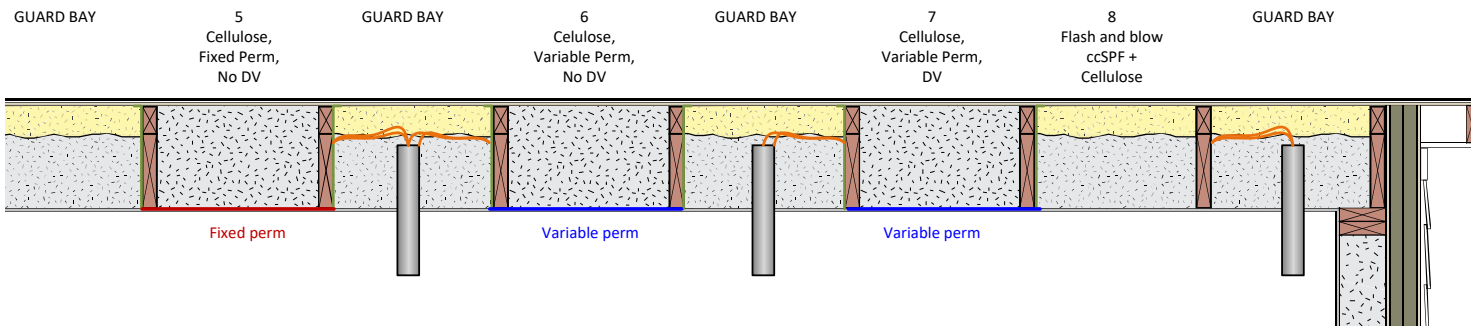
Figure 25. Test hut lateral roof cross section, showing Roofs 5 through 8

3 Test Roof Instrumentation

3.1 Roof Instrumentation: Experimental Roofs

The instrumentation package for all unvented/fibrous insulation experimental bays was identical; an instrumentation schematic is shown in Figure 26. A full description of instrumentation (including error and accuracy) is provided in the Appendices: Section 10.1: Testing and Monitoring Equipment and Section 10.2: Sensor Count Listing.

Typical Unvented Bay
- Asphalt shingles
- Self-adhered membrane
- OSB (5/8" ZIP roof panel)
- Cavity insulation (dense pack cellulose or blown fiberglass)
- Interior vapor control layer (fixed or variable perm membrane)

MC/T Sheathing High

RH/T Sheathing Mid
MC/T Sheathing Mid

RH/T Ridge

Wafer at Ridge

MC/T Sheathing Low

Wafer (South only)
RH/T Mid Interior

Notes
- "MC/T Sheathing High" is at top edge of sheathing at diffusion vent, or equivalent location in non-DV roofs
- Wafer and RH/T at ridge are directly under ridge

Sensor Key:
- ● Relative humidity/temperature
- ■ Moisture content/temperature
- ◥ Moisture content block "wafer"

Figure 26. Unvented test roof instrumentation plan (Roofs 1 through 7)

The groups of sensors are broken down as follows with their associated role/function; sensors are highlighted with Sensor Key symbols, as shown in Figure 26.

At the ridge:

- There is a temperature/RH sensor to measure moisture accumulation (expected worst-case location, per previous work), and a "wafer" sensor (wood moisture RH surrogate sensor; see Ueno and Straube 2008) to provide a backup of the T/RH sensor. The installed instrumentation is shown in Figure 27, showing a non-diffusion-vent roof (left) and a diffusion vent roof (right).
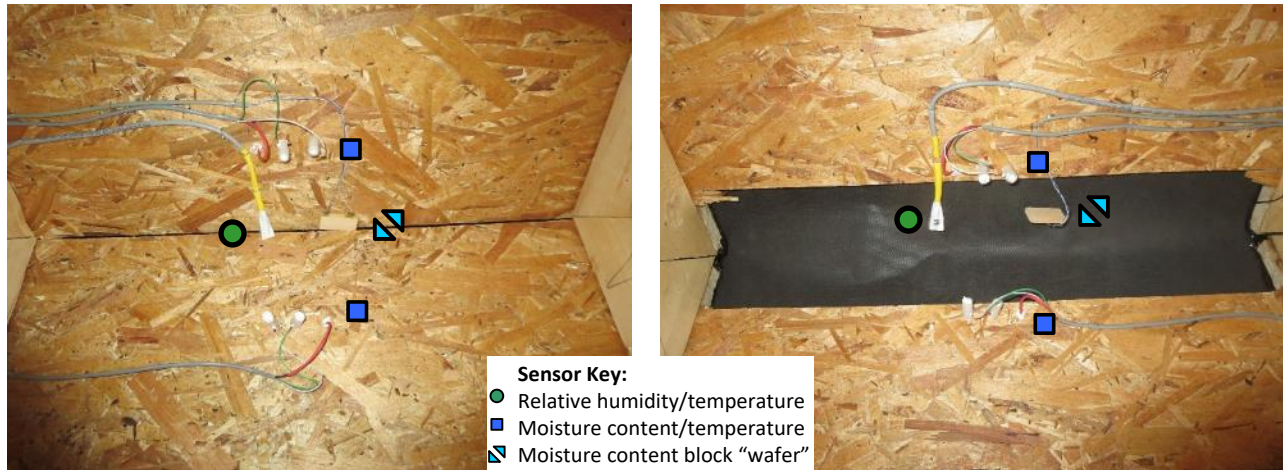
Figure 27. Ridge instrumentation package for non-diffusion-vent (left) and diffusion vent (right) roofs

At the roof sheathing:

- There are MC/Ts low, middle, and high on each orientation (north and south), per Figure 28. The MC pins are protected from short-circuiting issues (common with damp cellulose insulation) by a piece of 3/8-in. O.D./1/4-in. I.D. polyethylene tubing, filled with silicone sealant.

- "MC/T Sheathing High" is at the top edge of sheathing at the diffusion vent, or equivalent location in non-diffusion-vent roofs (Figure 27, left and right).

- There is a T/RH sensor at the middle sheathing-to-insulation interface, mirroring the measurements of the middle-height MC/T sensor (Figure 28, left and right).
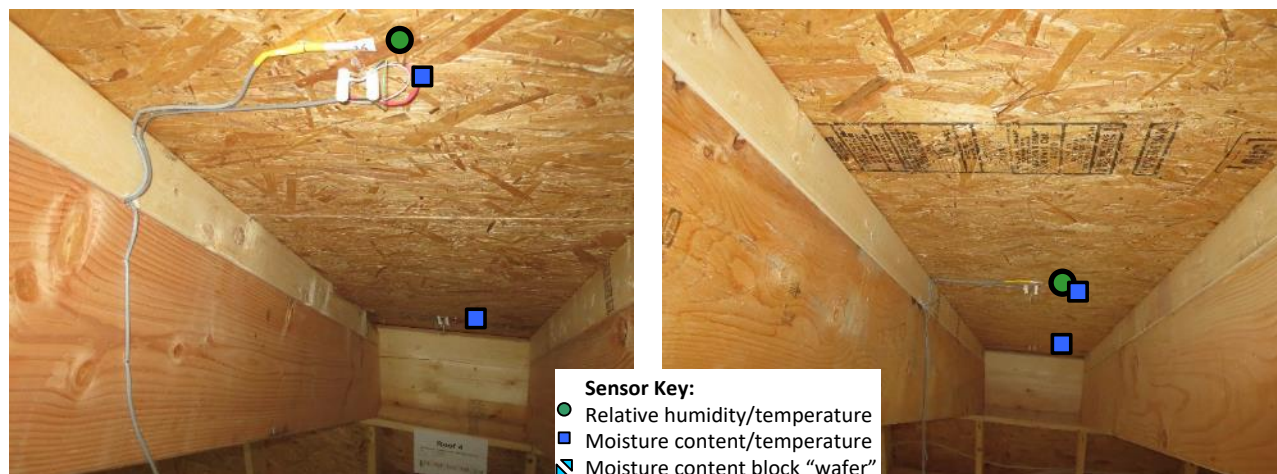
Figure 28. Middle and lower height sheathing MC/T sensors, with surface RH/T

At the roof interior side (between insulation and vapor control membrane):

- There is a T/RH sensor to measure inward vapor drive (thus measuring the difference in interior vapor retarders); this phenomenon is expected during warmer weather.

- It is "mirrored" by a wafer sensor, but only on the south side—inward drive was expected to be lower in magnitude on the north side. This was a compromise due to limitations on available data collection channels.

- Sensors were protected in plastic bags during insulation installation, hanging free of the rafter bay (Figure 29, left); after completion, they were inserted between the vapor control membrane and the fibrous insulation (Figure 29, right).
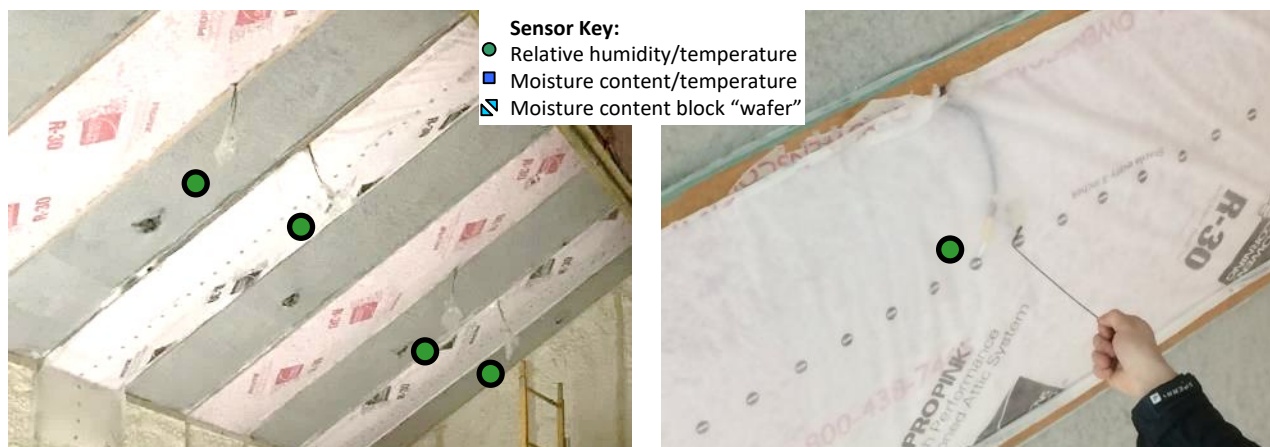
Figure 29. Interior sensors left free of rafter bays (left), insertion of sensor (right)

As shown in the schematic in Figure 24 and Figure 25, sensor wires are run via conduit penetrations into the guard bays. The conduit penetrations are shown in Figure 30 (left); the wires are run down the length of the guard bay and then penetrate laterally into the experimental

bay through a drilled hole in the rafter. The rafter penetration was air sealed with silicone sealant, and then covered with ccSPF from the guard bay side (Figure 30, right).

Figure 30. Conduit penetrations at guard bay (left), sealing of wiring holes with ccSPF (right)

3.2 Roof Instrumentation: Control Comparison Roof

The control comparison flash-and-blow bay has a slightly different instrumentation package, because different phenomena are of interest, as shown in Figure 31.

Control "Flash and Blow" Bay
- Asphalt shingles
- Self-adhered membrane
- OSB (5/8" ZIP roof panel)
- 4" ccSPF insulation
- Dense pack cellulose (±10")
- Interior gypsum board

MC/T Sheathing High
RH/T Ridge
RH/T Sheathing Mid
MC/T Sheathing Mid
RH/T Ridge Interface
Wafer at Interface
MC/T Sheathing Low
Wafer Mid Interface (North only)
RH/T Mid Interface

Notes
- "MC/T Sheathing High" is at top edge of sheathing at diffusion vent, or equivalent location in non-DV roofs
- Wafer and RH/T at ridge are directly under ridge
- "Interface" denotes spray foam-to-fibrous insulation interface

Sensor Key:
- Relative humidity/temperature
- Moisture content/temperature
- Moisture content block "wafer"

Figure 31. Unvented flash-and-blow control roof instrumentation plan (Roof 8)

Differences from the previous experimental bays are highlighted in blue:

At the ridge:

- There is a temperature/RH sensor to measure moisture accumulation; no matching wafer sensor to mirror the T/RH sensor was installed (lower priority given expected moisture-safe performance).

- There is a T/RH sensor and wafer sensor at the ridge interface between the ccSPF and fibrous insulation to measure evidence of condensation at the ridge, where problems are expected (due to moisture concentration), per Figure 32 (left).

Sensor Key:
- Relative humidity/temperature
- Moisture content/temperature
- Moisture content block "wafer"

Figure 32. ccSPF-cellulose interface sensors at ridge (left) and mid-height (right)

At the roof sheathing:

- There are MC/Ts low, middle, and high on each orientation (north and south).

- "MC/T Sheathing High" is at top edge of sheathing at diffusion vent, or equivalent location in non-diffusion-vent roofs.

- There is a T/RH sensor at the middle sheathing-to-insulation interface, mirroring the measurements of the middle MC/T sensor.

At the roof interface between the ccSPF and fibrous insulation:

- There is a T/RH sensor to measure moisture levels at the interface (evidence of condensation), per Figure 32 (right).

- It is mirrored by a wafer sensor, but only on the north side (greatest condensation risks); this is a compromise due to limitations on data collection channels.

3.3   Boundary Condition Measurements

Test hut interior conditions were recorded via four temperature/RH sensors; they were placed in high/low pairs, hanging from two locations along the ridge beam (Figure 33). The heights were set at approximately the 1/3 and 2/3 points of the distance from the floor to the top of the ridge beam (underside of the ceiling).

Figure 33. Interior high/low temperature/RH sensors

Exterior T/RH was recorded via a sensor located in a radiation shield, below the overhang of the north wall (Vaisala HMP60 Temperature and Relative Humidity Probe; Figure 34, right). Insolation (solar radiation) on the north and south roofs was measured with two pyranometers, oriented to match the roof slope (Davis Instruments 6450; Figure 34, left).

Figure 34. Exterior temperature/RH sensor (left), roof solar radiation sensor (right)

All sensors were connected to a central data acquisition system (Campbell Scientific CR1000) located in the test hut (Figure 35). Instrumentation specifications are detailed in Section 10.1: Testing and Monitoring Equipment. Data downloads were via in-person direct connection.

Figure 35. Measurement and control (data acquisition) system

4 Experimental Narrative and Roof Modifications

The data analysis sections of this report are extensive and include many graphs. To provide an initial overview, a narrative of the experiment and results are provided next, which covers the findings in a qualitative manner. The experiment covered three winters and the following spring/summer periods; the experimental program included the following:

- Winter 1 (2016–2017) had normal (uncontrolled) interior RH conditions; measured levels were typically in the 30%–40% RH range.

- Winter 2 (2017–2018) had interior conditions of constant 50% RH to stress the roof assemblies due to the interior moisture load.

- Winter 3 (2018–2019) was also run at 50% RH for the first portion of the winter (through February 2019). This was followed by controlled injection of interior air into the rafter cavities to simulate the effect of inadvertent air leakage.

In addition, the results from Winter 1 and Winter 2 informed iterative modifications to the roofs between winters, as covered in the tables in this section.

4.1 Winter 1: Tested Assemblies and Test Hut Commissioning

Eight experimental unvented roofs were compared in this work; the numbering and characteristics in Winter 1 are shown in Table 2. This includes four netted loose-fill fiberglass roofs (#1–4), three dense-pack cellulose roofs (#5–7), and one code-compliant flash-and-blow control comparison roof (#8).

Table 2. Roof Assembly Test Matrix (Winter 1)

Roof #	Insulation	Interior Vapor Barrier	Diffusion Vent	Short Name
1	Fiberglass	Fixed perm (Owens Corning 1 perm)	Yes	FG-VB-DV
2	Fiberglass	Variable perm (MemBrain)	Yes	FG-SVR-DV
3	Fiberglass	Fixed perm (Owens Corning 1 perm)	No	FG-VB-nDV
4	Fiberglass	Variable perm (MemBrain)	No	FG-SVR-nDV
5	Dense pack cellulose	Fixed perm (DuPont 1 perm)	No	Cell-VB-nDV
6	Dense pack cellulose	Variable perm (DuPont Variable)	No	Cell-SVR-nDV
7	Dense pack cellulose	Variable perm (DuPont Variable)	Yes	Cell-SVR-DV
8	ccSPF + cellulose flash-and-blow §R806.5	None	No	ccSPF-Cell

Roof #8 and other guard bays were built as roof assemblies that meet the current code requirements for unvented roofs/conditioned attics (§R806.5 in 2012 IRC; ICC 2012b).

The roof assemblies were completed, and data collection began in early December 2016. Part of the commissioning process was measurement of test hut airtightness, as covered in Section 11.2: Enclosure Airtightness Measurement. The key finding was that the hut is exceptionally airtight, at 46–50 CFM 50, or 4.2 to 4.8 square in. of equivalent leakage area (EqLA). This is consistent with the construction of the hut, using sheathing with taped joints, spray foam, and other air sealing details (Figure 8 and Figure 9). In addition, the low air leakage was a good indication that inadvertent air leakage through the test assemblies was unlikely.

Air leakage was then examined further using fan depressurization and infrared thermography to localize the leaks, per Section 11.4: Air Leakage Localization. Key findings were that air leakage occurs at the building corner roof-to-wall joints (in guard bays, not test bays) and mechanical penetrations. Infrared examination of the roof showed thermal bridging at the framing, but no interior indication of airflow at the test assemblies.

One issue stemming from the low air leakage of the test hut was that operating the 70 CFM nominal exhaust fan (Figure 14) created significant depressurization, as covered in Section 11.3: Mechanical-Enclosure Interaction. Running the fan resulted in a -22 Pa building depressurization, which can have a significant effect on enclosure monitoring studies. This was confirmed by examining the data: turning the exhaust fan on and off correlated with increases and declines in roof ridge RH. The likely explanation is that during periods when the exhaust fan is on, induced infiltration (small amounts of inward air leakage through the cavity) protects the ridge from interior moisture. Turning off the fan removes this effect, as shown by a sharp rise in ridge RH. After the exhaust fan was turned off, RHs remained high for several weeks (possibly storage of accumulated moisture), but then dropped. After confirming these findings, the exhaust fan was turned off in early March 2017.

During this depressurization testing, the pressure differences across the interior air-vapor control membrane into the roof test bays were measured, per Section 11.5: Roof Bay Pressure Difference Comparison. This pressure difference (ΔP) indicates whether disproportionate air leakage is occurring in one of the test bays. Measurements were taken at the roof-wall connection/eave at the north and south sides and at the ridge. Overall, the results show a small pressure drop across the interior air/vapor control membrane, compared to the total pressure drop (0.3% to 3.5% of total). This indicates that the exterior sheathing is the most airtight layer, which is consistent with its construction (taped sheathing with an integrated water-resistive barrier). Roof 1 (fiberglass, fixed-perm vapor retarder, diffusion vent) showed ΔPs higher than the remaining roof bays, which suggested that there might be an air leakage anomaly in this roof bay.

Roof 1 was therefore disassembled in the spring (March 2017) by opening the ridge diffusion vent from the exterior to search for air leakage anomalies, per Section 11.6: Roof 1 Disassembly

and Retesting. However, no issues were found; further investigation was not pursued, given the extensive demolition required.

4.2 Winter 1: Data Results

Key findings from Winter 1 data analysis include the following. The full set of data graphs are covered in following sections, but are summarized here.

- The non-diffusion-vent ridges accumulate significant moisture over the winter:

  - All the non-diffusion-vent roofs (3, 4, 5, 6) reached 95%+ RH conditions early in the winter, stayed at high RH levels (95%–100%) for most of the winter, and only showed significant drying in April. Wafer sensors (operating in parallel with the ridge RH sensors) showed substantial moisture accumulation in non-diffusion-vent roofs, with sustained MCs over 40%, which indicate liquid water condensation at the ridge. "Upper" position roof sheathing (~3-4 in. from the ridge) MCs peaked in winter at 30%–35% in the fiberglass roofs, and higher in the cellulose roofs. However, the cellulose measurements are likely spurious data, caused by borate salt migration into the wood during liquid water condensation conditions.

  - In contrast, the diffusion vent roof (1, 2, 7) ridge conditions have lower sustained RH levels than non-diffusion-vent roofs, which is consistent with localized drying at the ridge. Brief peaks in the 95% RH range were observed, followed by drying to safer ranges. Wafer MC levels remain well below condensation levels. "Upper" sheathing MCs peaked under 20%.

  - These results are consistent with previous Building America research (Ueno and Lstiburek 2015, 2016a, 2016b), which show that roofs insulated with fibrous insulation concentrate moisture at the ridge or highest point. These roofs are essentially solar-powered machines that redistribute moisture from the lower portions of the roof to the ridge.

  - The disassembled non-diffusion-vent roofs did not show visible mold growth or damage to the sheathing from openings at the ridge exterior. However, signs of moisture issues included corrosion of metal hardware exposed to the rafter cavity, including roofing nails and instrumentation staples. This disassembly work is covered in Section 13: Diffusion Vent Retrofit and Insulation Settling (Prior to Winter 2) and Figure 147.

- The sensors at the exterior sheathing-to-insulation interface (typical condensation plane in winter) at mid-height in the roof also showed moisture accumulation, albeit not as severe.

  - The north-side roof RHs rose to the 95%–100% range in the winter, and remained at this level through roughly April. Some of the roofs had long sustained winter periods

at 100% RH. The associated sheathing MCs peaked at slightly over (fiberglass) or under (cellulose) 20% MC.

o The south-side roof RHs showed diurnal swings due to solar gain; they all remained drier than the north-facing roofs. There are periods with steady conditions/no diurnal swings, which are linked to snow cover on the roof. Peak south sheathing MCs were below 15%.

o In the spring and summer, all roofs dried down to reasonably safe RH and MC levels. Whether this drying is sufficiently fast to avoid mold growth problems was determined by the mold index calculations.

o Winter 1 measurements seemed to indicate that the diffusion vent provides localized drying at the ridge, but only limited (if any) assembly-wide drying. At these mid-height sensor locations, the diffusion vent and non-diffusion-vent roofs were difficult to distinguish.

o Roof sheathing MCs showed the expected spatial pattern, with greater accumulation higher in the roof, and the north side wetter than the south side. In fact, the sheathing MC levels seen at the middle and lower locations are generally below levels that would cause alarm (rare excursions over 20% MC in mid-winter).

- The inward drive measurements at the insulation-vapor retarder interface showed RH and wafer MC spikes corresponding to warmer outdoor conditions, with sustained high moisture levels during the summer.

  o The fiberglass roofs with fixed-perm interior vapor retarders showed extended periods at 100% RH in the summer. In contrast, the variable-perm vapor retarder roofs showed lower maximum values, reflecting the inward drying available with these membranes.

  o However, wafer sensors indicate that condensation is not occurring at the interface. The cellulose roofs have much lower moisture peaks (RH peaks below 90%), due to the greater moisture storage available in cellulose compared to fiberglass.

  o Disassembly of interior vapor retarders revealed that the worst inward drive issues are occurring near the ridge (top 3 ft of the rafter bay), which is consistent with locally accumulated moisture being driven downward by the summertime thermal gradient. Liquid water condensation was observed at the fiberglass bays, and surface wetness at the cellulose bays. This disassembly work is shown in Section 12.3: Inward Vapor Drive Condensation. The inward drive instrumentation does not capture the worst-case conditions.

  o The cellulose roofs showed insignificant inward vapor drive accumulation compared to the fiberglass roofs. This is ascribed to the much higher moisture storage available

in the cellulose insulation: it is an order of magnitude higher on a weight basis, and a factor of 30 greater when density differences are taken into account (see Section 12.4: Fiberglass vs. Cellulose Sorption Isotherms).

- The §R806.5 code-compliant hybrid ccSPF-cellulose roof showed consistently excellent performance, with sheathing RH and MC levels much drier than the fibrous unvented roofs, and no signs of significant moisture accumulation or mold risk at the ccSPF-cellulose interface (the potential condensation plane).

- The roofs with a variable-perm vapor retarder and a diffusion vent (roofs 2 and 7) demonstrated the lowest moisture accumulation out of all the roofs, and no indicators exceeded danger thresholds. In contrast, the remaining fibrous unvented roofs indicated possible moisture risks, including possible condensation at the ridge, high sheathing MCs, and sustained high RH levels.

- Mold index values were calculated based on collected temperature and RH data, consistent with *ASHRAE Standard 160: Addendum e* (ASHRAE 2016) methods. Mold indices were all below 3.0 (the failure criterion); typical areas showing risk had mold indices between 1.0 and 2.0. The mold index calculations showed greater safety at the ridge in the diffusion vent roofs, and at the insulation-vapor retarder interface for variable-perm vapor retarder roofs. Calculations were hampered by periods with missing data.

- Disassembly at the ridge revealed substantial fiberglass and cellulose insulation settling (2 to 8 in., commonly), specifically at the ridge. In addition, the cellulose roofs showed a pattern of settling on the entire north roof slope, likely due to cycling to high humidity levels. In contrast, the south side did not show the same degree of settling, consistent with lower wintertime humidity peaks. This is documented in Section 13: Diffusion Vent Retrofit and Insulation Settling (Prior to Winter 2).

4.3 Winter 2: Tested Assemblies and Modifications

The plan for Winter 2 was to operate at humidified interior conditions (constant 50% RH) to increase risks of moisture failures. 50% RH is a high loading, but quite possible given humidification and/or modern airtight construction. Specifics of the humidification system are covered in Section 12.1: Humidification System Installation.

Given the moisture accumulation measured in the non-diffusion-vent roofs, the team decided to eliminate the poor-performing roofs (3, 4, 5, and 6), replacing them with alternate assemblies. Continued monitoring of high-risk non-recommended assemblies with more challenging interior conditions would be a waste of time and resources.

The existing diffusion vent ridge design provides disproportionately high drying. The ridge detail is highly vapor-open (300+ perms), and is 6-in. wide, comprising roughly 3% of the roof area flat plane (roughly a 1:30 ventilation ratio). Therefore, the non-diffusion-vent roofs were

replaced with assemblies that examined the effect of lower vapor permeance and smaller diffusion vents, as shown in Table 3. The abbreviations shown in the Short Name column in Table 3 are presented in Table 4.

Roofs 3, 4, 5, and 6 received a 2-in. wide diffusion vent slot at the ridge; this is roughly a 1:100 ventilation ratio (compared to the 6-in. wide diffusion vent slot providing a 1:30 ventilation ratio):

- Roofs 4 and 6 were covered with the same 300+ perm membrane used at the other diffusion vent roofs (Dörken Delta Foxx), creating the small diffusion vent (sDV) condition.

- Roofs 3 and 5 were covered with a lower vapor permeance membrane that still allows outward drying (DuPont Tyvek Commercial Wrap; 23 perms dry cup, 28 perms wet cup), creating the tight diffusion vent (tDV) condition.

- To limit experimental variables, Roofs 3 and 5 were retrofitted with a variable perm interior vapor retarder/air barrier membrane, matching adjacent roofs.

Table 3. Roof Assembly Test Matrix (Winter 2), Modifications Redlined

Roof #	Insulation	Interior Vapor Barrier	Diffusion Vent	Short Name
1	Fiberglass	Fixed perm (Owens Corning 1 perm)	6"/~300 perm (Yes)	FG-VB-DV
2	Fiberglass	Variable perm (MemBrain)	6"/~300 perm (Yes)	FG-SVR-DV
3	Fiberglass	Variable perm (MemBrain) ~~Fixed perm (Owens Corning 1 perm)~~	2"/~25 perm ~~No DV~~	FG-SVR-tDV ~~FG VB nDV~~
4	Fiberglass	Variable perm (MemBrain)	2"/~300 perm ~~No DV~~	FG-SVR-sDV ~~FG-SVR-nDV~~
5	Dense pack cellulose	Variable perm (DuPont Variable) ~~Fixed perm (Owens Corning 1 perm)~~	2"/~25 perm ~~No DV~~	Cell-SVR-tDV ~~Cell VB nDV~~
6	Dense pack cellulose	Variable perm (DuPont Variable)	2"/~300 perm ~~No DV~~	Cell-SVR-sDV ~~Cell-SVR-nDV~~
7	Dense pack cellulose	Variable perm (DuPont Variable)	6"/300 perm (Yes)	Cell-SVR-DV
8	ccSPF + cellulose flash-and-blow §R806.5	None	No	ccSPF-Cell

Table 4. Abbreviations for Short Roof Names in Winter 2 Table

Abbreviation	Meaning
SVR	smart vapor retarder (variable perm)
VB	fixed-perm vapor barrier (retarder)
DV	diffusion vent
nDV	no diffusion vent
sDV	small diffusion vent (~300 perm, 2-in. wide)
tDV	tight (lower perm) diffusion vent (~25 perm, 2-in. wide)

During the diffusion vent retrofit process, failed sensors were replaced, including the ridge T/RH sensors at Roofs 4 and 6 and the wafer sensors at Roofs 5 and 6 (borate salt contamination). Sheathing and insulation conditions were examined during this exterior disassembly work. This process is covered in Section 13: Diffusion Vent Retrofit and Insulation Settling (Prior to Winter 2).

Several interior air-vapor barriers failed over the course of Winter 2, and were repaired on a bay-by-bay basis. This is documented in Section 12: Humidification and Vapor Barrier Issues (Prior to Winter 2). That section also covers the replacement of interior air-vapor barriers after Winter 2, and upgrading the perimeter sealing methods in other roof bays.

4.4 Winter 2: Data Results

Key findings from the Winter 2 data analysis are summarized in this section; the full set of data graphs are covered in following sections.

- Winter 2's constant 50% RH created much more challenging conditions for all of the roof assemblies. Many roofs that showed low or limited risks in Winter 1 (30%–40% interior RH) showed much greater moisture accumulation in Winter 2 (50% interior RH)—into high risk levels.

- Roof 3, the tight diffusion vent (~25 perms vs. ~300 perms) fiberglass roof, showed markedly higher moisture accumulation at the ridge than other experimental roofs; it was the high outlier in terms of RH, wafer MC, and sheathing MC. More importantly, the tight diffusion vent roof was consistently the slowest to dry during warmer weather, retaining wet conditions within the assembly. This indicates that a ~25-perm material is insufficient for a ridge diffusion vent material, at least under these experimental conditions.

- Roof 4, the small diffusion vent (2 in. wide) fiberglass roof, showed moisture accumulation and drying between the tight diffusion vent roof (Roof 3) and the full-size diffusion vent (6 in. wide) roofs (Roofs 1 and 2).

- Cellulose roof analysis was hampered by RH sensor failures (two of the three ridge RH sensors failed in Winter 2) and suspected borate contamination of wood materials.

  - The borate contamination resulted in wafer and sheathing MC measurements far higher than reasonable levels. This was ascribed to borate salt migration from the cellulose to the wood products during condensing (liquid water) conditions, which would transport borate salts by capillarity. The MC data indicate the wetting and drying of these cellulose roofs over time, but the absolute measurements are not reliable.

  - The cellulose roofs did not show as clear differentiation between roof assemblies; this might be ascribed to the substantial moisture storage of 14-in. dense-pack cellulose, which would tend to buffer moisture-concentrating events.

- Multiple roof assemblies had sheathing MCs over 25%, with some higher than 30%. Roof sheathing MCs showed expected patterns of greater accumulation at upper portions of the roof and greater accumulation on the north side versus south (due to solar gain). Multiple roofs had insulation-to-sheathing interface RHs that rose to 90%–95%+ RH in the winter and remained there for most of the winter. This included the best-performing experimental fibrous insulation roofs from Winter 1.

- Roof rankings (in terms of wetness/dryness) were not always consistent; a roof showing safe results at one sensor sometimes showed risky behavior in other sensors.

- Inward vapor drives were measured in summer 2018; they were typically less significant than in summer 2017.

  o This is consistent with the change of most of the roofs to variable-permeance ("smart") interior vapor retarders by summer 2018. The fixed-perm (1 perm) vapor retarder roof showed greater accumulation than SVRs.

  o Previous (summer 2017) disassembly work revealed that inward drives can result in condensation on the vapor retarder 2 to 3 ft from the roof ridge (away from the mid-bay measurements), per Section 12.3: Inward Vapor Drive Condensation.

  o Surprisingly, inward drive problems were worse on the north side than the south; this was ascribed to the accumulation of wintertime moisture.

- Mold index values were calculated based on collected temperature and RH data. Mold indices were all below 3.0 (the failure criterion); typical areas showing risk had mold indices well below 2.0. However, these results were hampered by sensor failures in several roofs.

- The §R806.5 code-compliant hybrid ccSPF-cellulose roof (Roof 8) was compared with experimental (all-fibrous insulation) assemblies:

  o Roof 8 consistently showed safe behavior at the sheathing-to-insulation interface compared to the experimental fiberglass and cellulose roofs. Winter 2 conditions, which strongly stressed the performance of the experimental all-fibrous insulation roofs, resulted in safe conditions in the hybrid assembly.

  o One challenge in the hybrid ccSPF-cellulose assembly was moisture accumulation at the ccSPF-to-cellulose interface. Minimal accumulation occurred in Winter 1 (30%–40% RH interior), but substantial accumulation and potential mold risks occurred during Winter 2 (50% RH interior). Note that this assembly has no interior air barrier or Class III (1–10 perm) vapor control, so this interface is exposed to interior vapor flows. This indicates that this assembly is pushing performance limits at this extreme (50% RH interior) loading. However, disassembly of the interface found no adverse effects, such as cellulose "caking," staining, or microbial growth, per Section 14.4: Guard Bay Conditions.

- Disassembly of the roof ridges revealed substantial mold growth, corrosion of metal fasteners, and staining/delamination in multiple roof assemblies. This is documented in Section 14: Disassembly and Ridge Examination (Prior to Winter 3). This occurred despite calculated mold index values below 3.0.

  o In general, some of the worst-performing roofs (based on monitoring) showed the most noticeable damage, such as the tight diffusion vent roofs. Damage was

concentrated at the ridge and on the north-side rafter bay. Roof 1 showed staining consistent with sheathing condensation and water rundown, resulting in a brown stain at the interior vapor control layer.

o The most concentrated damage occurred on the 2x4 rafter extension stacked on top of the main 2x12 rafter. This was ascribed to worst-case conditions (top of rafter bay) and possibly greater vulnerability of the lighter-colored 2x4 lumber to mold growth.

o The cellulose roofs showed some of the worst mold growth, including substantial mold growth on both the framing and north-side sheathing. A possible explanation is the extensive cellulose settling, which created a continuous air channel above the insulation.

o Mold growth typically occurred on one rafter side or another, but not in all cases. Correlation was not tied to a single cardinal orientation, or location of instrumentation wiring penetrations.

o Based on the summer 2018 disassembly, the timing of the damage (Winter 1 vs. Winter 2) cannot be positively determined. But based on limited observations at roof ridge openings in summer 2017, it appears that the most substantial damage occurred in Winter 2, consistent with greater interior moisture loading.

- All three cellulose roofs showed substantial (2 to 2.5 in., typically) settling of the insulation, which created an air gap between the insulation and the roof sheathing, from the eave to the ridge, per Section 14.3: Cellulose Roof Conditions. This created a pathway for airflow and/or rapid air-transported moisture movement. This would tend to accelerate the concentration of moisture to the ridge. The settling was worse on the north side than the south, which is consistent with the greater moisture cycling that occurred on the north side (no wintertime solar gain).

4.5 Winter 3: Recommissioning, Tested Assemblies, and Modifications

Recommissioning work in preparation for Winter 3 included the following:

- While the ridge was disassembled for visual inspection of the sheathing, roof ridge RH and wafer sensors were replaced in all seven experimental roofs, given sensor failures and intermittent data in Winter 2 (see Section 14.1: Disassembly and Sensor Replacement).

- A suspected issue was air and/or water leakage at the diffusion vents; Section 15.1: Air and Water Leakage Testing provides further detail.

o The vapor-open diffusion vent material is listed at <0.69 l/(s·m²) @ 75 Pa, which is higher than air barrier material requirements of 0.02 l/(s·m²) @ 75 Pa. However, the

small area of this diffusion vent would tend to make this air leakage negligible overall. Air leakage was tested directly by depressurizing the hut and searching for airflow at the ridge; none was detected either by hand or a hot-wire anemometer.

- Another possible issue was that the visible bulk water staining was due to precipitation leakage rather than condensation rundown. Therefore, the test hut was depressurized to -75 Pa, and water was sprayed, aiming at the diffusion vent ridge detail, to simulate the effect of wind-driven rain. This test was conducted for 10 minutes of water spraying from each side, with no detectable water leakage visible from the interior.

- Insulation was reinstalled after this testing. This work included installation of dense-pack cellulose in the settled air gap between the insulation and the north-side roof sheathing, and repacking of the fiberglass insulation at the ridge. Further detail is provided in Section 15.2: Roof Reassembly.

- Similar to commissioning at the start of the experiment, air leakage at the hut was tested, localized, and air leakage was compared between roof bays.

  - Overall hut air leakage was comparable to the original commissioning measurements of 39 CFM 50 (2018) versus 50 CFM 50 (2017). The sliding glass door seal had a noticeable effect on overall air leakage. Further detail is provided in Section 15.3: Enclosure Airtightness Measurement.

  - Depressurization and infrared thermography were again used to localize air leakage; they were evident at the roof corners (guard bays) and at the sliding glass door. Further detail is provided in Section 15.4: Air Leakage.

  - The ΔP across the interior air-vapor barrier was measured with the building depressurized. Roof 1 (a previous anomaly) was more in-line with the remaining roofs; again, the majority of the airtightness was at the roof sheathing. Further detail is provided in Section 15.4: Roof Bay Pressure Difference Comparison.

The tight diffusion vent roofs (Roofs 3 and 5) showed limited drying, moisture accumulation, and poor performance in Winter 2. Therefore, as shown in Table 5, these roofs were retrofitted with full-size (~6 in.) ridge vapor diffusion openings. This work is documented in Section 16.1: Diffusion Vent Retrofit (Removal of Tight Diffusion Vents): the existing tight diffusion vent was removed, the opening enlarged by cutting the sheathing, and the new diffusion vent (Dörken Delta Foxx) installed and sealed with tape.

Subtle differences between roof moisture levels were perhaps caused by differences in permeance curves of the interior air-vapor retarders (Figure 21). The suspected behavior in Winter 2 was higher-than-desired vapor permeance in the existing SVR (CertainTeed

MemBrain; ~4 perms at 50% RH). This is covered in more detail in Section 16.2: Interior Vapor Control Effect.

Therefore, as shown in Table 5, Roofs 3 and 5 were also reconfigured by replacing the CertainTeed MemBrain interior vapor retarder with Isover Vario Xtra (tight vapor retarder or tVR). The material was installed in the same manner as existing interior vapor retarders. The multistep air seal included spray adhesive on the rafter surfaces, double-sided tape on the rafters, installation of the vapor retarder, mechanical fasteners (staples), sealing the perimeter with clear housewrap tape, and rolling the seal for positive adhesion. Further information is provided in Section 16.3: Vapor Retarder Reconfiguration.

The resulting roof reconfiguration is shown in Table 5, with Winter 2 to Winter 3 modifications redlined. The abbreviations shown in the Short Name column in Table 5 are presented in Table 6.

In Winter 3, the test hut was operated at humidified interior conditions (constant 50% RH), similar to Winter 2. Then, controlled air leakage was introduced into the rafter bays in late winter (February 2019). The air leakage system was designed to introduce controlled amounts of interior air into the rafter bay cavities (an "interior-to-interior air leak"), thus demonstrating their vulnerability to air barrier imperfections. The system provided 15 liters/minute (l/min), or 0.53 CFM of interior air into each rafter bay, consistent with a small leak in relatively airtight construction. Full background on air leakage into the assembly cavities and construction of the air leakage system is provided in Section 17: Air Injection System (Prior to Winter 3).

Table 5. Roof Assembly Test Matrix (Winter 3), Modifications Redlined

Roof #	Insulation	Interior Vapor Barrier	Diffusion Vent	Short Name
1	Fiberglass	Fixed perm (Owens Corning 1 perm)	6 in./~300 perm (Yes)	FG-VB-DV
2	Fiberglass	Variable perm (MemBrain)	6 in./~300 perm (Yes)	FG-SVR-DV
3	Fiberglass	Tight variable perm (Isover) ~~Variable perm (MemBrain)~~	6 in./~300 perm ~~2 in./~25 perm~~	FG-tVR-DV ~~FG SVR tDV~~
4	Fiberglass	Variable perm (MemBrain)	2 in./~300 perm	FG-SVR-sDV ~~FG-SVR-nDV~~
5	Dense pack cellulose	Tight variable perm (Isover) ~~Variable perm (DuPont Variable)~~	6 in./~300 perm ~~2 in./~25 perm~~	Cell-tVR-DV ~~Cell SVR tDV~~
6	Dense pack cellulose	Variable perm (DuPont Variable)	2 in./~300 perm	Cell-SVR-sDV
7	Dense pack cellulose	Variable perm (DuPont Variable)	6 in./300 perm (Yes)	Cell-SVR-DV
8	ccSPF + cellulose flash-and-blow	None	No	ccSPF-Cell

Table 6. Abbreviations for Short Roof Names in Winter 3 Table

Abbreviation	Meaning
SVR	smart vapor retarder (variable perm)
VB	fixed-perm vapor retarder
tVR	tight vapor retarder (Isover)
DV	diffusion vent
nDV	no diffusion vent
sDV	small diffusion vent (~300 perm, 2 in. wide)
tDV	tight (lower perm) diffusion vent (~25 perm, 2 in. wide)

4.6 Winter 3: Data Results

Key findings from Winter 3 data analysis are summarized here; the full set of data graphs are covered in subsequent sections.

- Winter 2 and Winter 3 were run at identical interior conditions of 50% RH to provide an interior-source moisture load to the assemblies. During the first portion of Winter 3 (prior to late February 2019), the roofs had substantially different moisture behavior (compared to Winter 2), despite identical interior conditions. Roof moisture levels were consistently

lower in Winter 3, including sheathing-insulation interface RHs, wafer MCs, and sheathing MCs.

- Given the identical interior conditions and mostly identical roof assemblies, this change in moisture behavior is likely due to the reinsulation or repacking of the roof assemblies. This reinsulation specifically targeted the voids found at the roof ridges (fiberglass and cellulose) and on the north slope of the cellulose roofs. For reference, all three cellulose roofs showed substantial (2 to 2.5 in., typically) settling of the insulation, which created an air gap between the insulation and the roof sheathing, from the eave to the ridge. Post-Winter 3 density measurements showed that the fiberglass was retrofitted at a higher density near the ridge than the remainder of the roof (see Section 18.2: Density Measurements). Eliminating voids and increasing installed density would tend to suppress convective looping in cavities and inadvertent airflow through and/or around the body of the insulation.

- This finding from early Winter 3 indicates that the unvented fibrous insulation roof assemblies can function with acceptable moisture risks even at high (50%) interior RH levels if insulation is installed in a mostly void-free and high-density manner. However, consistently assuring this level of quality in field installations may be difficult to achieve; this is especially critical given that the roof assembly relies on suppressing airflow to function in a moisture-safe manner. Furthermore, the voids that appeared in the cellulose roof north bays occurred after Winter 1; this was likely settling due to humidity fluctuations. Unfortunately, this means that moisture safety is not assured unless this humidity-based settling phenomenon can be eliminated.

- When air injection was added low on the north-side roofs, sheathing MCs rapidly rose to 30%–40%, which is a risk range for mold growth and decay. These high MCs were seen at the low- and mid-height roof locations on the north side. The air injection system induced a small (~0.5 CFM) leak, which is consistent with a small imperfection in relatively airtight construction. However, disassembly during the following summer (see Section 18.1: Lower North Roof Disassembly) showed no indication of moisture distress at the sheathing, including mold growth, staining, or physical damage. One possible explanation is that this roof OSB formulation uses a significant fraction of methyl diisocyanate (MDI) resin adhesive, which is known to improve moisture resistance and is anecdotally reported to improve mold resistance.

- The seven fibrous insulation test roofs were compared against each other for Winter 3's performance. All had similar construction, including ridge-top diffusion vents (small and normal size), and interior air-vapor control layers (fixed-perm or variable perm). The roofs had generally similar behavior. The roof with fixed-perm vapor control (Roof 1) was a higher moisture outlier in some measurements, but not by a significant degree.

- When fiberglass and cellulose roofs were compared, there was a general trend of the cellulose roofs damping moisture extremes (both wintertime and summertime) due to hygric storage. As discussed previously, cellulose moisture storage is more than an order of magnitude higher than fiberglass at higher RH conditions on a weight basis.

- Inward moisture drive measurements indicated lower risks in Winter 3 than Winter 2. In general, inward vapor drives were found to be a non-issue with any roofs with variable-perm interior air and vapor control layers.

- Mold index values were not calculated for Winter 3's data. Calculations from Winters 1 and 2 showed no periods exceeding the mold growth threshold of 3.0. Given that all roof measurements were consistently drier in Winter 3 compared to Winter 2, safer conditions would result. Of course, one finding after Winter 2 was visible mold growth at the ridge of multiple roofs, despite a safe calculated mold index value.

- The §R806.5 code-compliant hybrid ccSPF-cellulose roof (Roof 8) consistently showed safe behavior compared to the experimental fiberglass and cellulose roofs. There were some measurements indicating a constantly increasing ("ratcheting") ridge RH; however, based on comparisons with other sensors and handheld instruments, this was ascribed to sensor drift.

- One challenge in the hybrid ccSPF-cellulose assembly was moisture accumulation at the ccSPF-to-cellulose interface. Minimal moisture accumulation occurred in Winter 1 (30%–40% interior RH), but substantial accumulation and potential mold risks occurred during Winters 2 and 3 (50% interior RH). Note that this assembly has no interior air barrier or Class III (1–10 perm) vapor control, so this interface is exposed to interior vapor flows. However, disassembly of the interface found no adverse effects, such as cellulose "caking," staining, or microbial growth. This indicates that whatever moisture accumulation occurred at this interface could dry downward in warmer weather without issues.

5 Boundary Conditions Results

5.1 Experimental Timeline

This section presents results from December 2016 through mid-July 2019, covering three winters and most of three summers of data. As a reminder, the interior conditions over the three winters of the project were as follows:

- Winter 1 (2016–2017): Normal interior conditions (30%–40% RH)

- Winter 2 (2017–2018): Elevated interior RH (50% constant)

- Winter 3 (2018–2019): Elevated interior RH (50% constant), with air injection into rafter bays in late winter (February 2019).

5.2 Heating Degree Days/Climate

Monthly heating degree days (HDD) for the nearest weather station (KLWM—Lawrence Municipal Airport) are plotted in Figure 36.
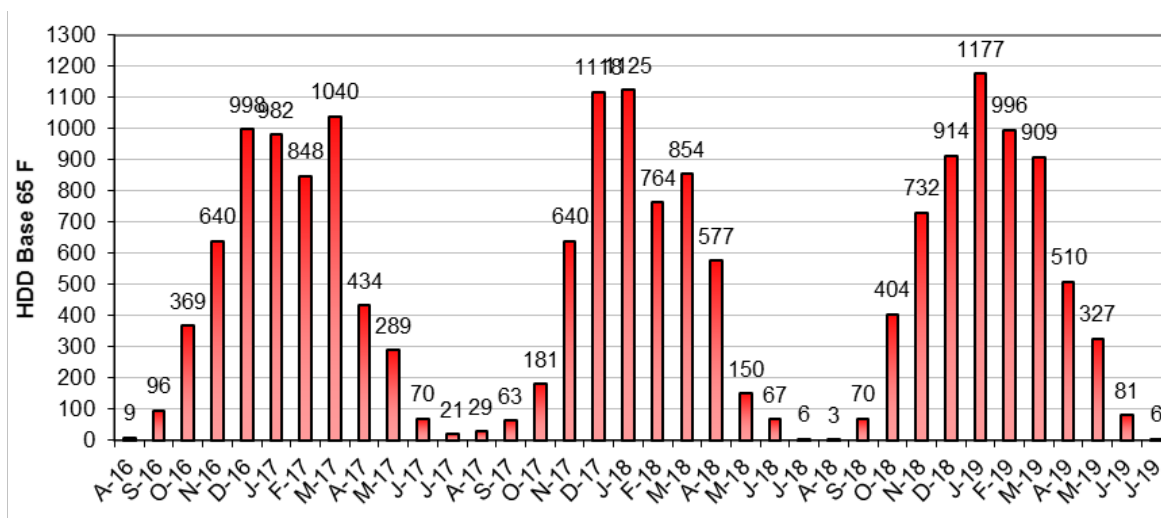
Figure 36. Heating degree days (base 65°F) for KLWM, summer 2016–summer 2019

Comparisons between the climate average and wintertime HDD are shown in Table 7. The HDD totals indicate that winter 2018–2019 was noticeably colder than previous winters.

Table 7. Heating Degree Days (HDD) for Experimental Winters for KLWM

Period	HDD Base 65°F	% of Normal HDD
Climate Average	6,539 HDD	100%
Winter 2016–2017	5,796 HDD	89%
Winter 2017–2018	5,574 HDD	85%
Winter 2018–2019	6,129 HDD	94%

5.3 Temperatures

Exterior and interior temperatures are graphed in Figure 37.

Winter 3 (2018–2019) had higher HDD than previous winters, but Winter 2 (2017–2018) had colder extreme lows (-8°F/-22°C).

Interior conditions were measured at four locations (high and low pairs at east and west sides of the structure). The "lower" of each pair is plotted in blue, and "upper" in red. Interior setpoint was typically 72°–74°F (22°–23°C), with some excursions due to seasonal changeover and controls issues. Interior temperatures showed thermal stratification, with "high" sensors typically slightly warmer than "low" sensors.
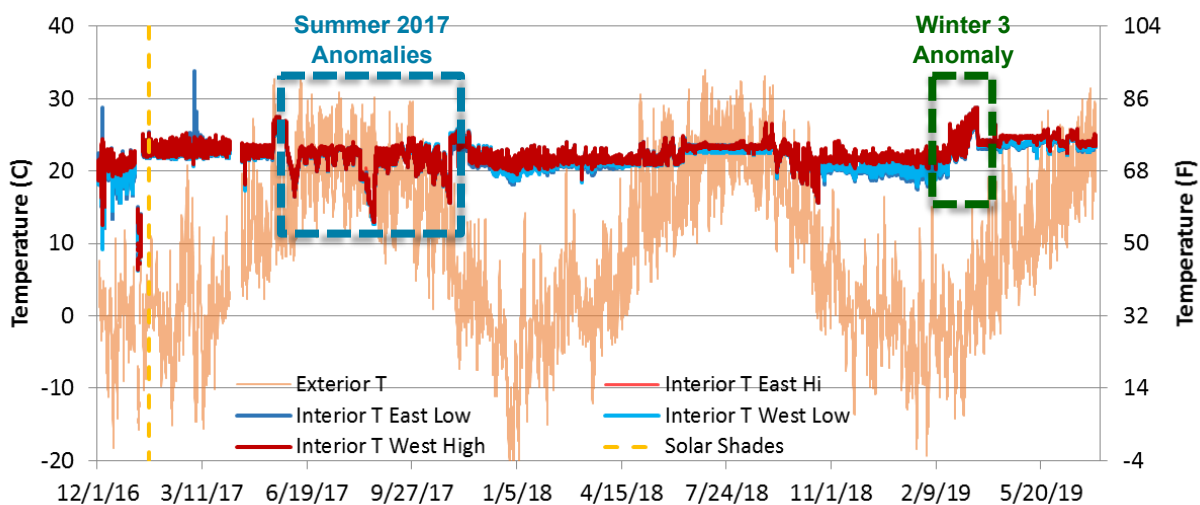
Figure 37. Exterior and interior temperatures (four interior locations)

There was a substantial temperature excursion in Winter 1 (prior to "Solar Shades," **GOLD** line); this was due to a power failure at the test hut, including a loss of space conditioning.

There were several temperature anomalies during summer 2017 (**BLUE**); these were due to controls and setpoint issues.

A temperature anomaly occurred in Winter 3 (late February 2019, **GREEN**), when interior temperatures rose above the setpoint. This was due to heat generated by the air injection system shop vacuum motor; operation was sufficient to increase temperatures in late winter in a small superinsulated building. This problem was addressed by switching space conditioning to heating/cooling auto-changeover mode, resulting in a constant interior temperature. In addition, the air movement created by the air injection system (from fan motor operation and/or rising heated air "plume") was sufficient to break up the vertical stratification seen in the remainder of the temperature data.

5.4 Relative Humidity

Interior RH levels are plotted in Figure 38. Winter 1 had varying interior RH levels due to air change from exhaust fan operation (as noted by orange and green lines; see Section 11.3: Mechanical-Enclosure Interaction). Winter 2 had a rise in RH in spring 2018 (**GREEN**); this was addressed by adding a dehumidifier, bringing interior RH levels down to 50%. Winter 3 ran with relatively stable 50% RH levels; interior conditioning transitioned smoothly from humidification to dehumidification.
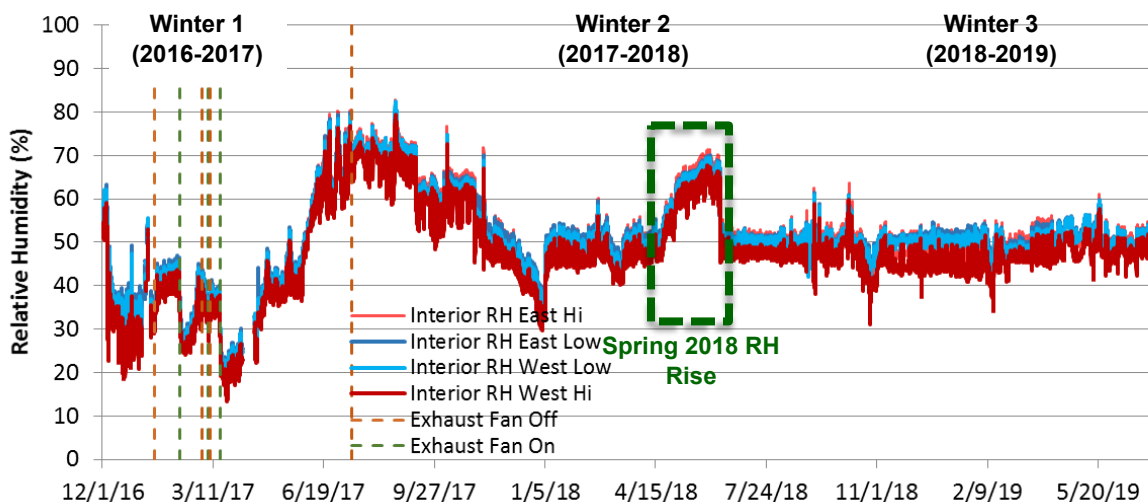
Figure 38. Interior RH measurements (four locations), with exhaust fan operation

5.5 Dewpoint Temperatures

Interior dewpoint temperatures (air absolute moisture content) had a similar plot to interior RH, due to the near-constant interior temperatures. They are plotted with exterior dewpoint in Figure 39, which shows the seasonal rise and fall of exterior dewpoint.

In Winter 3, the temperature anomaly due to air injection system operation (see Figure 37) was mirrored in the dewpoint measurements. Rising interior temperatures and a constant RH setpoint (50%) resulted in a temporary increase in interior dewpoint, until interior temperatures were brought back under control. However, interior dewpoint ran slightly higher after the temperature anomaly due to a higher interior temperature setpoint.
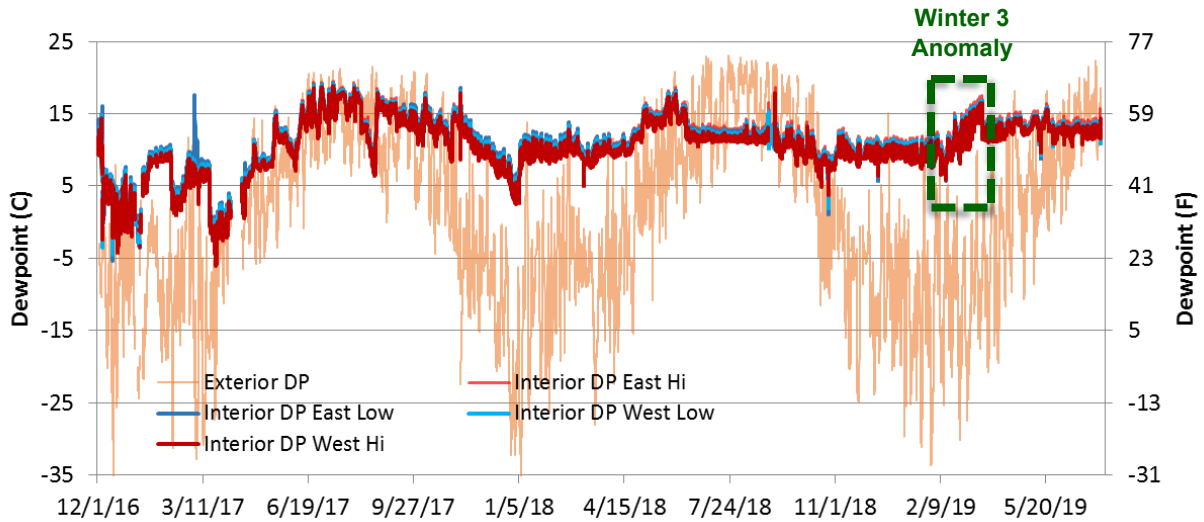
Figure 39. Exterior and interior dewpoint temperatures (four locations)

5.6 Solar Gain (Insolation) Measurements

Insolation/solar gain, as measured on the north and south roof slopes, is plotted in Figure 40 (in W/m^2); insolation was typically cross-referenced with other data to understand observations.

One notable point is that insolation of the north roof is significant with this slope and latitude; peak radiation was more than 500 W/m^2 in the summer.
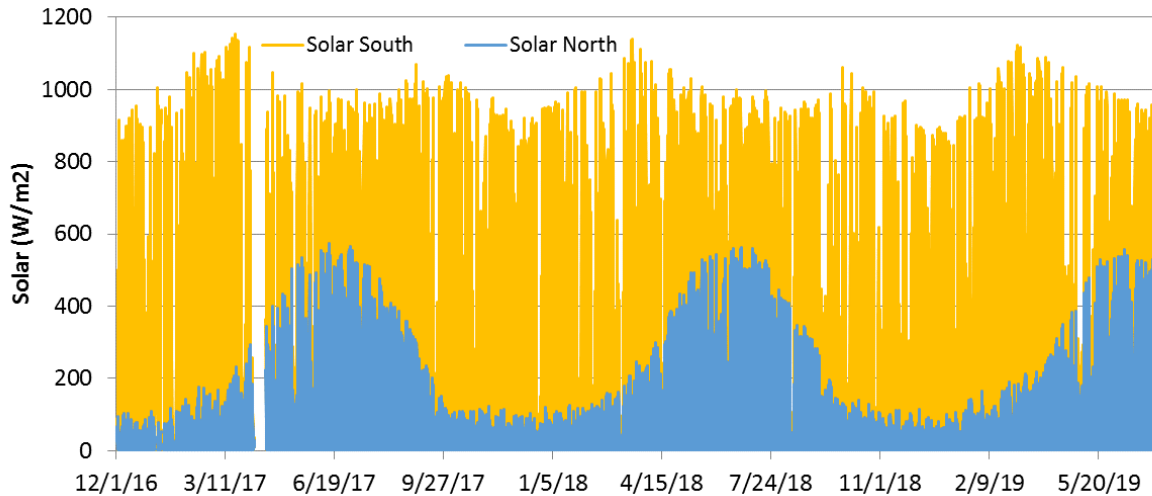
Figure 40. North and south roof insolation/solar gain, in W/m^2

6 Fiberglass Roof Results

6.1 Fiberglass Roof Identification

The color codes and abbreviations shown in Table 8 are used to identify the different roofs in subsequent graphs. The fiberglass roofs (1–4) are shown in shades of tan (Roof 1 and Roof 2, with diffusion vent in Winter 1), pink, and blue (Roof 3 and Roof 4, no diffusion vent in Winter 1). Characteristics that were modified between winters are underlined; note that Roof 1 and Roof 2 (diffusion vents) remained unchanged throughout the experiment.

The abbreviations can be keyed to the information shown in Table 2, Table 3, and Table 5.

Table 8. Fiberglass Experimental Roof Numbering with Short Name and Color Coding Scheme (Winters 1, 2, and 3), Changes Underlined

Roof	Winter 1 Short Name	Winter 2 Short Name	Winter 3 Short Name
1	FG-VB-DV	FG-VB-DV	FG-VB-DV
2	FG-SVR-DV	FG-SVR-DV	FG-SVR-DV
3	FG-VB-nDV	FG-SVR-tDV	FG-tVR-DV
4	FG-SVR-nDV	FG-SVR-sDV	FG-SVR-sDV

6.2 Ridge Relative Humidity Conditions

The ridge has a concentration of sensors because of the likelihood of moisture problems from localized accumulation. The sensors include a temperature/relative humidity (T/RH) sensor and wafer surrogate moisture sensor (Figure 41); the RH data are covered here.

Roof #	Short Name	Winter 3	
1	FG-VB-DV		OC Facer
2	FG-SVR-DV	DV Roofs	Membrain
3	FG-tVR-DV		Isover SVR
4	FG-SVR-sDV	DV-small	Membrain

Sensor Key:
- ● Relative humidity/temperature
- ■ Moisture content/temperature
- ◨ Moisture content block "wafer"
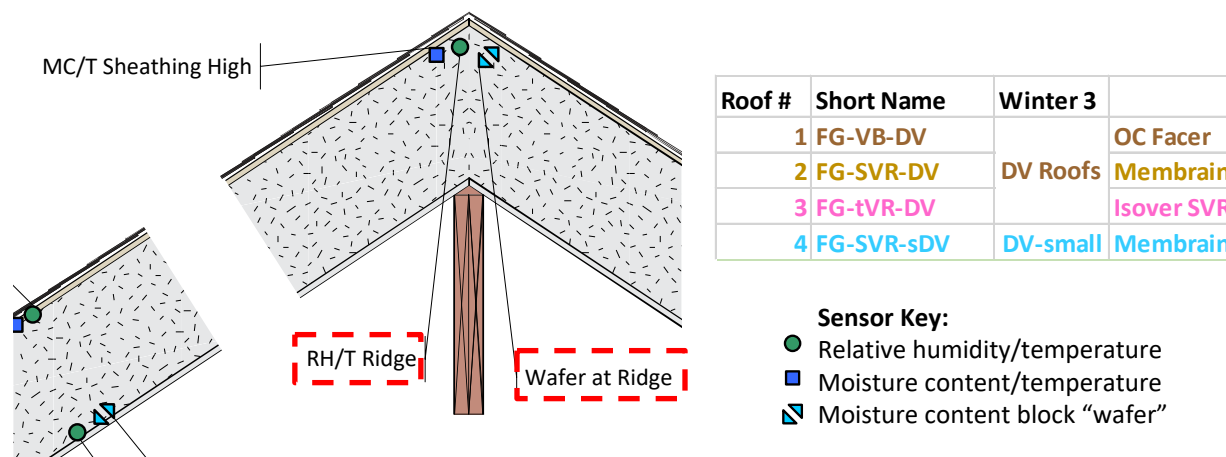
Figure 41. Roof ridge instrumentation, highlighting T/RH and wafer sensors

The raw RH results for the fiberglass roofs are almost unreadable due to diurnal variations (from solar gain). Therefore, ridge RH 24-hour rolling average RH data are shown in Figure 42 for all three winters. These sensors were all replaced between Winter 2 and Winter 3.
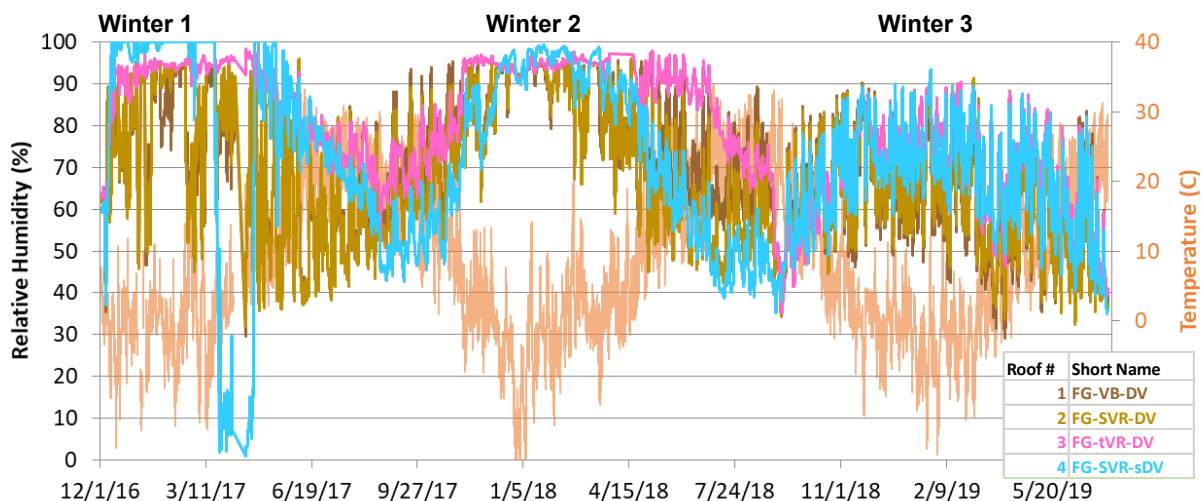
Figure 42. Fiberglass roofs' (1–4) ridge RH conditions, 24-hour moving average

In Winter 1, the non-diffusion-vent roofs (Roof 3 and Roof 4) reached 95%+ RH conditions early in the winter, stayed at high RH levels (95%–100%) for most of the winter, and only showed significant drying in April. In contrast, the diffusion vent roofs' (Roof 1 and Roof 2) ridge conditions oscillated between 95% and much lower RHs. This results in lower sustained RH levels than non-diffusion-vent roofs, which is consistent with localized drying at the ridge.

Winter 2 had long extended periods at high humidity at the ridge in all four roofs: levels rose to ~95% in early winter, and remained there into spring. This shows the more challenging effect of 50% interior RH on these assemblies. Note that Roof 1 and Roof 2 are unchanged from Winter 1, but show markedly worse behavior in Winter 2. Lastly, the tight diffusion vent roof (Roof 3) is an outlier, being the slowest to dry in the spring. This indicates that a ~25-perm material is insufficient for a ridge diffusion vent material, at least under these experimental conditions.

In contrast, in Winter 3, ridge RH levels were much lower than in Winter 2, despite identical interior conditions and similar outdoor temperatures. As discussed previously, a likely reason is that repacking the roof bays with insulation resulted in greater densities, elimination of voids, and therefore less convective airflow within the rafter bay. The settling and insulation retrofit are covered in Section 13: Diffusion Vent Retrofit and Insulation Settling (Prior to Winter 2) and Section 15.2: Roof Reassembly.

A detail of Winter 3 is shown in Figure 43: Roof 3 (tight vapor retarder, full-size diffusion vent) and Roof 4 (small diffusion vent) appear to remain wetter than Roofs 1 and 2. However, performance is relatively close between all four roofs. The addition of air leakage in late February 2019 is not discernable in the ridge data.
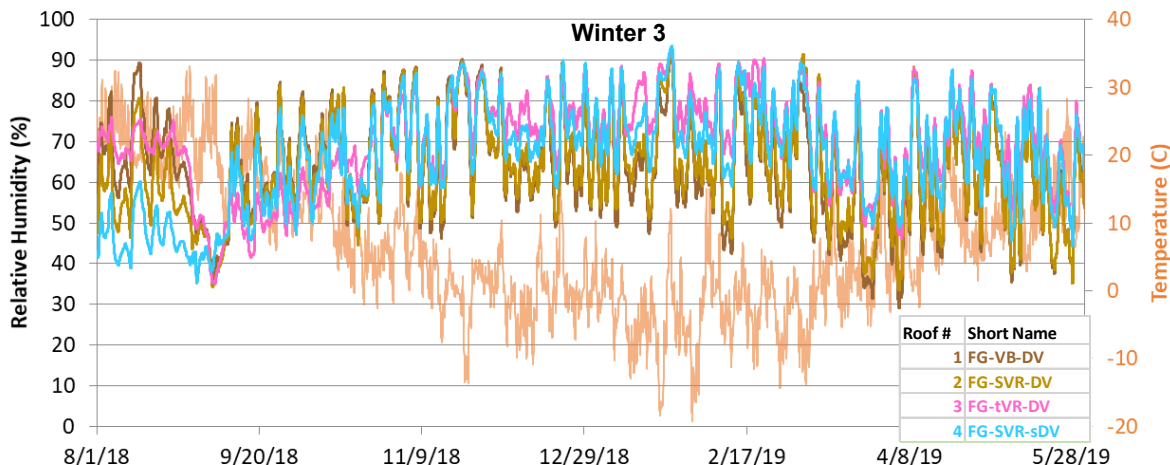
Figure 43. Fiberglass roofs' (1–4) ridge RH conditions, 24-hour moving average, Winter 3 detail

These data can also be shown as box-whisker plots, which show the overall range and distribution of measured data. The plots show median (center of box), lower and upper quartile (extent of box), and maximum/minimum (lines extending from box) data. They are plotted below with Winter 1 at left and Winter 2 at right; winter was defined as December, January, and February. The Winter 1 and 2 roof identities are also shown in a key, given that they change between winters.

The ridge RH plots are shown in Figure 44: in Winter 1, they demonstrate the greater drying (range of RHs) for Roof 1 and Roof 2 (full-size diffusion vent) compared to Roof 3 and Roof 4 (no diffusion vent). Note that Roof 4 (no diffusion vent) had sensor anomalies resulting in the range of outlier data points in Winter 1 (see Figure 42). In Winter 2, however, interior humidification pushes all roofs into the 90%–95% RH range. Roof 3 had an RH sensor failure, but it occurred after the December–February window (late March 2018).
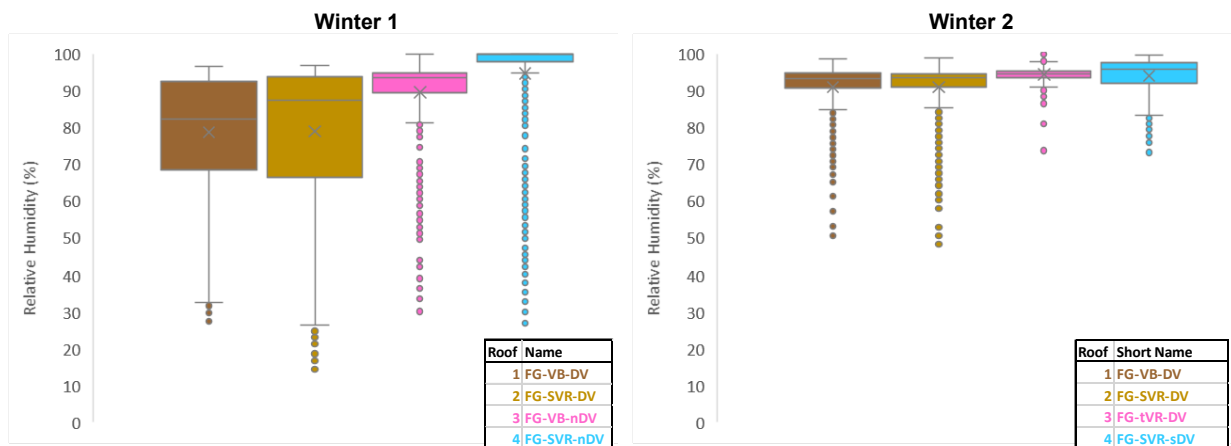
Figure 44. Fiberglass roofs' (1–4) ridge RH box-whisker plots, Winter 1 vs. Winter 2

6.3 Ridge Wafer Conditions

The ridge conditions were also measured with a wafer (wood surrogate moisture) sensor (Figure 41), which provides an indication of moisture accumulation over time. The results are shown in Figure 45.

Wafer measurements are not equivalent to sheathing MC measurements; the wafers are small sensors with a corresponding small amount of storage. The wafer sensors will typically have higher MCs than sheathing measurements at the same interface.
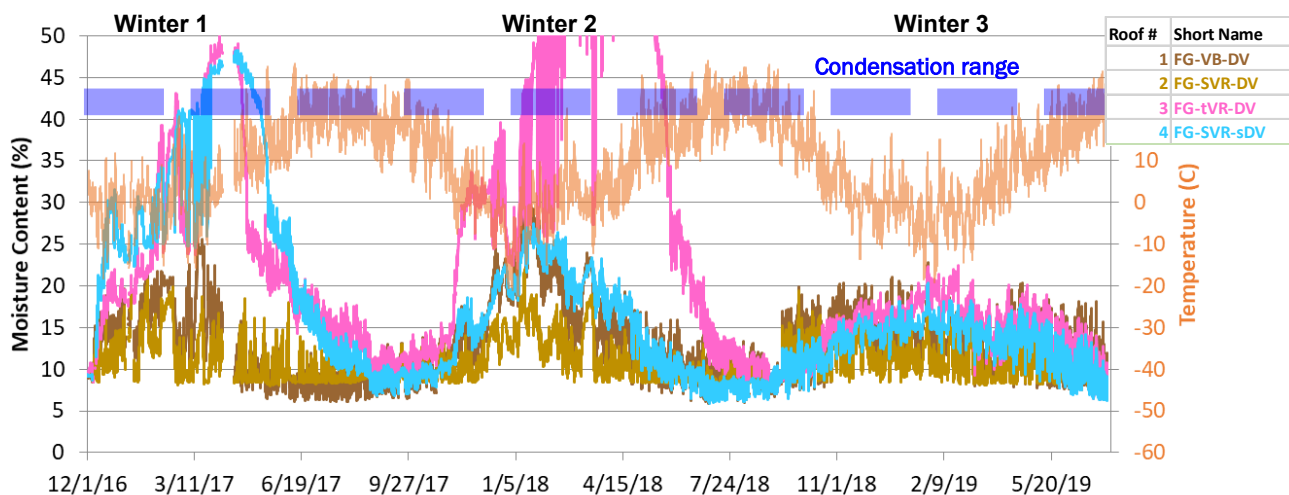
Figure 45. Fiberglass roofs' (1–4) ridge wafer MC measurements

In Winter 1, Roof 3 and Roof 4 (no diffusion vent) have MC peaks of 45%–50%, while Roof 1 and Roof 2 (diffusion vent) have peaks under 25%. These measurements can be compared with previous calibration of the wafer sensor (Ueno and Straube 2008). In that work, the wafer sensors came to equilibrium with 100% RH conditions (air in closed container over water) at 28%–30% MC. However, immersing the sensors in liquid water increased their MC to the 40%–

45% range ("Condensation range" is the dotted blue/purple line in Figure 45). Therefore, 40%–45% wafer MCs indicate possible liquid water condensation.

The wafer measurements therefore indicate that Roof 3 and Roof 4 (no diffusion vent) ridges are at 100% RH conditions for much of the winter, and with possible condensation in February–May 2017. In comparison, Roof 1 and Roof 2 (diffusion vent) are below 100% RH, with no condensation.

In Winter 2 ridge RH measurements, Roof 3 (tight diffusion vent) shows much greater accumulation than Roof 1, Roof 2, and Roof 4 (diffusion vent/small diffusion vent). Roof 3 has peaks over 50% MC, indicating liquid water condensation. This indicates that the ~25-perm diffusion vent material provides insufficient drying. In contrast, the other roofs did not show indications of condensation in this measurement (peak wafer values of 20%–30% MC), but did indicate extended high humidities (95%–100% RH-equivalent).

Roof 3 (tight diffusion vent) remained at high moisture levels through much of the spring, taking the longest to dry, reflecting its greater wintertime accumulation and poor drying. In comparison, the other roofs had lower peak MCs and dried more rapidly.

All wafer sensors were replaced between Winters 2 and 3. In Winter 3, wafer data showed much lower moisture levels, with rare excursions over 20%—essentially, safe behavior. The contrast between Winters 2 and 3 is notable given identical interior conditions (50% RH) and three unchanged roof assemblies (Roof 1, Roof 2, and Roof 4; diffusion vent/small diffusion vent). This is an indication of the positive effect of repacking the fiberglass insulation at the ridge; further detail is provided in Section 15.2: Roof Reassembly.

Similar to previous winters, conditions at the ridge dry to very safe levels during the summer.

Box and whisker wafer plots contrasting Winters 1 and 2 are shown in Figure 46. They demonstrate the greater drying of Roof 1 and Roof 2 (full-size diffusion vent) in Winter 1, compared to Roof 3 and Roof 4 (no diffusion vent). In Winter 2, they show that Roof 3 (tight diffusion vent) is the high outlier with poor performance.
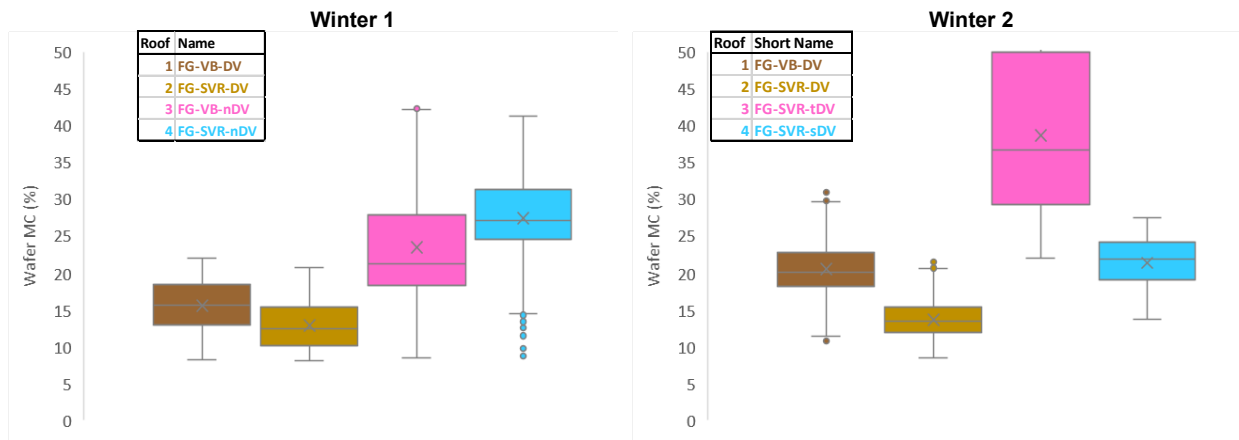
Figure 46. Fiberglass roofs' (1–4) ridge wafer MC box-whisker plots, Winter 1 vs. Winter 2

Note that these box-whisker plots only cover the three winter months; they only capture wintertime wetting of the assemblies, not spring drying. As discussed below, drying during warmer weather may be critical to avoid mold growth, when temperatures are more amenable to biological activity.

6.4 Mid-Bay Relative Humidity Conditions

RH sensors are placed mid-height in the rafter bay at the interface between the insulation and the exterior sheathing (Figure 47) on both the north and south orientations. This is intended to capture condensation or high RH levels at the cold (in winter) interface.
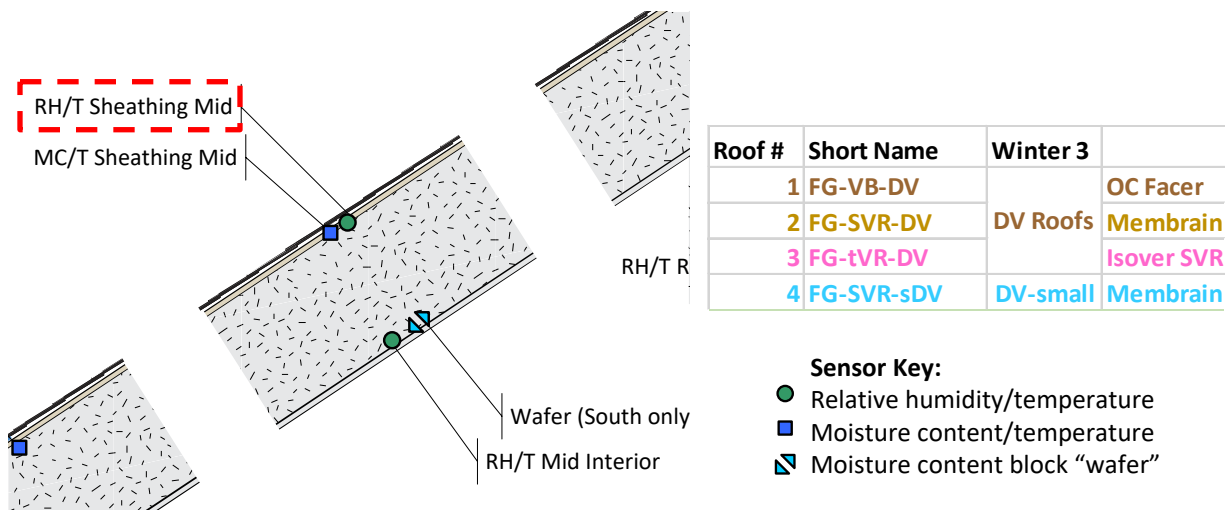
Figure 47. Roof mid-bay instrumentation, highlighting outboard T/RH sensor

Results for the fiberglass bays' north-side RHs are shown in Figure 48:
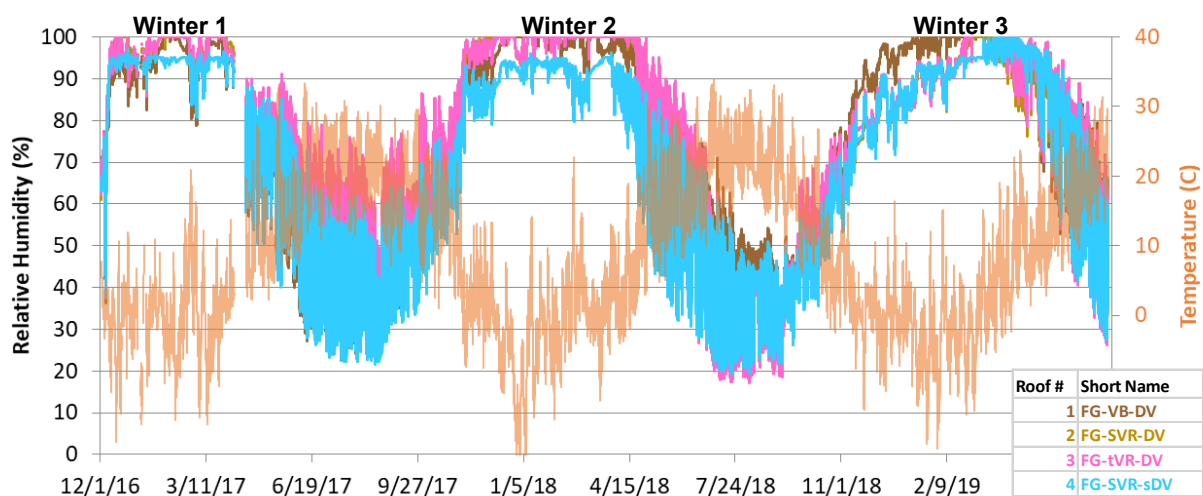
Figure 48. Fiberglass roofs' (1–4) mid-bay RH north conditions

During Winter 1, all four roofs rose uniformly rose to ~90%–100% RH and remained there for most of the winter. There was a brief dip to the 80%–90% RH range during unseasonably warm February 2017 temperatures. By April 2017 (after missing data), dropping RHs indicated drying of the insulation-sheathing interface. RHs also begin to show a strong diurnal swing pattern; this is due to greater diurnal temperature cycling caused by solar gain to the north-side roof (see Figure 40).

Roof 4 (no diffusion vent) is a low outlier; based on multiple winters of measurements, it appears that this may be a sensor issue. For instance, the sensor might have shifted inward into the rafter bay, rather than staying at the sheathing-insulation interface. Also, for reference, the stated accuracy of the sensor is ±3.5% RH.

In Winter 2, all roofs also rose to 90%–100% RH for the entire winter, remained at that level into spring, and eventually fell in late April as the temperature gradient shifted inward. Roof 4 (small diffusion vent) consistently shows drier conditions than the remaining roofs; this is ascribed to a sensor anomaly. Roof 3 (tight diffusion vent) has the highest mid-height north RH levels, providing evidence that the ~25-perm diffusion vent inhibits drying for the remainder of the assembly, not just the ridge. In other words, it indicates that the diffusion vent provides more than localized ridge drying, and instead dries the entire rafter bay (given sufficient moisture accumulation).

In Winter 3, north-side interface RH levels took longer to rise to the 95%–100% range than in Winter 2, despite identical interior conditions. This measurement is consistent with the previous theory of higher insulation density reducing airflow and moisture movement.

The north-side mid-height insulation-to-sheathing RH box-whisker plots are shown in Figure 49 (Winter 1 vs. Winter 2) and Figure 50 (Winter 2 vs. Winter 3). Figure 49 shows the severity of Winter 2's humidified load, pushing interface RHs near 100% for much of the winter, with no low-RH outliers. As discussed earlier, Roof 4's drier performance appears to be a sensor anomaly rather than an actual performance difference.
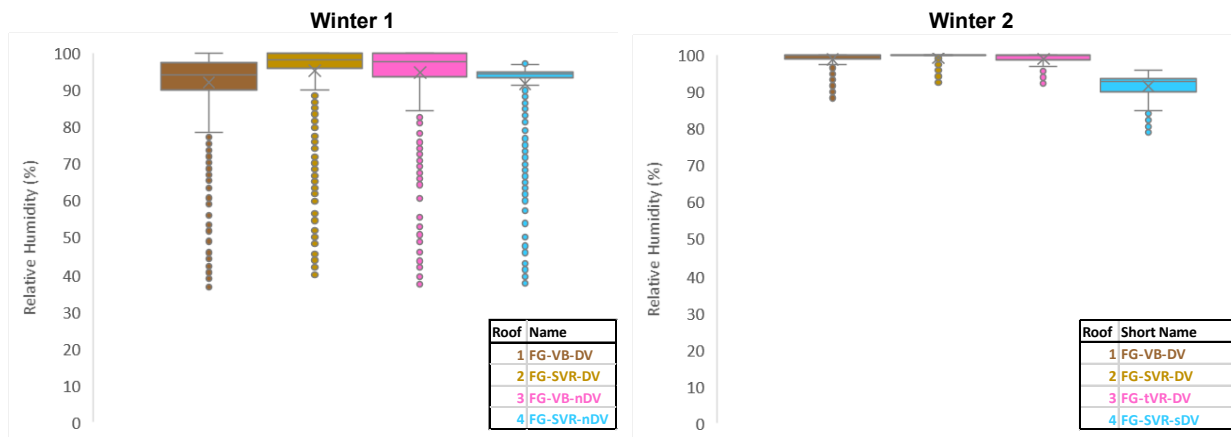
Figure 49. Fiberglass roofs' (1–4) mid-height north RH box-whisker plots, Winter 1 vs. Winter 2

Figure 50 (Winter 2 vs. Winter 3) demonstrates that Winter 3 had much drier (lower RH) conditions than Winter 2 (despite identical interior conditions), and the fact that Roof 1 (fixed-perm vapor barrier, diffusion vent) was a wetter outlier in Winter 3.
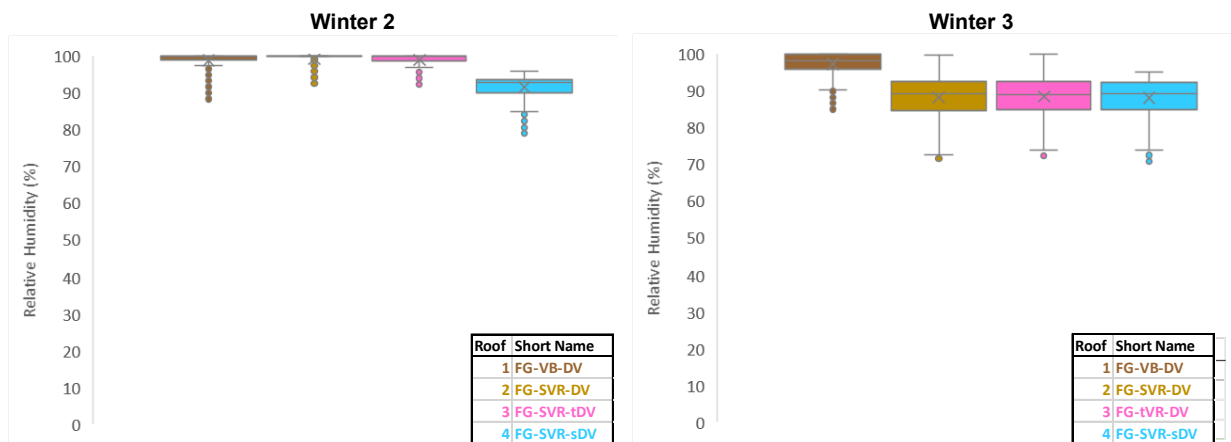
Figure 50. Fiberglass roofs' (1–4) mid-height north RH box-whisker plots, Winter 2 vs. Winter 3

A closer examination of Winter 3 (January–March 2019) conditions is shown in Figure 51: Roof 1 (fixed-perm vapor barrier/DV) is the high outlier. However, almost all roofs converge on 100% RH in late February; this is roughly consistent with the addition of air injection into the north-facing roof and/or the associated slight increase in interior dewpoint. One exception is Roof 4, which remains slightly drier (again, a possible sensor issue).
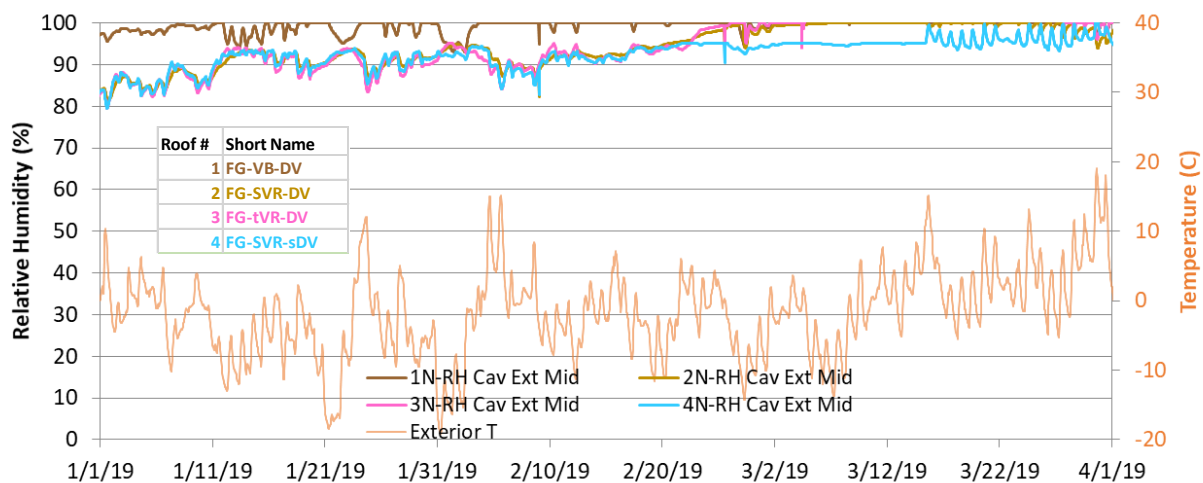
Figure 51. Fiberglass roofs' (1–4) mid-bay RH north conditions, Winter 3 detail

The north fiberglass roof data can be contrasted with the south data; the raw data are practically unreadable due to diurnal variations from solar heating of the roof bay. Therefore, 24-hour moving average RH data are plotted (Figure 52).
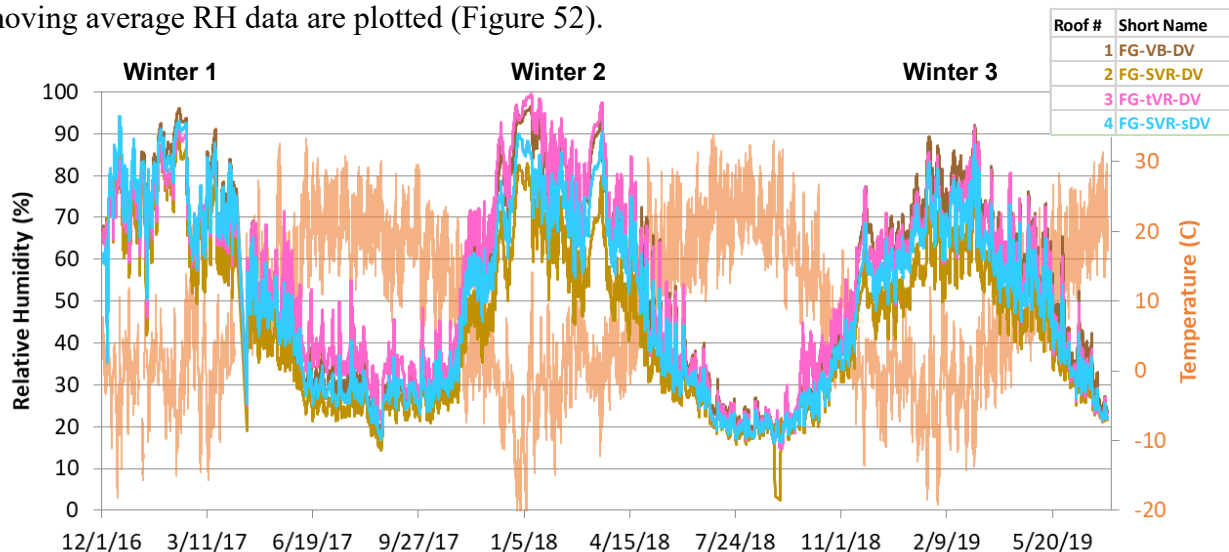
Figure 52. Fiberglass roofs' (1–4) mid-bay RH south conditions, 24-hour moving average

Of course, RH levels on the south side are consistently lower than the corresponding north measurements, due to warmer wintertime temperatures from solar gain. Peak values are lower than the 95%–100% RH levels seen on the north side.

A comparison between Winter 1 and Winter 2 shows markedly higher RHs due to the interior humidification load in Winter 2. Most roofs had extended periods above 90% RH in Winter 2, compared to brief excursions in Winter 1.

Similar to previous measurements, all roofs are much drier in Winter 3 compared to Winter 2, despite identical interior conditions. This is again ascribed to the improvement in insulation density suppressing convective airflow.

One point of interest is shown in the following excerpt from Winters 1 and 2, which plots the raw south fiberglass roof RH data (Figure 53). Sheathing-insulation RHs vary strongly on a diurnal cycle due to solar heating of the roof bay for most of the data. Winter periods lacking diurnal swings are due to snow cover (**BLUE** highlights in Figure 53). The temperatures during these snow periods show roof sheathing temperatures "locked" at 32°F or lower, consistent with expected snow behavior.
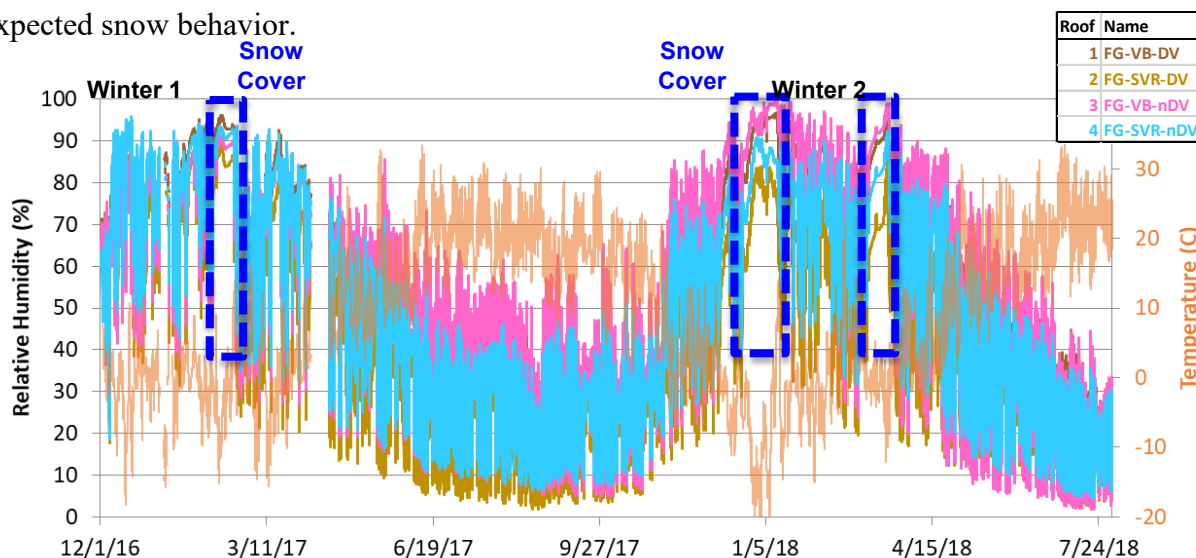
Figure 53. Fiberglass roofs' (1–4) mid-bay RH south conditions, Winter 1 and 2 excerpt

The south-side mid-height insulation-to-sheathing RH box-whisker plots are shown in Figure 54 (Winter 1 vs. Winter 2) and Figure 55 (Winter 2 vs. Winter 3). Figure 54 shows the higher RHs associated with Winter 2 humidification, and Figure 55 shows lower RHs associated with repacking the roofs.
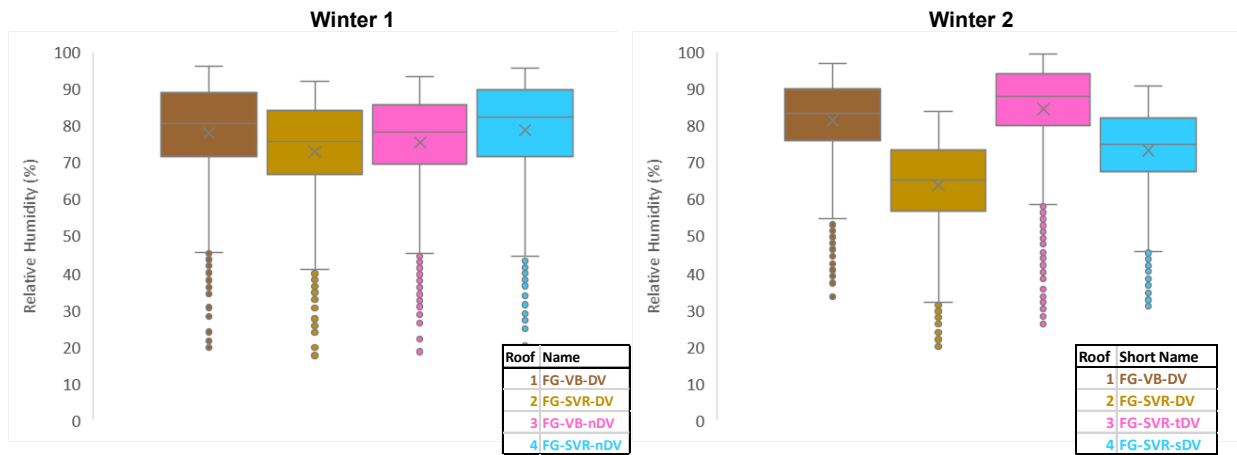
Figure 54. Fiberglass roofs' (1–4) mid-height south RH box-whisker plots, Winter 1 vs. Winter 2

Winter 2 and 3 plots (Figure 55) also show a pattern between roofs year-to-year; however, this type of consistent pattern was not seen across other sensors.
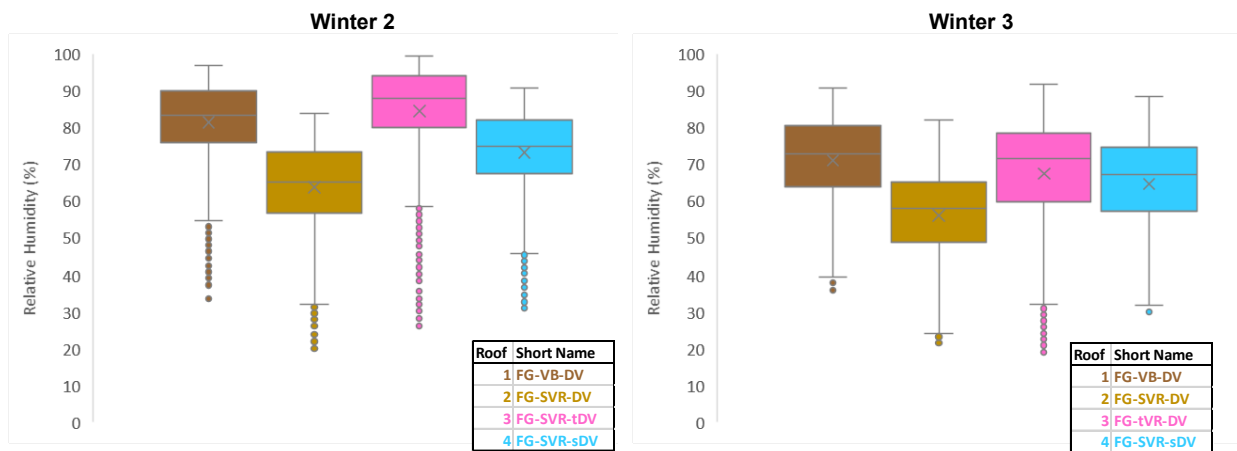
Figure 55. Fiberglass roofs' (1–4) mid-height south RH box-whisker plots, Winter 2 vs. Winter 3

6.5 Sheathing Moisture Contents

When framed assemblies fail due to wintertime moisture accumulation, the structural sheathing typically shows the greatest damage, as it is the cold condensing surface. Wood MCs were measured on north and south, low, mid, and high (Figure 56).
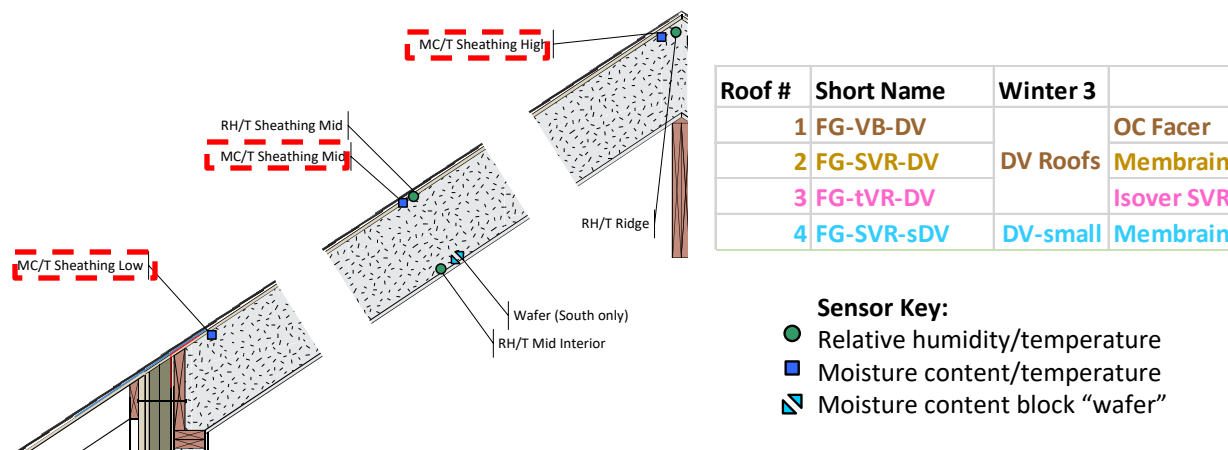
Figure 56. Roof sheathing MC measurements, highlighted

Moisture-related failures of building enclosures are typically defined by risks of mold growth or growth of decay fungi on vulnerable substrates. Traditional guidance is to keep wood MC below 20%; decay fungi are inhibited below this level (Carll and Highley 1999), with optimum growth occurring above the 25%–30% MC range. Decay fungi become active at MC levels above 28% (Straube and Burnett 2005).

Previous unvented roof monitoring in Chicago, Houston, and Orlando (Ueno and Lstiburek 2015, 2016a, 2016b) demonstrated that sheathing moisture accumulation typically increases from low to high, and is greater on the north side than the south side.

The sheathing MCs for the fiberglass roofs are shown for the north side (Figure 57) and the south side (Figure 58), ordered from high to low. The expected pattern is seen throughout all winters, with greater accumulation higher in the roof, and greater accumulation in north roofs vs. south roofs.

In Winter 1, on the north side (Figure 57), upper sheathing MCs in the diffusion vent roofs (Roof 1 and Roof 2) reach the 15%–20% range in mid-winter, but the non-diffusion-vent roofs (Roof 3 and Roof 4) have much higher peak MCs of 25%–35%, which is in the risk range for moisture-related damage. However, the middle and lower sheathing MCs are lower, with wintertime peaks slightly above 20% and 15% respectively, which is a safer range.

The uppermost MCs show a pattern indicating drying from the diffusion vent, but patterns are not as clear the mid- and lower-height locations.

Operation of the humidification equipment in Winter 2 is shown by the dotted **BLUE** line, which resulted in a sharp increase in roof MCs. All roofs showed concerning MCs near the ridge, and Roof 3 (tight diffusion vent) showed the worst performance by a large margin. In addition to high wintertime peaks, Roof 3 also took the longest to dry in the spring.

In Winter 3, before air injection (to the left of the **GREEN** vertical dotted line in Figure 57), all roof MCs were much lower than Winter 2, despite identical interior conditions. This is consistent

with repacking of insulation suppressing airflow and associated moisture deposition into the roofs. The rate of moisture uptake in the roof sheathing was much lower in Winter 3 compared to Winter 2.

Then, after activation of the air injection system (late February 2019, to the right of the **GREEN** vertical dotted line in Figure 57), there was a sharp rise in sheathing MCs, especially at the low location (directly above the air injection port). Sheathing MCs rose to the 30%–40% MC range at the low location, and similar levels at the mid-height location. However, no discernable rise occurred at the high (near-ridge) location.

Air injection was ended in mid-April 2019; sheathing MCs then declined, falling to safe levels by the summer. The wettest was Roof 1 (fixed-perm vapor retarder), but not by a significant margin; this is consistent with inhibited inward drying.

Overall, the Winter 3 north-side MC measurements indicate that a small (~0.5 CFM) air leak can result in significant wetting of the roof sheathing in these unvented roof assemblies.
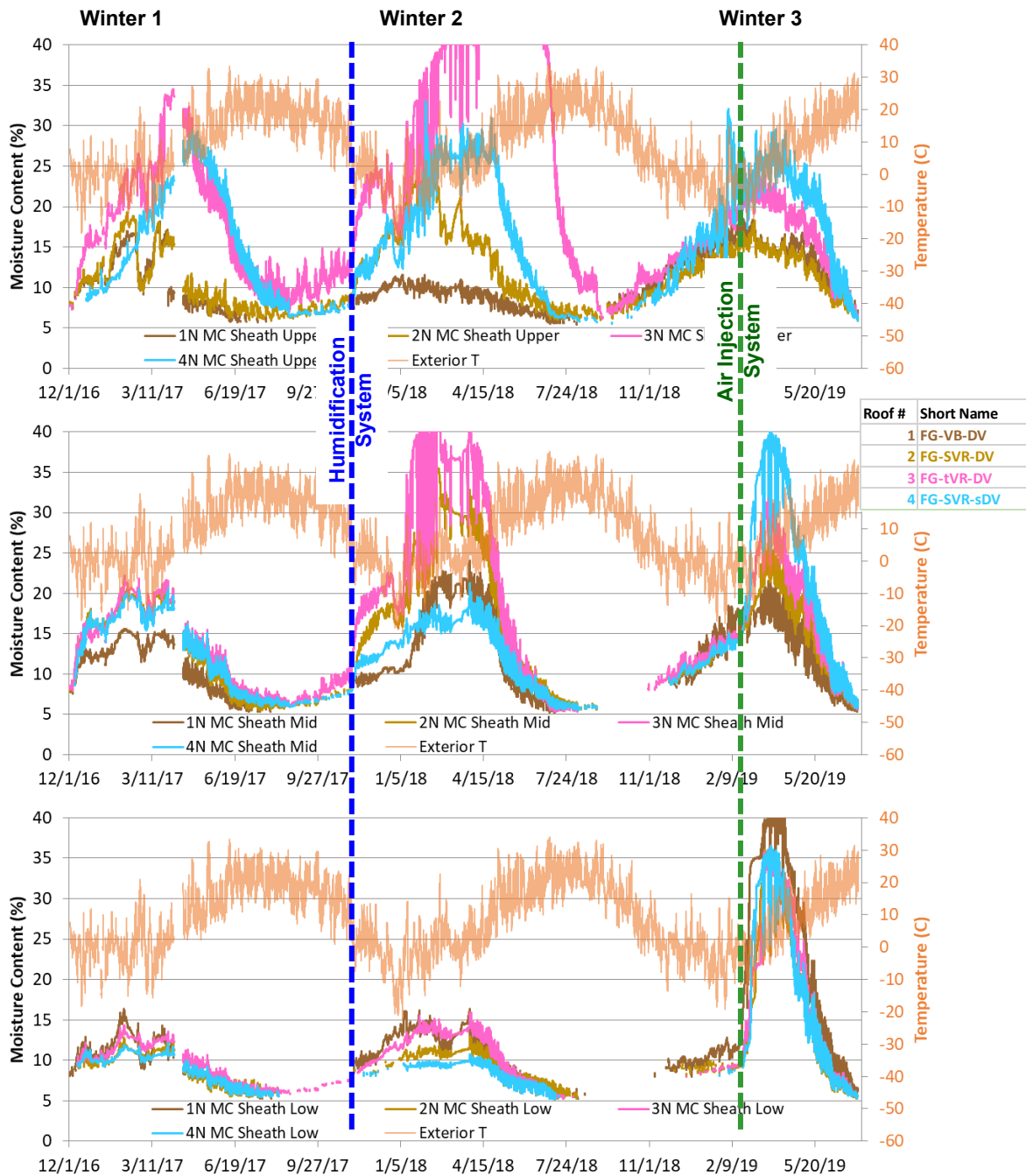
Figure 57. Fiberglass roofs' (1–4) sheathing MC north measurements

The sheathing MCs for the south fiberglass roofs are shown in Figure 58. This showed similar patterns of Winter 2 having higher MCs than Winter 1 (due to humidification). As expected, all south MCs are drier than the corresponding north measurements.

In Winter 2, operation of the humidification system increases MCs, which is particularly noticeable at the mid and lower heights. However, MCs remain within the safe range at those locations.

Winter 3 results are drier than Winter 2 (again consistent with repacking of insulation suppressing convective airflow). The air injection system was not designed to impact the south-facing roofs, so no response was expected.
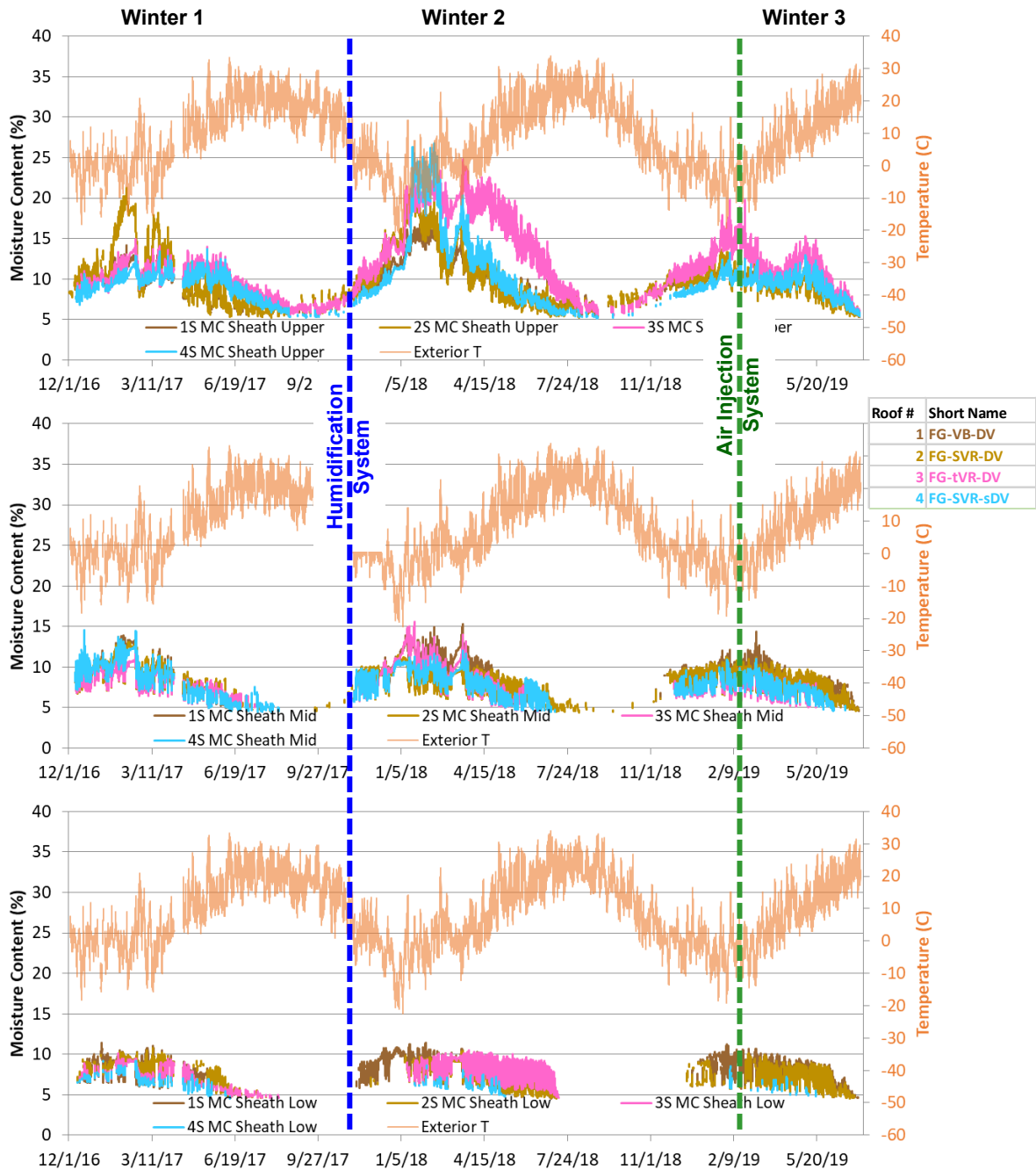
Figure 58. Fiberglass roofs' (1–4) sheathing MC south measurements

6.6 Inward Vapor Drive Measurements

Sensors were installed to measure the effect of inward vapor drives, which are caused by warm-season temperature gradients that tend to push accumulated moisture inward. The risk is that this moisture would accumulate at the interior vapor control layer, due to its low vapor permeance. Sensors were installed at the insulation-vapor retarder interface: T/RH sensors on the north and south sides, and a wafer sensor on the south side, per Figure 59.

RH/T Sheathing Mid

MC/T Sheathing Mid

RH/T Ridge

Wafer (South only)

RH/T Mid Interior

Roof #	Short Name	Winter 3	
1	FG-VB-DV		OC Facer
2	FG-SVR-DV	DV Roofs	Membrain
3	FG-tVR-DV		Isover SVR
4	FG-SVR-sDV	DV-small	Membrain

Sensor Key:
- ● Relative humidity/temperature
- ■ Moisture content/temperature
- ◪ Moisture content block "wafer"
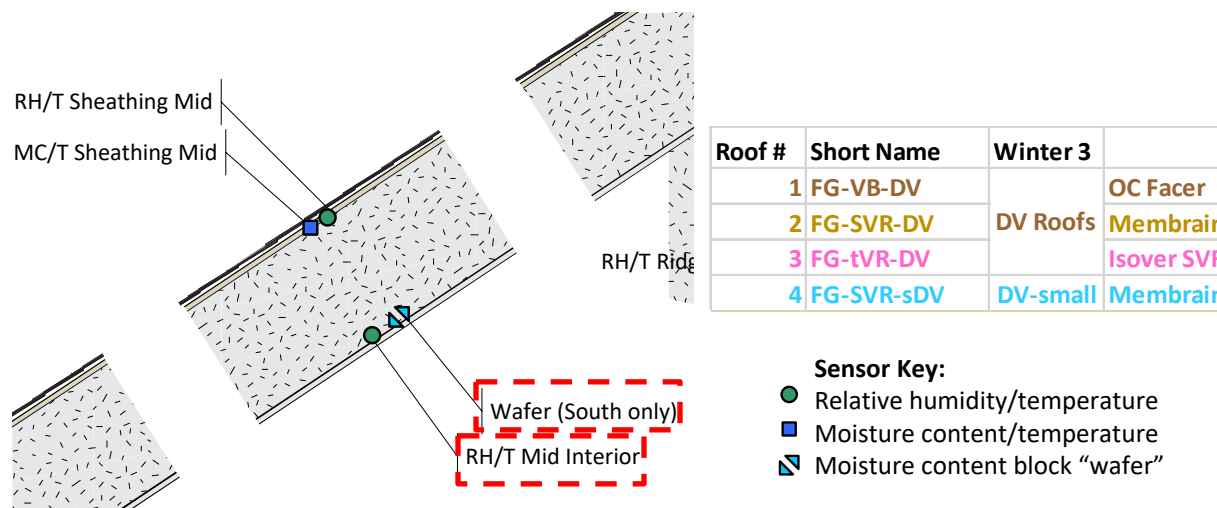
Figure 59. Roof mid-bay instrumentation, highlighting inboard T/RH and wafer sensors

The south-side wafer sensor (Figure 60) reflects moisture accumulation; the condensation range is shown by the dotted **BLUE** line.

Roof #	Short Name
1	FG-VB-DV
2	FG-SVR-DV
3	FG-tVR-DV
4	FG-SVR-sDV

— 1S Int Drive Wafer MC — 2S Int Drive Wafer MC — 3S Int Drive Wafer MC
— 4S Int Drive Wafer MC — Exterior T
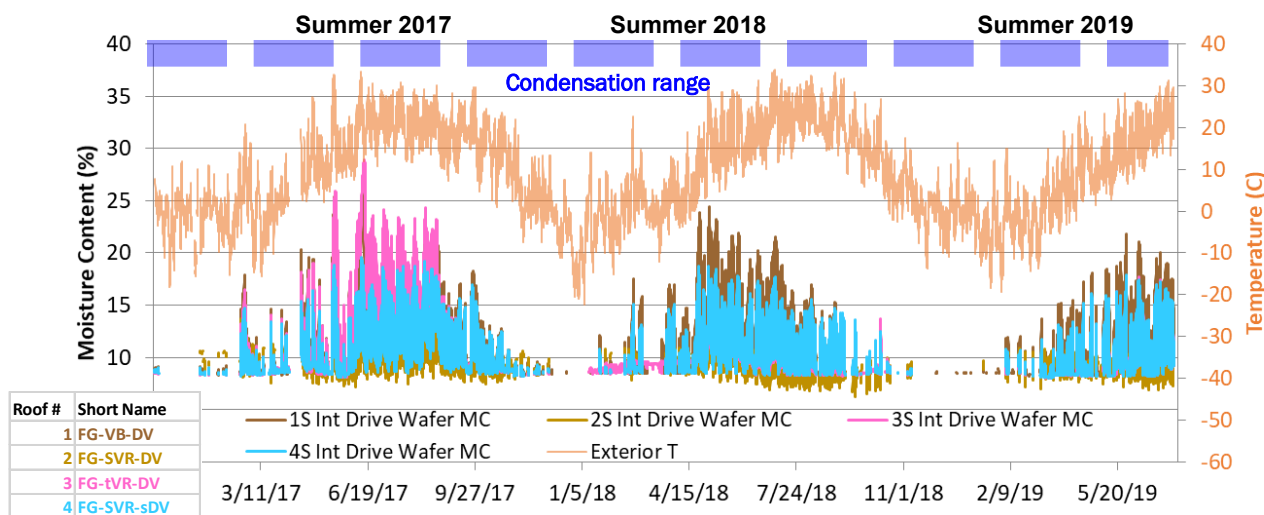
Figure 60. Fiberglass roofs' (1–4) inward drive wafer MC south measurements

In 2017, wafer peaks first occurred in February 2017, during unusually warm outdoor conditions. As exterior temperature warmed, moisture spikes occurred more frequently, and in proportion to outdoor temperatures. Moisture spikes remained well below the 40% MC range that indicates condensation. However, summertime spikes were above levels consistent with 100% RH.

The highest moisture spikes occurred in Roof 1 and Roof 3, which both had fixed-perm (1 perm) interior vapor and air barriers. In contrast, Roof 2 and Roof 4 (variable-perm vapor retarders) had noticeably lower peaks and accumulation of moisture.

The presence of liquid water condensation was noted during roof disassembly work (vapor retarder replacement) in summer (August) 2017. Specifically, condensation was found on Roof 3 (fixed-perm vapor retarder in Winter 1) within 3 ft of the ridge; this disassembly work is covered in Section 12.3: Inward Vapor Drive Condensation. The instrumentation at mid-height did not capture this extreme accumulation.

In summer 2018, Roof 1 (fixed-perm vapor barrier) appears to be the worst performer. Note that Roofs 2–4 were switched to variable permeance vapor retarders for Winter 2, which allow greater inward drying in summer. However, all MC peaks were below 25%, and well below the 40%–45% MC condensation range.

Similar results were seen in summer 2019, albeit with lower peaks. This might be due to lower wintertime moisture accumulation in Winter 3 (compared to Winter 2).

The south-facing inward drive RH sensors' 24-hour moving average data are plotted in Figure 61, for summer 2018 and summer 2019. Averaging was used to make the data readable. Again, Roof 1 (fixed-perm vapor barrier) is the consistent high outlier, although moisture levels remain in the safe range (mostly below 90% RH).
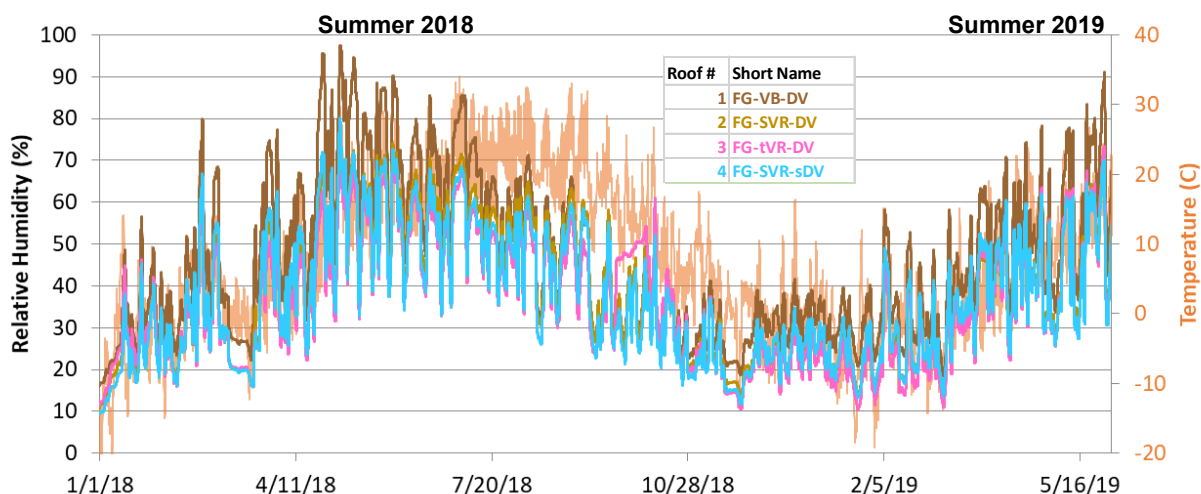
Figure 61. Fiberglass roofs' inward drive 24-hour average RH, south measurements, 2018–2019

The north orientation RH sensors' 24-hour moving average were plotted in Figure 62, for summer 2018 and summer 2019.
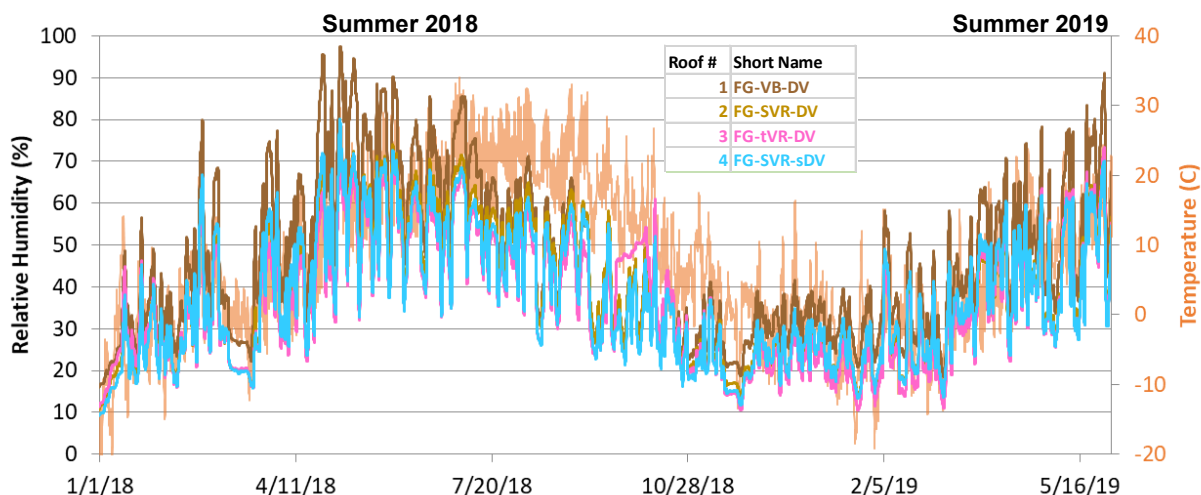
Figure 62. Fiberglass roofs' (1–4) inward drive 24-hour average RH, north measurements 2018–2019

Again, Roof 1 (fixed-perm vapor barrier) is the high outlier, although other roofs operate in a similar range. Summertime peaks on the north side reach 100% RH.

One observation when comparing Figure 61 (south RHs) and Figure 62 (north RHs) is that inward drive problems appear to be worse on the north side. This was surprising, given the greater solar gain on the south roof elevation. This is ascribed to greater wintertime moisture accumulation in the north-side assembly, which provides a greater reservoir of moisture.

6.7 Mold Index Calculations

The RH, wood MC, and wafer surrogate measurements indicate that many of the roofs experienced extended periods at high moisture levels under certain conditions, which are a risk factor for degradation and failure. However, these metrics alone do not account for temperature and time, which are critical for determining whether mold growth occurs.

Therefore, the data were analyzed using the Viitanen mold index (Ojanen et al. 2010), which accounts for RH, temperature, time, and substrate conditions. This is consistent with the methodology used in *ANSI/ASHRAE Standard 160-2009: Criteria for Moisture-Control Design Analysis in Buildings* (ASHRAE 2009b), Addendum e (ASHRAE 2016).

The failure criterion used for this work was a mold index over 3.0 (visible mold growth 10% coverage), per Table 9. Other inputs and assumptions include use of the "sensitive" class index (planed wood, paper coated products, wood-based boards), a Surface Quality of 0.0 (materials other than sawn wood), and a Decline Coefficient of 1.0.

Table 9. Viitanen Mold Index (Ojanen et al. 2010)

Index	Description of Growth Rate
0	No growth
1	Small amounts of mold on surface (microscope), initial stages of local growth
2	Several local mold growth colonies on surface (microscope)
3	Visual findings of mold on surface, < 10% coverage, or < 50% coverage of mold (microscope)
4	Visual findings of mold on surface, 10%–50% coverage, or > 50% coverage of mold (microscope)
5	Plenty of growth on surface, > 50% coverage (visual)
6	Heavy and tight growth, coverage about 100%

The mold index results for the fiberglass ridge T/RH sensor are shown in Figure 63 for Winters 1 and 2 and the following summers.
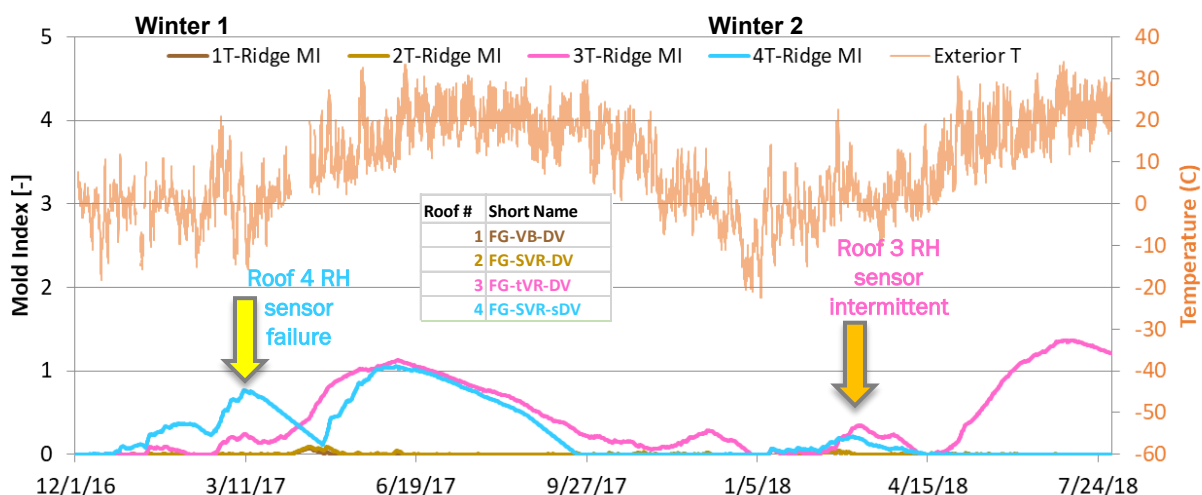
Figure 63. Fiberglass roofs' (1–4) ridge mold index calculations

In Winter 1, Roof 3 and Roof 4 (no diffusion vent) had extended winter periods at high RH (95%–100%) and indications of condensation. In contrast, Roof 1 and Roof 2 (diffusion vent) had much lower RH levels and no indication of condensation. The calculated mold index shows a rise slightly above 1.0 (microscopic mold growth levels) in Roof 3 and Roof 4 in the spring, as outdoor temperatures warmed while RH levels remained high. In contrast, Roof 1 and Roof 2 mold index values barely exceeded 0.

The decline seen in Roof 4 (YELLOW arrow in Figure 63) is an artifact of sensor failure; the ridge RH sensor failed in March 2017, returning unrealistically low measurements and zeroes. Roof 4 would likely have a higher mold index than Roof 3 if the sensor returned valid data.

In Winter 2, all roofs had extended periods at 95%–100% RH (Figure 43). Roof 3 (tight diffusion vent) showed indications of extensive wintertime ridge condensation (Figure 45); other fiberglass roofs remained below the condensation range. Roof 3's RH ridge sensor was intermittent during April 2018, also causing an artificial decline (**GOLD** arrow in Figure 63). However, the calculated mold index remained below 2.0, and well below the failure criterion of 3.0.

One variable to adjust in the mold index calculation is the decline coefficient. It was changed from 1.0 (default value) to 0.25 ("relatively low decline"), with results for the ridge T/RH sensor shown in Figure 64. For reference, a decline coefficient of 0.1 is "almost no decline." These results can be compared between Figure 63 (1.0 value) and Figure 64 (0.25 value). The smaller decline coefficient results in higher peak mold indices; however, maximum values remain below 3.0.
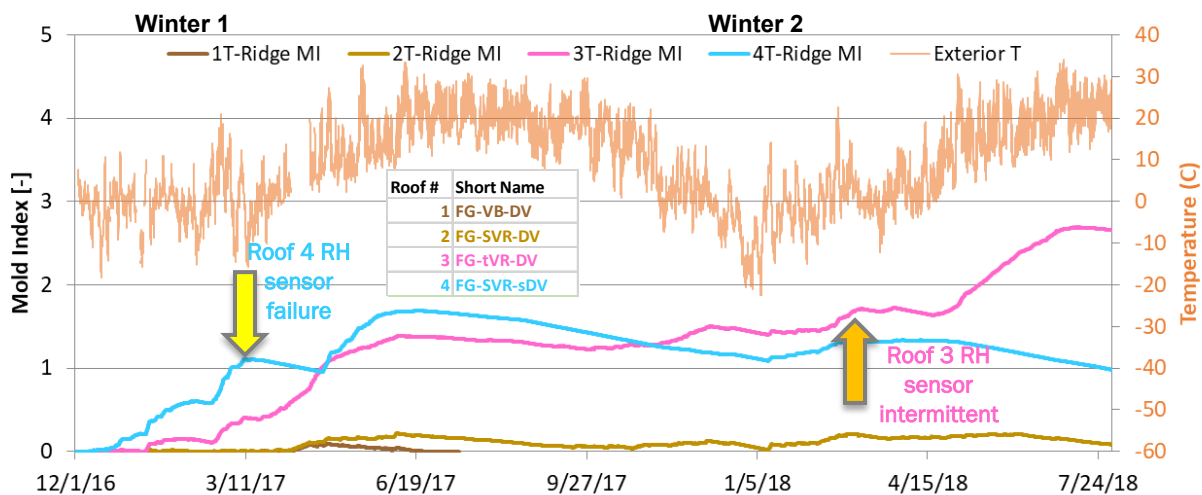
Figure 64. Fiberglass roofs' (1–4) ridge mold index calculations, with decline coefficient 0.25 (versus 1.0 default)

Given the RH sensor failures, the ridge wafer sensor was used to approximate RH levels. A generic wood sorption isotherm from Straube and Burnett (2005) was used to generate a polynomial curve fit to calculate RH from wafer MC. This calculation did not account for hysteresis effects and/or the asymmetric response of wafer sensors (slow adsorption, faster desorption), as discussed by Ueno and Straube (2008).

The mold index results are shown in Figure 65 for both Winter 1 and Winter 2. Winter 1 showed higher risks of Roof 3 and Roof 4 (no diffusion vent) but below the risk threshold of 3.0.

Winter 2 shows Roof 3 (tight diffusion vent) with a mold index rising over 3.0 in late spring/early summer, which is consistent with the sustained high moisture levels measured at the ridge.
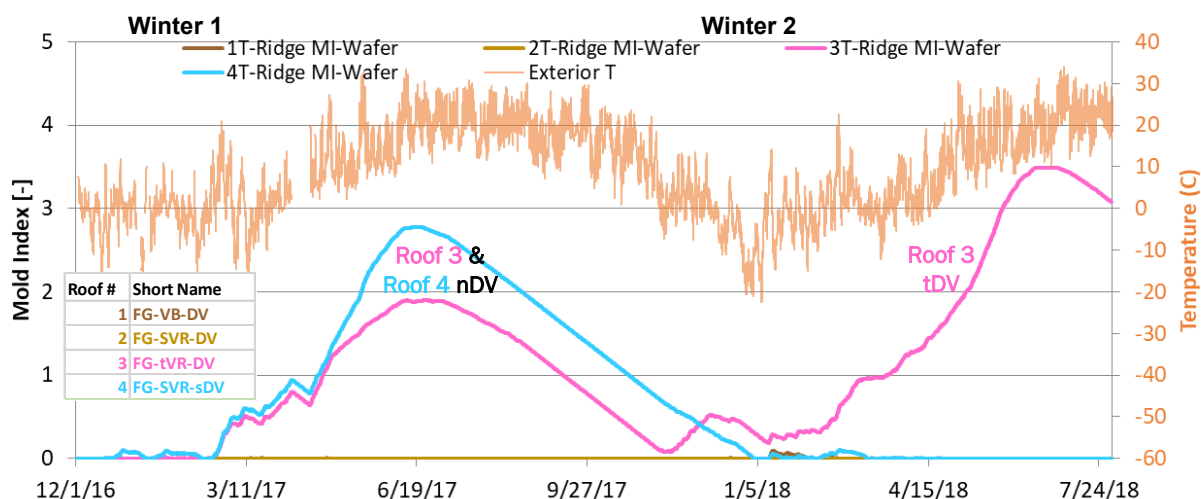
Figure 65. Fiberglass roofs' (1–4) ridge mold index calculations (derived from wafer MCs)

Another high-risk location was the north-side sheathing-insulation interface. In Winter 2, this interface had extended periods at 95%–100% RH in all four roofs (Figure 48) and sheathing MCs over 25% in some roofs (Figure 57). The mold index calculation results are shown in Figure 66: peak values were well below 2.0 for Winter 2, indicating low risk. Roof 4 (small diffusion vent) had lower interface RHs, which was ascribed to a sensor anomaly, rather than an actual performance difference; the mold index for this roof remains near zero for the winter. Given these low risks, mold indices were not calculated for the drier south sheathing-insulation interface.
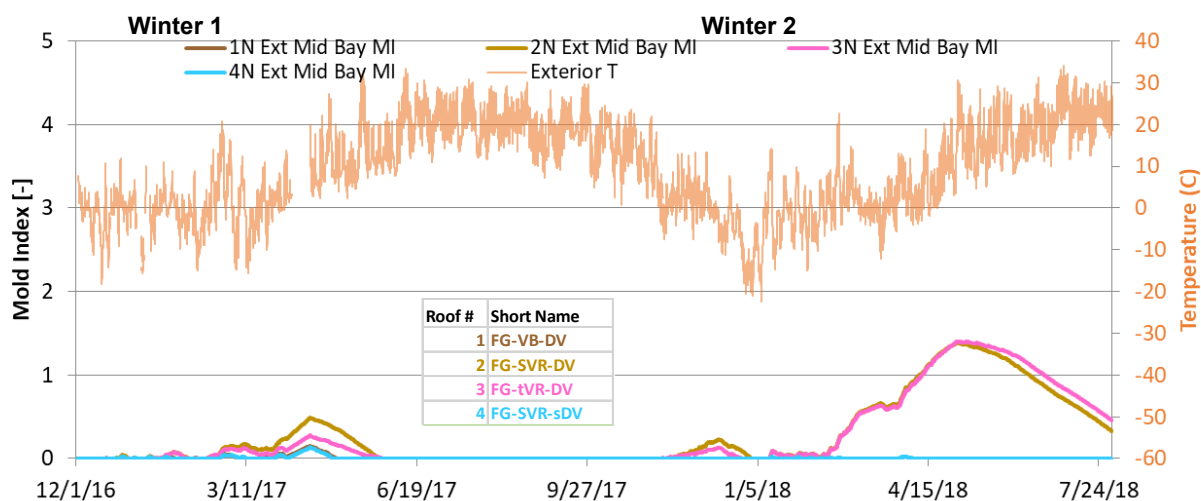
Figure 66. Fiberglass roofs' (1–4) north sheathing-insulation interface mold index calculations

A final area at risk was the insulation-vapor retarder interface, given the measurements of inward vapor drive and accumulation in fixed-perm vapor retarder roofs. The variable-perm vapor retarders showed lower RH peaks, indicating that the membrane allowed drying to the interior when loaded with moisture. The results are shown for the south side (Figure 67) and the north side (Figure 68).

In summer 2017, consistent with RH and wafer measurements, Roof 1 and Roof 3 (fixed-perm vapor retarder) showed higher risk than Roof 2 and Roof 4 (variable-perm vapor retarder). Mold indices for the fixed-perm vapor retarder roofs rose slightly above 1, which is below the failure threshold, but greater than the ridge mold index maximum. In addition, the north side had higher maxima than the south side, which was ascribed to greater stored moisture from the winter in the north-facing roof.
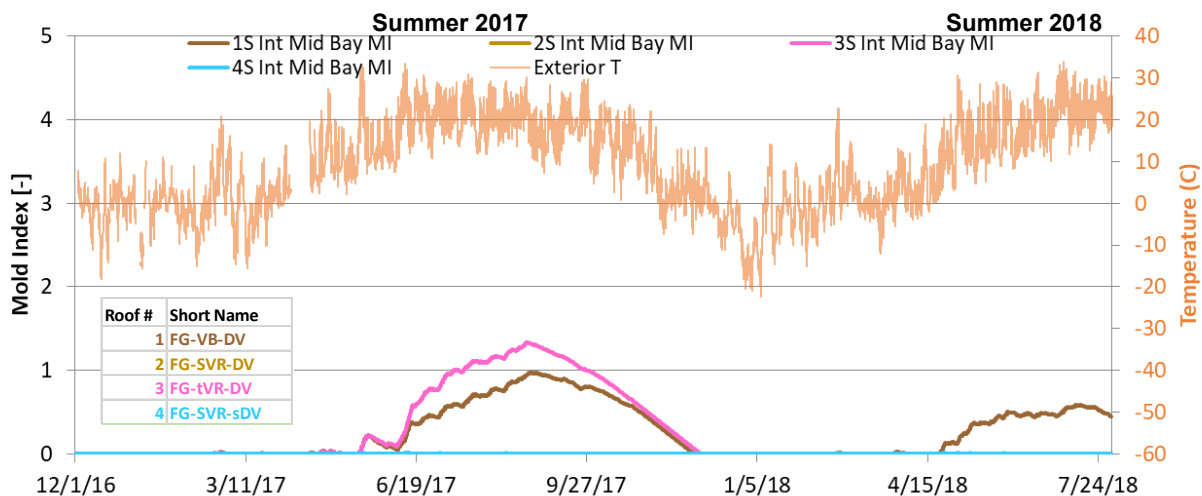
Figure 67. Fiberglass roofs' (1–4) south inward drive mold index calculations
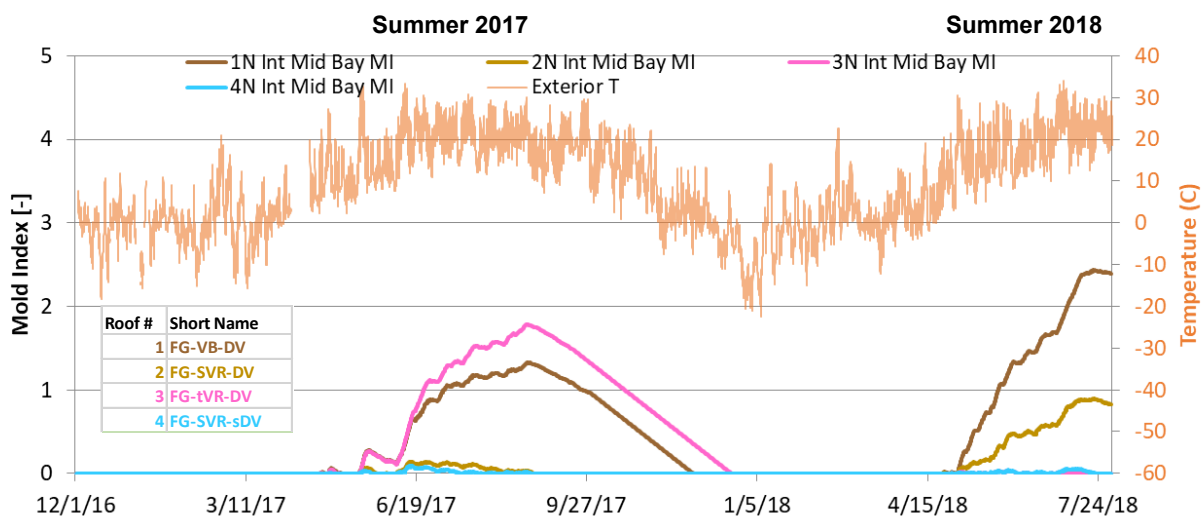
Figure 68. Fiberglass roofs' (1–4) north inward drive mold index calculations

In summer 2018, Roof 1 (fixed-perm vapor barrier) was the higher outlier on both the north and south sides, consistent with a lack of inward drying, compared to SVRs used in Roof 2, Roof 3, and Roof 4. Note that summer 2018 follows Winter 2 (humidified condition) with substantial moisture accumulation in the rafter bays. However, mold index remained below 3.0 on both orientations. The north-side roofs showed higher mold indices than the south side, again consistent with inward drive of stored wintertime moisture.

The mold index results were calculated using the "sensitive" class (planed wood, paper coated products, wood-based boards). It is fair to argue that the "medium resistant" class (cement or plastic-based materials, mineral fibers) is correct for interface, given the adjacent materials are the vapor retarder and fiberglass insulation. However, in inward moisture drive failures, the degradation often occurs on the wood framing members adjacent to the stud or rafter bay.

The analysis of Winter 1 and 2 showed no periods exceeding the mold growth threshold of 3.0. Given that all roof measurements were consistently drier in Winter 3 compared to Winter 2, safer conditions would result. Therefore, mold index values were not calculated for Winter 3.

7 Cellulose Roof Results

7.1 Cellulose Roof Identification

A similar set of plots was generated for the cellulose roofs (Roof 5, Roof 6, and Roof 7) and the flash-and-blow roof (hybrid ccSPF and cellulose; Roof 8). In the following graphs, the color codes and abbreviations shown in Table 10 are used to identify the roofs. The ccSPF-to-cellulose interface condition in Roof 8 is analyzed in a subsequent section. Characteristics that were modified between winters are underlined; note that Roof 7 and Roof 8 remained unchanged throughout the experiment.

The abbreviations can be keyed to the information shown in Table 2, Table 3, and Table 5.

Table 10. Cellulose Experimental Roof Numbering with Short Name and Color Coding Scheme (Winters 1, 2, and 3), Changes Underlined

Roof	Winter 1 Short Name	Winter 2 Short Name	Winter 3 Short Name
5	Cell-VB-nDV	Cell-SVR-tDV	Cell-tVR-DV
6	Cell-SVR-nDV	Cell-SVR-sDV	Cell-SVR-sDV
7	Cell-SVR-DV	Cell-SVR-DV	Cell-SVR-DV
8	ccSPF-Cell	ccSPF-Cell	ccSPF-Cell

7.2 Ridge Relative Humidity Conditions

The ridge sensors include a T/RH and wafer surrogate moisture sensor (Figure 69); the section below covers RH sensors.

Roof #	Short Name			
5	Cell-tVR-DV	Isover SVR w. DV		
6	Cell-SVR-sDV	DuPont SVR w. DV-small		
7	Cell-SVR-DV	DuPont SVR w. DV		
8	ccSPF-Cell			

Sensor Key:
🟢 Relative humidity/temperature
🟦 Moisture content/temperature
◨ Moisture content block "wafer"
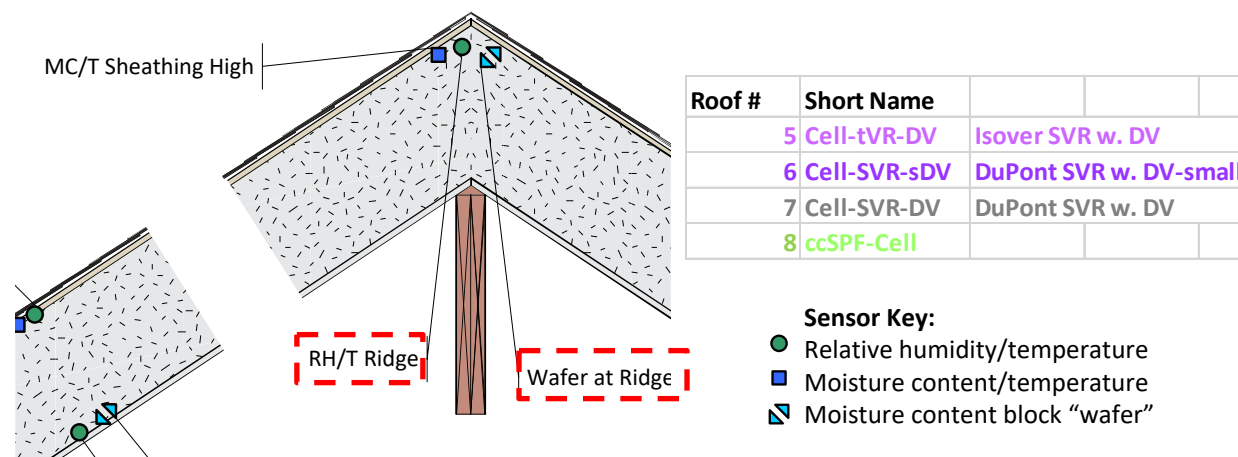
Figure 69. Roof ridge instrumentation, highlighting T/RH and wafer sensors

The ridge RH 24-hour moving average values for the cellulose roofs are shown in Figure 72; diurnal variations make the raw data graphs essentially unreadable.
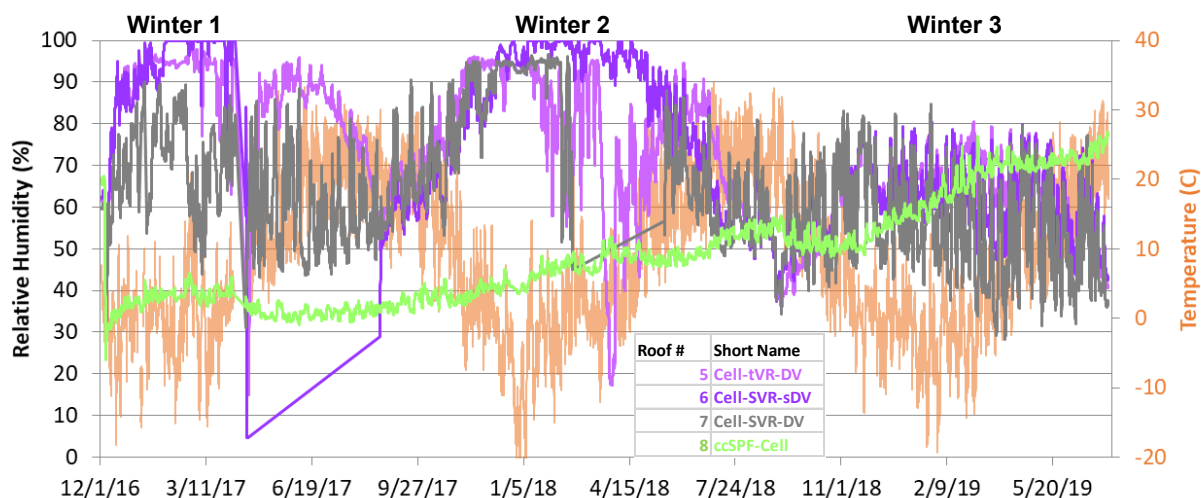
Figure 70. Cellulose roofs' (5–8) ridge RH conditions, 24-hour moving average

In Winter 1, Roof 5 and Roof 6, (no diffusion vent) have similar behavior to the equivalent fiberglass roofs: RH levels rise to 95%–100% RH and remain there over the course of the winter. However, Roof 7 (SVR and diffusion vent) has markedly drier behavior, with only brief excursions over 90% RH through the winter.

During spring drying, Roof 5 (no diffusion vent) remained wetter than Roof 7 (diffusion vent). The ridge RH sensor in Roof 6 failed in April 2016, so spring drying data are not available; however, this sensor started to return data in fall 2017.

Lastly, Roof 8 (ccSPF and cellulose) had consistently low RHs at the ridge, remaining in the 35%–45% range. This is consistent with the air- and vapor-impermeable ccSPF protecting the sheathing from interior moisture; the code-compliant roof has the driest conditions. These moisture levels continued through the spring dry-down.

In Winter 2, all ridge RHs were higher than Winter 1 due to interior humidification. For instance, Roof 7 (full-sized diffusion vent) can be compared between Winters 1 and 2, as it is unchanged between those two periods. In Winter 1 (moderate interior RH), ridge RH seldom peaked above 90%, but in Winter 2 (humidification to 50% RH), RHs rose to ~95% and remained there until sensor failure. Roof 5 also showed drops in RH consistent with sensor issues rather than actual drying.

These sensors appeared to return valid data again in late spring (drying of the sensors); however, this data is suspect, given the previous failure. Arguably, summertime data show Roof 7 (full-size diffusion vent) drying faster than Roof 6 (small diffusion vent), which is consistent with greater drying through a larger surface area. Roof 5 (tight diffusion vent) has the slowest drying, consistent with behavior in the fiberglass roofs.

In contrast, Roof 8 (hybrid ccSPF-cellulose) only shows a slight rise from 40%–50% RH over the course of the winter, which is well below risk thresholds. The cellulose ridge RH sensors were replaced between Winter 2 and Winter 3, except Roof 8 (hybrid).

Winter 3 ridge RH sensors showed much drier conditions than Winter 2, with identical interior conditions. This is consistent with results from the fiberglass roofs, suggesting that repacking of insulation and eliminating voids (especially on the north side) greatly reduces wetting, due to less convective airflow in the rafter bays. Average RHs remain below 80% for most of Winter 3.

These maximum values (~80% RH) are drier than those measured in the fiberglass roofs (~90% RH); this difference is ascribed to the moisture/hygric storage of the cellulose insulation.

Roof 8 (ccSPF-cellulose) shows a slow increase in RH over the three years. This trend does not match expected behavior or typical observed field conditions for this type of assembly. Ridge conditions at this roof were examined more closely with handheld instruments, as covered in Section 8.5: Ridge Sensors and Long-Term Moisture Accumulation. These measurements indicate that the upward trend is likely sensor drift.

Box and whisker plots for the cellulose roof ridges in Winters 1 and 2 are shown in Figure 71. Winter 1 shows the superior performance of Roof 7 (diffusion vent) and Roof 8 (hybrid ccSPF-cellulose). But in Winter 2, interior humidification pushes all cellulose roofs into the 85%–95% RH range, including the best-performing Roof 7. The Winter 2 plot should be interpreted with caution: the RH sensor in Roof 5 and Roof 7 showed erratic data for much of the winter, as denoted by the gray shaded bars.
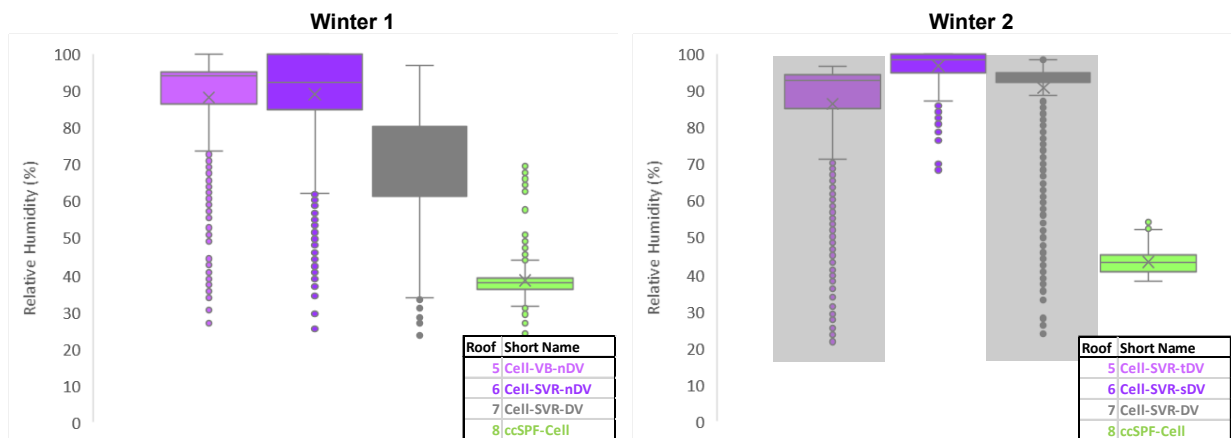
Figure 71. Cellulose roofs' (5–8) ridge RH box-whisker plots, Winter 1 vs. Winter 2

7.3 Ridge Wafer Conditions

The ridge wafer results are shown in Figure 72, with the condensation range for these sensors shown in **BLUE**.
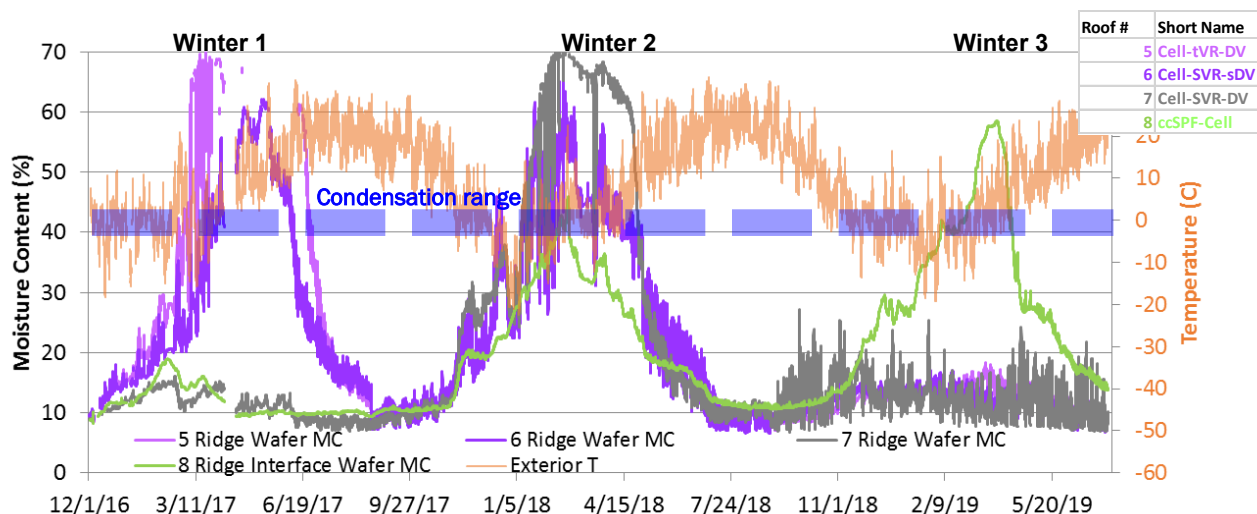
Figure 72. Cellulose roofs' (5–8) ridge wafer MC measurements

In Winter 1, wafer MC rose sharply in Roof 5 and Roof 6 (no diffusion vent). The MC measurements are well outside the realistic range, with maxima of 60%–70% MC. This is ascribed to migration of borate salts from the cellulose insulation into the wafer, which lowers electrical resistance, resulting in these false high readings. Migration of borate salts occurs at high moisture levels (in the presence of liquid water due to capillary salt transport); this is consistent with wafer measurements rising above 40%–45% MC (condensation range). These moisture levels remain high well into spring; this matches the Roof 5 ridge RH measurements, but the absolute wafer MCs are suspect.

In contrast, Roof 7 (diffusion vent) has much drier ridge conditions, with MCs under 20%, demonstrating drying at the ridge. Similarly, Roof 8 (ccSPF-cellulose hybrid) shows a peak under 20% MC and then dries in the spring. This is consistent with the protection from interior moisture provided by air- and vapor-impermeable spray foam.

In Winter 2, humidification to 50% RH caused a sharp increase in all wafer MCs, indicating possible condensation in all of the cellulose roofs (Roof 5, Roof 6, and Roof 7). Even the hybrid ccSPF and cellulose roof (Roof 8) showed a noticeable increase. However, all roofs dried in the spring to safe levels.

Ridge wafers were replaced in all cellulose roofs between Winters 2 and 3 (not Roof 8 hybrid). In Winter 3, all cellulose roofs were much drier (rarely exceeding 20% MC) than Winter 2, consistent with previous measurements, indicating the protective effect of greater insulation density and the elimination of air voids.

Roof 8 (ccSPF-cellulose) had ridge wafer measurements indicating very high moisture accumulation (50%–60% MC, above the condensation range) in Winter 3. This accumulation dried at the end of the winter. This wafer sensor was not replaced between Winters 2 and 3. It is not clear if this is a sensor anomaly or an indication of actual conditions; the fact that this sensor was in service for a third year suggests sensor issues. The wafer MCs are much higher than the co-located RH measurements, even if RH sensor drift is ignored.

The ridge wafer sensor plots are shown in Figure 73. They demonstrate the greater drying of Roof 7 (full-size diffusion vent) and safe behavior of Roof 8 (ccSPF-cellulose hybrid) in Winter 1.

In Winter 2, Roof 5 (tight diffusion vent, SVR) had no sensor and is not plotted. Roof 6 and Roof 7 had very high wafer MCs, ascribed to borate contamination.
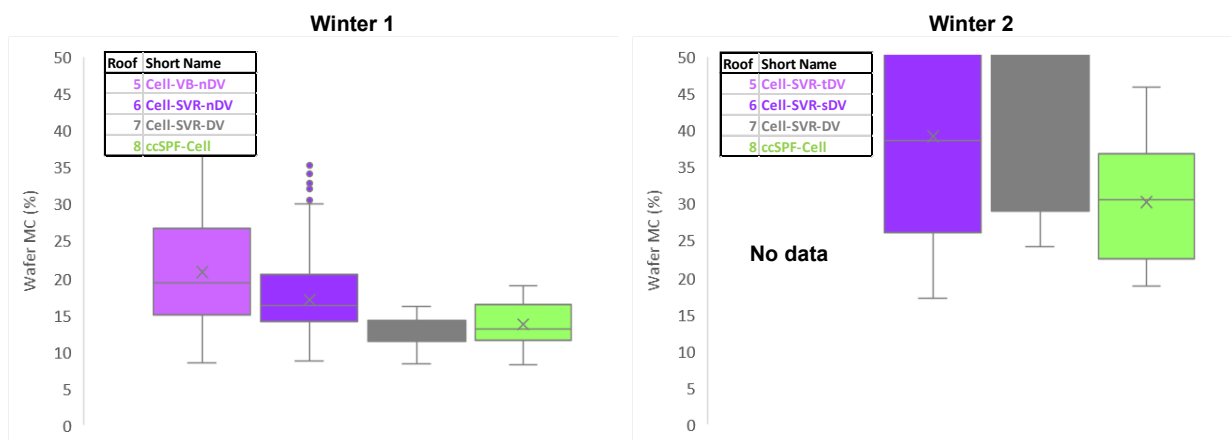
Figure 73. Cellulose roofs' (5–8) ridge wafer MC box-whisker plots, Winter 1 vs. Winter 2

7.4 Mid-Bay Relative Humidity Conditions

RH sensors at mid-height in the rafter bay, at the interface between the insulation and the exterior sheathing (Figure 74), are installed on both the north and south orientations. They are intended to capture high RH levels or condensation at the cold (in winter) interface.

Roof #	Short Name			
5	Cell-tVR-DV	Isover SVR w. DV		
6	Cell-SVR-sDV	DuPont SVR w. DV-small		
7	Cell-SVR-DV	DuPont SVR w. DV		
8	ccSPF-Cell			

Sensor Key:
- ● Relative humidity/temperature
- ■ Moisture content/temperature
- ◪ Moisture content block "wafer"
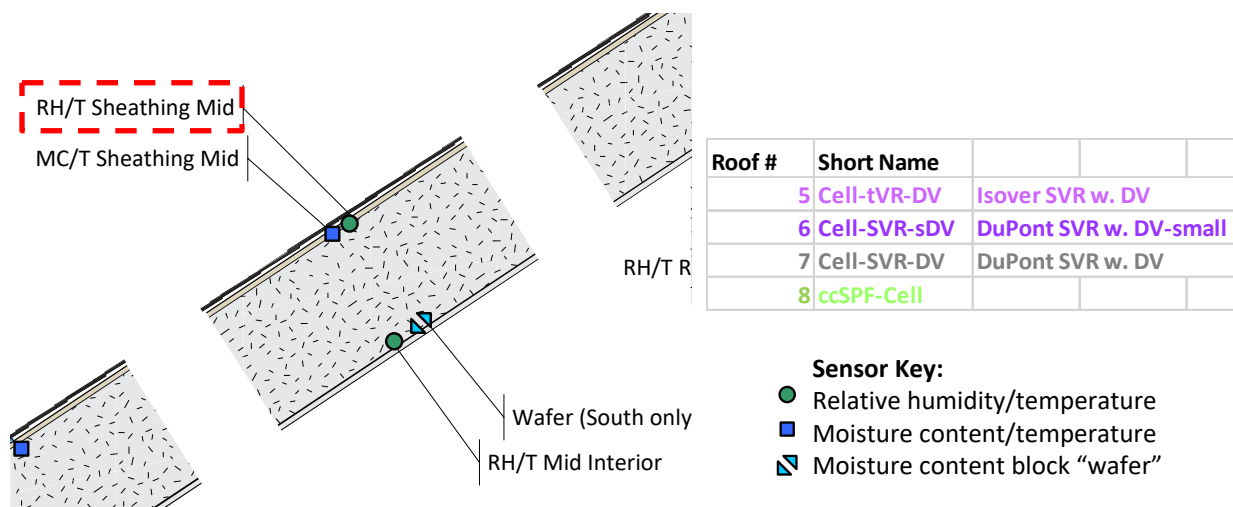
Figure 74. Roof mid-bay instrumentation, highlighting outboard T/RH sensor

Mid-bay RH data for the cellulose roof are shown in Figure 75 (north) and Figure 76 (south, 24-hour moving average).
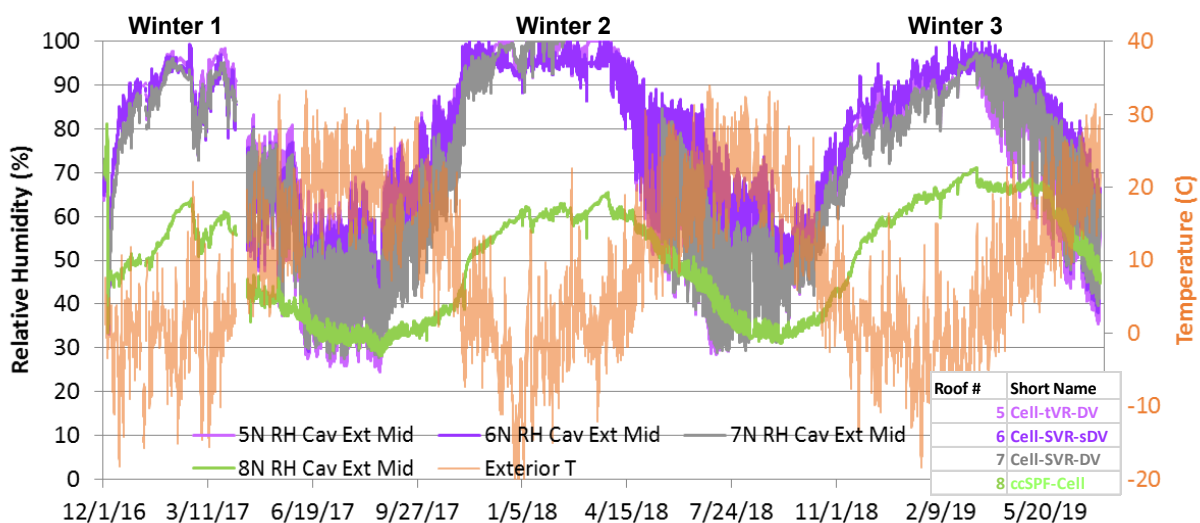
Figure 75. Cellulose roofs' (5–8) mid-bay RH north conditions

In Winter 1, the north-facing cellulose roof RHs (Figure 75) follows patterns similar to the fiberglass roofs, with RHs rising over the course of the winter to 90%–100% RH. However, the winter rise is more gradual in the cellulose roofs (compared to fiberglass), due to the moisture storage of the cellulose insulation. Consistent 90%+ RH levels only occur by mid-January in the cellulose roofs, compared to early December in the fiberglass roofs. In addition, the north-facing cellulose roofs do not reach 100% RH, unlike the fiberglass roofs.

Roof 5, Roof 6, and Roof 7 show very similar behavior, arguably showing that the diffusion vent (Roof 7) only provides localized drying, as opposed to systemic whole-roof drying. However, Roof 7 is the driest of the three cellulose roofs. During the spring and into the summer, all three roofs dry to a safe level (30%–60% RH typical).

In Winter 2, all three cellulose roofs (Roof 5, Roof 6, and Roof 7) rose to 95%–100% RH, and remained there for most of the winter; this difference was due to interior humidification. The fiberglass roofs showed similar behavior. Roof 8 (hybrid ccSPF-cellulose) showed RH levels well below risk ranges at the ccSPF-to-sheathing interface (peaking at 60%–65% RH). In the spring, Roof 7 (full-size diffusion vent) showed faster drying than Roof 5 (tight diffusion vent) and Roof 6 (small diffusion vent), consistent with greater surface area for diffusion drying.

Winter 3 north sheathing RHs (Figure 75) are much lower than Winter 2, with a much briefer period in the 95%–100% range. This is consistent with repacking of insulation improving hygrothermal performance. Roof 6 (small diffusion vent) is the high outlier, consistent with reduced drying through a smaller diffusion vent. Roof 8 (ccSPF-cellulose) is consistently much drier than the experimental cellulose roofs, well in the safe range.

The 24-hour moving average of south sheathing interface RH data (Figure 76) show expected trends, including drier conditions than the north side, Winter 2 (humidification) being wetter than Winter 1, and drier conditions in Winter 3 compared to Winter 2. Sheathing-insulation interface RHs remain below risk levels.
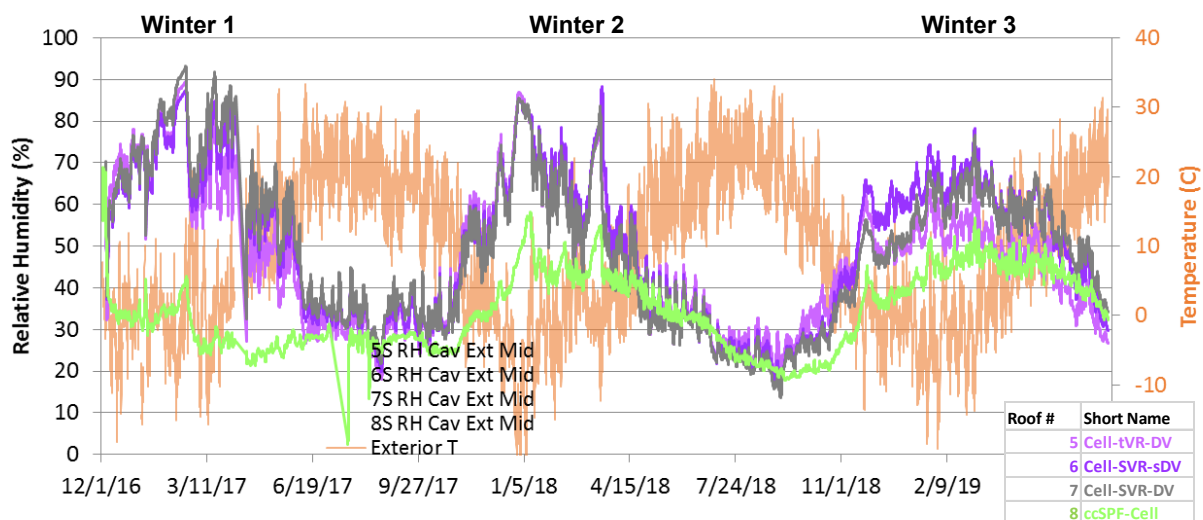
Figure 76. Cellulose roofs' (5–8) mid-bay RH south conditions, 24-hour moving average

Mid-height insulation-to-sheathing RH box-whisker plots for the north side are shown in Figure 77 (Winter 1 vs. Winter 2) and Figure 78 (Winter 2 vs. Winter 3).

The Winter 1 vs. Winter 2 plots (Figure 77) show the severity of Winter 2's humidified load, pushing interface RHs near 100% for much of the winter, with no low-RH outliers as seen in Winter 1. There is no clear differentiation between the experimental cellulose roofs, although Roof 7 (full-size diffusion vent) is the driest in Winter 1, consistent with its greater outward drying. Roof 8 (hybrid ccSPF-cellulose) runs at much lower (drier) RHs throughout both winters.
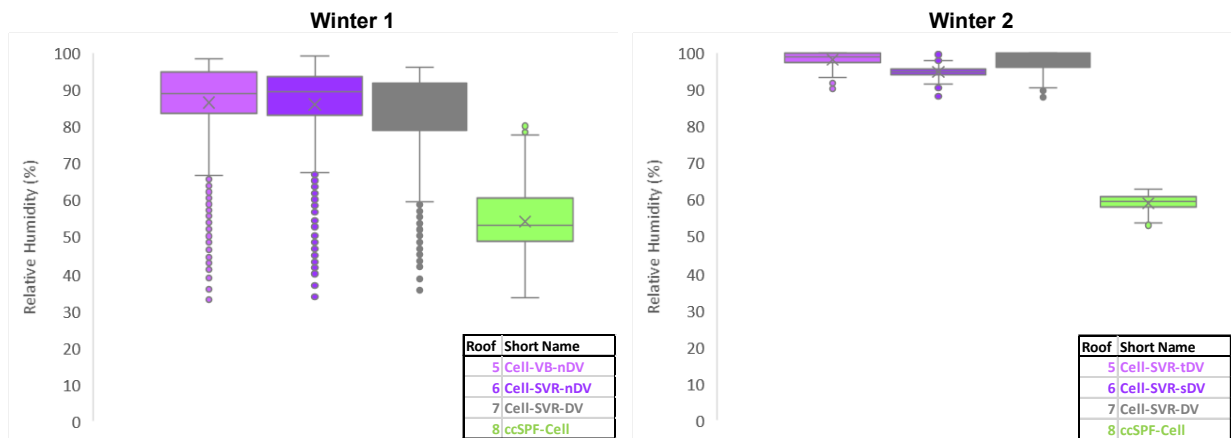
Figure 77. Cellulose roofs' (5–8) mid-height north RH box-whisker plots, Winter 1 vs. Winter 2

The Winter 2 vs. Winter 3 plots (Figure 78) show drier conditions in Winter 3 compared to Winter 2, and the fact that Roof 6 (small diffusion vent) appears to be the higher outlier relative to Roof 5 and Roof 7 (full-size diffusion vents). This suggests that the diffusion vent might provide more than localized drying at the ridge. However, this difference is close to RH sensor accuracy limits (±3.5% RH).
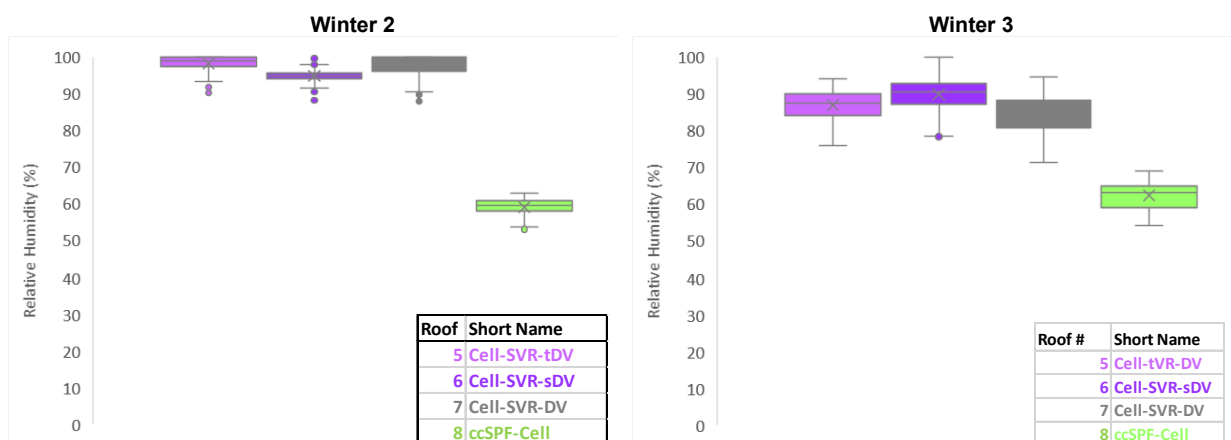
Figure 78. Cellulose roofs' (5–8) mid-height north RH box-whisker plots, Winter 2 vs. Winter 3

South-side interface RH box-and-whisker plots are not shown, as they show less useful characterization of the roofs.

7.5 Sheathing Moisture Contents

Roof sheathing MCs were measured on north and south sides, low, mid, and high (Figure 79).

Roof #	Short Name		
5	Cell-tVR-DV	Isover SVR w. DV	
6	Cell-SVR-sDV	DuPont SVR w. DV-small	
7	Cell-SVR-DV	DuPont SVR w. DV	
8	ccSPF-Cell		

Sensor Key:
● Relative humidity/temperature
■ Moisture content/temperature
◩ Moisture content block "wafer"
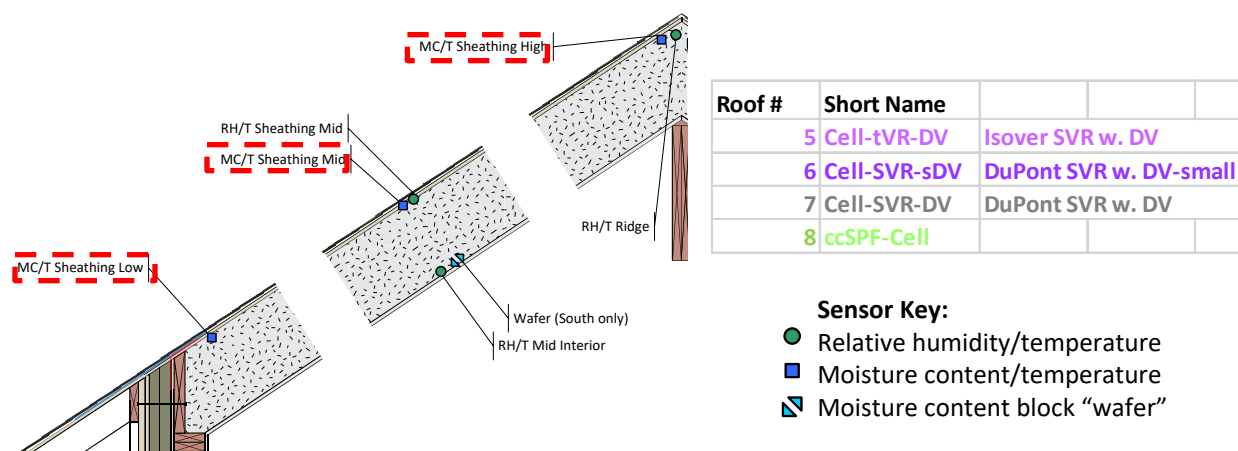
Figure 79. Roof sheathing MC measurements highlighted

The sheathing MCs for the cellulose roofs are shown for the north side (Figure 80) and the south side (Figure 81), ordered from high to low. The expected pattern is seen, with greater accumulation higher in the roof and drier conditions on the south side.

On the north side in Winter 1, Roof 5 and Roof 6 (no diffusion vent) have a substantial rise in MC, above 40%; reported values peaked in the 45%–50% MC range. Like the wafer sensor results (Figure 72), these results appear to be spurious values due to borate salt migration from the cellulose into the wood sheathing caused by liquid water condensation. However, it does indicate that these roofs are experiencing severe moisture loading at the roof ridge, with likely condensation. The plotted values should not be taken as valid wood MC measurements, though.

In contrast, Roof 7 (diffusion vent) and Roof 8 (ccSPF-cellulose) both had safe conditions at the north upper location. Roof 7 had peak MCs under 15%, and Roof 8 below 10%. The middle and lower wood north-side MCs all remained below 20%.

Winter 2 has much higher MCs than Winter 1; operation of the humidification system is highlighted in **BLUE**. For instance, in Winter 1, Roof 7 (full-sized diffusion vent) remained at dry (under 15% MC) conditions, while in Winter 2, it rose to wet (over 40% MC) conditions. A similar contrast can be shown at the mid-height sensors: all sheathing MCs remained in the safe range in Winter 1, but maximums exceeded 25% in Winter 2.

In summer 2018, Roof 7 (full-sized diffusion vent) showed safer behavior than Roof 5 (tight diffusion vent) and Roof 6 (small diffusion vent). For instance, at the upper location, it was the fastest-drying roof in spring. Roof 7 was also the driest in winter at the mid-height sheathing, again indicating that the greater drying of the diffusion vent is not limited to localized ridge conditions.

At the low sheathing measurements, all MCs remained in the safe range (under 15%), showing the stratification effects in the rafter bays. Roof 8 (hybrid) showed dry sheathing MCs, well below levels of concern.

Winter 3's performance before air injection is much drier than Winter 2, consistent with all other measurements. After air injection in late February 2019 (**GREEN** vertical dotted line), sheathing MCs rapidly increase at the low location (to 30%–35% MC), and to a lesser degree at the middle sheathing location. The upper sheathing measurements do not show a response. In addition, the maximum MCs are lower than in the fiberglass roofs, likely due to cellulose moisture storage.

After the conclusion of air injection (mid-April), sheathing MCs declined to safe levels.

Roof 8 (ccSPF/cellulose) shows a cycling rise in MC at the upper sheathing location, which appears to peak in late spring/early summer; this seasonal response is different than the cellulose roofs, and could indicate slow moisture accumulation in the assembly. However, peak MCs are within the safe range. These trends are further examined below.
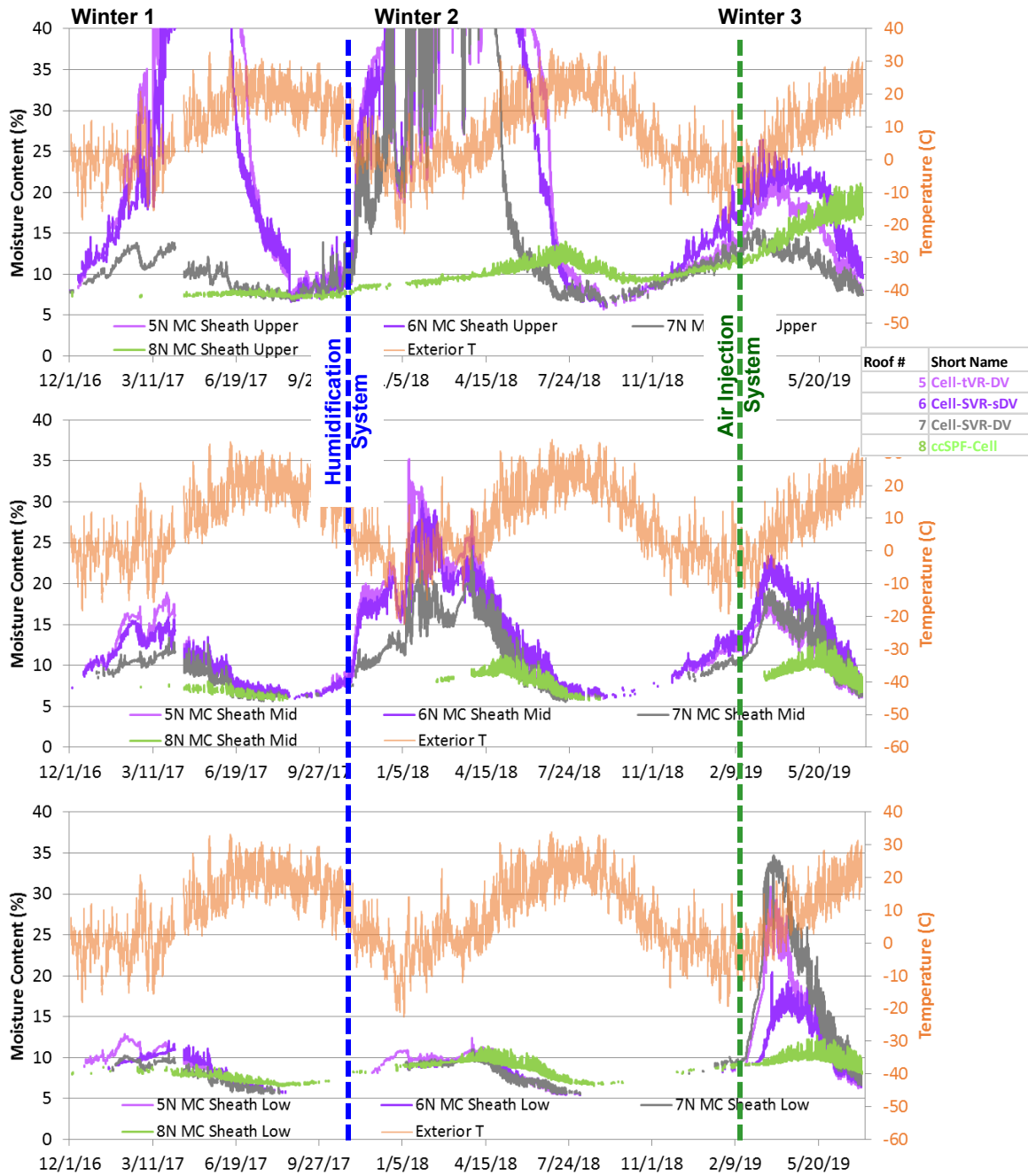
Figure 80. Cellulose roofs' (5–8) sheathing MC north measurements

The south-side roof sheathing MCs are plotted in Figure 81. Again, south-side measurements are much drier than the north side, and the expected spatial pattern (wettest at upper location) is observed.
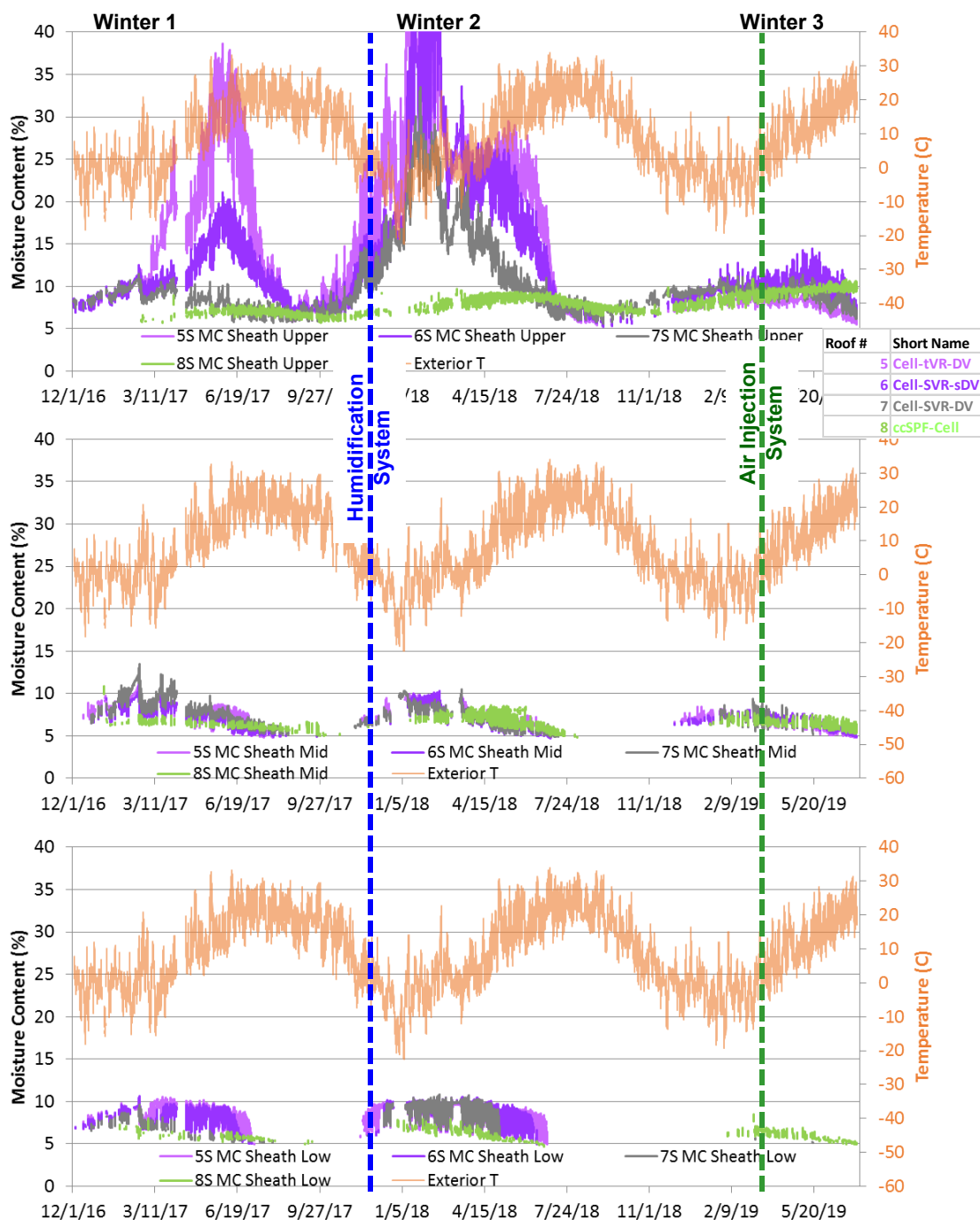
Figure 81. Cellulose roofs' (5–8) sheathing MC south measurements

On the south side, in Winter 1, the same pattern was seen of Roof 5 and Roof 6 (no diffusion vent) showing greater moisture accumulation near the ridge than Roof 7 (diffusion vent). However, unlike the north side, this rise began during warmer spring conditions (March–April 2017). MCs rose to 20% (Roof 6) and over 35% (Roof 5); again, these results are suspect due to condensation and possible migration of borate salts into the sheathing. Roof 8 (ccSPF-cellulose)

both had safe conditions at the south upper location (under 10% MC). The middle wood south-side MCs all remained below 15%, and the lower MCs below 10%.

In Winter 2, the south side shows similar issues of much higher MCs than Winter 1 due to interior humidification. Roof 7 (full-sized diffusion vent) appears drier than Roof 5 (tight diffusion vent) and Roof 6 (small diffusion vent) at the upper location, consistent with greater wintertime drying. Roof 5 and Roof 6 show peak MCs over 40%, which is likely a combination of high moisture levels and borate migration. As expected, Roof 8 (hybrid ccSPF-cellulose) shows low sheathing MCs throughout, including the humidified Winter 2.

Winter 3 results are drier than Winter 2 (again consistent with repacking of insulation suppressing convective airflow). The air injection system was not designed to impact the south-facing roofs, so no response was expected. Maximum south-side MCs all remained below 15%, well within the safe range.

7.6 Inward Vapor Drive Measurements

Inward vapor drive sensors were installed at the insulation-vapor control layer interface: T/RH sensors on the north and south sides, and a wafer sensor on the south side (where the greatest inward drive issues are expected), per Figure 82.

Roof #	Short Name	
5	Cell-tVR-DV	Isover SVR w. DV
6	Cell-SVR-sDV	DuPont SVR w. DV-small
7	Cell-SVR-DV	DuPont SVR w. DV
8	ccSPF-Cell	

Sensor Key:
🟢 Relative humidity/temperature
🟦 Moisture content/temperature
◨ Moisture content block "wafer"
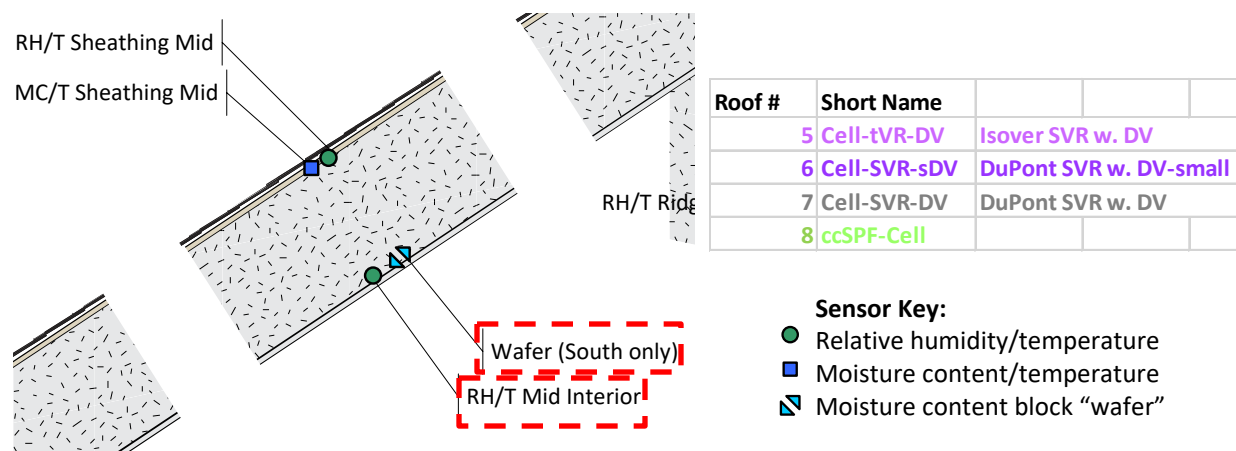
Figure 82. Roof mid-bay instrumentation, highlighting inboard T/RH and wafer sensors

The cellulose roof south-facing inward drive RH measurements (Figure 83) rose and fell in a pattern matching outdoor temperatures, which would dominate the vapor drive direction in this closed cavity.
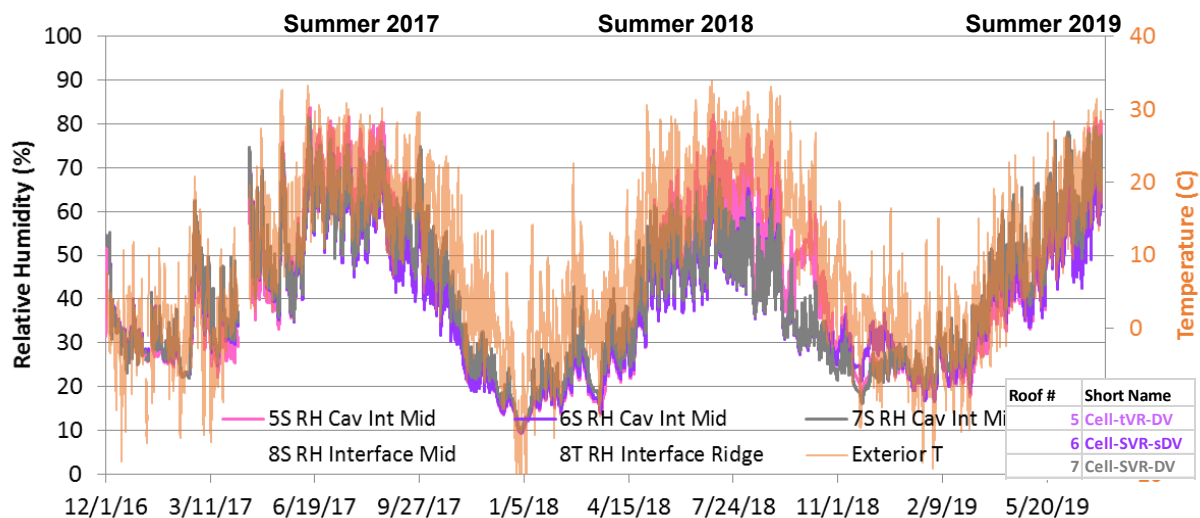
Figure 83. Cellulose roofs' (5–8) inward drive RH south measurements

In all three summers, peak RHs rarely exceeded 80%, compared to extended 100% RH peaks seen in the fiberglass roofs. This demonstrates safer behavior in the cellulose roofs due to moisture storage.

A detail of June 2017 conditions (Figure 84) was used to try to differentiate roof behaviors. Roof 5 (fixed-perm vapor retarder) had slightly higher peaks than Roof 6 and Roof 7 (variable-perm vapor retarders), but the difference was very small. This contrasts with the fiberglass roofs, where interior vapor retarder permeance created a large difference in behavior. The lack of difference between these two vapor control materials (Roof 5, Roof 6, and Roof 7) is ascribed to the fact that very high RHs did not occur at the interface, which would "activate" the open vapor permeance of the variable-perm vapor retarder.
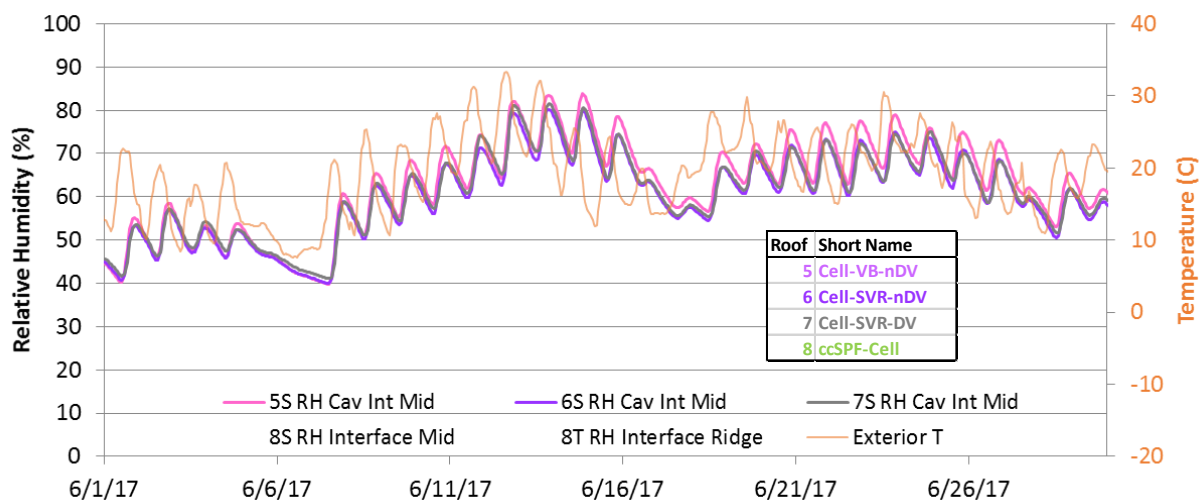
Figure 84. Cellulose roofs' (5–8) inward drive RH south measurements, June 2017 detail

The north-facing inward drive RH sensor results are shown in Figure 85, with behavior similar to the south-facing roof. RH peaks were slightly over 90% on the north side (vs. 80% on the south

side); this is likely due to greater stored moisture in the assembly from the winter. These north RH peaks were also lower than those observed in the fiberglass roofs, due to greater moisture storage of cellulose insulation, compared to fiberglass or mineral fiber.
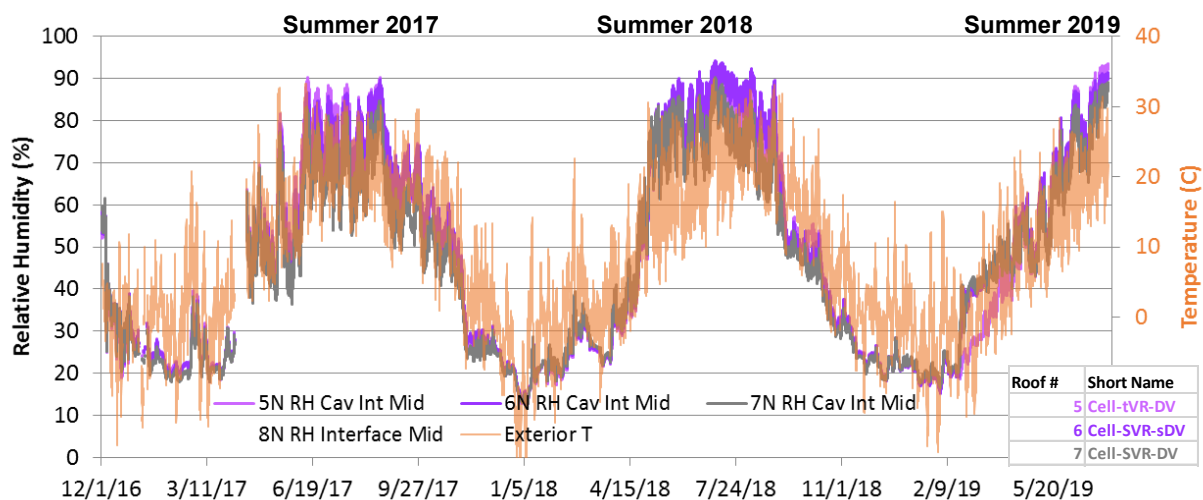
Figure 85. Cellulose roofs' (5–8) inward drive RH north measurements

The inward drive south-side cellulose wafer sensors (Figure 86) showed a small rise during summer conditions, but MCs remained well below 15%. In contrast, the equivalent fiberglass wafers had peaks in the 20%–25% range, again demonstrating hygric storage of cellulose.
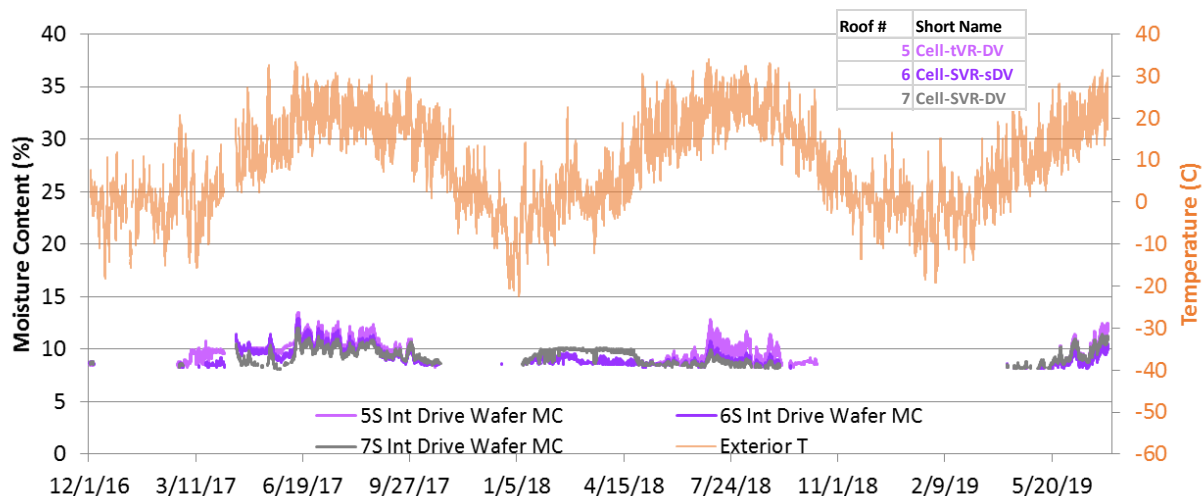
Figure 86. Cellulose roofs' (5–8) inward drive wafer MC south measurements

7.7 Mold Index Calculations

Mold indices were calculated for key locations using the same parameters described for the fiberglass roofs. The mold index results for the fiberglass ridge conditions are shown in Figure 87 for Winters 1 and 2 and the following summers.

In Winter 1, Roof 5 and Roof 6 reached 95%–100% RH early in the winter, while Roof 7 remained drier (Figure 70). In Winter 2, all three cellulose roof ridges rose to 95%–100% RH

early in the winter, and remained there until RH sensors failed. Sensor failures included Roof 6 in Winter 1 (mid-April 2017) and Roof 5 in Winter 2 (January 2018), as noted by yellow arrows. As a result, these mold index results are suspect; based on the raw data, all mold indices remain below 2.0. Unfortunately, the wafer sensors cannot be used as surrogates for RH, due to the borate salt migration issues.
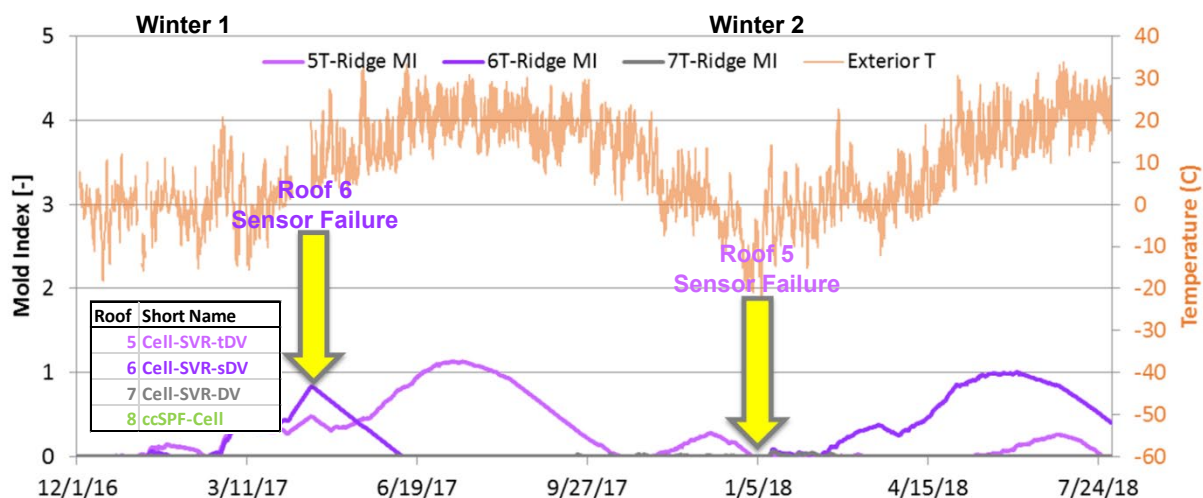
Figure 87. Cellulose roofs' (5–8) ridge mold index calculation results

The north mid-bay insulation-sheathing interface mold index results are plotted in Figure 88. RHs were higher in Winter 2 compared to Winter 1, with 90%–100% RH conditions for most of the winter. This results in higher mold index values for Roof 5 and Roof 6; however, mold index values did not exceed 1.0. The south orientation had even lower RH levels, so mold index values were not plotted.
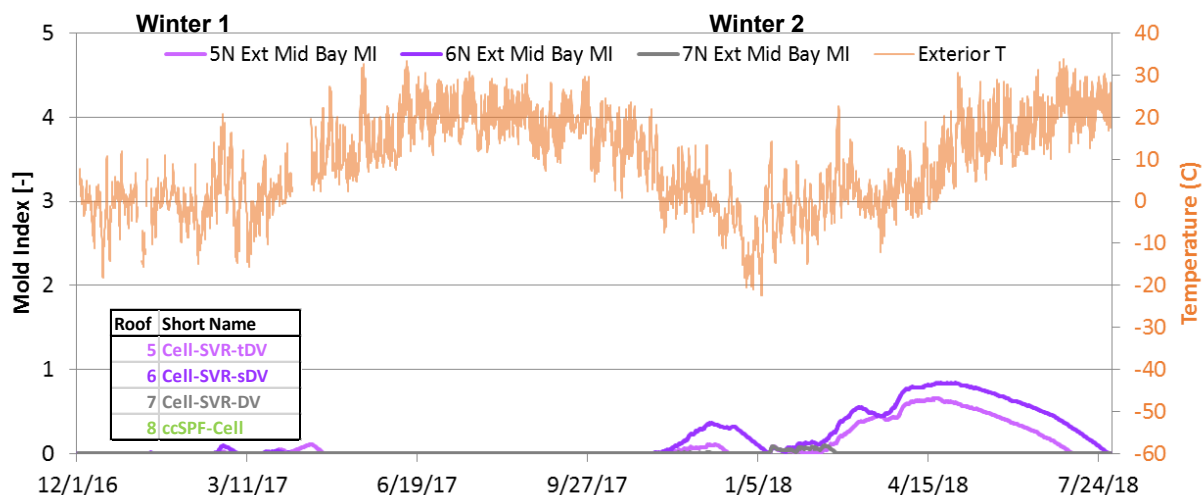
Figure 88. Cellulose roofs' (5–8) north mid-bay interface mold index calculation results

The south-side inward drive insulation-vapor retarder interface mold index results are shown in Figure 89; previous measurements demonstrated lower risks in the cellulose roofs than the fiberglass roofs. This is consistent with near-zero mold index values (peak value 0.004).
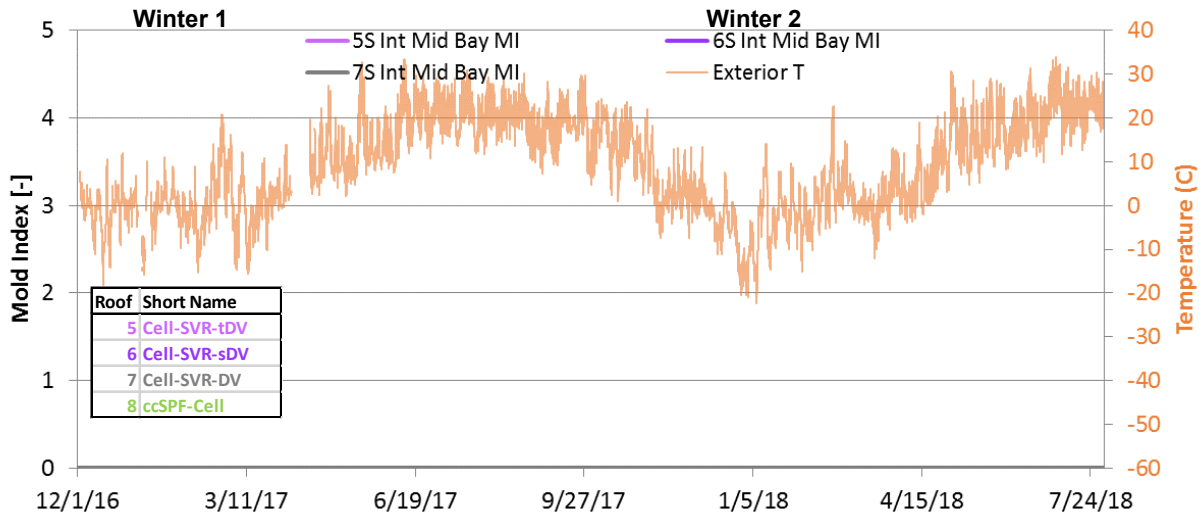
Figure 89. Cellulose roofs' (5–8) south mid-bay inward drive mold index calculation results

As discussed in the fiberglass roofs analysis, mold index values are not calculated for Winter 3, given drier/safer behavior in Winter 3. In addition, these low mold index values can be contrasted with visible mold growth found on framing and sheathing between Winters 2 and 3, per Section 14: Disassembly and Ridge Examination (Prior to Winter 3).

8 Hybrid ccSPF-Cellulose Roof Measurements

8.1 Interface Overview

Roof 8 (hybrid ccSPF-cellulose roof) had multiple instruments placed at the interface between the two insulation materials, which is the likely condensation plane for interior-sourced moisture.

These sensors included multiple T/RH and wafer sensors, placed at the ridge and mid-height in the rafter bay (Figure 90). The roof sheathing-to-ccSPF interface was covered in the previous section; this roof consistently had conditions drier than the experimental all-fiberglass and all-cellulose roofs.

Roof #	Short Name			
5	Cell-tVR-DV	Isover SVR w. DV		
6	Cell-SVR-sDV	DuPont SVR w. DV-small		
7	Cell-SVR-DV	DuPont SVR w. DV		
8	ccSPF-Cell			

Sensor Key:
- ● Relative humidity/temperature
- ■ Moisture content/temperature
- ◹ Moisture content block "wafer"
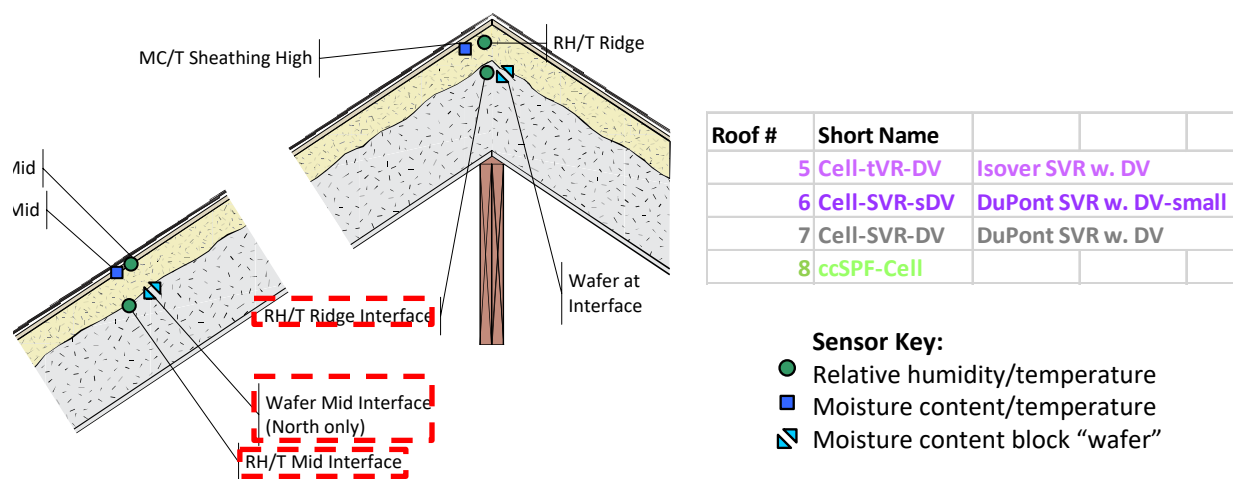
Figure 90. Hybrid ccSPF-cellulose interface measurements highlighted

8.2 Interface RH Measurements

The interface RH measurements for the north, south, and ridge are shown in Figure 91. In Winter 1, the north side and ridge have the highest RHs (with short peaks ~95% RH), and the south side has lower peaks. This matches previous measurements of moisture stratification and cooler temperatures on the north-side roof assembly. The RH levels track roughly inversely to the exterior temperature, as exterior temperature will affect interface temperature (assuming a constant interior temperature).
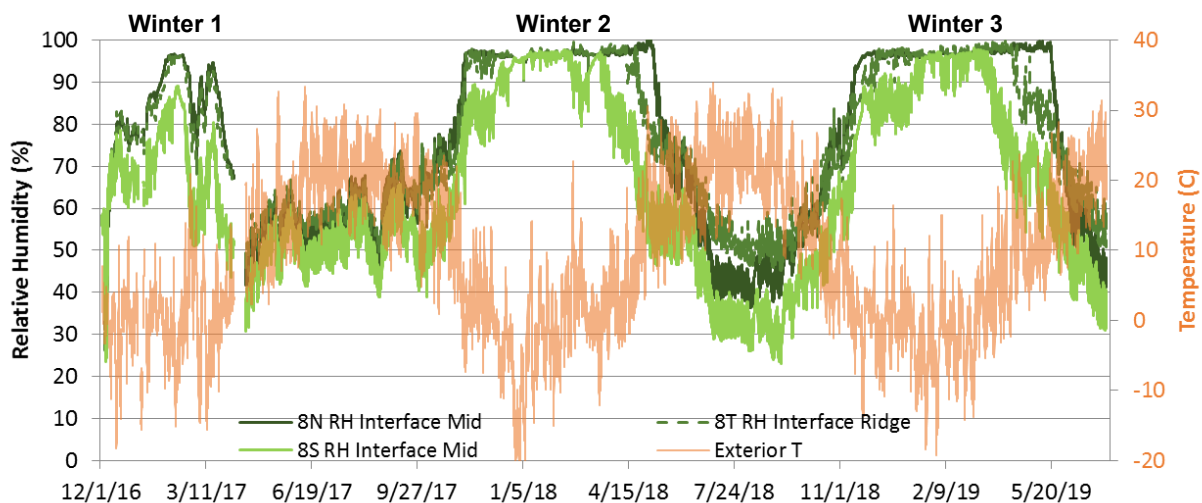
Figure 91. Hybrid ccSPF-cellulose interface RH measurements, with exterior T

However, Winters 2 and 3 (humidified 50% RH interior) resulted in higher moisture risks at the interface; RH levels rose to 95%–100% for most of the winter. RHs were highest at the ridge/peak and on the north side.

For reference, visual inspection from the interior after Winter 2 did not reveal any moisture issues from the interior (dripping or staining). Disassembly of a guard bay after Winter 2 revealed no caking or visible moisture issues at the interface (see Section 8.6: Interface Surface Examination). Interface RH levels fell rapidly (to 30%–60%) each spring as exterior temperatures warmed.

8.3 Interface Wafer Measurements

The wafer sensors at the interface (Figure 92) run roughly parallel to the RH measurements. Winter 1's maximum MCs are under 25%—far below the 100% RH or condensation range. However, in Winters 2 and 3, wafers rose over 40% MC, into the condensation risk range (BLUE). Liquid water condensation and borate contamination of the wafers likely plays a part in these high MCs.
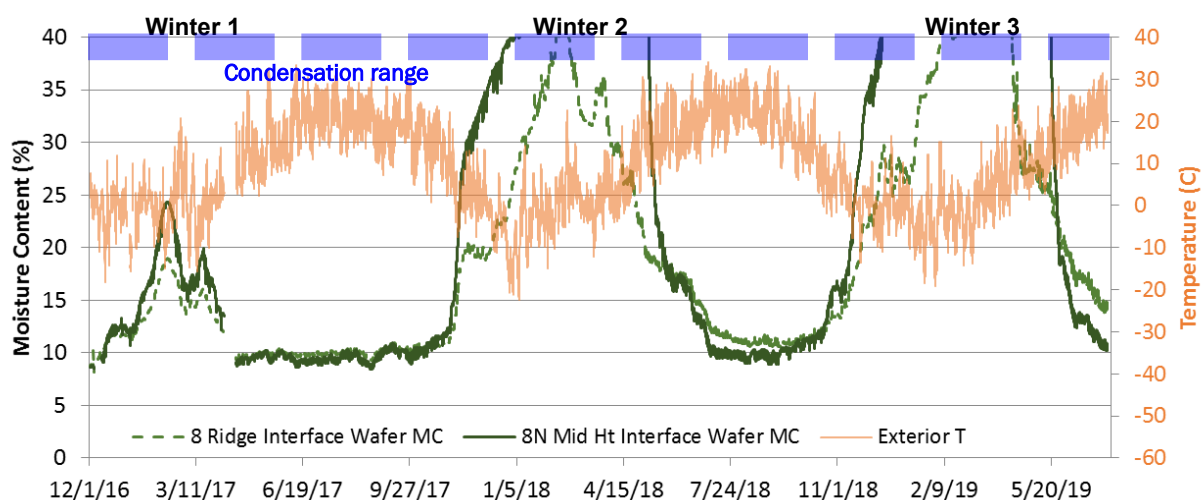
Figure 92. Hybrid ccSPF-cellulose interface wafer measurements, with exterior T

8.4 Interface-to-Dewpoint Comparison

The moisture accumulation at the interface is covered in more detail below. These graphs plot the interface temperature (at the ridge and mid-height, north/south, **GREEN**) with interior dewpoint (**RED**) for Winter 1 (Figure 93) and Winter 2 (Figure 94).

In Winter 1 (Figure 93), interior dewpoint (**RED**) mostly remained below interface temperatures (**GREEN**). When the interior dewpoint overlapped with interface temperature (late January 2017), there was a noticeable rise in RH and wafer MC (Figure 91 and Figure 92).
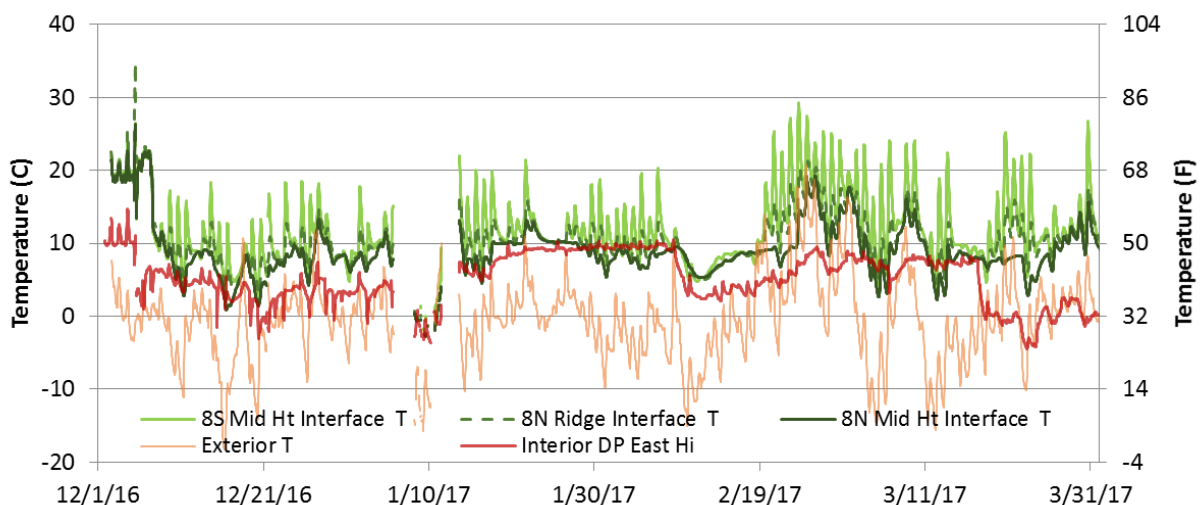
Figure 93. Hybrid ccSPF-cellulose interface Winter 1 temperature, with interior dewpoint

In contrast, in Winter 2 (Figure 94), interior dewpoint (**RED**) was higher than the interface temperatures (**GREEN**) for much of the winter, resulting in the measurements of high RH and possible condensation.
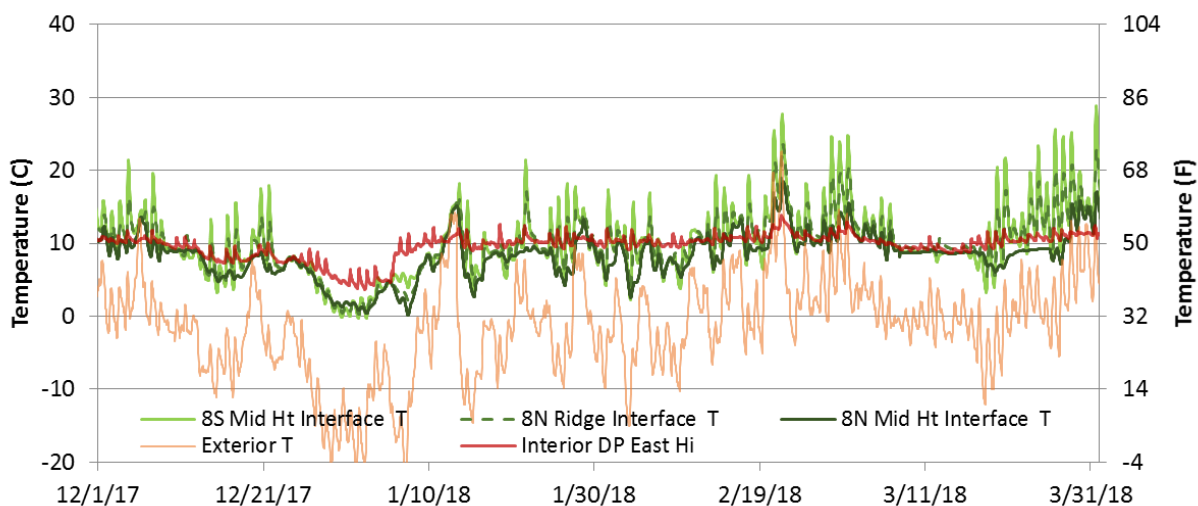
Figure 94. Hybrid ccSPF-cellulose interface Winter 2 temperature, with interior dewpoint

The interface conditions during Winter 2 and Winter 3 are shown for reference in Figure 95. With 50% RH interior conditions, the interior dewpoint was often greater than the interface temperature.
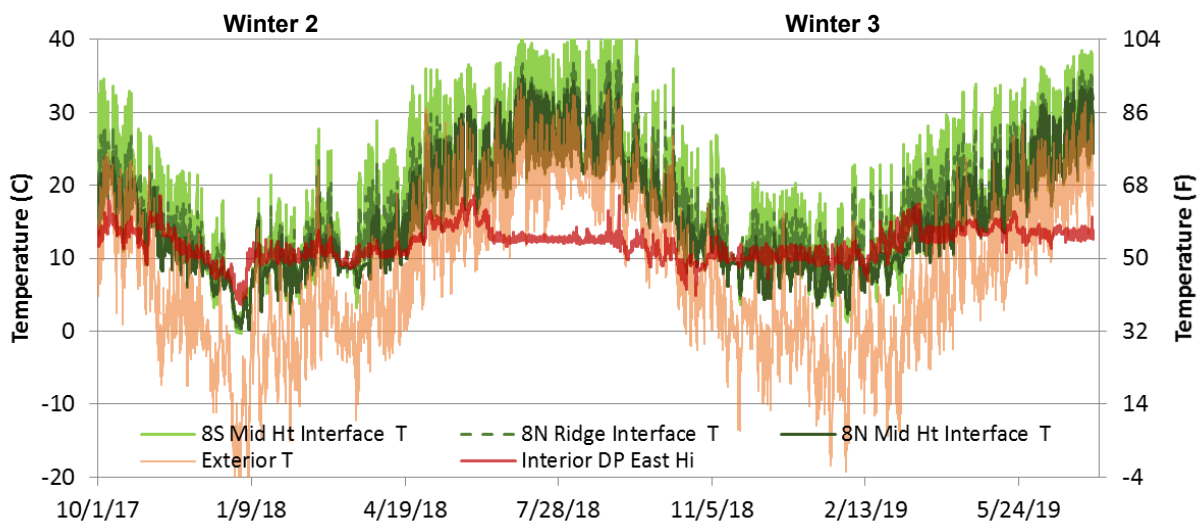
Figure 95. Hybrid ccSPF-cellulose interface Winter 2 and 3 temperatures, with interior dewpoint

8.5 Ridge Sensors and Long-Term Moisture Accumulation

The §R806.5 code-compliant hybrid ccSPF-cellulose roof (Roof 8) showed a concerning trend at one sensor over the three-year experiment: the ridge RH sensor showed a constantly increasing accumulation of moisture (Figure 70). It was unclear if this was due to sensor drift or an

indication of actual accumulation. Therefore, four sensors localized at the ridge were examined together, as shown in Figure 96.
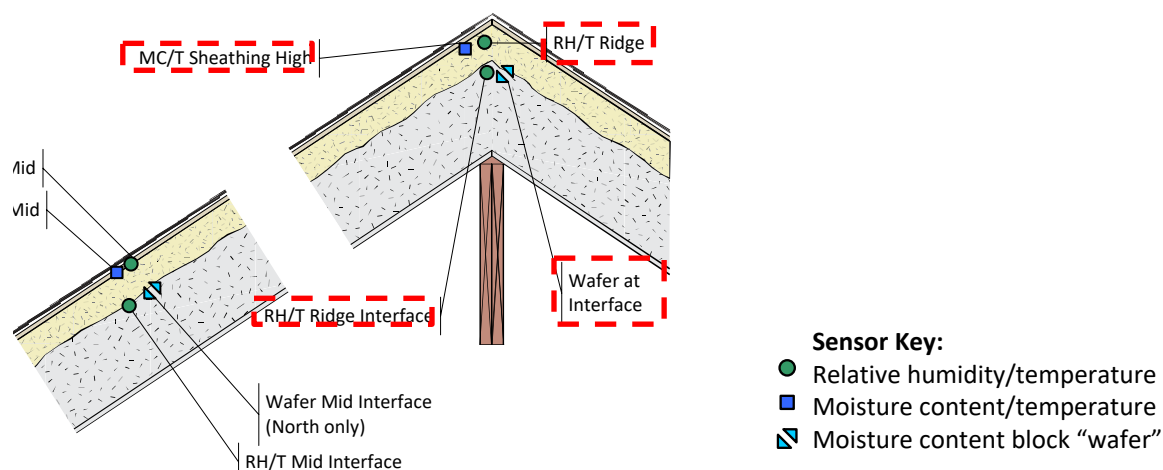
Figure 96. Hybrid ccSPF-cellulose interface measurements highlighted

The ridge RH and upper sheathing MC (north and south) are plotted together in Figure 97; these reflect moisture conditions at the ccSPF-to-sheathing interface near the roof ridge. Ridge wafer MC (cellulose-to-ccSPF conditions) is also plotted; outdoor temperature is also plotted for reference.
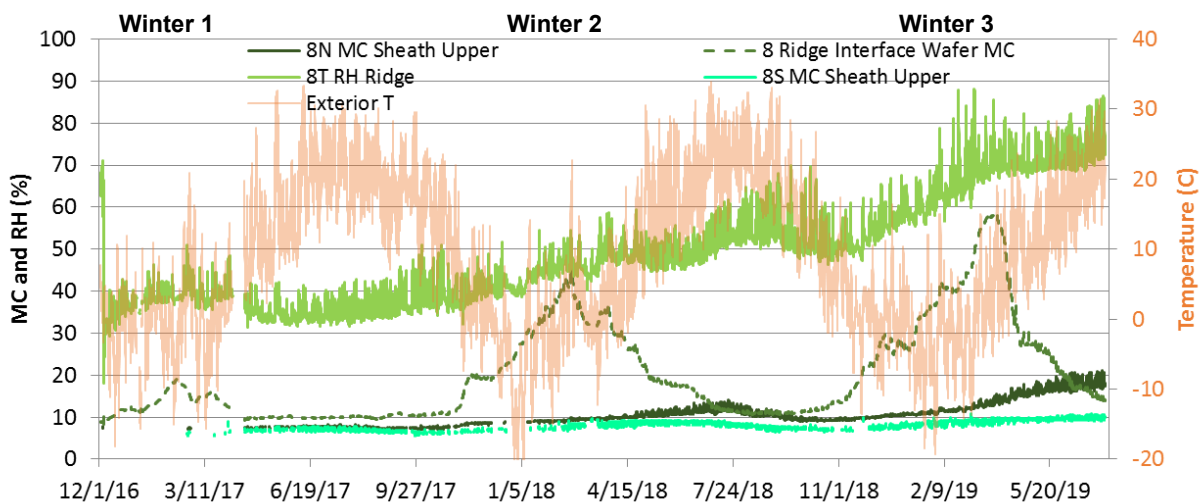
Figure 97. Hybrid ccSPF-cellulose interface RH measurements, with exterior T

The continuous increase in RH (from 30% to 80%) would result in MCs rising from roughly 6% to 16%, assuming a typical sorption isotherm; this is roughly comparable to the north sheathing upper MC patterns. However, sheathing MCs indicate generally dry conditions and low risk. Wafer and sheathing MCs are not directly comparable; the wafer has a small form factor and is not subject to the same temperature gradients as roof sheathing, and is a different wood species than those composing OSB.

Given the uncertainty of the RH sensor measurements, conditions were also measured on a "spot" basis in mid-July 2019 using a handheld temperature/RH meter (Vaisala HMI41 indicator

and HMP42 probe). Measurements were taken at multiple points at the guard bay between Roofs 6 and 7, and in Roof 8 (ccSPF/cellulose). The probe was inserted through the cellulose and into the ccSPF until hitting the roof sheathing at the ridge (Figure 98).

Figure 98. Measurement of T/RH at ridge using Vaisala probe

The Vaisala measurements showed temperatures consistent with instrumentation results, but RHs roughly 10% lower than logger data. This is consistent with the ridge RH sensor drifting upward over time. The roof ridge hits temperatures over 120°F/50°C during summertime conditions, which is a likely cause of long-term damage to sensors, especially capacitive polymer RH sensors.

8.6 Interface Surface Examination

Given the high ccSPF-cellulose interface moisture levels, conditions were visually examined at the conclusion of the experiment. The guard bay between Roofs 6 and 7 was opened and the cellulose at the ridge removed (Figure 99).
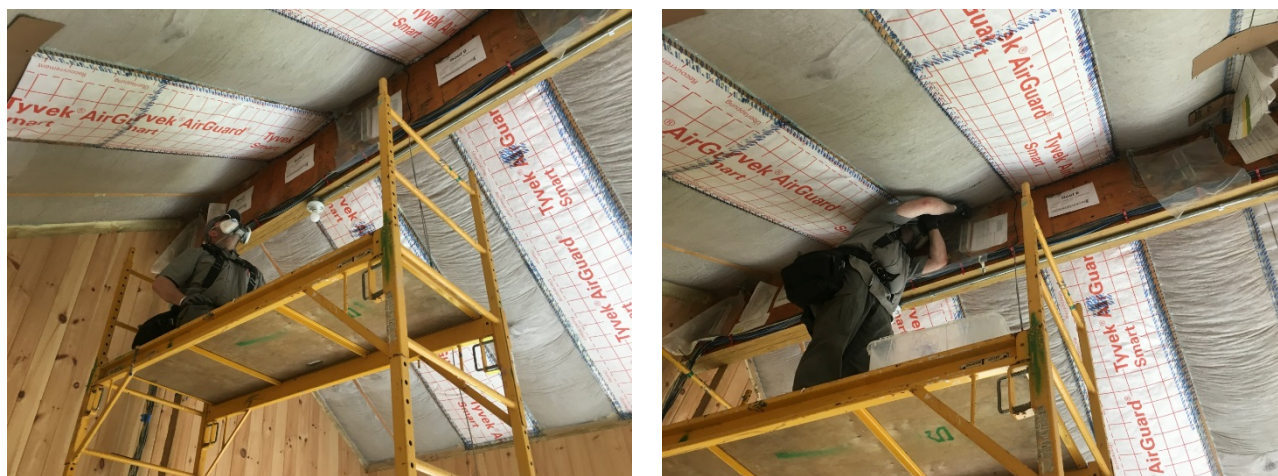
Figure 99. Cellulose insulation removal at guard bay between Roofs 6 and 7

The cellulose was not "caked" or "packy" at the ccSPF-to-cellulose interface, as would be expected after liquid water wetting. The cellulose fell away freely when removed from the netting, leaving the ccSPF exposed. There was no visual indication of mold damage or staining on the ccSPF surface. Overall, this indicates that whatever wetting occurred safely dried without creating moisture issues. No insulation voids were noted between the ccSPF and cellulose in this disassembly.

Figure 100. ccSPF surface conditions after removal of cellulose insulation

8.7 Mold Index Calculations

Mold index values were calculated for the ccSPF-cellulose interface (Figure 101); one potential risk is that warmer wintertime temperatures at this interface would be more amenable to mold growth. In Winter 1, the mold index at the north and ridge conditions remains low (well below 0.5). However, Winter 2 and the following spring showed mold index values over 3.0, in the risk range.
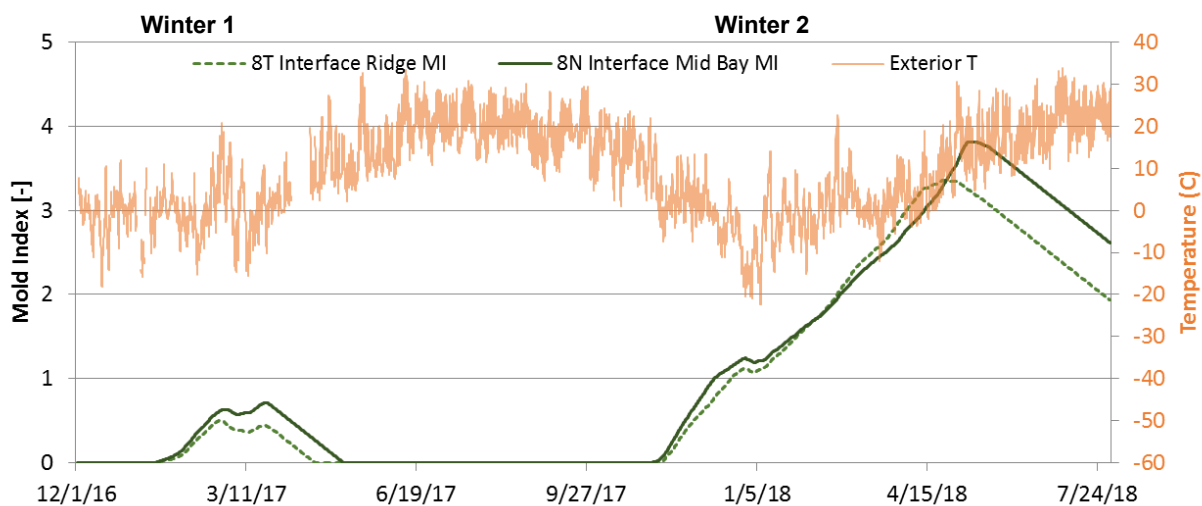
Figure 101. Hybrid ccSPF-cellulose interface mold index, with exterior T

However, direct observation of the interface (Figure 99 and Figure 100) showed no indication of mold growth. Note that in cellulose insulation assemblies, the combination of hygric storage and borate preservatives have been noted to reduce incidence of mold; the safety of this interface with other insulation materials is unknown.

9 Conclusions, Recommendations, and Further Work

9.1 Monitoring and Observation Conclusions

This research examined seven experimental unvented roofs and one code-compliant control hybrid ccSPF-cellulose roof over three winters and the following summers. Examined variables included the presence or absence of a ridge diffusion vent (vapor-open material at the roof ridge to promote drying), the effect of various interior vapor control membranes (fixed and variable permeance), the effect of interior RH, and the effect of interstitial airflow (from the interior into the cavity).

Findings from Winter 1 (2016–2017, normal 30%–40% interior RH) include the following:

- All the non-diffusion-vent roofs (Roofs 3, 4, 5, 6) reached 95%+ RH conditions at the roof ridges early in the winter, and remained at high RH levels (95%–100%) for most of the winter, only showing significant drying in spring. Wafer sensors indicated liquid water condensation at the ridge. High sheathing MCs were measured near the ridge, with less-risky conditions at lower and south-facing sheathing locations.

- Despite these indications of problems in the roofs, mold index values remained below 3.0 (failure threshold of visible mold without magnification).

- The roofs with a variable-perm vapor retarder and a diffusion vent (Roofs 2 and 7) showed much safer performance: Winter 1 data for these roofs indicated the lowest moisture accumulation out of all the roofs, with no measurements going over danger thresholds.

Findings from Winter 2 (2017–2018, addition of 50% interior RH humidification) include the following:

- Based on the poor performance of the non-diffusion-vent roofs, they were eliminated in Winter 2, and replaced with the small and tight diffusion vent roofs.

- Higher interior RH levels resulted in worse moisture performance across all roofs; all were at higher risks than Winter 1, with evidence of condensation at the ridges of all roofs. This included Roofs 2 and 7, which showed acceptable behavior in Winter 1. The exception was the code-compliant flash-and-blow roof (Roof 8), which showed few signs of durability risks.

- The data also demonstrated that the 25-perm (lower-permeance) tight diffusion vent did not provide adequate drying, and was the worst outlier in terms of moisture accumulation.

- Mold index calculations remained below 3.0 in Winter 2's data. However, ridge disassembly in summer 2018 revealed mold spotting on sheathing and framing in all fibrous insulation roofs, with some of the worst damage in the tight diffusion vent roofs.

- In addition, the cellulose roofs showed full-length settling at the north-side rafter bays, which created an airflow pathway for any interior-sourced moisture entering the rafter cavities. The fiberglass roofs showed limited settling near the ridge. All roofs were reinsulated between winters, with a complete and dense rafter cavity fill.

Findings from Winter 3 (2018–2019, 50% RH indoors, addition of air leakage in late winter/February 2019) include the following:

- Based on the poor performance of the tight diffusion vent roofs, they were eliminated in Winter 3 and replaced with full-size diffusion vents with an alternate interior variable-perm vapor barrier.

- Interior conditions were first run at 50% RH without air injection, which is identical to Winter 2's conditions. All roofs demonstrated less moisture accumulation than Winter 2, remaining below risk thresholds. This likely demonstrates the effect of suppressing airflow with a complete cavity fill (elimination of air voids due to insulation settling).

- This finding from early Winter 3 indicates that these unvented fibrous insulation roof assemblies can function with acceptable moisture risks even at high (50%) interior RH levels, if insulation is installed in a mostly void-free and high-density manner. This is consistent with Hulstrunk (2020), who noted that unvented cellulose roof failures are associated with lower packing density, and that higher insulation densities (4 PCF or higher) are required for deep rafter cavities. Consistently assuring this level of quality in field installations may be difficult to achieve; this is especially critical given that the roof assembly relies on suppressing airflow to function in a moisture-safe manner. Furthermore, the voids that appeared in the cellulose roof north bays occurred after Winter 1; this was likely settling due to humidity fluctuations. Unfortunately, this means that moisture safety is not assured unless this humidity-based settling phenomenon can be eliminated.

- Interior air was injected into north-side roof cavities in late winter; the system induced a small (~0.5 CFM) leak, which is consistent with a small imperfection in relatively airtight construction. This resulted in severe localized wetting (30%–40% MC maximums), which is a risk range for mold growth and decay. These high MCs were seen at the low- and mid-height roof locations on the north side. However, disassembly during the following summer showed no indication of moisture distress at the sheathing, including mold growth, staining, or physical damage. One possible explanation is that this roof OSB formulation uses a significant fraction of MDI (methyl diisocyanate) resin adhesive, which is known to improve moisture resistance, and is anecdotally reported to improve mold resistance (Davidovic 2019).

- Mold index values were not calculated for Winter 3's data, given the drier conditions than Winter 2, which showed no mold risks (below 3.0).

Other observations that apply over multiple winters include:

- Inward vapor drives were found to be a non-issue with any roofs with variable-perm interior air and vapor control layers. The only issue found with inward vapor drives was liquid water condensation near the ridge at the fixed-perm (1 perm) fiberglass roofs.

When fiberglass and cellulose roofs were compared, there was a general trend of the cellulose roofs damping moisture extremes (both wintertime and summertime) due to hygric storage. For instance, inward drive issues were insignificant in the cellulose roofs due to adsorption of moisture in the cellulose. As discussed in Section 12.4: Fiberglass vs. Cellulose Sorption Isotherms, cellulose moisture storage is over an order of magnitude higher than fiberglass at higher RH conditions on a weight basis. Accounting for installed insulation density, the actual hygric storage is closer to a factor of 30.

- The §R806.5 code-compliant hybrid ccSPF-cellulose roof (Roof 8) consistently showed safe behavior compared to the experimental fiberglass and cellulose roofs. There were some measurements indicating a constantly increasing ("ratcheting") ridge RH; however, based on comparisons with other sensors and handheld instruments, this was ascribed to sensor drift.

- However, one challenge in the hybrid ccSPF-cellulose assembly was moisture accumulation at the ccSPF-to-cellulose interface. Minimal moisture accumulation occurred in Winter 1 (30%–40% interior RH), but substantial accumulation and potential mold risks occurred during Winters 2 and 3 (50% interior RH). Note that this assembly has no interior air barrier or Class III (1–10 perm) vapor control, so this interface is exposed to interior vapor flows. However, disassembly of the interface found no adverse effects, such as cellulose "caking," staining, or microbial growth. This indicates that whatever moisture accumulation occurred at this interface could dry downward in warmer weather without issues.

- All of this research was done using dark-colored roof shingles; lighter-colored roofs have been linked with moisture-related failures due to lower temperatures and less inward solar drying. The north-facing roof still had significant summertime solar gain (peak values ~550 W/m^2). Lighter-colored roofing would make these assemblies more vulnerable to wintertime moisture accumulation.

9.2 Takeaway Recommendations

Based on this research, unvented all-fibrous insulation assemblies have greater moisture risks than current code-compliant air impermeable insulation or exterior insulation assemblies. These fibrous insulation-only unvented roofs can function in a moisture-safe manner, especially with measures that increase their drying (ridge-top diffusion vent and variable-perm interior vapor retarder), or either at lower interior RH levels or with a complete cavity fill. However,

widespread adoption of unvented fibrous roof assemblies will likely result in an unacceptable failure rate. In addition, air injection indicated that the assemblies are still highly vulnerable to small air leaks (0.5 CFM), which resulted in significant localized sheathing moisture uptake.

Finally, the high moisture accumulation and visible mold growth seen in the test roofs after Winter 2 (despite mold index values in the safe range) indicate that these roofs can have significant moisture risks at high interior RH levels.

As a result, it is difficult to recommend these experimental all-fibrous insulation assemblies for any application that might experience high wintertime humidity levels. Although wintertime humidity levels in cold climate are commonly in the 30% RH or lower range, inadvertent operation at 40%–50% RH in winter is becoming more common. This occurs in modern construction with greater airtightness, low outdoor air change rates, and in particular, buildings with high occupant densities (e.g., multifamily construction). Given these risks, acceptance of these assemblies for general use and code acceptance is not recommended.

9.3 Construction Recommendations (§R806.5 Compliant Options)

If a project goal is to eliminate the use of plastic foam materials in roof assemblies, non-foam roofs can be built while still complying with IRC §R806.5. These roofs would include non-foam continuous exterior insulation (e.g., semi-rigid mineral fiber, wood fiberboard) outboard of the roof structural sheathing and air barrier and rafter cavity fibrous insulation (Figure 102). The ratio of exterior insulation to interior (rafter cavity) insulation must comply with the ratios provided in §R806.5, per climate zone.

In addition, fibrous insulation roof assemblies that use a waterproof but vapor-open membrane on the outboard side of the insulation, adjacent to a ventilated air cavity, have been documented to have very safe long-term moisture performance (Corson 2015, Figure 103).
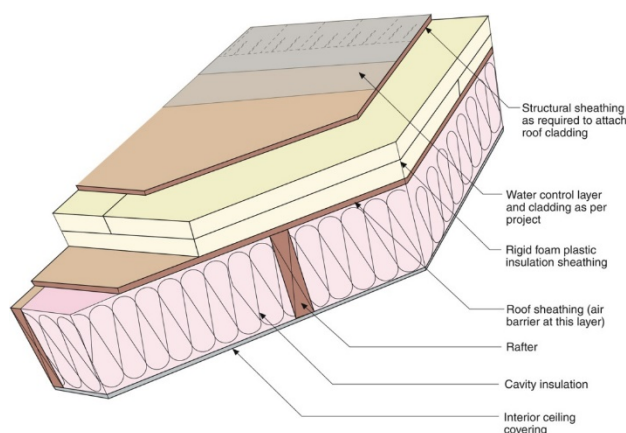
Figure 102. Unvented roof assembly with exterior rigid insulation per IRC §R806.5
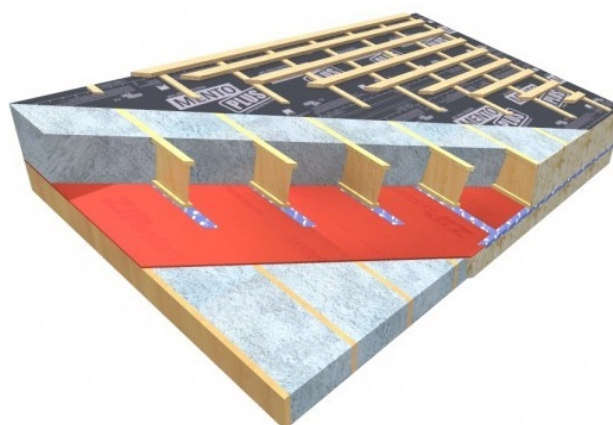
Figure 103. Fibrous insulation roof assembly with ventilated cavity above (Corson 2015)

9.4 Construction Recommendations (Non-Code-Compliant Systems)

Unvented fibrous roof assemblies might be useful in retrofit situations where a failing assembly must be addressed, but interior/exterior demolition followed by code-compliant assemblies (polyurethane spray foam and/or exterior rigid insulation overclad) is not a realistic, affordable, or acceptable option. Unfortunately, there is no code provision allowing "use only to address existing failing assemblies."

If the goal is to implement these unvented fibrous roof assemblies in cold climates with the least moisture risk, the following items are recommended:

- Ensure low wintertime relative humidities (~30% RH) for the life of the building. As discussed, this may be difficult to ensure in practice, especially in high-performance (low air leakage) buildings and multifamily or high occupant density construction. Controlled mechanical ventilation systems are required to control interior humidity levels in winter, and can be disabled by occupants or become non-functional due to poor maintenance.

- Airtightness of the interior air and vapor control layer must be ensured and tested. As demonstrated during Winter 3, small air barrier imperfections and airflows can have a significant impact on sheathing MC.

- A variable-perm air-vapor retarder should be used to allow for one avenue of drying of the assembly. Roof exterior waterproof underlayments and claddings generally have very low vapor permeance, allowing for no effective outward drying. The fixed 1-perm vapor retarder showed condensation during summertime inward vapor drive events, and more importantly, only allows minimal inward drying. Commercially available variable-perm vapor retarders allow much greater inward drying (e.g., 10+ perms at 90%+ RH, Figure 21).

- A large ~300 perm ridge diffusion vent should be used. This research has not quantified go/no-go diffusion vent dimensions, but a recommended level is a ~6-in. opening, which fits under commercially available asphalt shingle ridge vents, or larger. This is intended to apply to residential-scale roofs, rather than large commercial sloping roofs where this opening would be disproportionately small.

- The fibrous insulation must be installed in a manner that eliminates voids and empty cavities; as discussed previously, this may be difficult to ensure consistently in the field, especially given in-service insulation settling problems over time.

- Light-colored roof membranes and shading (from adjacent obstructions or rooftop solar arrays) will reduce roof temperatures and solar drying of the roof. Either of these will increase risks of moisture accumulation in these assemblies.

9.5 Further Work

Overall, this research has run fibrous insulation unvented roof assemblies through a variety of conditions and exposures, with multiple vapor control materials and details. Further research on this topic may be of limited value, given the demonstrated moisture risks of these assemblies. A possible exception might be monitoring of roofs with an exterior vapor-permeable membrane and a ventilated cavity above the fibrous insulation, although previous work (Corson 2015) found low risks.

Another potential research topic is the retrofit of "story and a half" or Cape Cod-style houses, where the living space is enclosed within the sloping roof/ceiling assembly (Figure 104). This results in roughly 4-ft-tall kneewalls, and portions of sloping ceiling, topped by a small attic. Figure 105 shows typical conditions in this type of kneewall attic geometry.
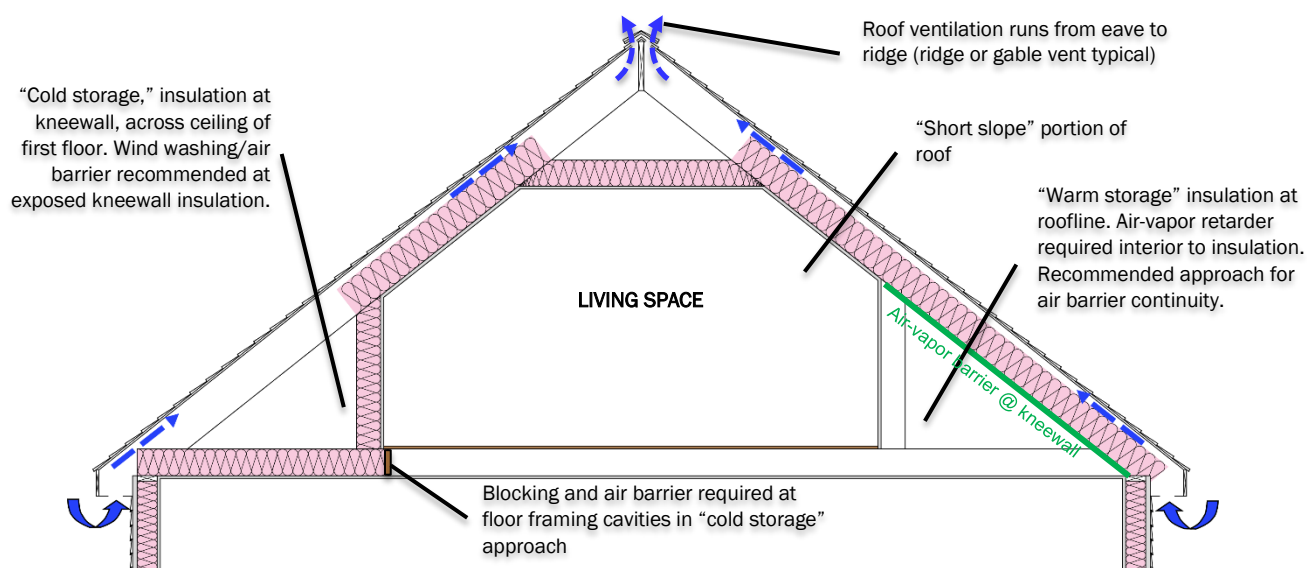
Figure 104. Story and a half (Cape Cod house) geometry and insulation options (kneewall left, roofline right)

Background on the problems associated with air sealing and insulating these geometries are covered by Holladay (2015). Typical solutions for the lower triangular attic include insulating at the first floor ceiling and kneewall, with associated air sealing details ("cold storage" per Figure 104, left, and Figure 105, left), or insulating at the roofline ("warm storage" per Figure 104, right). The "warm storage" option (insulation at roofline) is the recommended approach for superior air barrier continuity.

Figure 105. Attic kneewall area (left) with polystyrene vent chute over fiberglass batt insulation (right)

In both cases, at the sloping "compact" roof-ceiling assembly (referred to as the "short slope"), code compliance requires the installation of a ventilation air space or chute (1-in. minimum per IRC/ICC 2012b, and shown in Figure 105, right). This clear airspace is difficult to retrofit in long thin roof cavities without interior demolition, and it reduces R-value in typically limited-depth roof framing (commonly 2x6 to 2x8).

Based on this research, it may be possible to use blown-in insulation in this "short slope" roof/ceiling assembly but omit the ventilation chute, resulting in a short section of unvented roof. Sheathing MCs in this research indicated that high MCs occurred near the ridge, but safe conditions occurred at lower portions of the slope. This "short slope" Cape Cod geometry is equivalent to the "lower half of the roof," with what is effectively an unrestricted vapor diffusion port the size of the rafter bay into the upper vented attic.

This technique has been used by multiple weatherization practitioners in various regions without reported callback issues. These locations are known to include upstate NY (Kornbluth 2019), Minnesota, and Massachusetts.

A study of Minnesota homes weatherized during airport sound insulation (Bohac and Cheple 2002) included inspections of retrofitted attics for moisture damage. A research team member from that work (Fitzgerald 2019) mentioned that more than 10,000 existing homes have been weatherized with a "short slope" dense pack retrofit, starting in the early 1990s, and moisture issues at this geometry were not noted in return visits. CLEAResult (formerly Conservation Services Group/CSG), in partnership with Mass Save (Massachusetts energy efficiency organization funded by utility providers), has proposed a state building code change allowing this type of unvented roof retrofit in a short (8 ft or less) sloped assembly. Their supporting evidence included the fact that this retrofit has been implemented for roughly three decades on thousands of homes in Massachusetts with no known issues (Harley 2011).

A field monitoring study deploying this retrofit and comparing various geometries, materials, and interior conditions would provide the most robust demonstration of this technique's safety.

References

475 High Performance Building Supply. 2015. "Unvented Foam-Free Roof Retrofit with Dolphin Insulation." https://foursevenfive.com/blog/unvented-foam-free-roof-retrofit-with-dolphin-insulation/.

475 High Performance Building Supply. 2016a. "INTELLO & DB+ Approved by DIBt for Use in Unvented Hot Roof Assemblies." https://foursevenfive.com/blog/intello-db-approved-by-dibt-for-use-in-unvented-hot-roof-assemblies/.

475 High Performance Building Supply. 2016b. "The 8 Golden Rules for Foam-Free Unvented Asphalt Shingled Roofs." https://foursevenfive.com/blog/the-eight-golden-rules-for-foam-free-unvented-asphalt-shingled-roofs/.

ASHRAE. 2009a. *2009 ASHRAE Handbook—Fundamentals*. Atlanta, GA.

ASHRAE. 2009b. *ASHRAE Standard 160-2009—Criteria for Moisture-Control Design Analysis in Buildings (ANSI/ASHRAE Approved)*. Atlanta, GA.

ASHRAE. 2016. *ANSI/ASHRAE Addendum e to ANSI/ASHRAE Standard 160-2009—Criteria for Moisture-Control Design Analysis in Buildings*. Atlanta, GA.

Bohac, D. and M. Cheple. 2002. "Ventilation and Depressurization Information for Houses Undergoing Remodeling." Report for Minnesota Department of Commerce, State Energy Office, DE-FG45-96R530355, by Center for Energy and Environment.

Carll, C.G.; Highley, T.L. 1999. "Decay of Wood and Wood-Based Products Above Ground in Buildings. *Journal of Testing and Evaluation* 27(2):150–158.

Corson, C. 2015. "Super Insulated Walls and Moisture: Does Bad Stuff Happen?" Northeast Sustainable Energy Association Building Energy Conference 2015 (BE15). March 4, 2015. https://www.nesea.org/sites/default/files/session-docs/super_insulated_walls_and_moisture_corson.pdf.

Davidovic, D. 2019. Building Science Manager at Huber Engineered Woods. Personal communication.

Derome, D. 2005. "Moisture Accumulation in Cellulose Insulation Caused by Air Leakage in Flat Wood Frame Roofs." *Journal of Thermal Envelope and Building Science*, Vol. 28, No. 3.

Desmarais, G, Derome, D. and Fazio, P. 2000. "Mapping of Air Leakage in Exterior Wall Assemblies." *Journal of Thermal Envelope and Building Science*. Vol. 24.

Fitzgerald, J. 2019. Senior Building Analyst, Minnesota Center for Energy and the Environment. Personal communication.

Fox, M. 2014. "Hygrothermal Performance of Highly Insulated Wood Frame Walls with Air Leakage: Field Measurements and Simulations." Master of Applied Science Thesis, Ryerson University. http://digital.library.ryerson.ca/islandora/object/RULA%3A2603/datastream/OBJ/download/Hygrothermal_performance_of_highly_insulated_wood_frame_walls_with_air_leakage___field_measurements_and_simulations_.pdf.

Harley, B. 2011. "Technical Bulletin: Dense-packing vs. Venting of Sloped Roofs." Conservation Services Group, September 28, 2011.

Holladay, M. 2015. "Insulating a Cape Cod House: Capes are notoriously difficult to air seal and insulate." *Green Building Advisor*, December 11, 2015, https://www.greenbuildingadvisor.com/article/insulating-a-cape-cod-house.

Hulstrunk, B. 2020 "Dense-Packing Unvented Roofs." *Journal of Light Construction*, July-August 2020.

ICC. 2007. *Excerpt from the 2007 Supplement International Residential Code*. Country Club Hills, IL: International Code Council.

ICC. 2012a. *2012 International Energy Conservation Code*. Country Club Hills, IL: International Code Council.

ICC. 2012b. *2012 International Residential Code*. Country Club Hills, IL: International Code Council.

Janssens, A. and Hens, H. 2003. "Interstitial Condensation Due to Air Leakage: A Sensitivity Analysis." *Journal of Thermal Envelope and Building Science.*, Vol. 27, No. 1.

Kalamees, T., and Kurnitski, J. 2010. "Moisture Convection Performance of External Walls and Roofs." *Journal of Building Physics*, Vol. 33, No. 3.

Kornbluth, D., 2019. Dick Kornbluth, LLC, Building Performance Institute Board Member. Personal communication.

Lawrence Berkeley National Laboratory (LBNL). 2012. THERM 6.3 Two-Dimensional Building Heat-Transfer Modeling Software.

Lstiburek, J. 2015. "Building Sciences: WUFI*: Barking Up the Wrong Tree?." *ASHRAE Journal*, October, pp. 62–70, Atlanta, GA: ASHRAE. https://www.buildingscience.com/documents/building-science-insights-newsletters/bsi-089-wufi%E2%80%94barking-wrong-tree.

Lstiburek, J. 2018. "Building Sciences: Doubling Down-How Come Double Vapor Barriers Work?" *ASHRAE Journal*, January, pp. 52–59, Atlanta, GA: ASHRAE, Inc.

https://www.buildingscience.com/documents/building-science-insights-newsletters/bsi-092-doubling-down%E2%80%94how-come-double-vapor-barriers.

Marra, A. 1992. *Technology of Wood Bonding: Principles in Practice.* New York, NY: Van Nostrand Reinhold.

Ojanen, T. and Kumuran, K. 1996. "Effect of Exfiltration on the Hygrothermal Behaviour of a Residential Wall Assembly." *Journal of Thermal Insulation and Building Envelope*. Volume 19.

Ojanen, T., H. Viitanen, R. Peuhkuri, K. Lähdesmäki, J. Vinha, and K. Salminen. 2010. "Mold growth modeling of building structures using sensitivity classes of materials." Thermal Performance of the Exterior Envelopes of Buildings XI International Conference, Clearwater Beach, FL.

Salonvaara, M., Karagiozis, A., and Desjarlais, A. 2013. "Moisture Performance of Sealed Attics in Climate Zones 1 to 4." Proceedings: Thermal Performance of the Exterior Envelopes of Buildings XII. Atlanta, GA: ASHRAE.

Straube, J., Onysko, D., and Schumacher, C. 2002. "Methodology and Design of Field Experiments for Monitoring the Hygrothermal Performance of Wood Frame Enclosures." *Journal of Thermal Envelope and Building Science*, 26(2).

Straube, J., E. Burnett. 2005. *Building Science for Building Enclosures*, Building Science Press, Westford, MA.

TenWolde, A., Carll, C., Malinauskas, V. 1998. "Air Pressures in Wood Framed Walls." *Thermal Envelopes VII*. Clearwater, FL. https://www.fs.usda.gov/treesearch/pubs/5950.

Trainor, T. 2014. "The Hygrothermal Performance of Exterior Insulated Wall Systems." Master of Applied Science Thesis, University of Waterloo. https://uwspace.uwaterloo.ca/handle/10012/8550.

Ueno, K., and Straube, J. 2008. "Laboratory Calibration and Field Results of Wood Resistance Humidity Sensors," *Proceedings of BEST 1 Conference*, Minneapolis, June 10–12, 2008.

Ueno, K. 2015. "Monitoring of Double-Stud Wall Moisture Conditions in the Northeast." Building Science Corporation for the U.S. Department of Energy Building America Program. DOE/GO-102015-102015-4589. https://www1.eere.energy.gov/buildings/publications/pdfs/building_america/monitoring-doublestud-wall-northeast.pdf.

Ueno, K., and J. Lstiburek. 2015. "Field Testing Unvented Roofs with Asphalt Shingles in Cold and Hot Humid Climates." Building Science Corporation for the U.S. Department of Energy Building America Program. DOE/GO-102015-4705.

https://www1.eere.energy.gov/buildings/publications/pdfs/building_america/unvented-roofs-asphalt-shingles-cold-hothumid.pdf.

Ueno, K., and J. Lstiburek. 2016a. "Field Testing of an Unvented Roof with Fibrous Insulation, Tiles, and Vapor Diffusion Venting." Building Science Corporation for the U.S. Department of Energy Building America Program. DOE/GO-102016-4764. https://www1.eere.energy.gov/buildings/publications/pdfs/building_america/64999.pdf.

Ueno, K., and J. Lstiburek. 2016b. "Monitoring of Two Unvented Roofs with Air-Permeable Insulation in Climate Zone 2A." Thermal Performance of the Exterior Envelopes of Whole Buildings XIII International Conference. Atlanta, GA: ASHRAE, Inc.

Appendices

In order to limit the size of the main body of the report and improve its narrative flow, detailed explanations of field observations and equipment are covered in the following appendices.

10 Instrumentation and Roof Thermal Simulations

10.1 Testing and Monitoring Equipment

The testing and monitoring equipment used in this project is described in Table 11.

Table 11. Testing and Monitoring Equipment Specifications

Measurement	Equipment and Specifications
Temperature	Negative temperature coefficient thermistor, 0.1°C (±0.2°F)
RH	Thermoset polymer capacitive RH sensor, ±3.5% RH
Wood MC	Electric resistance-based MC pin sensors (per Straube et al. 2002; calculation of uncertainty is presented in Ueno and Lstiburek (2016a)
Data Acquisition and Collection	Campbell Scientific CR1000 measurement and control system with Campbell Scientific AM16/32B Multiplexers
Outdoor Temperature/RH	Campbell Scientific HMP60-L -40°C to +60°C (-40°F to 140°F) range; 0.6°C (±1.1°F) accuracy; RH accuracy at 0° to +40°C (32° to 104°F): ±3% RH (0%–90% RH); ±5% RH (90%–100% RH); RH accuracy at -40° to 32°F (-40°to 0°C) and +40° to +60°C (104° to 140°F): ±5% RH (0%–90% RH); ±7% RH (90%–100% RH)
Infrared Observation	FLIR ONE Infrared Camera (-20°C to 120°C [-4°F to 248°F] temperature range; 0.1°C [0.18° F] resolution)
Air Leakage	The Energy Conservatory Minneapolis Duct Blaster Series B Fan 10 to 1500 CFM (Ring 3/Open) Flow Accuracy: ±3% of reading or ±1 CFM, whichever is greater, with DG-700
ΔP Measurement	The Energy Conservatory DG-700 Pressure and Flow Gauge –1,250 to +1,250 Pa. Accuracy: 1% of pressure reading or 0.15 Pa, whichever is greater
Airflow Velocity and Temperature	Fieldpiece Model STA2 In-Duct Hot Wire Anemometer Temperature Range: -4°F to 140°F (-20°C to 60°C) Resolution: 0.1°C, 0.1°F; Accuracy: ±1.0°F for 32°F to 113°F Velocity Resolution: 1 fpm (0.01 m/s) Range: 40–3960 fpm (0.20–20.00 m/s) Accuracy: ± (5%+1 dgt) reading or ± (1%+1dgt) full scale
Temperature and RH	Vaisala HMI41 indicator and HMP42 probe Temperature Accuracy: ±0.2°C at 20°C RH Accuracy: ±2% (0%–90% RH); ±3% (90%–100% RH)

10.2 Sensor Count Listing

A table with the sensor count is provided in Table 12, divided into numbers of RH/T, MC/T, wafer MC sensors, T (green, blue, and orange text), and channel counts (in black). Several temperature sensors ("T Alone") are marked as -1 in the table; this signifies redundant

temperatures (e.g., T/MC and T/RH in same location), where only one temperature sensor will be connected to the logger.

The number of required temperature channels (69) exceeds the available channels on multiplexers (64). These excess temperature sensors were run to the data logger (CR1000), but redundant temperature sensors were omitted.

Table 12. Roof Sensor/Instrumentation Listing

#	Name	RH/T	MC/T	Wafer MC only	T Alone		RHs	MCs	Ts
Roofs 1-7	Ridge Package	1	0	1	-1		1	1	0
	Sheathing Sensors, North	1	3	0	-1		1	3	3
	Sheathing Sensors, South	1	3	0	-1		1	3	3
	Interior Sensors, North	1	0	0	0		1	0	1
	Interior Sensors, South	1	0	1	0		1	1	1
	Multiply by 7 roof bays	**35**	**42**	**14**	**-21**		**35**	**56**	**56**
Roof 8	Ridge Package	2	0	1	-1		2	1	1
	Sheathing Sensors, North	1	3	0	-1		1	3	3
	Sheathing Sensors, South	1	3	0	-1		1	3	3
	Interior Sensors, North	1	0	1	0		1	1	1
	Interior Sensors, South	1	0	0	0		1	0	1
Interior T/RH	2 locations, high and low, 4 total	4					4		4
Project Total		45	48	16	-24		45	64	69
						# Ch Avail	64	64	64

10.3 Roof Assembly Thermal Simulations

One issue raised by a team member was that the guard and experimental bays have different R-values, ranging from R-52 (cellulose) to R-63 (flash-and-blow cellulose/ccSPF hybrid). This difference might affect experimental roof sheathing temperatures.

Two-dimensional thermal simulations were run to determine the effect of these R-value differences. THERM 6.3 (LBNL 2012) Two-Dimensional Building Heat-Transfer Modeling Software was used on a section of roof. Note that this is a steady-state software package, so it does not capture dynamic effects, thermal mass, or any solar gain effects.

The simulated roof assembly includes two experimental and three guard bays, as shown in Figure 106; the ccSPF and cellulose ratio shown in the guard bays match installed thicknesses.
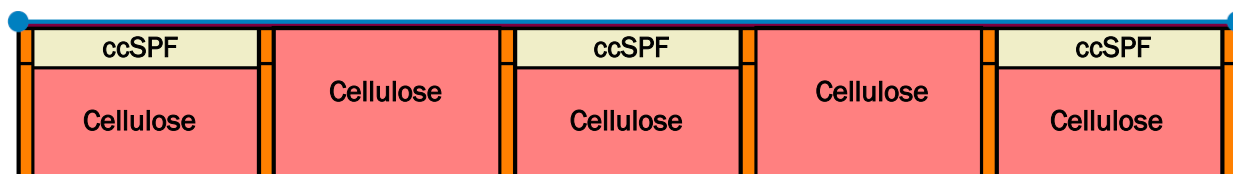
Figure 106. Roof insulation THERM simulation, showing assembly

Boundary conditions were set at 69.8°F interior and -0.4°F exterior. The resulting temperatures are shown in Figure 107. These results demonstrate that there is insignificant influence of the differing insulation materials on middle-of-bay conditions, where instrumentation is located. Despite the difference in R-values, there is a minimal difference in sheathing temperatures between the bay types, even at these extreme temperature conditions. Of course, sheathing temperature variation will be smaller at lower temperature differences (ΔTs).
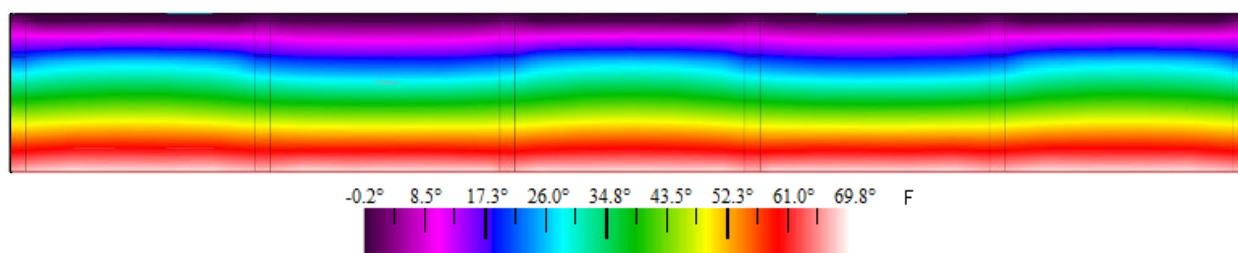
Figure 107. Roof insulation THERM simulation, showing temperatures, with temperature key

Heat flux is shown in Figure 108; as would be expected, guard bays have lower heat flux than experimental (cellulose) bays, and framing has significantly higher heat flux (thermal bridging).
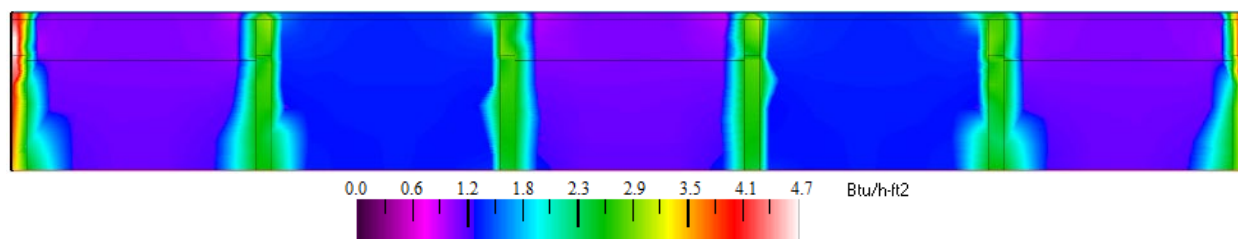
Figure 108. Roof insulation THERM simulation, showing heat flux, with flux key

The high heat flux seen at the left and right edges of the simulation (white/red colors) are simulation artifacts caused by the use of adiabatic conditions at those edges.

The greater heat flow at the framing is also evident in wintertime snow melt patterns (Figure 109), showing thermal bridging (and greater melting) at the rafters. In addition, there is clear lack of melting at the portions of the roof over unconditioned space (eave and rake end overhangs).

Figure 109. Snow melt patterns on north-facing roof, showing rafter thermal bridging

11 Commissioning Testing (Prior to Winter 1)

11.1 Commissioning Testing Overview

As part of the experimental commissioning process, the test hut was tested for airtightness in March 2017, and individual test rafter bays were tested using differential pressure measurement in insulation cavities to ensure that unequal air leakage is characterized as a variable. In addition, building depressurization due to mechanical system operation was evaluated.

11.2 Enclosure Airtightness Measurement

The airtightness of the test hut enclosure was tested via fan pressurization and depressurization, using an Energy Conservatory Duct Blaster (Model B). All exterior doors in this enclosure are large sliding glass doors, which are difficult to adapt to the typical door frame and shroud. Therefore, the exhaust fan was removed from its housing, and the Duct Blaster was connected to the opening (Figure 110). Measurements were taken with an Energy Conservatory DG700 manometer, connected to a computer running TECTITE 4.0 automated multipoint testing software.

Figure 110. Airtightness testing with fan connected to exhaust fan opening

The results of multipoint pressurization and depressurization testing are graphed in Figure 111, with key parameters summarized in Table 13:
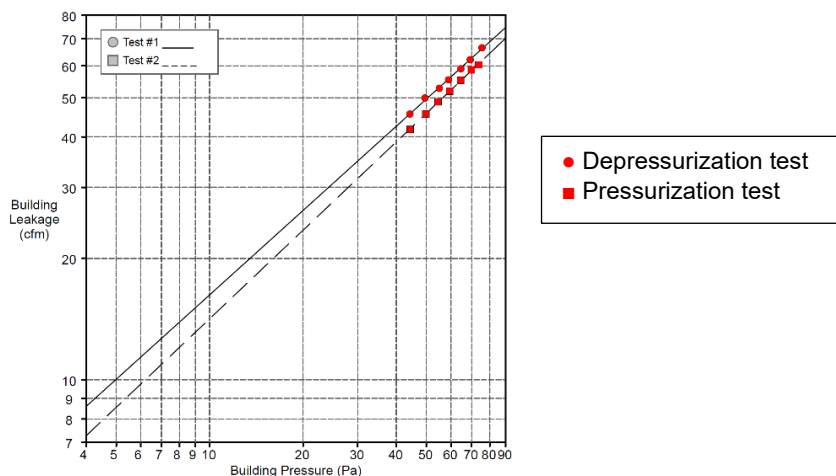
Figure 111. Multipoint pressurization and depressurization test results

Table 13. Air Leakage Testing (Full Enclosure) Results

Measurement	Label	Pressurization	Depressurization
Airflow @ 50 Pa	CFM50[1]	46	50
Air changes/hr @ 50 Pa	ACH50[2]	0.50	0.55
Surface area-normalized leak	CFM 50/ft² surface area	0.02	0.02
Leakage area (EqLA)	in²	4.2	4.8
Flow coefficient	C	2.6	3.3
Flow exponent	n	0.73	0.69
Coefficient of determination	r²	0.9995	0.9986

Clearly, these results indicate a very airtight enclosure in terms of interior-to-exterior air leakage.

11.3 Mechanical-Enclosure Interaction

Given the airtightness of the enclosure, the through-wall exhaust fan created significant depressurization. The 70 CFM nominal fan was operating at 28 CFM (due to the restriction of the shell/enclosure on airflow), resulting in a -22 Pa building depressurization. This was measured directly and is consistent with the calculated depressurization based on C and n values in Table 13.

The purpose of this exhaust fan is to promote indoor-outdoor air exchange and therefore reduce interior RH levels in winter. However, -22 Pa ΔP is a significant level of constant

---

[1] Cubic feet per minute at 50 Pascal pressure differential.
[2] Air changes per hour at 50 Pascal pressure differential.

depressurization and can have a significant effect on enclosure monitoring studies; this was confirmed by examining the data for the unvented fiberglass roofs (Roofs 1–4).

RH at the roof ridge is plotted in Figure 112, and the period with the exhaust fan turned off is noted in red. During this fan-off period, the RH levels in Roofs 1 and 2 (diffusion vent/fiberglass) rise markedly and remain high. The likely explanation is that during exhaust fan-on periods, induced infiltration (small amounts of inward air leakage around or though the diffusion vent) protects the ridge from interior moisture. Turning off the fan removes this effect, as shown by the sharp rise in ridge RH. After the exhaust fan is turned off, RHs remain high for several weeks (possibly storage of accumulated moisture), but then drop.

After these findings were confirmed, the exhaust fan was turned off in early March (Figure 113), and noted in the data collection.
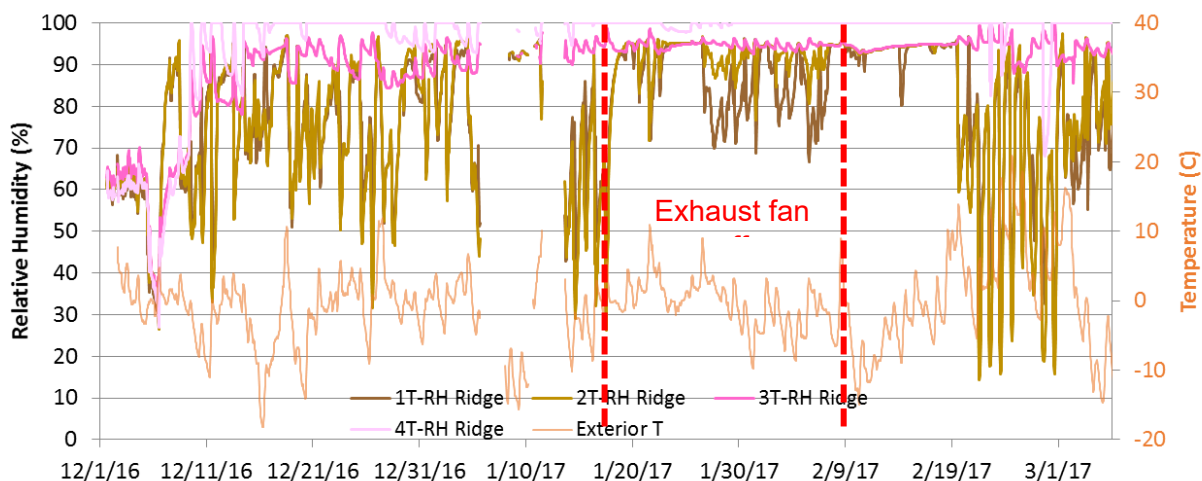
Figure 112. Fiberglass roof ridge RH measurements, showing exhaust fan on/off

In mid-March, the situation was addressed by putting a sliding glass door in a slightly open position to create greater leakage area/pressure relief (Figure 113, left). In addition, the intake of the exhaust fan was restricted (Figure 113, right), reducing airflow from 85 CFM to 43 CFM. These changes resulted in a fan depressurization effect of -1 to -2 Pa, which is well within the range for typical residential construction.

Figure 113. Door opening to relieve pressure (left), exhaust fan restriction (right)

Air leakage was retested after this modification, and the measurement was 367 CFM 50 (depressurization test only). The calculated EqLA was 34 square in., which is roughly consistent with the opening size (29-square-in. increase in calculated EqLA; sliding glass door opening roughly 28 square in.).

11.4 Air Leakage Localization

Although overall indoor-outdoor air leakage was small (4.2 to 4.8 square in. EqLA), depressurization and infrared thermography were used to locate air leakage, ensuring that it was not associated with the test roof bays. The interior surfaces of the building were examined with a FLIR ONE infrared camera (-4°F to 248°F; 0.18°F resolution). The infrared camera shows surface temperatures; warmer areas are brighter (yellow/orange) colors, and cooler areas are darker (blue/purple) colors.

With outdoor temperatures cooler than indoors, thermal bridging or air leakage appear as cool surfaces (colder than interior conditions). Temperatures were 28°F exterior and 73°F interior during these observations. Infrared thermography captures surface temperatures, which can be influenced by thermal bridging/conduction, thermal mass/storage, presence of moisture, and/or air leakage.

A baseline infrared observation of the building was done prior to depressurization to identify existing thermal bridges or other anomalies, to avoid ascribing them to depressurization air leakage. The test facility had been operating without the exhaust fan for 5 days prior to these observations.

Key findings include some thermal bridging at the ridge, rafters, and gable end/rake walls (Figure 114), as well as thermal bridging at the slab perimeter (Figure 115).

Figure 114. Visual and infrared image of interior of roof, no depressurization

Figure 115. Visual and infrared image of floor-to-slab joint, no depressurization

The slab edge is insulated (with 4-in. semi-rigid mineral fiber); however, the wall is an even higher R-value (4-in. mineral fiber and 5-in. ccSPF), potentially causing this thermal anomaly. There are no noticeable thermal anomalies between roof bays (interior surface temperatures); concerns of uneven heat distribution from the wall-mounted minisplit head appear to be unfounded.

The structure was then depressurized to -75 Pa with the same equipment used for air leakage testing, and an infrared camera was used to identify air leakage sites.

The most significant air leakage was associated with electrical conduit penetrations through the slab (Figure 116); leakage occurred both through the conduit and at the opening between conduits. Exterior-to-interior airflow was confirmed with air velocity and temperature measurements via a Fieldpiece STA2 In Duct Hot-wire Anemometer (Figure 118, left), at 650 ft per minute/FPM and 58°F.

Figure 116. Visual and infrared image of conduit penetration at slab, depressurization test

Another set of thermal anomalies was seen at the roof corners at the three-way intersection between the walls and roof (Figure 117). They were also examined with the anemometer (Figure 118); some corners showed airflow (99 FPM/66°F), but others had no measurable airflow despite the thermal anomaly.

Figure 117. Visual and infrared image of roof corner, depressurization test
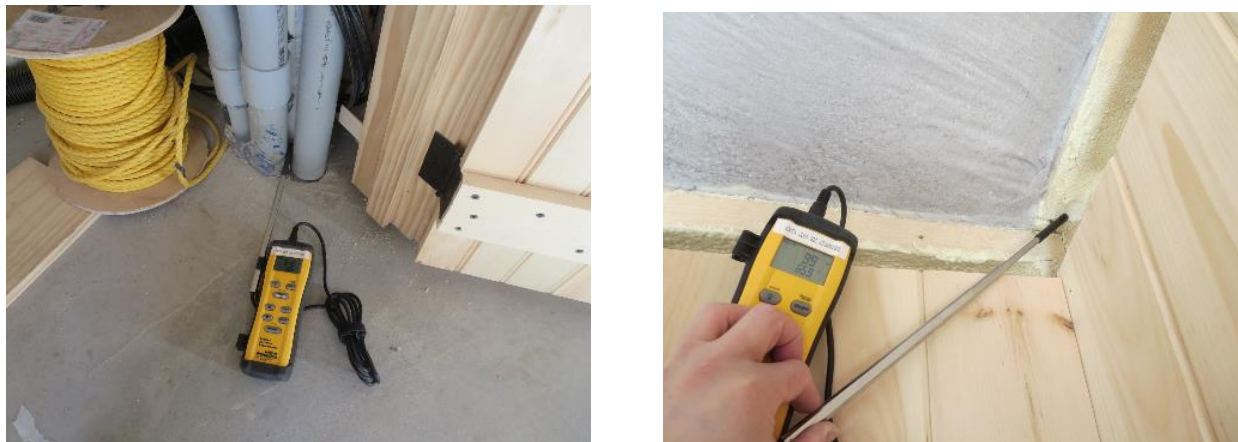
Figure 118. Air velocity measurements at slab conduit penetration (left) and roof corner (right)

An infrared overview of the roof under depressurization testing is shown in Figure 119; no clear difference between the unpressurized and depressurized test was evident. Although there might be air leakage hidden behind the fibrous insulation, if rates are low, they would be difficult to detect from the interior.
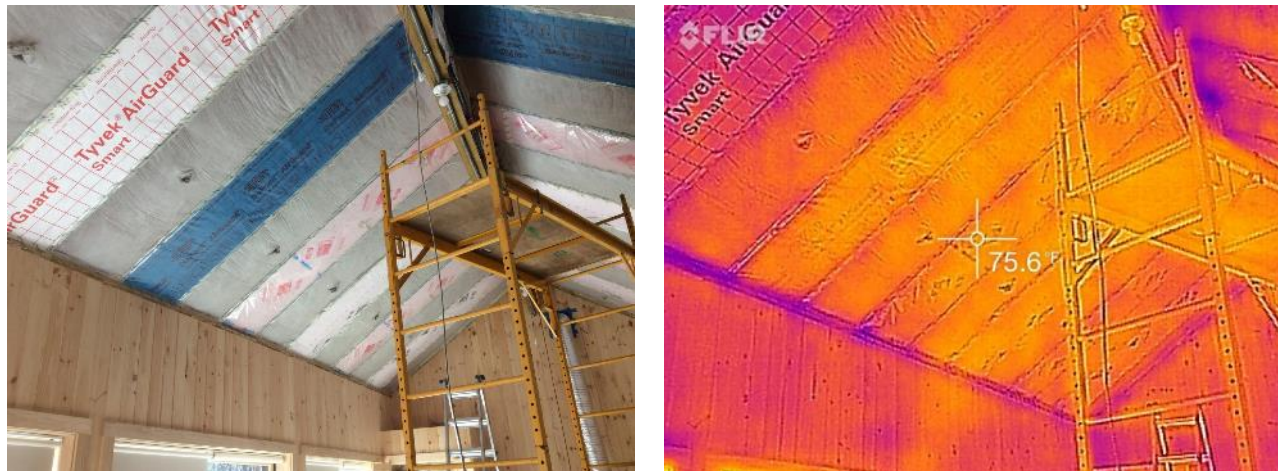
Figure 119. Visual and infrared image of overall roof, depressurization test

11.5 Roof Bay Pressure Difference Comparison

Another commissioning test was to measure the pressure difference (ΔP) across the interior air/vapor control membrane to determine whether disproportionate air leakage is occurring in one of the test bays. With the building depressurized to -75 Pa, ΔP measurements were taken with an Energy Conservatory DG-700 manometer. Measurements were taken at the roof-wall connection/eave at the north and south sides (Figure 120, left) and at the ridge (Figure 120, left). An opening was cut in the interior air/vapor control membrane, and then sealed with tape.

Figure 120. Measuring ΔP across air/vapor control membrane at eave (left) and ridge (right)

The results of these measurements are shown in Table 14, showing pressure drop (ΔP) in Pa, bar graphs for visual comparison, and as a percentage of the enclosure indoor/outdoor ΔP.

Overall, the results show a small pressure drop across the interior air/vapor control membrane, compared to the total pressure drop (0.3% to 3.5% of total). This indicates that the exterior sheathing is the most airtight layer, which is consistent with its construction (taped sheathing with an integrated water-resistive barrier). Roof 1 (fiberglass, fixed-perm vapor retarder, diffusion vent) shows ΔPs higher than the remaining roof bays, which suggests that there might be an air leakage anomaly in this roof bay. In addition, the north-side eave measurements showed consistently higher ΔPs than the south side or ridge. This could be consistent with an air leak at the north roof-wall eave connection.

Table 14. Roof Membrane ΔP Measurements at Eaves and Ridge, Before Roof 1 Retrofit

Location	1 FG-VB-DV	2 FG-SVR-DV	3 FG-VB-nDV	4 FG-SVR-nDV	5 Cell-VB-nDV	6 Cell-SVR-nDV	7 Cell-SVR-DV
North ΔP	2.6	1.0	0.7	1.1	1.5	1.9	1.9
Ridge ΔP	1.7	0.9	0.2	0.2	0.2	0.2	0.5
South ΔP	1.7	0.4	0.2	0.5	0.2	0.3	0.6
Average ΔP	2.0	0.8	0.4	0.6	0.6	0.8	1.0
North ΔP							
Ridge ΔP							
South ΔP							
Average ΔP							
North % of total	3.5%	1.4%	0.9%	1.5%	2.0%	2.6%	2.6%
Ridge % of total	2.3%	1.2%	0.3%	0.3%	0.3%	0.3%	0.7%
South % of total	2.3%	0.5%	0.3%	0.7%	0.3%	0.4%	0.8%
Average %	2.7%	1.0%	0.5%	0.8%	0.9%	1.1%	1.4%

11.6 Roof 1 Disassembly and Retesting

Roof 1 was investigated further in late March 2017 by opening the ridge diffusion vent, which was considered the most likely location for an air leakage anomaly. This work was delayed waiting for snow melt off the roof and temperatures warm enough to avoid damaging roof materials due to lack of pliability.

The ridge vent was removed and the diffusion vent material was opened to expose cavity conditions (Figure 121). The only notable anomaly was that the diffusion vent material was cut much larger than the sheathing opening. No empty nail holes penetrated the diffusion vent.

Figure 121. Cutting open existing diffusion vent ridge membrane, after vent removal

Conditions inside the cavity revealed incomplete fill of fiberglass insulation at the ridge (Figure 122, left). The ridge wafer was examined for any sign of moisture damage or mold spotting (Figure 122, right); none was seen. In the monitored data, Roof 1 has the driest ridge conditions out of the four fiberglass roof assemblies (1–4).
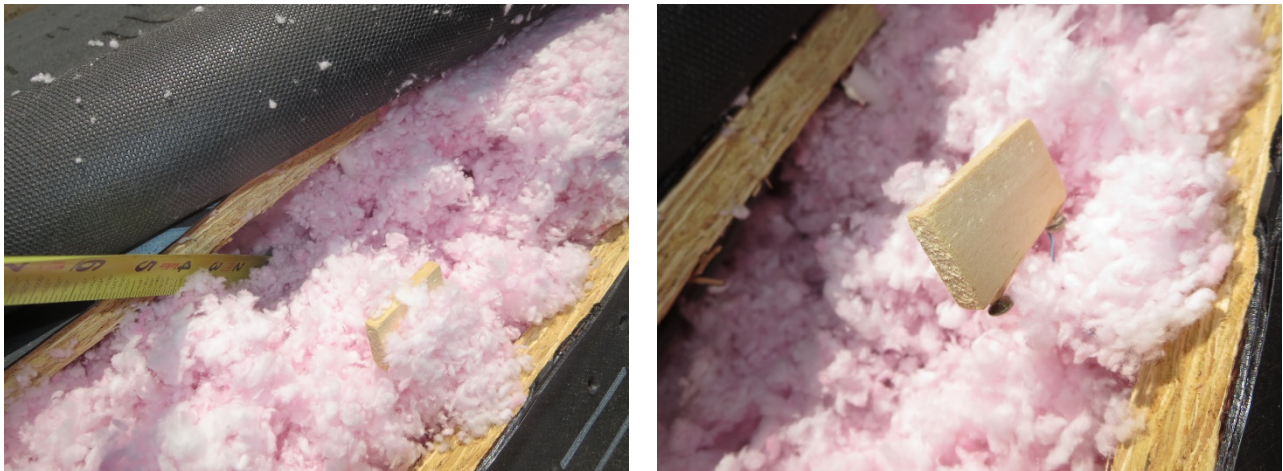
Figure 122. Void at Roof 1 ridge insulation (left) and ridge wafer condition (right)

The ridge was then reassembled, with taped edges closer to the sheathing opening (Figure 123, left), and Roof 2's ridge was also visually examined after removing the vent cap (Figure 123, right); no anomalies were seen.

Figure 123. Reassembled Roof 1 diffusion vent (left) and Roof 2 examination (right)

Interior cavity differential pressures were remeasured after the retrofit to determine whether this retrofit addressed the air leakage anomaly seen at Roof 1. The results with the building at -75 Pa are shown in Table 15; Roof 1 still has anomalously high air leakage. Almost all other ΔP measurements were 1 Pa or less, but all Roof 1 measurements were still anomalous—over 1 Pa.

Further examination of the Roof 1 air leakage anomaly would require extensive disassembly, so no further investigation was conducted.

Table 15. Roof Membrane ΔP Measurements at Eaves and Ridge, After Roof 1 Retrofit

Location	1 FG-VB-DV	2 FG-SVR-DV	3 FG-VB-nDV	4 FG-SVR-nDV	5 Cell-VB-nDV	6 Cell-SVR-nDV	7 Cell-SVR-DV
North ΔP	1.5	0.5	0.4	0.2	0.9	1.2	1.9
Ridge ΔP	1.3	1.0	0.1	0.0	0.1	0.1	0.4
South ΔP	1.9	0.4	0.3	0.5	0.5	0.4	0.5
Average ΔP	1.6	0.6	0.3	0.2	0.5	0.6	0.9
North ΔP							
Ridge ΔP							
South ΔP							
Average ΔP							
North % of total	2.0%	0.7%	0.5%	0.3%	1.2%	1.6%	2.6%
Ridge % of total	1.8%	1.4%	0.1%	0.0%	0.1%	0.1%	0.5%
South % of total	2.6%	0.5%	0.4%	0.7%	0.7%	0.5%	0.7%
Average %	2.1%	0.9%	0.4%	0.3%	0.7%	0.8%	1.3%

12 Humidification and Vapor Barrier Issues (Prior to Winter 2)

12.1 Humidification System Installation

To stress the roof assemblies through Winter 2 (2017–2018), the test hut interior space was run at a high RH of 50% RH, as discussed in the test plan and other documents. This equipment was used for humidification in previous work (Ueno and Lstiburek 2016b). An overview of the installed humidification system is shown in Figure 124 and Figure 125.

Figure 124. Overview of humidification system

Figure 125. Humidifier bucket, heater, and float switch

A schematic of the system is shown in Figure 126: on a call for humidification, water in the insulated 5-gallon bucket is heated with a resistance immersion heater, and a fan blows over the water surface to distribute water vapor. This bucket is in turn fed by an immersion pump in the water reservoir (gray trash receptacle), controlled by the float level switch at the heated bucket. The heated bucket and controller are placed on a white cooler to elevate the bucket waterline above reservoir water levels, thus avoiding siphon effects.
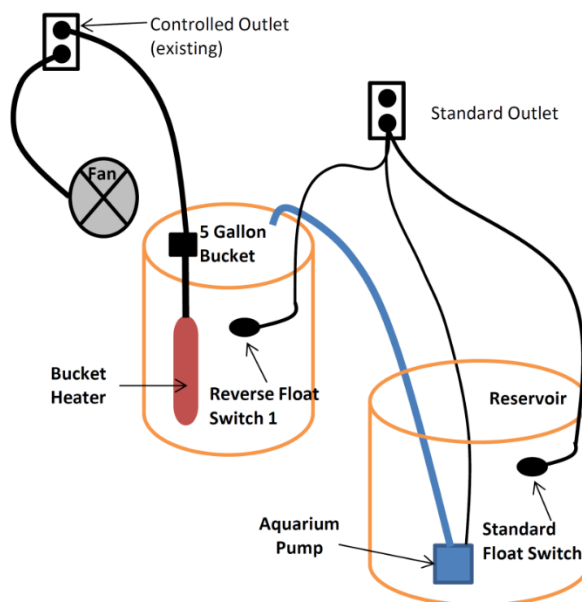
Figure 126. Conceptual schematic of humidification setup

The humidifier was installed in early October 2017, before the start of winter 2017–2018 (Winter 2).

12.2 Interior Air Barrier/Vapor Retarder Issues and Repairs

Measurements of ridge conditions during Winter 1 indicated that Roof 2 had signs of disproportionate leakage of interior air near the ridge. Inspection of current conditions at Roof 2 showed a loss of adhesion of the housewrap tape and the double-sided tape near the ridge, thus connecting the bay to interior conditions (Figure 127). In addition, several roofs were retrofitted with alternate interior vapor retarders. Instead of repairing this installation, the existing vapor retarder was removed and a new interior membrane was installed.

Figure 127. Roof 2, showing loss of adhesion of housewrap tape near ridge

A multistep process was used to improve the air seal (Figure 128), including (a) removal of all old tapes and seals, (b) using contact spray adhesive (3M 90) on the face of the wood rafter, (c) using double-sided tape on the rafter to form a primary seal (Saint-Gobain Norbond foam tape), (d) using high-performance housewrap tape on the rafter as a secondary seal (Dow Weathermate Construction Tape), and (e) using a roller and/or squeegee to improve the adhesive bond.

Figure 128. Reinstallation of Roof 2 vapor retarder: spray adhesive (left) and taped edges (right)

However, even after this retrofit, several roofs had vapor retarder seal failures, including Roof 3 North (October 2017/Figure 129, then January 2018/Figure 130) and Roof 2 (December 2017).

Figure 129. Roof 3 north vapor retarder failure (October)

Figure 130. Roof 3 north vapor retarder failure (January)

Each was repaired using mechanical fasteners (staples) in addition to the sealing materials listed previously. These seal failures occurred at fiberglass roofs where there was noticeable "bellying" of the insulation, which resulted in a tensile load on the interior air/vapor retarder seal.

Some of the other roofs showed minor tape adhesion issues (Figure 131). This was addressed by retrofitting the tape seals in place, by cutting away the failed housewrap tape (leaving the double-

sided tape in place), applying high-performance construction tape, and rollering to improve adhesion (Figure 132). This was done at all bays that had the older housewrap tape.

Figure 131. Tape adhesion loss at Roof 6 along rafter and at ridge

The data were examined for a correlation between air barrier failures/repairs and roof responses; none was clear in the monitored data.

Roofs 3 and 5 were retrofitted with a variable-perm interior vapor retarder/air barrier membrane to control experimental variables. The installation technique was identical to that used at Roof 2 (removal of old seals, spray adhesive, and all new taping). However, disassembly revealed moisture accumulation issues, discussed in the following section.

Figure 132. Cutting away failed housewrap tape (left) application of replacement tape (right)

12.3 Inward Vapor Drive Condensation

The interior fixed-perm vapor retarders on Roofs 3 and 5 were removed from the ridge beam downward (Figure 133, left); this revealed the accumulation of liquid water condensation at the vapor retarder-insulation netting interface, as demonstrated by visible droplets and water indicator paper (Figure 133, right). Further demonstrations of this wetting are shown in Figure

134, including droplets of accumulation on the vapor retarder, pink stained water tinted by the fiberglass insulation pigment, and pink spots or droplet marks on the insulation installation netting.

The pattern of wetness was worst at the ridge and decreased down the slope of the roof. The most noticeable patterns of wetness extended roughly 3 ft from the ridge. Wetness appeared to be roughly similar on north and south slopes.

Figure 133. Roof 3 vapor retarder removal (left), condensation accumulation (right)

This condensation might not fully reflect normal operating conditions: due to a controls issues, the interior temperature was set at roughly 60°F for a period before these observations. However, even if the interior temperature is non-representative, the spatial accumulation patterns are useful information.

In addition, Roof 2 (FG-SVR-DV; variable-perm vapor retarder) was disassembled in the same manner immediately before Roofs 3 and 5 and had dry conditions (no condensation accumulation).

Figure 134. Roof 3 condensation wicking into water indicator paper, staining of insulation netting

The cellulose roof with a fixed-perm vapor retarder also had surface wetness at the vapor retarder-insulation interface, but without visible droplets of water. The accumulation was felt as surface dampness at the interface, and demonstrated with water indicator paper (Figure 135).
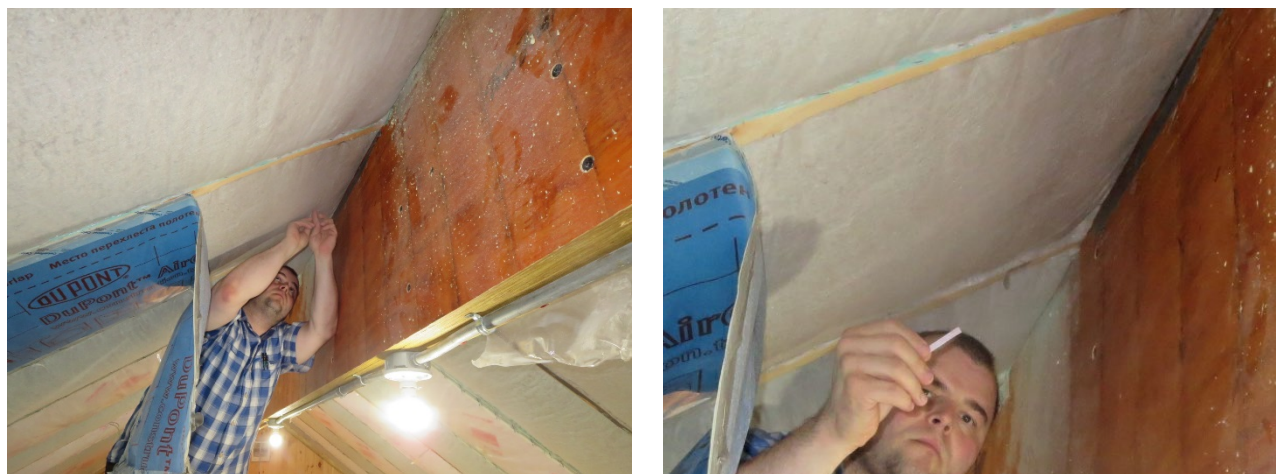
Figure 135. Roof 5 wetness at vapor retarder-netting interface

Wood MCs were measured at the framing with a handheld Delmhorst BD-10 meter (Figure 136). Consistent patterns were not seen, but MCs ranged from roughly 15% to 25%, with the highest MCs at the edges of the rafters near the ridge (per Figure 136, left).

Roof conditions were also examined with an infrared camera (FLIR ONE Pro, -20°C to 400°C/ -4°F to 752°F, accuracy ±3°C/5.4°F or ±5%, typical). With the interior vapor retarders removed, a pattern of cooler temperatures was observed at the ridge (Figure 114 and Figure 138), matching the wetted areas. This is ascribed to evaporative cooling of water from the exposed surfaces to the interior.

At Roof 5 (cellulose, Figure 138), the rafter framing was also cooler than adjacent bays, suggesting moisture accumulation at the wood. In addition, cooler surfaces were seen at the ridges of Roofs 6 and 7, suggesting possible ridge moisture accumulation in these variable-perm roof bays.

Overall, this pattern of summertime condensation at the ridge is consistent with moisture accumulating at the ridge, and then being dried down locally at this area. The instruments installed to capture inward vapor drive issues are installed mid-height in the rafter bays, so they do not capture the worst-case conditions occurring near the ridge. These observations make it clear that inward drive problems are a greater risk than recorded by the instrumentation, with observed condensation and water rundown at the interior.

Figure 136. Wood MC measurements at framing

Figure 137. Visual and infrared image of Roof 3 (fiberglass) after fixed-perm vapor retarder removal

Figure 138. Visual and infrared image of Roof 5 (cellulose) after fixed-perm vapor retarder removal

12.4 Fiberglass vs. Cellulose Sorption Isotherms

The difference in inward vapor drive behavior in the fiberglass and cellulose roofs is ascribed to moisture storage in the cellulose. This is demonstrated by plotting the sorption isotherms for fiberglass, mineral fiber, and cellulose (taken from *ASHRAE Handbook of Fundamentals*, ASHRAE 2009a), per Figure 139.

This shows that cellulose moisture storage is more than an order of magnitude higher than fiberglass at higher RH conditions. This plot shows storage on a weight percentage basis; if the installed density difference were factored in (1.4 PCF fiberglass vs. 3.5 PCF cellulose), the volume-based storage difference is roughly a factor of 30.
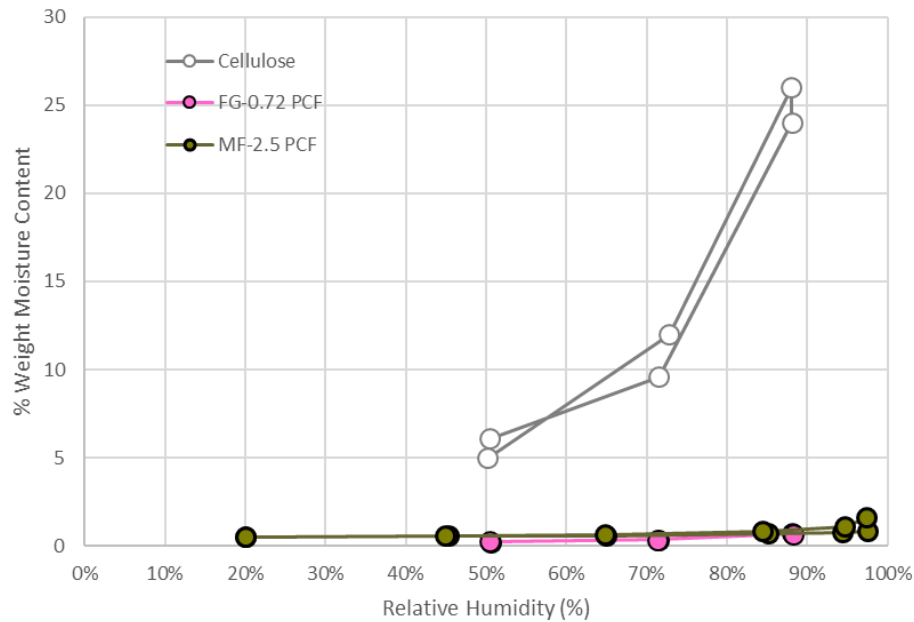
Figure 139. Sorption isotherm comparison of cellulose, mineral fiber, and fiberglass insulation (ASHRAE 2009a data)

13 Diffusion Vent Retrofit and Insulation Settling (Prior to Winter 2)

13.1 Diffusion Vent Retrofit

The non-diffusion-vent roofs (Roofs 3, 4, 5, and 6) were retrofitted with 2-in. wide diffusion vents (as detailed in Table 3) in late August 2017. The self-adhered membrane and sheathing were cut back to create a roughly 2-in. wide opening (Figure 140). The openings are roughly 22 in. wide (full width of the rafter bay).
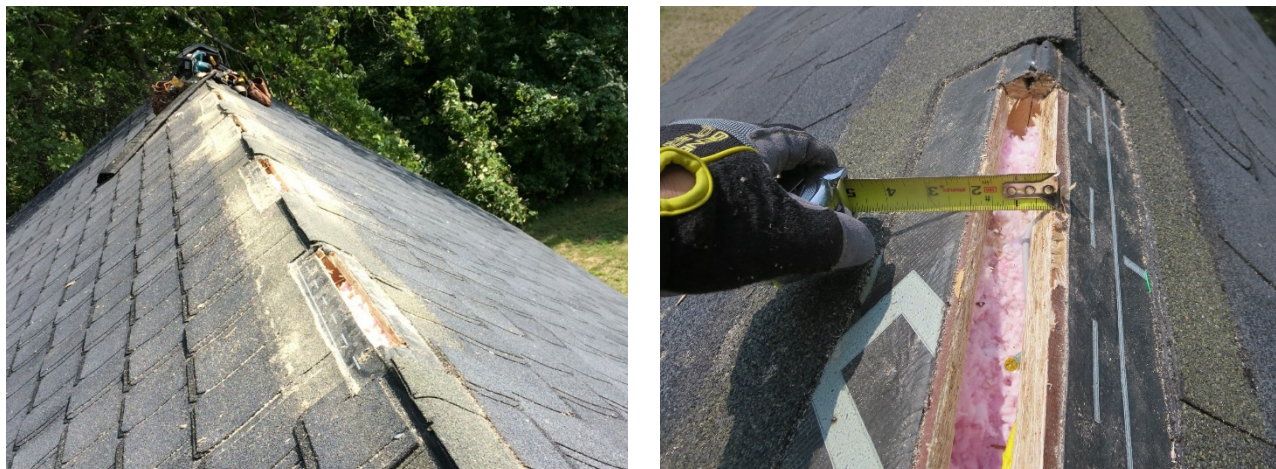
Figure 140. Retrofit of 2-in. wide diffusion vents at Roofs 4, 5, 6, and 7

The failed RH sensors (Roofs 4 and 6) were replaced. The wafer sensor at Roof 6 was replaced, but in Roof 5, insufficient wire was available to splice in a connection, so the sensor was abandoned.

The remaining diffusion vent details were per the existing diffusion vent roofs (1, 2, and 7), with the vapor-open membrane adhered to the roof self-adhered membrane with flashing tape, and the ridge cap covering the diffusion vent (Figure 141).

Figure 141. Diffusion vent material installation and ridge cap coverage

13.2 Insulation Settling—Fiberglass

The ridge opening allowed for observation of insulation and sheathing conditions. The fiberglass insulation showed varied amounts of settling at the ridge, ranging from 1 to 2 in. to more than 3 in. (exposing most of the 2x4 nailer), per Figure 142. This settling resulted in an open-air cavity near the ridge.

Figure 142. Settling of fiberglass insulation at ridge, Roof 4

13.3 Insulation Settling—Cellulose

Insulation settling was also seen at the cellulose roofs (Figure 143). This settling at the ridge was in the range of 4 to 8 in., typically (Figure 144).

Figure 143. Settling of cellulose insulation at ridge, Roof 5

Figure 144. Settling of cellulose insulation at ridge, Roof 6

However, a surprising finding was that there was significant settling on the north-facing slope in both Roofs 5 and 6, varying from minimal to roughly 1 in. (Figure 145, showing view down slope).

Figure 145. Settling of cellulose insulation on north-facing slope, Roof 5

The dimensions of the settling were examined by probing with a tape measure at the insulation-sheathing interface (Figure 146). On the north slope, the tape measure stopped at roughly 9.5 ft., or most of the length of the rafter bay. On the south slope, the tape measure stopped at less than 12 in. This indicates that the settling is likely a function of high wintertime RHs experienced on the north elevation, rather than uniform settling due to temperature cycling, time, or stretching of the netting.

Figure 146. Settling of cellulose insulation on north (left) and south (right) slopes, Roof 6

In addition, this roof disassembly allowed for examination of the assembly for signs of moisture issues. The sheathing removed to create the ridge diffusion vent was intact and did not show macroscopic signs of mold growth, delamination, or other damage. However, metal fasteners exposed to roof bay conditions shows signs of corrosion, including staples used for instrumentation wiring (Figure 147, left), and roofing nails, where they penetrated the sheathing (Figure 147, right). Note that the longer nails were used at the ridge cap, with less of the shank penetrating the sheathing.

Figure 147. Corrosion of wire staples (left) and corrosion of roofing nails (right)

14 Disassembly and Ridge Examination (Prior to Winter 3)

Roof ridge RH sensors saw multiple failures, due to extended periods at high RH (95%–100% and condensation) and temperature extremes. In addition, in the cellulose bays, the wafer sensors had issues likely caused by borate contamination. Therefore, in preparation for Winter 3, the interiors of the roof ridges were disassembled in all seven experimental bays for visual examination and sensor replacement.

Visual examination of building enclosure test assemblies often provides the best indication of long-term performance: sensors provide hourly condition data, but may miss anomalies away from the sensors. This dovetailed with sensor replacement work, as the worst-case moisture accumulation was at the ridge, based on monitored data.

Unfortunately, one limitation is that this inspection looks at conditions after both Winter 1 and Winter 2. Determining when damage occurred is difficult, apart from comparisons with ridge opening photos during summer 2017, as covered in Section 13: Diffusion Vent Retrofit and Insulation Settling (Prior to Winter 2).

14.1 Disassembly and Sensor Replacement

The interior vapor control and netting at the roof ridges were opened, roughly 2 to 3 ft from the ridge, on the north side. Insulation was carefully removed via vacuum cleaner (Figure 148).

Figure 148. Removal of fiberglass insulation at ridge of Roof 1

The interior conditions of the roof framing and sheathing were inspected (covered in later sections), and the ridge RH and wafer MC sensors were replaced in all seven experimental fibrous insulation roofs (Figure 149, left). The repair splices were made with snap-on silicone-filled insulation displacement connectors (3M Scotchlok IDC Butt Connector UY); the splices were kept away from ridge conditions.

One MC pin had been knocked out of place from the sheathing; it was replaced and redriven (Figure 149, right).
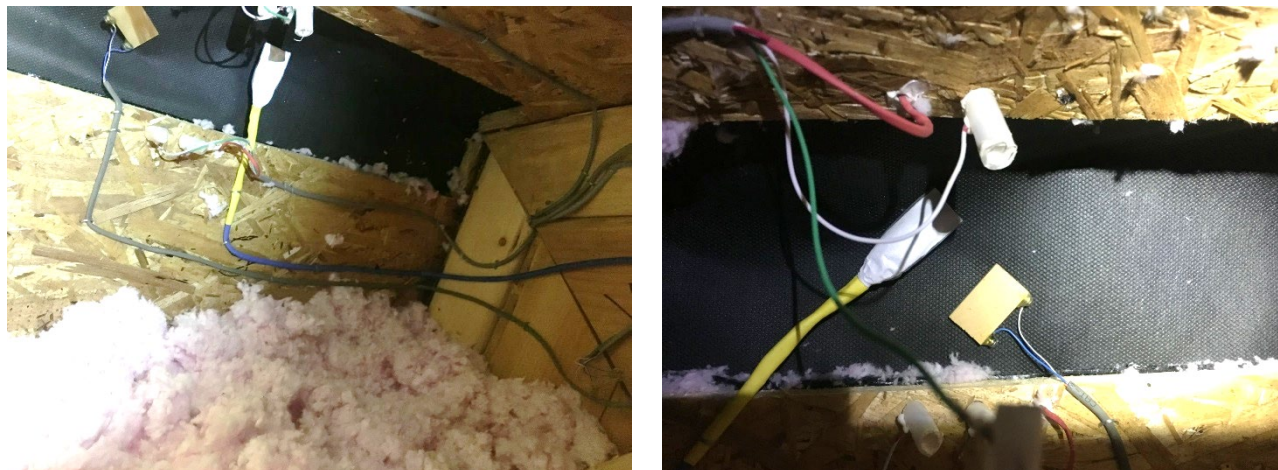
Figure 149. Sensor replacement (left) and repair of failed MC pin (right)

14.2 Fiberglass Roof Conditions

The fiberglass experimental roof characteristics in Winters 1 and 2 are shown in Table 16 for reference, allowing comparison between conditions and roof type. All photos below were taken standing on north side of ridge (facing south).

Table 16. Fiberglass Roofs' (1–4) Characteristics for Winter 1 vs. Winter 2

	Winter 1 Designations			Winter 2 Designations		
Roof #	Short Name	DV	VB	Short Name	DV	VB
1	FG-VB-DV	DV Full	OC Facer Fixed	FG-VB-DV	DV Full	OC Facer Fixed
2	FG-SVR-DV	Size	Membrain SVR	FG-SVR-DV	(original)	Membrain SVR
3	FG-VB-nDV	No DV	OC Facer Fixed	FG-SVR-tDV	DV-Tight	Membrain SVR
4	FG-SVR-nDV	Roofs	Membrain SVR	FG-SVR-sDV	DV-Small	Membrain SVR

Roof 1 (Winter 1 and 2-full-size diffusion vent; fixed-perm interior vapor barrier) disassembly showed noticeable water staining on the vapor retarder and netting, on the north side (Figure 150, left).

Figure 150. Roof 1 water staining on netting (left) and pink spotting on fixed-perm vapor barrier (right)

In addition, dried pink spotting was found on the exterior side of the interior vapor barrier (Figure 150, right), consistent with summertime inward drive condensation on the fixed-perm vapor retarder at the ridge (like Roof 3, Figure 133 and Figure 134).

Further disassembly revealed minor mold spotting on the framing. The rafters are framed with a "stacked" 2x12 and 2x4 assembly to achieve a ~14.75-in. cavity depth. The visible mold occurred in the north bay, on the west-side rafter, on the 2x4 (lighter colored wood, Figure 151, left). There was minor staining on the roof sheathing near the west-side rafter (Figure 151, left, and Figure 152, left). In comparison, the east-side rafter was mostly clean, but with some minor mold spotting on the 2x4 (Figure 152, right). Some minor spotting was also seen on the horizontal collar tie (similar light-colored lumber to "stacked" 2x4).

The west-side rafter showed a noticeable bulk water stain on the 2x4, originating at the sheathing joint (Figure 151, right). The most likely explanation based on the visible patterns was condensation and rundown from the roof ridge along the sheathing; at the sheathing joint, surface tension resulted in a "drip," causing the visible staining on the interior vapor control shown in Figure 150 (left).

Figure 151. Roof 1 mold spotting on sheathing/framing (left) and bulk water stain on 2x4 (right)

Figure 152. Roof 1 ridge sheathing conditions (left) and east-side rafter (right)

Roof 2 (Winter 1 and 2 full-size diffusion vent; variable-perm interior SVR) showed minor mold spotting on the east-side rafter (Figure 153, left) and no visible issues on the west side (Figure 153, right). This roof generally showed the least moisture accumulation, given the large ridge diffusion vent and variable-perm interior vapor control.

Figure 153. Roof 2 minor mold spotting on east rafter (left) clean conditions on west rafter (right)

Roof 3 (Winter 1 no diffusion vent, fixed-perm vapor barrier; Winter 2 tight diffusion vent, SVR) showed some of the worst moisture accumulation in monitoring, specifically during Winter 2. Roof 3 had extensive stains matching bulk water drainage near the ridge on the east rafter (Figure 154, left), and some visible spotting. This stain is consistent with ridge condensation that drained down from the sheathing.

At the sheathing, there was noticeable discoloration, raising of the wood grain/wafers or slight delamination, and extensive corrosion of the instrumentation staples (Figure 154, right).

Figure 154. Roof 3 mold and staining on east rafter (left); sheathing damage and rusted staples (right)

The west rafter appeared to be mostly intact and unstained.

A close-up of Roof 3's east-side water staining is shown in Figure 155 (left). Although the water rundown stain is noticeable, mold staining appears minor.

A final notable item is that there was significant ant infestation/nesting, per Figure 155 (right). The ants left to the adjacent guard roof bay when disturbed; however, the location of the nest was not determined via disassembly. Ant infestation is a common indicator of moist wood products.

Roof 3 had the tight diffusion vent (25-perm housewrap), which showed low drying and high moisture accumulation, consistent with the visible moisture problems.

Figure 155. Roof 3 close-up of water staining on east rafter (left) ant infestation from adjacent bay (right)

Roof 4 (Winter 1 no diffusion vent, SVR; Winter 2 small diffusion vent, SVR) showed minor staining on the 2x4 near the ridge on the east side (Figure 156, left and right) and minor damage to the sheathing on the north side.

Figure 156. Roof 4 mold and staining on east rafter (left) close-up of east rafter and sheathing stains (right)

The west rafter appeared to be mostly intact and unstained (Figure 157, left).

In addition to visual inspections, wood MC measurements were taken at all stained areas, using a handheld Delmhorst BD-10 meter (Figure 157, right); all conditions were dry, as would be expected for summertime measurements.

Figure 157. Roof 4 mostly clean conditions on west rafter (left) wood MC measurements (right)

The ridge wafers were also all inspected during this work; no visual evidence of mold growth on the wafers was found.

Overall, the damage patterns roughly match the severity of the wetting over two winters, in particular, Winter 2. The summer 2017 retrofit of the tight and small diffusion vents in Roofs 3 and 4 allowed for visual inspection of the sheathing; the extensive wetting seen in Roof 3 was not evident during that work. The greater wetting in Winter 2 is consistent with extended elevated RHs/MCs due to interior humidification. The staining on the 2x4 is due to both its vulnerable location (highest in the rafter bay) and possibly higher susceptibility to mold growth.

14.3 Cellulose Roof Conditions

The cellulose experimental roof characteristics in Winters 1 and 2 are shown in Table 17 for reference, allowing comparison between conditions and roof type. All photos below were taken standing on the north side of ridge (facing south).

Table 17. Cellulose Roofs' (5–8) Characteristics for Winter 1 vs. Winter 2

Roof #	Winter 1 Designations			Winter 2 Designations		
	Short Name	DV	VB	Short Name	DV	VB
5	Cell-VB-nDV	No DV	DuPont Fixed VB	Cell-SVR-tDV	DV-Tight	DuPont SVR
6	Cell-SVR-nDV	Roofs	DuPont SVR	Cell-SVR-sDV	DV-Small	DuPont SVR
7	Cell-SVR-DV	DV Roof	DuPont SVR	Cell-SVR-DV	DV Full	DuPont SVR
8	ccSPF-Cell	None	None	ccSPF-Cell	None	None

Roof 5 (Winter 1 no diffusion vent, fixed-perm vapor barrier; Winter 2 tight diffusion vent, SVR) disassembly showed significant mold spotting on both the east and west rafters in the north bay (Figure 158) on the "stacked" 2x4. This damage was not limited to the ridge; it occurred further down below the collar tie on the west side (Figure 159, right). The damage was concentrated on the 2x4, providing a further indication of the vulnerability of the lighter-colored framing lumber. Figure 159 (right) also shows corrosion of nail heads at the rafter tie.

There was extensive staining of the roof sheathing on the north side and corrosion of the instrumentation staples, indicating significant previous wetting (Figure 159, left). The sheathing damage included mold spotting, raised OSB grain, and visible water staining.

Figure 158. Roof 5 significant mold spotting on both east rafter (left) and west rafter (right)

Figure 159. Roof 5 sheathing damage, east-side (left) collar tie rusted nails, rafter mold (right)

Roof 5 had the tight (25-perm housewrap) diffusion vent in Winter 2, which generally showed poor drying, which is consistent with this extensive staining.

Another major issue in this rafter bay was settling of cellulose, per Figure 160. The cellulose was originally blown to fully fill the cavity, but had settled over two winters, leaving a 2- to 3-in. gap on the north side (Figure 160, right).

This settling definitely occurred after Winter 1, based on observations from the exterior ridge in Roofs 5 and 6, during the retrofit of the tight and small diffusion vents (see Section 13.3: Insulation Settling—Cellulose). The team agreed to leave the settled gap in place during Winter 2 in order to maintain identical roof conditions between Winters 1 and 2 and avoid damage to roof sensors.

Figure 160. Roof 5 north-side cellulose settling (left); gap size 2 to 2.5 in. (right)

One possible counter-argument to cellulose settling would be that the gap is caused by stretching of the fabric netting supporting the insulation. However, the interior height of the netting belly was measured (Figure 161); it was typically 1 to 1.5 in., or less than the observed settling in the rafter bay. In addition, the belly appears to be consistent with photos of the roofs' installed conditions (December 2016). The settling was less severe on the south side, consistent with settling problems being related to cycling through high RH levels.

Figure 161. Cellulose netting belly (left); belly depth ~1 to 1.5 in. (right)

This settling created an air channel that would allow rapid transfer of airborne moisture in the rafter bay, rather than the slower movement due to airflow resistance of dense-pack cellulose. This settled gap is possibly a contributor to the severity of the damage at the ridge.

Roof 6 (Winter 1 no diffusion vent, SVR; Winter 2 small diffusion vent, SVR) also showed extensive staining to the framing (east-side rafter) and north roof bay sheathing, per Figure 162. The sheathing showed discoloration, grain raise, mold spotting, and extensively corroded fasteners.

Figure 162. Roof 6 peak overview; extensive mold on east rafter and north sheathing

A close-up of the staining is shown on the east side (Figure 163, left) and west side (Figure 163, right).

Figure 163. Roof 6 mold and staining on east rafter (left) and west rafter (right)

Roof 6 showed the same cellulose settling seen on Roof 5; a shot down the north rafter bay (Figure 164) shows cellulose stuck between the sheathing instruments. This indicates that settling occurred after insulation installation.

Figure 164. Roof 6 cellulose settling and gap at north rafter bay; note cellulose stuck in instruments

Roof 7 (Winter 1 and 2-full-size diffusion vent; variable-perm interior SVR) showed mold spotting and staining, but less than Roofs 5 and 6; this is consistent with the greater outward drying available through the full-size diffusion vent in Roof 7. The east side showed minimal issues (Figure 165, left), but noticeable mold spotting was visible on the "stacked" 2x4 on the west rafter (Figure 165, right), concentrated near the ridge. The mold spotting extended on the sheathing near the west rafter.

Figure 165. Roof 7 minimal damage to east rafter (left); mold and staining on west rafter (right)

Roof 7 suffered from the same cellulose settling issues seen in Roofs 5 and 6; the gap was roughly 2 to 2.5 in. on the north side (Figure 166, left). Settling was less severe on the south side (roughly 1 in., Figure 166, right), which is consistent with drier conditions at the sheathing-insulation interface due to greater solar exposure.

Wood MCs were measured on a spot basis, showing dry conditions; ridge wafers were intact.

Figure 166. Roof 7 cellulose settling at north rafter bay (left) and south rafter bay (right)

14.4 Guard Bay Conditions

The hybrid ccSPF-cellulose roofs showed elevated moisture levels in Winter 2 (Figure 91), with mold index predictions of noticeable growth (over 3.0, Figure 101). Therefore, disassembly exposing this interface was prioritized. However, the guard bays have identical construction to the hybrid Roof 8. In addition, one of the guard bays appeared to be the source of the ant infestation in Roof 3 (Figure 155).

Therefore, the guard bay between Roofs 3 and 4 was disassembled, exposing the interface (Figure 167, left). No evidence was found of significant wetting, which would include "packy" or caked cellulose insulation, visible staining, or odors.

No indication was found of the ant infestation; it is possible that the tunnels are inside the closed-cell spray foam, which was not cut open.

Figure 167. Disassembly of guard bay (hybrid ccSPF-cellulose) ridge and examination

15 Roof Recommissioning (Prior to Winter 3)

15.1 Air and Water Leakage Testing

Several tests were run while the ridge insulation was removed to eliminate potential secondary factors that would influence the experiment.

One was airflow testing at the ridge diffusion vent. The vapor-open diffusion vent material is listed at <0.69 l/(s·m²) @ 75 Pa, which is higher than air barrier material requirements of 0.02 l/(s·m²) @ 75 Pa. However, the small area of this diffusion vent would tend to make this air leakage negligible overall.

Therefore, the test hut was depressurized to -75 Pa (Figure 168, left), and airflow at the diffusion vent was measured with a Fieldpiece STA2 In Duct Hot-wire Anemometer (Figure 168, right). No airflow was measured. However, later calculations demonstrate that an airflow of 0.69 l/(s·m²) @ 75 Pa is equal to a velocity of 0.13 ft per minute/FPM, which is far below the equipment's measurement range of 40 FPM. However, this testing showed no "bypass" air leakage, due to imperfect tape sealing of the diffusion vent.
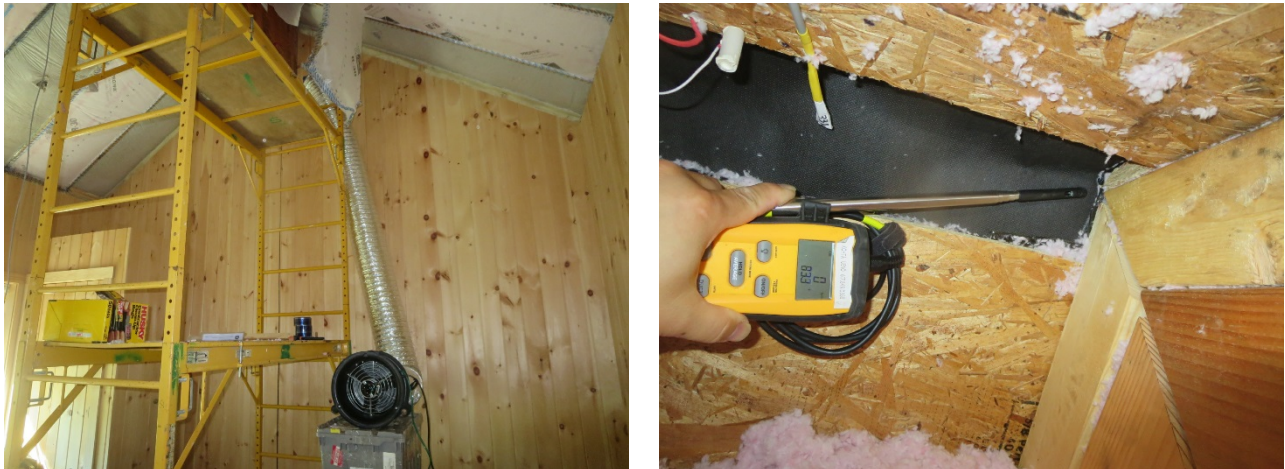
Figure 168. Test hut depressurization (left) and airflow measurement at diffusion vent (right)

Another possible issue was that the visible bulk water staining was due to precipitation leakage rather than condensation rundown. Therefore, the test hut was depressurized to -75 Pa, and water was sprayed, aiming at the ridge detail (Figure 169), to simulate the effect of wind-driven rain.

Figure 169. Hose spray testing of roof ridges with interior observation

This test was conducted for 10 minutes of water spraying from each side, with no detectable water leakage visible from the interior. Infrared observation during this testing distinctly showed cooling of the diffusion vent and ridge from water spraying, but no water penetration.

15.2 Roof Reassembly

After this sensor, observation, and testing work, the roofs were reassembled and reinsulated for Winter 3 testing.

In the cellulose roofs, the open cavity due to settling was filled with dense pack cellulose, maneuvering the hose throughout the rafter bay (Figure 170, left). Density measurements were not taken at that time (as it would require disassembly of the roof again); however, tactile measurements appeared to indicate complete filling of the cavity.

In the fiberglass roofs, the ridge area was filled, including additional fiberglass to infill low-density portions of the roof.

Figure 170. Reinsulation of roof ridge areas and repacking for cellulose (left) and fiberglass (right)

15.3 Enclosure Airtightness Measurement

As part of the experimental commissioning process, the test hut was tested for airtightness in March 2017, and individual rafter bays were tested using differential pressure measurement in insulation cavities to ensure that unequal air leakage is characterized as a variable. After the summer 2018 reconfiguration and recommissioning, these air leakage tests were repeated to ensure that conditions are comparable across multiple winters.

The airtightness of the test hut enclosure was tested via fan depressurization, using an Energy Conservatory Duct Blaster (Model B). All exterior doors in this enclosure are large sliding glass doors, which are difficult to adapt to the typical door frame and shroud. Therefore, the exhaust fan was removed from its housing, and the Duct Blaster was connected to the opening (Figure 171, Figure 110, left). Measurements were taken with an Energy Conservatory DG700 manometer, connected to a computer running TECTITE 4.0 automated multipoint testing software (Figure 171, Figure 110, right).

Figure 171. Airtightness testing with fan connected to exhaust fan opening

The results of multipoint pressurization and depressurization testing are graphed in Figure 172, with key parameters summarized in Table 13, comparing December 2018 and March 2017 results. The overall air leakage (39 CFM vs. 50 CFM) is comparable; based on multiple rounds of testing, it appears that the seal on the sliding glass doors can have a significant effect on overall airtightness measurements. Specifically, an early December 2018 test showed 97–109 CFM 50, due to door air sealing imperfections, before positively latching the door.

These results indicate a very airtight enclosure, in terms of interior-to-exterior air leakage.

Table 18. Air Leakage Testing (Full Enclosure) Results; December 2018 and March 2017

Measurement	Label	Dec 2018 Depressurization	Mar 2017 Depressurization
Airflow @ 50 Pa	CFM50[3]	39	50
Air changes/hr @ 50 Pa	ACH50[4]	0.43	0.55
Surface area-normalized leak	CFM 50/ft^2 surface area	0.02	0.02
Leakage area (EqLA)	in^2	4.3	4.8
Flow coefficient	C	3.6	3.3
Flow exponent	n	0.61	0.69
Coefficient of determination	r^2	0.9986	0.9986
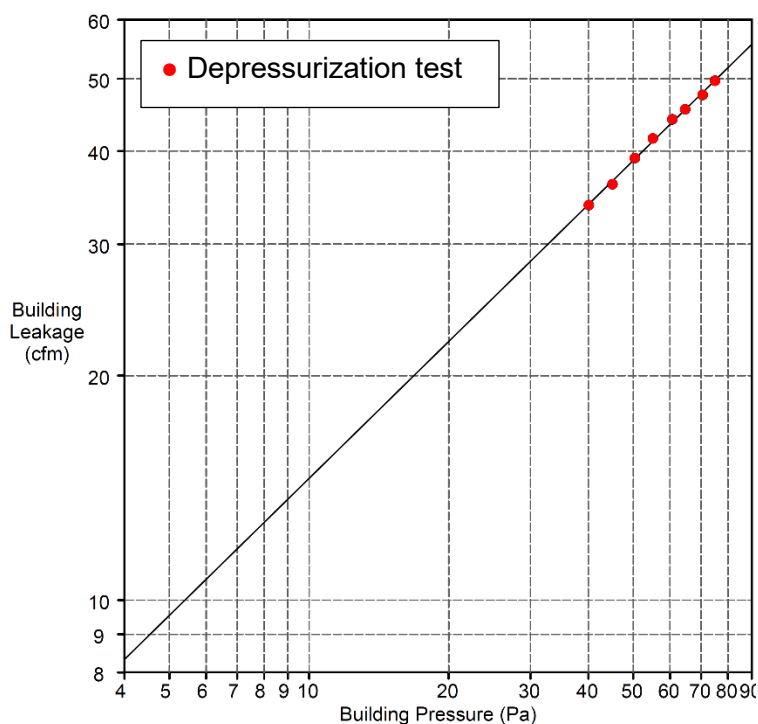
Figure 172. Multipoint depressurization test results

15.4 Air Leakage Location

Although overall indoor-outdoor air leakage was small, depressurization and infrared thermography were used to locate air leakage, thus ensuring that the leaks are not associated with the test roof bays. The interior surfaces of the building were examined with an FLIR ONE Pro

---

[3] Cubic feet per minute at 50 Pascal pressure differential.
[4] Air changes per hour at 50 Pascal pressure differential.

infrared camera; with outdoor temperatures cooler than indoors, thermal bridging or air leakage appear as cool surfaces (colder than interior conditions). Temperatures were 35°F exterior and 70°F interior during these observations.

A baseline infrared observation of the building was done prior to depressurization to identify existing thermal bridges or other anomalies and to avoid ascribing them to depressurization air leakage. Findings included thermal bridging at the roof framing (Figure 173), thermal stratification of the interior (consistent with interior temperature measurements), and thermal bridging at the slab perimeter (per previous observations).
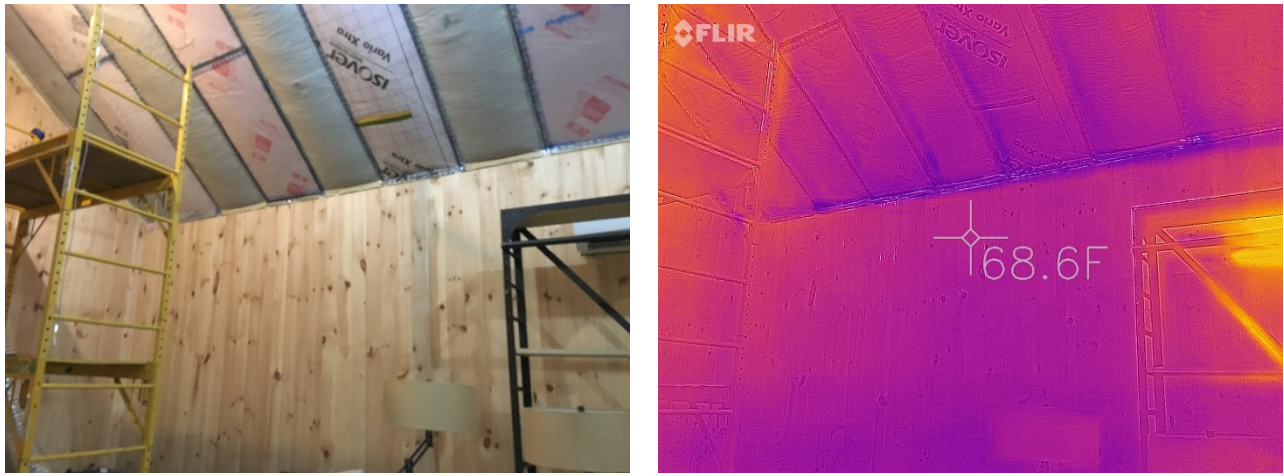
Figure 173. Visual and infrared image of interior of roof, depressurization testing

Then, infrared observation was combined with depressurization to search for air leakage. Figure 174 shows a point air leak at the corner of the building (triple point connection of walls to roof). However, this air leak is in a guard bay, not a test bay, so it does not affect the research. Similarly, a point air leak was found at an upper corner of a sliding glass door (Figure 175, Figure 116); again, this does not affect the test roofs.
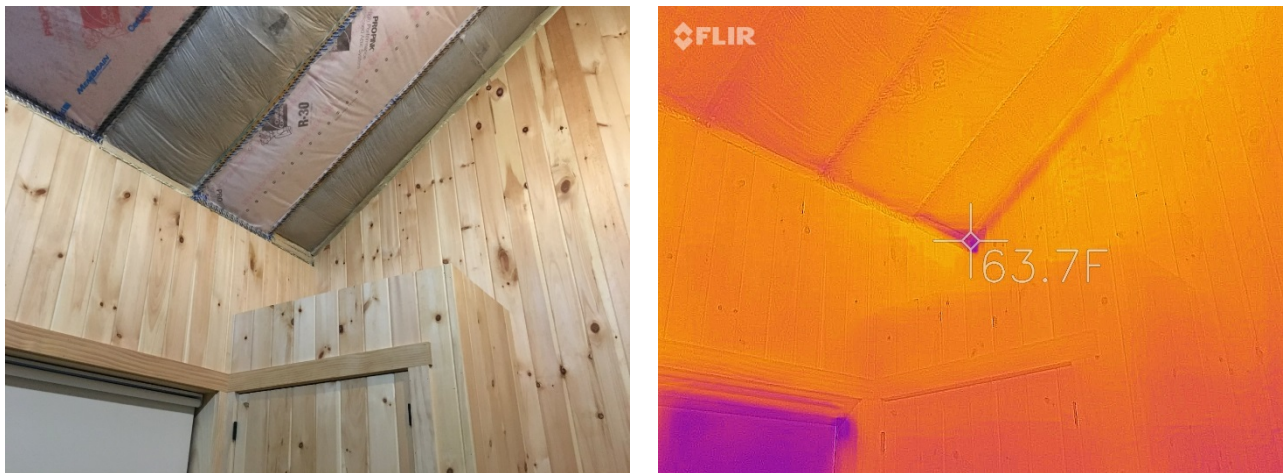
Figure 174. Visual and infrared image of interior of roof, depressurization testing

Figure 175. Visual and infrared image of air leakage at sliding glass door corner

15.5 Roof Bay Pressure Difference Comparison

Another commissioning test was to measure the pressure difference (ΔP) across the interior air/vapor control membrane to determine whether disproportionate air leakage is occurring in one of the test bays. With the building depressurized to -75 Pa, ΔP measurements were taken with an Energy Conservatory DG-700 manometer. Measurements were taken at the roof-wall connection/eave at the north and south sides (Figure 120, left) and at the ridge (Figure 120, left). An opening was cut in the interior air/vapor control membrane and then sealed with tape.

The results of these December 2018 measurements are shown in Table 19, showing pressure drop (ΔP) in Pa, bar graphs for visual comparison, and as a percentage of the enclosure indoor/outdoor ΔP. Overall, the results show a small pressure drop across the interior air/vapor control membrane, compared to the total pressure drop (0.9% to 4.1% of total). This indicates that the exterior sheathing is the most airtight layer, which is consistent with its construction (sheathing with an integrated water-resistive barrier and self-adhered membrane).

A comparison with March 2017 measurements (Table 14) shows that the anomaly seen in Roof 1 has been eliminated; it is much more consistent with other experimental roof bays. In addition, the 2018 south-side eave measurements showed consistently higher ΔPs than the north side or ridge. This is the opposite pattern from the 2017 measurements. A further explanation is unavailable without further disassembly and testing.

Figure 176. Measuring ΔP across air/vapor control membrane at eave (left) and ridge (right)

Table 19. Roof Membrane ΔP Measurements at Eaves and Ridge, December 2018

Location	1 FG-VB-DV	2 FG-SVR-DV	3 FG-tVR-DV	4 FG-SVR-sDV	5 Cell-tVR-DV	6 Cell-SVR-sDV	7 Cell-SVR-DV	ccSPF-Cell
North ΔP	1.0	1.0	0.7	0.7	1.0	0.6	1.4	n/a
Ridge ΔP	0.8	0.8	0.7	0.7	1.2	0.3	0.7	n/a
South ΔP	2.3	2.2	2.1	2.2	2.2	2.5	3.0	n/a
Average ΔP	1.4	1.3	1.2	1.2	1.5	1.1	1.7	n/a
North ΔP								
Ridge ΔP								
South ΔP								
Average ΔP								
North % of total	1.4%	1.4%	0.9%	0.9%	1.4%	0.8%	1.9%	
Ridge % of total	1.1%	1.1%	0.9%	0.9%	1.6%	0.4%	0.9%	
South % of total	3.1%	3.0%	2.8%	3.0%	3.0%	3.4%	4.1%	
Average %	1.8%	1.8%	1.6%	1.6%	2.0%	1.5%	2.3%	

Table 20. Roof Membrane ΔP Measurements at Eaves and Ridge, March 2017

Location	1 FG-VB-DV	2 FG-SVR-DV	3 FG-VB-nDV	4 FG-SVR-nDV	5 Cell-VB-nDV	6 Cell-SVR-nDV	7 Cell-SVR-DV	8 ccSPF-Cell
North ΔP	2.6	1.0	0.7	1.1	1.5	1.9	1.9	n/a
Ridge ΔP	1.7	0.9	0.2	0.2	0.2	0.2	0.5	n/a
South ΔP	1.7	0.4	0.2	0.5	0.2	0.3	0.6	n/a
Average ΔP	2.0	0.8	0.4	0.6	0.6	0.8	1.0	n/a
North ΔP								
Ridge ΔP								
South ΔP								
Average ΔP								
North % of total	3.5%	1.4%	0.9%	1.5%	2.0%	2.6%	2.6%	
Ridge % of total	2.3%	1.2%	0.3%	0.3%	0.3%	0.3%	0.7%	
South % of total	2.3%	0.5%	0.3%	0.7%	0.3%	0.4%	0.8%	
Average %	2.7%	1.0%	0.5%	0.8%	0.9%	1.1%	1.4%	

16 Diffusion Vent and Vapor Retarder Reconfiguration (Prior to Winter 3)

16.1 Diffusion Vent Retrofit (Removal of Tight Diffusion Vents)

The tight diffusion vent roofs (Roofs 3 and 5) showed limited drying, moisture accumulation, and poor performance in Winter 2. Therefore, as shown in Table 3, these roofs were retrofitted with full-size (~6-in.) ridge vapor diffusion openings. This work is documented in Figure 178: the existing tight diffusion vent was removed, the opening enlarged by cutting the sheathing, and the new diffusion vent (Dörken Delta Foxx) installed and sealed with tape.

Figure 177. Removal of tight (~25-perm) diffusion vent (left) and cutting new diffusion vent opening (right)

Figure 178. Retrofitting diffusion vent opening (left) and taping (~25-perm) diffusion vent (right)

16.2 Interior Vapor Control Effect

One unresolved difference in behavior was the sheathing MC on the north side, specifically when comparing Roof 1 (full-size diffusion vent, 1 perm VR) and Roof 2 (full-size diffusion vent, variable SVR). These two roofs are identical except for their interior vapor control layer.

In Winter 2, it appears that Roof 1 had noticeably drier MCs than Roof 2, as shown at the upper (Figure 179) and mid-height (Figure 180) sheathing measurements. This difference was not seen in Winter 1; it was seen only during Winter 2 with humidified interior conditions.
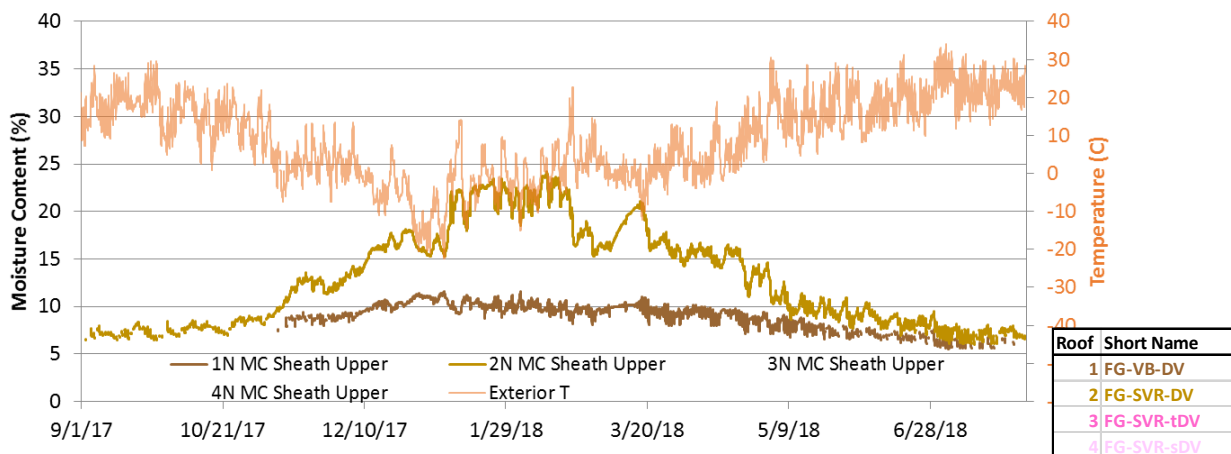
Figure 179. Fiberglass roofs' (1 and 2) sheathing MC north upper measurements, Winter 2
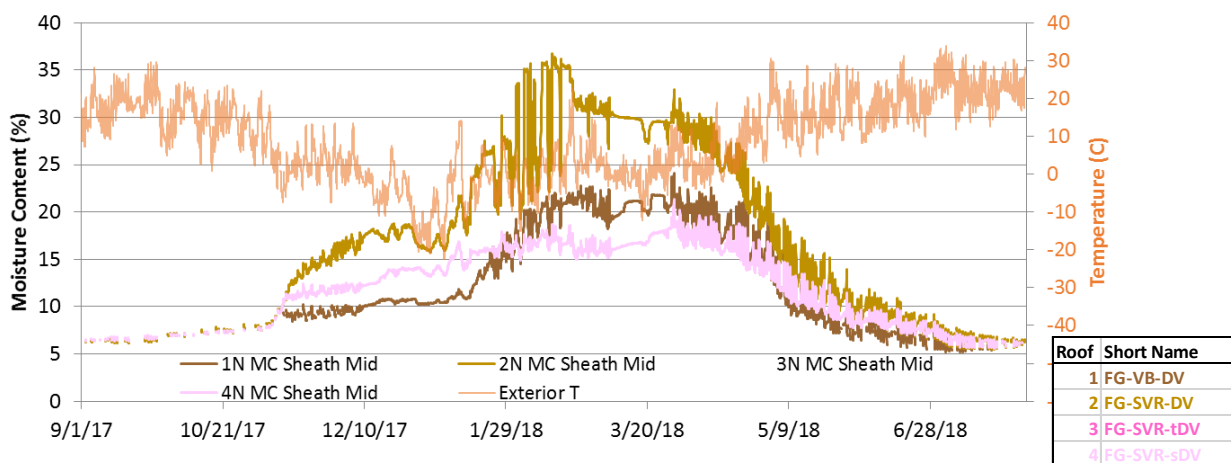
Figure 180. Fiberglass roofs' (1, 2, and 4) sheathing MC north mid-height measurements, Winter 2

One possible cause was that the selected smart variable-permeance vapor retarder (CertainTeed MemBrain, **BLUE** in Figure 21) has a permeance curve that opens noticeably at mid-range RHs. For instance, at 50% RH, it has a permeance of roughly 4 perms, which is higher than the 1 perm of the fixed-perm Owens Corning vapor retarder (**PINK** in Figure 21). This would be consistent with higher interior RHs exposing the rafter cavity to greater amounts of interior moisture.

However, there are some inconsistencies in this explanation. For one, Roof 4 (small diffusion vent, SVR) has similarly dry mid-height sheathing MCs, despite the use of the same CertainTeed

SVR (Figure 180). Second, the RHs shown in vapor permeance curves (Figure 21) is the average over the material. With an interior RH of 50% and a wintertime rafter cavity RH of 15%–45% (per inward drive measurements), the average RH over the material would be 33%–48% RH.

But, given the elimination of the tight diffusion vent (discussed below), an opportunity was available to test alternate materials. Therefore, two rafter bays (one fiberglass, one cellulose) were retrofitted with a variable-perm interior vapor retarder with lower mid-range permeances.

16.3 Vapor Retarder Reconfiguration

As shown in Table 3, Roofs 3 and 5 were also reconfigured by replacing the CertainTeed MemBrain interior vapor retarder with Isover Vario Xtra (tight vapor retarder/tVR). The material was installed in the same manner as existing interior vapor retarders (Figure 181). The multistep air seal included spray adhesive on the rafter surfaces, double-sided tape on the rafters, installation of the vapor retarder, mechanical fasteners (staples), sealing the perimeter with clear housewrap tape, and rolling the seal for positive adhesion.

Figure 181. Removing old interior vapor control (left) and newly retrofitted bays (right)

17 Air Injection System (Prior to Winter 3)

This appendix section provides selected background on air leakage through building enclosures and describes the construction and installation of an apparatus to inject controlled amounts of air leakage into the experimental roof rafter bays. The goal was to evaluate the vulnerability of assemblies to air barrier imperfections. This air leakage apparatus was put into operation late in Winter 3 (late February 2019) for comparison with baseline operation in early winter (50% RH interior, no imposed air leakage).

17.1 Air Leakage Background: Fox (2014) and Trainor (2014)

Fox (2014) and Trainor (2014) both completed research at the University of Waterloo field test facility (BEGHut), studying the hygrothermal behavior of high-R value wall assemblies in climate zone 6A. The test walls included stud frame walls with exterior insulation and thick superinsulated walls with a deep fibrous insulation cavity, such as double-stud and I-joist-framed walls. Part of their research involved injection of controlled amounts of interior air into the insulated cavities, which informs the current project.

These two authors' thesis work include technical background and a literature review on air leakage in insulated assemblies (see Section 3.2 "Previous Studies of Air Leakage Condensation and Drying Potential" in Trainor 2014, and Section 2.8 "Air Leakage" in Fox 2014). Key takeaways include:

- In a field study on wall assemblies with a controlled airflow path from the interior into the cavity, interior RH was the strongest influence on wintertime moisture accumulation in the assembly (TenWolde, Carll, and Malinauskas 1998).

- In hygrothermal simulations of air leakage into wall assemblies at various rates, moisture deposition into the assembly increases from 0.001 to 1.0 l/s/m^2. Above 1.0 l/s/m^2, moisture accumulation falls due to warming of the sheathing by exfiltration. "Short" air leakage paths result in greater moisture deposition, and RH levels strongly influence performance. Insulation outboard of the sheathing reduces wetting (Ojanen and Kumaran 1996).

- Hygrothermal simulations of air leakage into unvented roof assemblies show that these assemblies are vulnerable to wintertime moisture accumulation due to air leakage. Higher R-values correlate with greater moisture accumulation in all-cavity-fill assemblies, but exterior insulation reduces risks. Drying to the exterior via a vapor-permeable underlayment and an air gap above the sheathing reduces air leakage condensation accumulation (Janssens and Hens 2003).

- Laboratory study and computer modeling were conducted on the wall-to-roof joint with an unvented roof assembly (fibrous insulation in cavity), as this is a critical junction for air leakage-based condensation. Variables included interior RH, air pressure/airflow rates, exterior temperature, and insulated/uninsulated roof sheathing. The results showed expected

relationships between condensation accumulation and these variables, with greater moisture issues at higher interior RHs, airflow rates, lower temperatures, and uninsulated sheathing. The authors recommended an air leakage rate of 0.1 to 0.2 l/s/m² for a typical two-story house in a cold climate (Kalamees and Kurnitski 2010).

- Laboratory tests of a flat wood frame unvented roof assembly with dense-pack cellulose insulation were run varying interior and exterior conditions (T/RH) and air pressure. The work demonstrated that dense-pack cellulose alone is not an effective air barrier, and that air leakage resulted in moisture accumulation and cellulose "caking." Leakage path length had an effect on accumulation due to cellulose moisture storage (Derome 2005).

- A test hut was built to study air leakage and moisture accumulation patterns in wall assemblies; variables included wall assembly and air leakage path (long/direct/diffuse). The research found convective looping in wall cavities and the greatest moisture accumulation opposite the entry point. Eliminating air leakage resulted in low moisture accumulation. The exterior insulation wall had poor performance in this study due to liquid water condensation (rather than frosting) on the sheathing and low-permeance materials on both sides of the assembly (Desmarais et al. 2000).

Fox (2014) presented a variety of air leakage standards and air leakage metrics, which were used to gauge the realism of selected experimental airflow rates.

The overall results of Fox's field work were summarized in the literature search section of Ueno (2015). The key conclusion was that the work demonstrated that thick walls with cold sheathing (i.e., double-stud and I-joist walls) are more vulnerable to interior-sourced condensation than exterior insulated walls. In addition, Trainor (2014) demonstrated the measurable warming of the wall sheathing when subjected to forced air leakage.

The air leakage apparatus used by Fox and Trainor is shown in Figure 182; Building Science Corporation's air injection apparatus was based on this design. It included a central air pump (Figure 182, left), distributed to the walls via a manifold of 1-in. polyethylene tubing. This was in turn connected to flow meters/rotameters, connected to an opening low on the wall cavity (Figure 182, right). An exhaust port connected to the interior was created by drilling a 1-in. diameter hole through the interior air/vapor control layers (gypsum board and polyethylene).
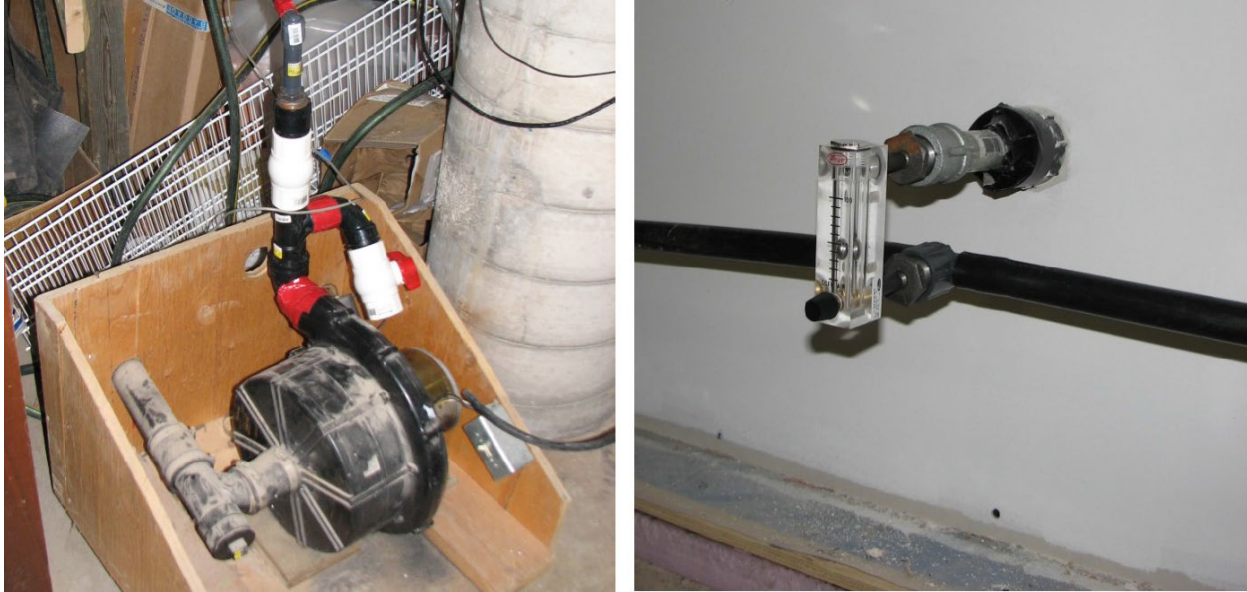
Figure 182. Air injection system used at University of Waterloo BEGHut (Fox 2014)

Air leakage was added at a rate of 0.315 l/s, or 40 standard cubic feet per hour, or 0.67 CFM per wall assembly. The area-normalized airflow rate was 0.24 l/s·m^2 (for the central 16-in. cavity alone) and 0.11 l/s·m^2 (for the total 4 ft. x 8 ft. test panel). This rate was comparable to the natural leakage rate calculated for U.S. Army Corps of Engineers and ASHRAE airtightness standards.

17.2 Air Leakage Background: Lstiburek (2015 and 2018)

Lstiburek (2015) discussed hygrothermal models (specifically WUFI/Wärme und Feuchte instationär/Heat and Moisture, Transient), their limitations, and various modeling techniques to overcome these limitations. One issue is airflow through the assembly; the current version of WUFI allows introduction of airflow (from interior or exterior sources) at interfaces to simulate air leakage ("source" and "sink" terms). Airflow can have a significant effect on building assemblies that contain multiple air spaces ("non-monolithic" or "hollow" assemblies) common in North America.

Modeling airflow in a one-dimensional simulation such as WUFI requires some judgement on how it should be incorporated. Twelve common airflow pathways through a stud frame wall assembly are shown in Figure 25. They are broken down into several categories: first convection within the stud bay, exterior-to-exterior, and interior-to-interior airflow. These are followed by infiltration/exfiltration pairs of short-pathway and long-pathway airflows. An exhaustive set of these airflow pathways combined with exterior rainscreen cavity ventilation is shown in Figure 183. Although WUFI does not handle interior-to-exterior airflows explicitly, it can essentially be simulated using careful source-sink terms.
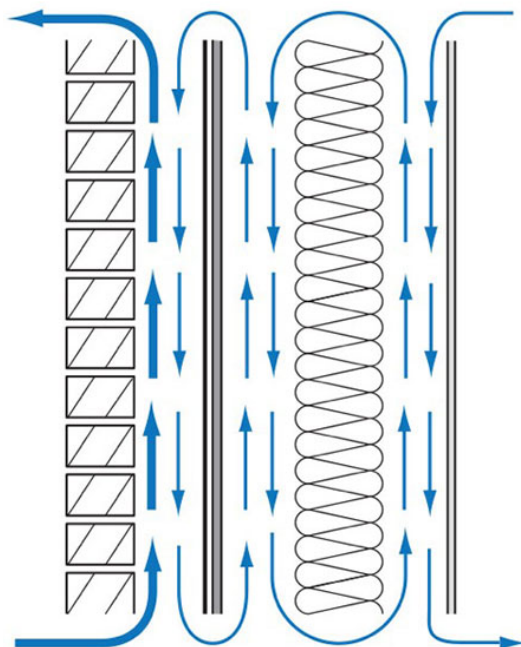
Figure 183. Combined airflow pathways (full level of complexity) (Lstiburek 2015)

Lstiburek (2018) also discussed why double vapor barriers (enclosure elements with low-perm materials on the interior and exterior of the assembly) can function without failure. Given their lack of inward and outward drying, some double vapor barrier assemblies have failed badly, given that inadvertent moisture penetration remains trapped within the assembly to cause damage. However, other double vapor barrier assemblies have acceptable to excellent performance. A typical example is a wall with extruded polystyrene foam sheathing (1 perm) and a polyethylene (Class I, 0.06 perm) vapor barrier. Airflow from the exterior into the stud cavity results in wintertime drying; combined with good interior airtightness, this assembly provides acceptable behavior.

Internal Cavity (Convective Looping)

Exterior-Exterior

Interior-Interior

Infiltration/Exfiltration - Short Path

Infiltration/Exfiltration - Long Path
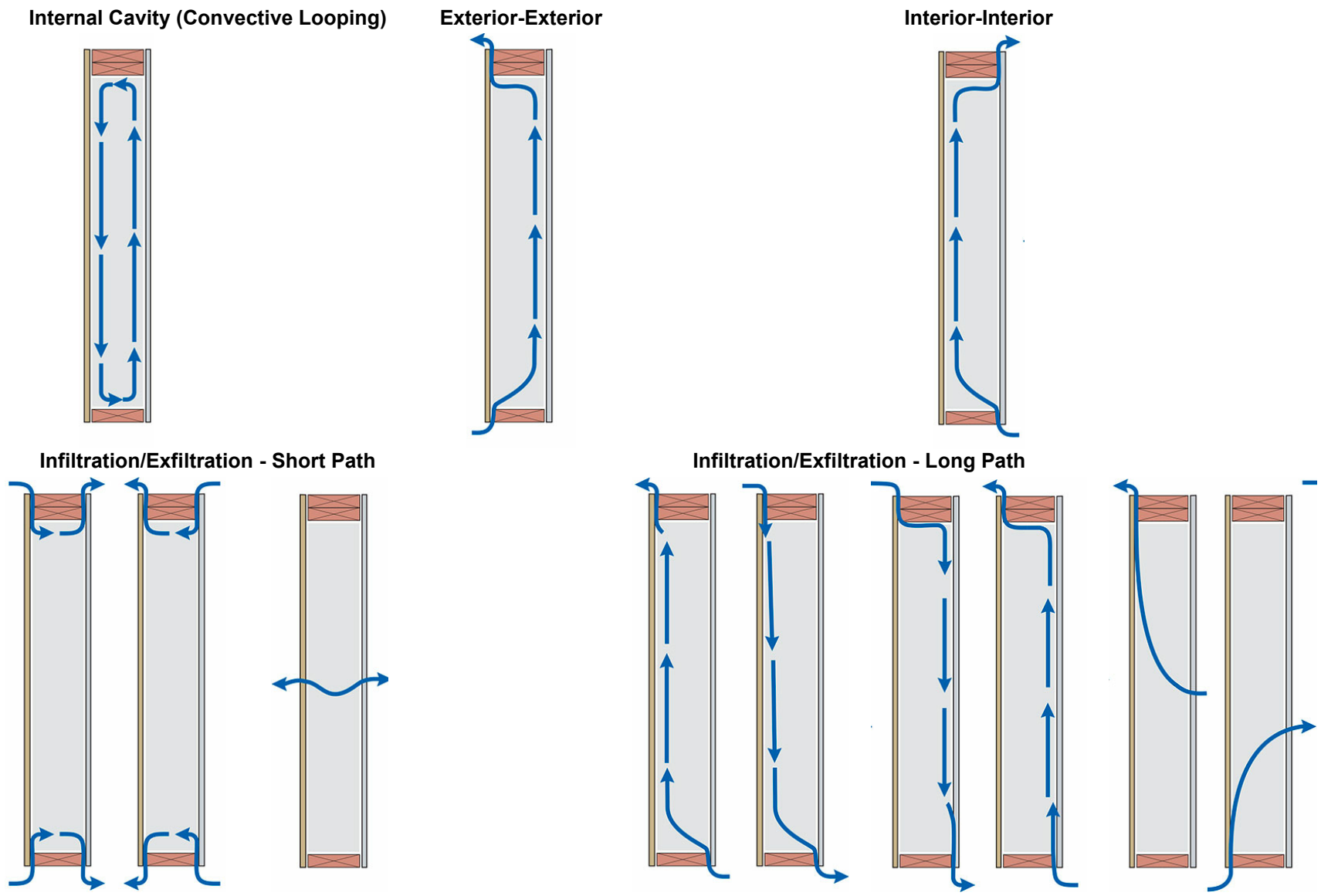
Figure 184. Twelve typical airflow pathways in multilayer systems (Lstiburek 2015)

17.3 Air Injection System and Airflow Path

The conceptual design of air leakage apparatus and its connections to the test rafter bays is shown in Figure 185. The intent is to inject interior air low into the north rafter bay (the side at higher risk for moisture failures) and for the air to travel upward in the bay to the "relief port" near the ridge. This would result primarily in an interior-to-interior airflow path (see Figure 25).

1" diameter polyethylene tubing as exhaust port, taped to air/vapor control membrane

Bulkhead/hose barb fitting; washer clamped to air/ vapor barrier membrane

Rotameter/flowmeter, 3-30 liters/minute (0.10-1.0 CFM)

Vacuum cleaner as blower, 150 CFM nominal capacity
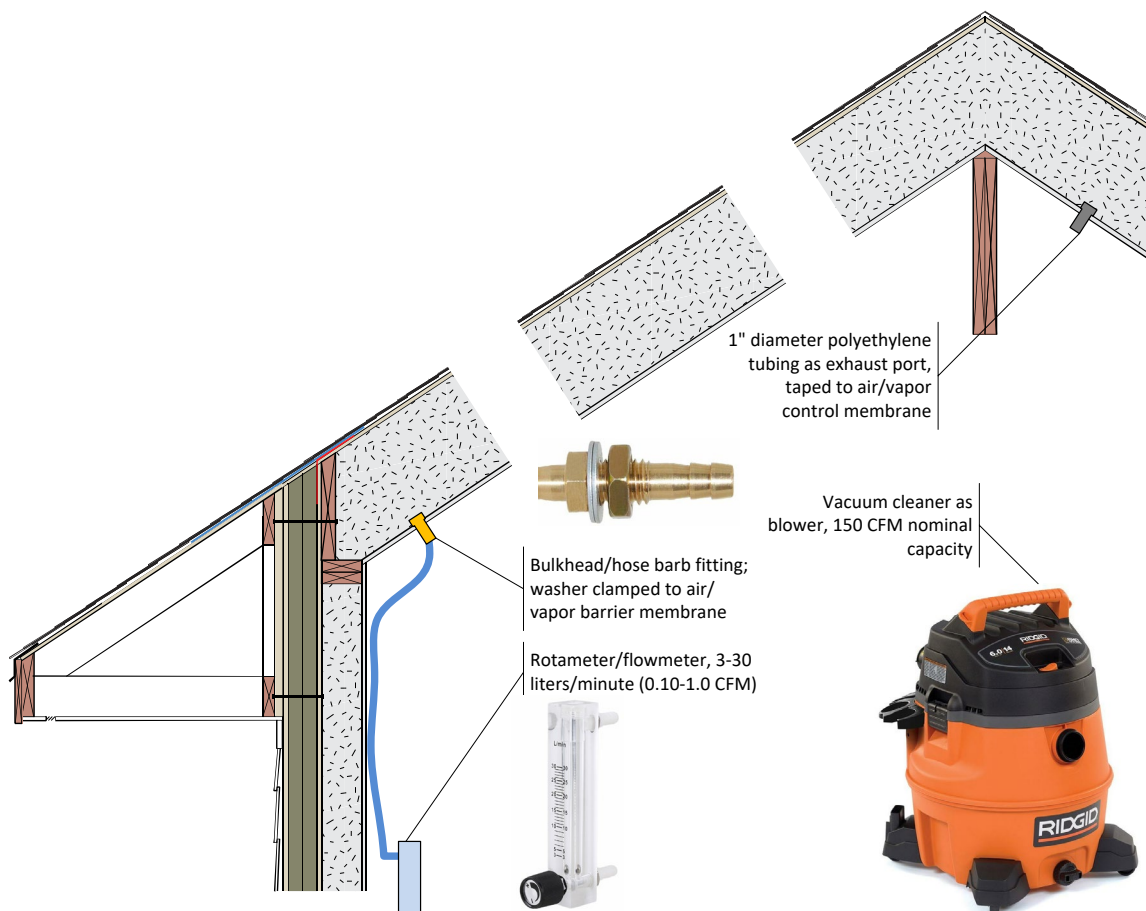
Figure 185. Conceptual design of air leakage apparatus and rafter bay connections

Interior-to-exterior airflow cannot be ruled out; however, previous testing indicated that the test hut as a whole is very airtight (39 CFM 50 or 0.02 CFM 50/sf enclosure area; see Table 18). Previous measurement of pressure drop across the air-vapor control membrane with the hut depressurized to -75 Pa (see Table 19) indicated that the exterior sheathing is the most airtight layer of the rafter assembly. Therefore, interior-to-interior air leakage will likely be the dominant airflow path with this imposed air leakage.

17.4 Air Injection System Installation

An overview of air injection system is shown in Figure 186; the loop-style manifold is built from 1-in. nominal polyethylene tubing, assembled using compression connector tees.

Figure 186. Overview of air injection system, showing manifold loop

Air injection is provided by a shop vacuum, using the output port (RIDGID 14 Gal. 6.0-Peak HP Wet Dry Vac, 150 CFM), per Figure 187 (left).

A tee is provided for each test roof, feeding a rotameter flow meter (CNBTR Multicolor Acrylic 3-30LPM LZQ-7 Oxygen Air Gas Flowmeter with Control Valve Adjustable Accuracy: 5%), per Figure 187 (right).
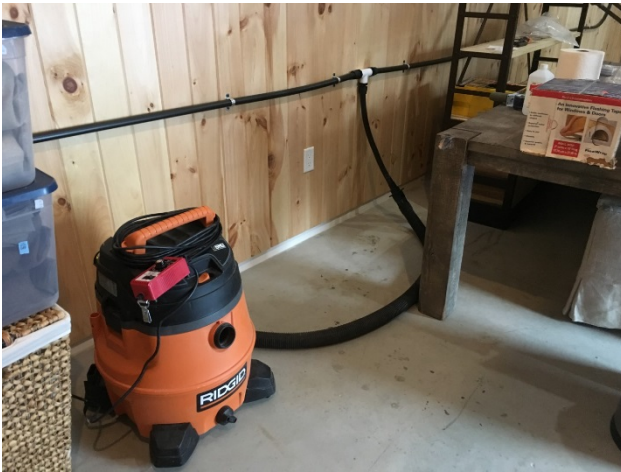
Figure 187. Shop vacuum used as blower (left); rotameter and tubing connection (right)

The injected air is in turn is fed to 7/16 O.D. x 5/16 I.D. flexible PVC tubing, which is connected to the interior air-vapor control membrane via a brass barb fitting, and sealed with flashing tape (3M 8067) and compression washers, per Figure 188. This injection port is roughly 8 in. from the bottom of the rafter bay.

Figure 188. Tubing hose barb penetration (left); tubing attachment for Roofs 4–7 (right)

Pressure relief at the rafter bays is provided by a relief port made of 1-in. nominal polyethylene tubing, attached to the interior air-vapor control membrane with flashing tape (Figure 189).

Figure 189. Roof ridge relief port close up (left); roof ridge relief port overview (right)

17.5 Airflow Rate and System Commissioning

When the air injection system was run, the maximum airflow that could be applied consistently to all rafter bays was 15 liters/minute, or 0.53 CFM, in each rafter bay (Figure 190, left).

This airflow rate is equal to 0.07 l/s·m^2 if applied to both rafter bays (north and south), or 0.14 l/s·m^2 if applied to only the north rafter bay. This can be compared to the airflows used in Fox (2014) and Trainor (2014) of 0.24 l/s·m^2 (for the central 16-in. cavity alone) and 0.11 l/s·m^2 (for the total 4 ft. x 8 ft. test panel). This air leakage is comparable to relatively airtight construction.

Figure 190. 15 liters/minute airflow rate (left), measuring pressure difference at relief opening (right)

A commissioning test was performed to seal the relief port and measure the developed pressure (Figure 190, right). The results are shown in Table 21.

Table 21. ΔP Measurements (in Pascals) at Exhaust Ports With Air Injection System Running

Location	1 FG-VB-DV	2 FG-SVR-DV	3 FG-tVR-DV	4 FG-SVR-sDV	5 Cell-tVR-DV	6 Cell-SVR-sDV	7 Cell-SVR-DV	ccSPF-Cell
North ΔP	0.1	0.1	0.1	0.3	0.2	0.1	0.1	n/a

These results suggest that Roof 4 (fiberglass, SVR, small diffusion vent) is either more airtight or receives more airflow than other bays. However, previous air leakage testing of pressure drop across the air-vapor control membrane with the hut depressurized to -75 Pa did not identify this roof bay as anomalous (Table 19). Differences in airflow are unlikely given the metering through rotameters. Another possibility is that the airflow pathways and/or airflow resistance through the insulation affect the pressure drop at the relief port.

The air injection system and roof bays were inspected with an infrared camera while in operation. The shop vacuum was noticeably hot in operation (maximum temperature 113°F, Figure 173); this is consistent with the unit operating with constricted flow and in continuous operation. This was concerning, as injecting high-temperature air into the rafter bays is not representative of in-service air leakage in the field.
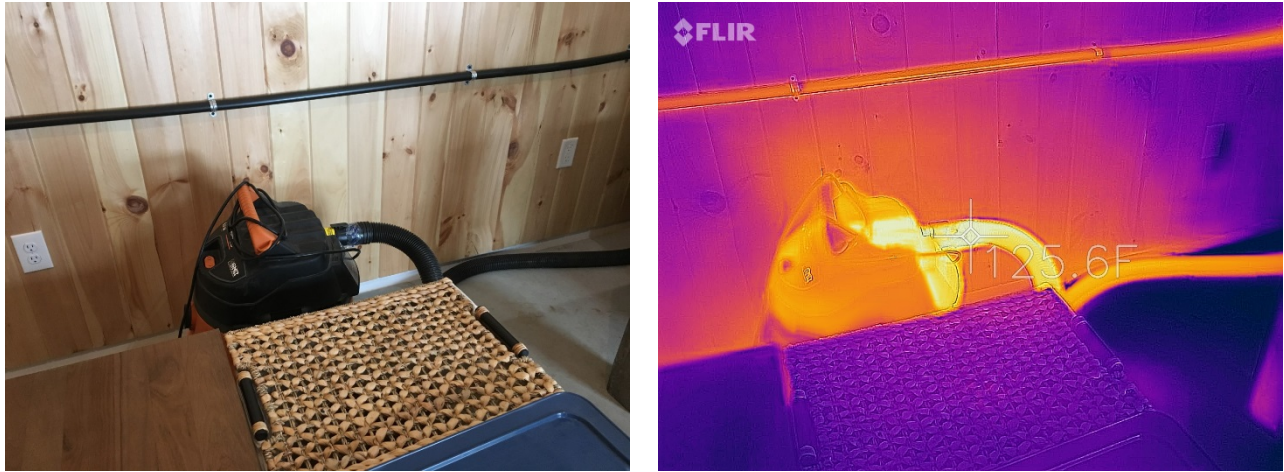
Figure 191. Visual and infrared image of show vacuum; heat generation visible

However, examining the upper manifold tube and the small-diameter PVC tubing (Figure 192), the air had cooled to ambient test hut conditions. This is consistent with the small airflow (0.5 CFM per rafter bay) and exposed surface area of the tubing.
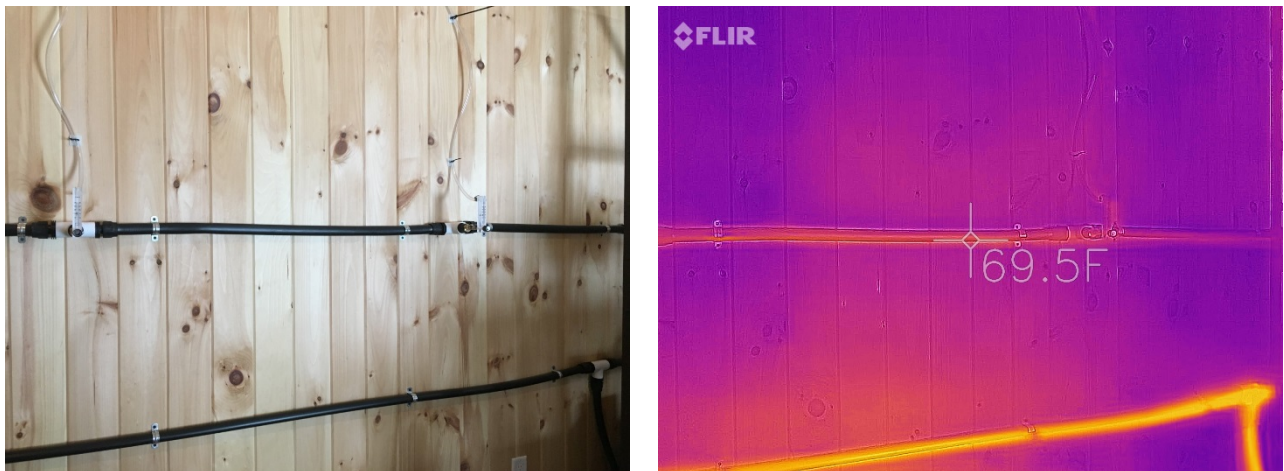
Figure 192. Visual and infrared image of manifold and tubing; PVC tubing at ambient temperature

18   Lower Roof Disassembly and Density Measurements (After Winter 3)

18.1 Lower North Roof Disassembly

Given the high sheathing MCs measured at the north lower roofs after running the air injection system (Figure 57 and Figure 81), the assembly was visually inspected to examine indications of moisture damage and/or mold. The interior vapor control and netting were opened directly above the air injection port, low on the north roof, 1 or 2 ft up. Cardboard baffles were inserted to hold back the insulation, fastened in place, and the insulation removed, per Figure 193 and Figure 194.

Figure 193. Installation of cardboard baffles for north roof sheathing examination

Figure 194. Overview of north-side roof openings

Roof sheathing conditions were then visually examined. No roof showed signs of sheathing moisture distress, such as mold or staining (Figure 195 and Figure 196). At most, there was arguably some raised grain at the OSB surface. While removing the insulation, no "packy" or adhered conditions (indicating previous wetting) were observed.

Given the lack of visual indications of problems, Roofs 6 and 7 were only opened for a 1-ft distance along the roof, rather than 2 ft (Figure 194).

Figure 195. Opening at north-side roof sheathing and OSB conditions (Roof 2 fiberglass)

Figure 196. Opening at north-side roof sheathing and OSB conditions (Roof 5 cellulose)

A possible contribution to the intact OSB conditions is the fact that the roof OSB was Huber ZIP sheathing. Their OSB formulation uses a significant fraction of MDI (methyl diisocyanate/polymeric diphenylmethane diisocyanate) resin adhesive, which is known to improve moisture resistance and reduce water uptake. This adhesive has been documented to improve performance in accelerated exposure tests (Marra 1992), and is anecdotally reported to improve mold resistance compared to commodity OSB (Davidovic 2019). This is consistent with previous studies of double-stud walls in Massachusetts (Ueno 2015). That work found that

assemblies with ZIP sheathing and cellulose and open-cell foam subjected to wintertime condensation did not develop mold growth on the inboard side of the sheathing.

18.2 Density Measurements

These north roof openings were also used to take insulation density measurements. Insulation was carefully removed in multiple bins and the weights summed (Figure 197); the dimensions of the opening were measured and/or estimated (based on the belly of the insulation netting).

Figure 197. Removal of fiberglass for density measurement and weighing

Installed insulation density was then calculated based on these measurements, as shown in Table 22. Two measurements were taken at Roofs 3 (fiberglass) and 5 (cellulose), both low (at the air injection port) and high (near the ridge on the north side).

Table 22. Weight, Volume, and Density Calculations for Test Roof Openings

Roof	Total Lbs	Cubic Ft	PCF
1 FG-VB-DV	5.8	4.6	1.3
2 FG-SVR-DV	6.2	4.6	1.3
3 FG-VB-nDV (Low)	6.6	4.6	1.4
3 FG-VB-nDV (Hi)	5.0	2.3	2.2
4 FG-SVR-nDV	6.4	4.6	1.4
5 Cell-VB-nDV (Low)	19.2	4.6	4.1
5 Cell-VB-nDV (Hi)	10.0	2.3	4.3
6 Cell-SVR-nDV	10.6	2.3	4.6
7 Cell-SVR-DV	8.6	2.3	3.7

The resulting installed fiberglass densities were typically 1.3 to 1.4 PCF, which is consistent with the manufacturer's stated 1.4 PCF (based on a timed installation technique). The exception was the measurement near the ridge (Roof 3), where the measured density was 2.2 PCF. This is consistent with additional material being installed at the ridge during the retrofit work, in an attempt to address voids at the roof ridge (see Section 15.2: Roof Reassembly).

The installed cellulose densities ranged from 3.7 to 4.6 PCF, averaging 4.2 PCF. This is consistent with typical densities for "dense pack" insulation (~4 PCF).